TESIS DE LA UNIVERSIDAD DE ZARAGOZA

2013

33

Julie Movellan

Dendritic derivatives as building blocks for biomedical applications

Departamento
Química Orgánica

Director/es
Serrano Ostáriz, José Luis
Martínez de la Fuente, Jesús

ISSN 2254-7606

Prensas de la Universidad
Universidad Zaragoza

Universidad Zaragoza
1542

Tesis Doctoral

DENDRITIC DERIVATIVES AS BUILDING BLOCKS FOR BIOMEDICAL APPLICATIONS

Autor

Julie Movellan

Director/es

Serrano Ostáriz, José Luis
Martínez de la Fuente, Jesús

UNIVERSIDAD DE ZARAGOZA

Química Orgánica

2013

Dendritic derivatives as building blocks for biomedical applications

2012

Julie Movellan

University of Zaragoza,

Institute of Nanoscience of Aragon

DOCTORAL THESIS

DENDRITIC DERIVATIVES AS BUILDING BLOCKS FOR BIOMEDICAL APPLICATIONS

Author

JULIE MOVELLAN

Directors

JOSÉ LUIS SERRANO OSTÁRIZ

JESÚS MARTÍNEZ DE LA FUENTE

Organic Chemistry Department

Institute of Nanosciences of Aragon

University of Zaragoza

Zaragoza, 2013.

D. JOSÉ LUIS SERRANO OSTÁRIZ, Catedrático del Departamento de Química Orgánica de la Facultad de Ciencias perteneciente al Instituto de Nanociencia de Aragón de la Universidad de Zaragoza y

D. JESÚS MARTÍNEZ DE LA FUENTE, investigador ARAID del Instituto de Nanociencia de Aragón de la Universidad de Zaragoza

HACEN CONSTAR:

Que el trabajo original titulado "DENDRITIC DERIVATIVES AS BUILDING BLOCKS FOR BIOMEDICAL APPLICATIONS", ha sido realizado bajo nuestra supervisión por JULIE MOVELLAN en el Instituto de Nanociencia de Aragón de la Universidad de Zaragoza y reúne las condiciones para su presentación como tesis doctoral.

Zaragoza, a 30 de enero de 2013

Fdo.: Dr. José Luis Serrano Ostáriz Fdo.: Dr. Jesús Martínez de La Fuente

Index

ACRONYMS

AB	Antibody
AR	Aspect ratio
***bis*-MPA**	2,2-bis(methylol)propionic acid
bp	Base pair
$CDCl_3$	Deuterated chloroform
COS-7	African Green Monkey SV40 transf-d-kidney fibroblast cell line
COSY	Correlation Spectroscopy
CQ	Chloroquine
CuAAC	Copper-Catalyzed Azide-Alkyne cycloaddition
CVS	Crystal Violet Staining
D_2O	Deuterated water
Da	Daltons
DCC	N,N'-dicyclohexylcardiimide
DCM	Dichloromethane
DCU	Dicyclohexylurea
DMAP	4-(dimethylamine) pyridine
DMEM	Dulbecco's modified eagle medium
DMF	Dimethylformamide
DNA	Deoxyribonucleic Acid
DOTA	1,4,7,10-tetraazacyclododecane-1,4,7,10-tetraacetic acid
DPTS	4-(Dimethylamino)pyridinium p-toluenesulfonate
EDC	*N*-(3-Dimethylaminopropyl)-*N*′-ethylcarbodiimide
EDTA	Ethylenediaminetetraacetic acid
EE	Encapsulation Efficiency
ESI	Electrospray ionization
EtOAc	Ethyl Acetate
EtOH	Ethanol
FA	Folic Acid

FACS	Fluorescence-Assisted Cell Sorting
FT-IR	Fourier Transform Infrared Spectroscopy
G	Glycine
G1	Generation 1
GFP	Green Fluorescent Protein
HATU	N-methylmethanaminium hexafluorophosphate
HeLa	Human epithelial carcinoma cells
HEPES	4-(2-hydroxyethyl)-1-piperazineethanesulfonic acid
HER2	Human epidermal growth factor receptor 2
HOAt	1-hydroxy-7-azabenzotriazole
HSQC	Heteronuclear Single Quantum Coherence
HUVEC	Human Umbilical Vein Endothelial Cells
J	Coupling constant
kDa	kilo Dalton
mAb	Monoclonal antibody
MALDI-TOF	Matrix assisted Laser Desorption Ionization-Time of Flight
MCF-7	Michigan Cancer Foundation – 7, human breast adenocarcinoma cell line
MeOD	Deuterated methanol
MeOH	Methanol
MRI	Magnetic Resonance Imaging
MS	Mass spectroscopy
MSCs	Mesenchymal stem cells
MW	Molecular Weight
NMR	Nuclear Magnetic Resonance
p-TsOH	Para-Toluenesulfonic acid
PAMAM	Poly(amidoamine)
PBS	Phosphate buffered saline
pDNA	Plasmid DNA
PEG	Poly(ethylene glycol)

PEI	Poly(ethylene imine)
PEO	Poly(ethylene oxide)
PLL	Poly-L-lysine
PPO	Poly(propylene oxide)
PQ	Primaquine
***p*RBCs**	*Plasmodium* infected red blood cells
r	Relaxivity
RBCs	Red Blood Cells
RNA	Ribonucleic acid
Rhod	Rhodamine
RT	Room Temperature
SEM	Scanning Electron Microscopy
TBE	Tris, Borate, EDTA buffer
THF	Tetrahydrofurane
TMS	Tetramethylsilane
U251MG	Human Neuronal Glioblastoma (Astrocytoma) cell line

PRÓLOGO

Los polímeros forman parte de nuestra vida diaria, un elevado número de los objetos que usamos están hechos a partir ellos. El almidón, la celulosa, la seda y el ADN son algunos ejemplos de polímeros naturales. Entre los polímeros sintéticos podemos citar, entre otros, el nylon, el polietileno o la baquelita. Los dendrímeros, por sus características específicas, constituyen actualmente un área de gran interés en la investigación en el campo de la Ciencia de los Polímeros. El nombre de este tipo de moléculas, "dendrímero", refleja su arquitectura particular: en griego *dendron* significa árbol y *meros* significa parte. La principal característica de este tipo de polímeros es su arquitectura tridimensional altamente ramificada, cuyo tamaño y propiedades pueden ser controlados perfectamente durante su síntesis. Son muy numerosos los grupos de investigación que trabajan actualmente en este campo de investigación. En España, la mayor parte de las Universidades tienen equipos, en muchos casos multidisciplinares, trabajando con dendrímeros para diversas aplicaciones. En nuestro país, estos grupos se reúnen cada dos años en el "Encuentro de Dendrimeros" (EDEN), que celebró su tercera edición en Ciudad Real en 2011.

La historia de los derivados dendríticos empezó en los años 80 cuando Denkewalter[1] y colaboradores prepararon el primer dendrón. A partir del trabajo vanguardista de Vögtle,[2] Tomalia[3] y Newkome[4] en la síntesis de dendrímeros al principio de la misma década, varios grupos de investigación contribuyeron al desarrollo del método de síntesis así como de las aplicaciones específicas de los dendrímeros.

Las técnicas de síntesis de los dendrímeros permiten introducir grupos funcionales en posiciones específicas, resultando en un elevado control de su arquitectura y funcionalidad. Así, se pueden introducir funciones a su superficie,

[1] R.G. Denkewalter, J. Kolc and W.J. Lukasavage*, US Pat.* 4289872, **1981.**

[2] E. Buhleier, W. Wehner, F. Vögtle, *Synthesis,* **1978**, 155-158.

[3] D.A. Tomalia, H. Baker, J. Dewald, M. Hall, G. Kallos, S. Martin, J. Roeck, J. Ryder, P. Smith*, Polym. J. (Tokio)* **1985**, *17*, 117-132.

[4] G.R. Newkome, Z. Yao, G.R. Baker and V.K. Gupta, *J. Org. Chem*. **1985**, *50*, 2004-2006.

en sus ramas y su núcleo. Para la síntesis de esas macromoléculas, se usan fundamentalmente dos métodos, el método divergente, desarrollado en el año 1985 por Tomalia y Newkome, permite un crecimiento del dendrímero desde el interior hacia el exterior. El método convergente, presentado en el año 1990 por Hawker y Fréchet,[5] y en 1992 por Miller y Neenan,[6] permite un crecimiento desde el exterior hacia el interior de la molécula. Cada uno de esos métodos tienen sus ventajas e inconvenientes, y han permito sintetizar moléculas de peso molecular parecido al de las bio-macromoléculas. Posteriormente otros autores han introducido mejoras y modificaciones en estos métodos de síntesis.[7] La caracterización de las moléculas dendríticas es una tarea difícil y se utilizan técnicas específicas como RMN-MS, GPC, DLS.[8]

La mayoría de los dendrímeros son de naturaleza orgánica, sin embargo, actualmente algunos grupos trabajan con dendrímeros basados en Si, P, Ge, Bi y otros derivados organometálicos. De entre todos estos dendrímeros dos de ellos se sintetizan actualmente a escala de kilogramos y son comercializados por diversas empresas: el PAMAM y el PPI. El PAMAM es un dendrímero formado por poliamidoaminas y está comercializado bajo el nombre STARBURST®. El PPI es un dendrímero de polipropilenimina que se comercializa bajo el nombre de ASTRAMOL®.

La posibilidad de diseñar y sintetizar dendrímeros con características estructurales únicas hace que su estudio sea muy atractivo para los científicos que trabajan en una gran variedad de objetivos para diferentes aplicaciones. Nuestro grupo de investigación comenzó a trabajar en este campo en 1996, combinando las propiedades de estos materiales con las de los cristales líquidos, en lo que se denominan dendrímeros cristales líquidos o materiales dendromesógenos.

Los dendrímeros, como compuestos con múltiples grupos terminales funcionalizables, son plataformas idóneas para combinar las unidades promesógenas, responsables del orden y la orientación, con otras unidades funcionales que introduzcan otra propiedad física. Esta combinación de función

[5] C.J. Hawker and J.M.J. Fréchet, *J. Am. Chem. Soc.*, **1990**, *112*, 7638-7647.
[6] T.M. Miller, E.W. Kwock and T.X. Neenan, *Macromolecules,* **1992**, *25*, 3143.
[7] M.V. Walter and M. Malkoch, *Chem. Soc. Rev.,* **2012**, *41,* 4593-4609.
[8] V. Biricova and A. Laznickova, *Bioorganic Chemistry,* **2009**, *37,* 185-192.

más orientación en un mismo material, convierte a los dendrímeros cristal líquido en una herramienta apropiada para la consecución de materiales multifuncionales con una ordenación y una orientación macroscópica preferente, lo que es fundamental para gran número de aplicaciones.[9]

Los dendrímeros se han utilizado en el área de catálisis como catalizadores *per-se* o como soporte.[10] También se han utilizado sensores dendríticos para detección de moléculas orgánicas e inorgánicas.[11] Además, se usaron los dendrímeros como promotores de cristalización[12] y como soportes para síntesis en fase sólida.[13] Se han estudiado sus aplicaciones como antenas para la captación y transferencia de energía[14] y como receptores.[15]

[9] a) S. Hernández, J. Barberá, M. Marcos, P. Romero, J.L. Serrano*, Macromol. Chem. Phys*., **2012**, *213*, 270-277; b) S. Hernández, J. Barberá, M. Marcos, J.L. Serrano*, J. Pol. Sci. A. Pol. Chem.,* **2011**, *49*, 278-285; c) S. Hernández, J. Barberá, M. Marcos, J.L. Serrano*, Soft Matter,* **2011**, *7*, 2560-568; c) J. Vergara, N. Gimeno, M. Cano, J. Barberá, P. Romero, J.L. Serrano, M.B. Ros*, Chem. Mater.,* **2011**, *23*, 4931-4940; d) A. Viñuales, J.L. Serrano, R. Giménez, M. Piñol, J. Tomczyk, J. Stumpe*, J. Pol. Sci. A. Pol. Chem.,* **2011**, *49*, 3499-3512; e) S. Hernández, M. Marcos, J. Barberá, J.L. Serrano*, Angew. Chem. Int. E.,* **2010**, *49*, 1990-1994; f) J. Del Barrio, R.M. Tejedor, S. Chinelatto, C. Sánchez, M. Piñol, L. Oriol*, Chem. Mater.,* **2010**, *22*, 1714-1723; g) J. Del Barrio, L. Oriol, C. Sánchez, J.L. Serrano, A. Di Cicco, P. Keller, M.-H. Li*, J. Am. Chem. Soc.,* **2010**, *132*, 3762-3769; h) S. Hernández, R. Alcalá, J. Barberá, M. Marcos, C. Sánchez, J.L. Serrano*, Macromolecules,* **2010**, *43*, 2660–2663; i) S. Hernández, J. Barberá, M. Marcos, J.L. Serrano*, Chem. Mater.* **2010**, *22*, 4762–4768.

[10] a) D. Astruc and F. Chardac, *Chem. Rev.* **2001***, 101*, 2991-3023; b) J.N.H. Reek, S. Arevalo, R. Van Heerbeek, P.C.J. Kamer, P.W.N.M. Van Leeuwen*, Advances in Catalysis,* **2006***, 49*, 71-151; c) J.W.J. Knapen, A.W. van der Made, J.C. de Wilde, P.W.N.M. van Leeuwen, P. Wijkens, D.M. Grove, G. van Koten, *Nature,* **1994***, 372*, 659-663; d) T. Kehat, K. Goren and M. Portnoy, *New J. Chem.,* **2012***, 36*, 394-401; e) H. Brunner, *J. Organomet. Chem.,* **1995***, 500*, 39-46; f) Q.H. Fan, Y.M Chen, X.M. Chen, D.Z. Jiang, F.Xi, A.S.C. Chan*, Chem. Commun.,* **2000**, 789-790.

[11] a) V. Balzani, P. Ceroni, S. Gestermann, C. Kauffmann, M. Gorka, F. Vogtle*, Chem. Commun.,* **2000**, 853–854; b) H. Cavaye, P.E. Shaw, A.R.G. Smith, P.L. Burn, I.R. Gentle, M. James, S.C. Law, P. Meredith*, J. Phys. Chem.* **2011**, *115*, 18366-18371; c) C. Valerio, J.L. Fillaut, J. Ruiz, J. Guittard, J.C. Blais, D. Astruc*, J. Am. Chem. Soc.* **1997***, 119,* 2588-2589.

[12] a) K. Nata, Y. Tanaka, Y. Chujo, Y. Ito*, Chem. Commun.* **1999**, 1931-1932 ; b) S. Mann, *Angew. Chem. Int. Ed.* **2000***, 39,* 3393-3406.

[13] a) C. Fromont and M. Bradley, *Chem. Commun.,* **2000**, 283-284 ; b) A. Basso, B. Evans, N. Pegg and M. Bradley, *Tetrahedron Lett.,* **2000***, 41*, 3763-3767.

[14] a) C. Devadoss, P. Bharathi and J.S. Moore*, J. Am. Chem. Soc.,* **2000***, 118*, 9635-9644; b) Y.J. Mo, D.L. Jiang, M. Uyemura, T. Aida, T. Kitagawa*, J. Am. Chem. Soc.,* **2005***, 127*, 10020-10027; c) M.S. Choi, T. Aida, T. Yamakasi and I. Yamakasi, *Angew. Chem. Int. Ed.* **2001***, 113*, 3294-3298.

[15] a) J.H. Hardy, I. Ashworth, C. Brennam and D.K. Smith, *Org. Biomol. Chem*., **2007**, *5*, 900-906; b) S. Mattei, P. Seiler and F. Dietrich, *Helv. Chim. Acta,* **1995**, *78*, 1904-1912; c) D.K. Smith, A. Zingg and F. Dietrich, *Helv. Chem. Acta* **1999***, 82*, 1225-1241.

Por otro lado, en la última década, se han descrito también numerosas aplicaciones de los dendrímeros en el campo de la Biomedicina.[16] Así los dendrímeros se han usado como agentes antivirales[17] y antibacterianos,[18] materiales de contraste,[19] vehículos de ADN para terapia génica,[20] en ingeniería de tejidos,[21] y como transportadores de fármacos.[22]

La aplicación de los dendrimeros en las áreas de medicina y química farmacéutica se esta convirtiendo rápidamente en un tema de investigación de gran interés. Los dendrímeros son excelentes candidatos para el desarrollo de transportadores de fármacos por su capacidad de encapsular moléculas pequeñas y por la posibilidad de formar complejos mediante uniones covalentes o supramoleculares. La primera tesis de nuestro grupo que incorporó aplicaciones biomédicas fue la de Silvia Hernández en 2012 con la formación de nano-objetos formados a partir de derivados iónicos de PAMAM capaces de encapsular moléculas hidrófilas e hidrófobas.[23]

Esta tesis doctoral pretende seguir profundizando en este tema, y está orientada hacia la búsqueda el estudio de derivados dendríticos con aplicaciones potenciales en biomedicina en los campos de la terapia génica, resonancia magnética de imagen y transporte de fármacos. Este trabajo es multidisciplinar y se encuentra a medio camino entre la química, por la síntesis, la caracterización de moléculas orgánicas, y la bioquímica, por el estudio de las aplicaciones de esas moléculas utilizando los métodos bioquímicos o biológicos a nuestra disposición.

---

[16] W.-D. Jang, K.M.K. Selim, C.-H. Lee, I.K. Kang*, Prog. in Polym. Sci.,* **2009,** *34*, 1-23.

[17] J.L. Jiménez, M. Pion and F.J. de la Mata, R. Gómez, E. Muñoz, M. Leal, A. Muñoz-Fernández*, New J. Chem.* **2012***, 36,* 299-309.

[18] A. Castonguay, E. Ladd, T.G.M. van de Ven and A. Kakkar, *New J. Chem.* **2012***, 36*, 199-204.

[19] C. Ghobril, G. Lamanna, M. Kueny-Stotz, A. Garofalo, C. Billotey, D. Felder-Flesch*, New J. Chem.,* **2012***, 36*, 310-323.

[20] X. Liu, P. Rocchi and L. Peng, *New J. Chem***., 2012***, 36*, 256-263.

[21] N. Joshi and M. Grinstaff, *Curr. Top Med. Chem.,* **2008***, 8*, 1225-1236.

[22] a) S.H. Medina and M.E.H. El Sayed, *Chem. Rev.,* **2009***, 109*, 3141–3157; b) M. Liu and J.M.J. Fréchet, *PSTT,* **1999***, 2*, 393-401.

[23] S. Hernández, *Nuevos materiales funcionales basados en dendrímeros cristales líquidos iónicos*, **2012**, Universidad de Zaragoza.

GENERAL INTRODUCTION

Dendrimers

Definition

A dendrimer is a three-dimensional macromolecule that is part of the polymer family. The term dendrimer graphically describe its architecture: the word is derived from the Greek words *dendron,* meaning "tree", and *meros* meaning "part".

Dendrimers differ from polymers because of their highly controlled structure: they have a single molecular weight, a large number of controllable peripheral functionalities and a tendency to adopt a globular shape once a certain size is reached.

Dendrimers are members of a versatile, fourth new class of polymer architecture: the dendritic polymers family composed by dendritic-linear hybrids (a), hyperbranched polymers (b), dendrons (c) and dendrimers (d)[24,25] (Figure 1). The order, from (a) to (d), reflects the relative degree of structural control presents in each of these dendritic architectures.[24,26] This class of polymer is distinct because of the repertoire of new properties they manifest.[27,28]

[24] D. A. Tomalia, J. M. J. Fréchet, *J. Polym. Sci. Part. A Polym. Chem.,* **2002**, *40*, 2719–2728.
[25] D. A. Tomalia, *Prog. Polym. Sci.,* **2005**, *30*, 294–324.
[26] J. M. J. Fréchet, D. A. Tomalia, Dendrimers and other dendritic polymers. Chichester: Wiley; **2001**.
[27] D. A. Tomalia, A. M. Naylor and W. A. Goddard, *Angew. Chem. Int. Ed.,* **1990**, *29*, 138–175.
[28] M. Fischer, F. Vögtle, *Angew. Chem. Int. Ed.,* **1999**, *38*, 884–905.

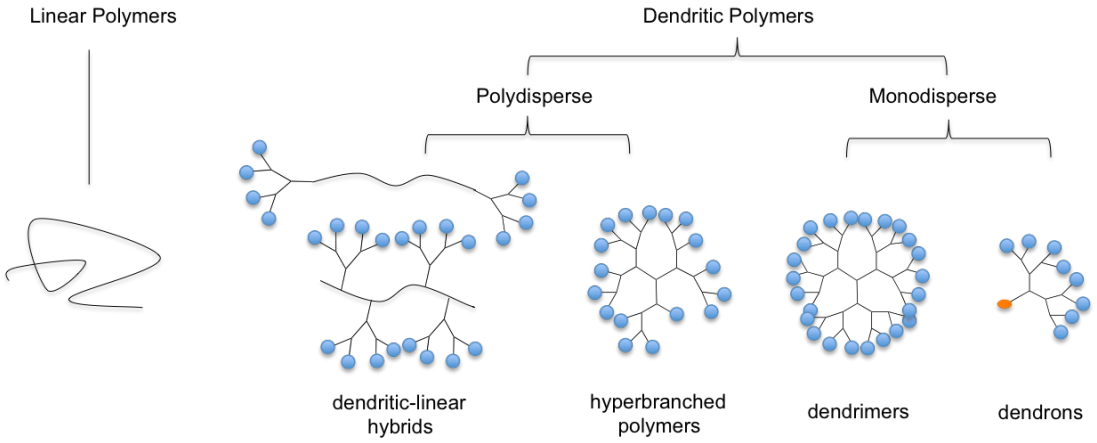

Figure 1: Linear and dendritic polymers.

The dendrimer structure can be divided into three main components: the core, the interior, and the shell. The core is an important part of the dendrimer as it affects the shape of the dendrimer, its directionality and multiplicity, and can be functionalized (for instance for imaging).[29] The interior affects the host-guest properties, and the solubility. Dendritic macromolecules present a generational growth (G); the first generation is generally called G1, the second one G2, etc. Finally, the surface can be modified with a large number of functional peripheral groups and the properties of the dendrimer can be modulated.

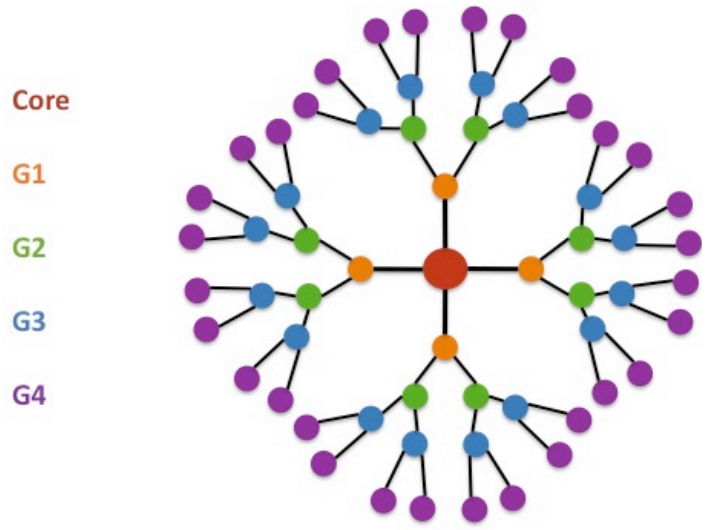

Figure 2: Dendrimer structure.

[29] M. Takahashi, *Tetrahedron Lett.*, **2000**, *41*, 8485.

The first dendritic wedge, reported by Denkewalter,[30] used lysine residues as branching units. Since the pioneering work of Vögtle,[31] Tomalia[32] and Newkome[33] on dendrimer synthesis in the early 1980s, several research groups have contributed to both the development of synthetic methodology and specific applications of dendrimers. One of the most appealing features of dendrimers is the existence of a high number of functional groups at the periphery, by which the properties of these macromolecules can be modulated. As a result, a large number of dendrimers with a broad variety of architectures have been developed. Some of the commonly referenced dendrimer structures are Tomalia's polyamidoamine (PAMAM),[3] Denkewalter's poly(L-lysine) (PLL),[7] Newkome's polyamide,[4] Grinstaff's polyester (PGLSA-OH),[34] Vögtle's polypropylenimine (PPI),[31] and Hult's poly(2,2-bis(hydroxymethyl)propionic acid (*bis*-MPA)[35] structures (Figure 3).

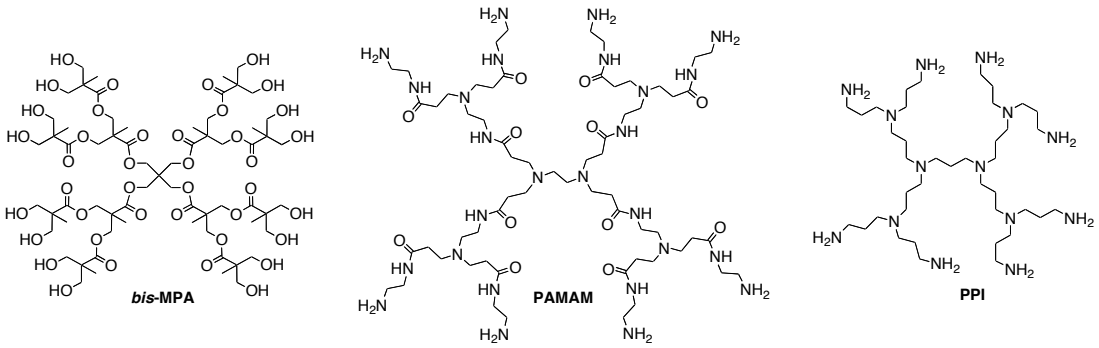

Figure 3: Chemical structures of some commonly used dendrimers.

[30] R.G. Denkewalter, J.F. Kole, W.J. Lukasavage, *US Pat.* 4289872, **1981.**

[31] E. Buhleier, W. Wehner, F. Vögtle, *Synthesis,* **1978**, 155-158.

[32] D.A. Tomalia, H. Baker, J. Dewald, M. Hall, G. Kallos, S. Martin, J. Roeck., J. Ryder., P. Smith*, Polym. J. (Tokio),* **1985**, *17*, 117-132.

[33] G. R. Newkome, Z. Yao, G.R. Baker, V.K. Gupta, *J. Org. Chem*., **1985**, *50*, 2004-2006.

[34] M. A. Carnahan, M. W. Grinstaff, *Macromolecules,* **2006**, *39*, 609-616.

[35] H. Ihre, A. Hult, E. Söderlind, *J. Am. Chem. Soc.,* **1996**, *118*, 6388-6395.

Approaches in dendrimer synthesis

Two distinct strategies exist for the preparation of dendrimers: the divergent approach developed by Tomalia[3] and Newkome[4], and the convergent approach pioneered by Hawker and Fréchet[36].

In the divergent synthesis (Figure 4), dendrimer growth starts from a polyfunctional core and proceeds radially outward with the stepwise addition of successive layers of building blocks. Another accelerated synthesis method, called the orthogonal coupling strategy, uses two different monomers to eliminate protection or activation steps.

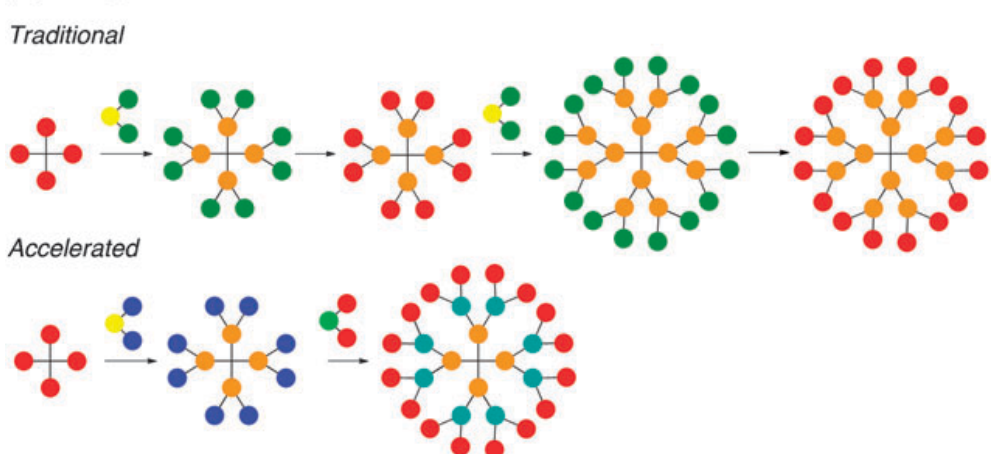

Figure 4: Divergent synthesis. Adapted from M.A. Mintzer et Al.[37]

In convergent synthesis (Figure 5), the dendrimer growth begins at the chain ends and proceeds inwards through successive additions of the growing dendritic molecules to a single monomer unit. This synthetic approach is more demanding but produces dendrimers of very high purity and allows the production of dendrons, which are useful either by themselves or as building blocks for asymmetric dendrimers. The "double-stage" convergent growth approach, in which a dendritic "hypercore" with a larger number of reactive surface functional groups is prepared first, followed by attachment of convergent dendritic "wedges".

[36] C. J. Hawker, J. M. J. Fréchet, *J. Am, Chem, Soc.,* **1990**, *112*, 7638-7647.
[37] M. A. Mintzer and M. W. Grinstaff, *Chem. Soc. Rev.,* **2011***, 40,* 174-190

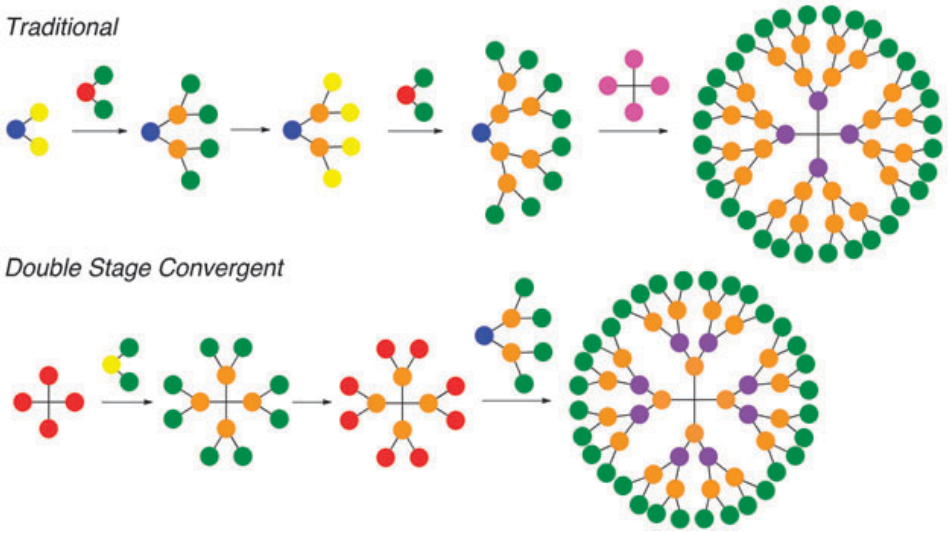

Figure 5: Convergent synthesis. Adapted from M.A. Mintzer et Al.[37]

Drug delivery

Drug delivery is the process of administrating a pharmaceutical compound in order to achieve a therapeutic effect. It focuses on the development of technologies to deliver biomolecules to the site of the disease in order to maximize therapeutic effect and minimize side effects.

When free drugs are administrated, they are confronted to various metabolic processes, non-specific distribution and renal clearance. All these processes lead to a reduction of efficiency of the drug and to the augmentation of non-desired side effects, which can easily be observed with chemotherapeutic agents for example.

These problems can be partially limited by designing carriers that perform multiple tasks like encapsulations, controlled release, minimization of immune-clearance, penetration of biological barriers and targeting the specific site of the disease.[38]

[38] a) O. Farokzhad and R. Langer, *Adv. Drug Delivery Rev.,* **2006**, *58*, 1456–1459 ; b) N. Doshi and S. Mitragotri, *Adv. Funct. Mater.,* **2009**, *19*, 3843-3854.

Applications of dendrimers for drug delivery

Dendritic polymers can differ significantly from linear polymers in their properties. The stepwise growth of dendrimers affords nearly monodisperse products, whereas polymerization involves chain growth procedures that afford statistical mixture of products. By controlling details of the core, interior and periphery, it is possible to design macromolecules with nearly perfectly defined structures and compositions. For biological applications, monodispersity allows the investigation of structure-activity relationships. Dendrimers are also multivalent molecules, with the number of surface groups increasing with the generation.

Dendrimers have a number of beneficial attributes for biomedical applications, including the following:

- Biodistribution and pharmacokinetic properties that can be tuned by controlling dendrimer size and conformation (generation number, dendrimer-polymer hybrids).
- High structural and chemical homogeneity: dendrimer biological properties can be attributable to a single molecular entity and not to a statistical distribution.
- Ability to be functionalized with multiple molecules of drugs, chromophores or ligands either at their peripheries and/or their interiors.
- High ligand density, increasing with the generation of the dendrimer.
- Controlled degradation, which can be achieved by judicious choice of dendrimer chemistry.

Dendrimer conjugates with therapeutic and diagnostic agents

The targeted delivery of diagnostic and therapeutic agents is one of the great challenges of today's medicine. Since their development in the mid-80s, dendrimers have become prominent synthetic macromolecules in the field of biomedical science. The dendrimers properties previously enounced make them excellent candidates for evaluation as drug carriers. A variety of applications

have been explored such as gene transfection, medical imaging, tissue engineering, and drug delivery.

Gene therapy is being of great interest because of its potential for treating numerous diseases. The problematic to overcome is the fast degradation of the DNA or *si*RNA by serum nucleases. Vectors that are able to compact and protect the nucleic acids from these attacks are of huge importance. The main barriers for gene delivery are related to toxicity, cell targeting and membrane permeation, complex stability under physiological conditions, and release of the gene from the complex.[39] Dendriplexes is the term use to describe the complex formed from the electrostatic interactions between cationic dendrimers and anionic DNA/RNA.

Magnetic resonance imaging (MRI) has become a widely employed technique for disease diagnosis. In order to enhance the sensibility MRI, contrast agents, typically gadolinium-based (*i.e.* DOTA, DPTA), are used. In this domain, the interest for dendrimers has come from the ability to attach multiple contrast ligands to a single scaffold and the possibility to combine the imaging with drug delivery and/or targeting to specific tissues.

Dendrimers can be used as potential drug delivery agents in at least three ways (Figure 6): drug molecules can be physically **encapsulated** inside the dendritic structure; drug molecules can be covalently or non-covalently bound onto the surface or other functionalities to afford **dendrimer-drug conjugates**; and dendritic molecules can form **supramolecular assemblies** like vesicles able to encapsulate small molecules.

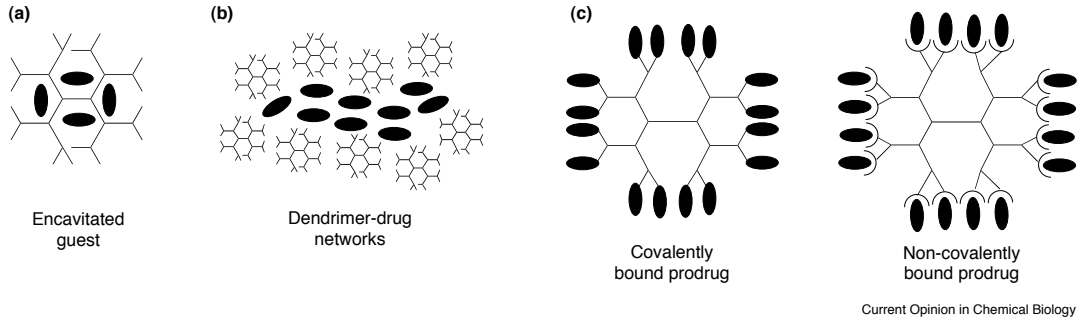

Figure 6: Drug-dendrimer possible interactions. Adapted from M.J. Cloninger et Al.[40]

[39] M. A. Mintzer and M. W. Grinstaff, *Chem. Soc. Rev.*, **2011**, *40*, 173-190.
[40] M.J. Cloninger, *Curr. Opin. in Chem. Biol.*, ***2002***, *6*, 742-748.

Furthermore, dendrimers can be used as **drugs** themselves, for example as antimicrobial[41] and antiviral agents.[42] Dendrimers are moreover being studied in the area of tissue engineering as crosslinked collagen **scaffolds**,[43] and as primary tissue scaffold components for ophthalmic [44] and orthopedic [45] applications.

Dendritic derivatives have the potential to overcome the problems of most chemotherapeutic drugs by **encapsulating** them. In this way, their water solubility can be enhanced, their bloodstream elimination slowered, and their specificity improved. Dendrimers can function as unimolecular micelles capable of encapsulating and solubilizing drug into the empty space within the dendrimer's interior. The drug can remain in circulation for a longer period if the size of the complex drug/dendrimer is bigger than 5 nm, so its kidney filtration can be reduced. Finally, due to the difference of vasculature in the tumor, complexes with a size superior to 250 nm will be passively targeted to the cancerous cells (Enhanced Permeation and Retention effect), which is very interesting for chemotherapy.

However, the encapsulation of drugs inside dendrimers presents some limitations as the poor loading capacity and the limitation in size of the drug. To overcome these problems, significant research has been done on **covalent attachment**. Various linkers have been studied to attach drugs to dendrimers,

---

[41] a) C.Z. Chen, N.C. Beck-Tan, P. Dhurjati, T.K. van Dyk, R.A. LaRossa, S.L. Cooper, *Biomacromol*., **2000**, *1*, 473-480 ; b) M.K. Calabretta, A. Kumar, A.M. McDermott, C. Cai, *Biomacromol.,* **2007**, *8*, 1807-1811 ; c) S. R. Meyers, F.S. Juhn, A.P. Griset, N.R. Luman, M.K. Grinstaff, *J. Am. Chem. Soc.,* **2008**, *130*, 14444-14445.

[42] a) A. Pérez-Anes, G. Spatato, Y. Coppel, C. Moog, M. Blanzat, C.-O. Turrin, A.-M. Caminade, I. Rico-Lattes, J.-P. Majoral, *Org. Biomol. Chem*., **2009**, *7*, 3491-4398 ; b) S.K. Wang, P.H. Liang, R.D. Astronomo, T.-L. Hsu, S.-L. Hsieh, D.R. Burton, C.-H. Wong, *PNAS U. S. A.,* **2008**, *105*, 3690-3695.

[43] a) J.C.Y. Chan, K. Burugapalli, H. Naik, J.L. Kelly, A. Pandit, *Biomacromolecules,* **2008**, *9*, 528-536 ; b) S. Zhong and L.Y.L Yung, *J. Biomed. Mater. Res., Part A,* **2009**, *91*, 114-122 ; c) X. Duan and H. Sheardon, *Biomed. Mater. Res., Part A,* **2005**, *75*, 510-518 ; d) X. Duan, C. McLaughlin, M. Griffith, H. Sheardon, *Biomaterials,* **2007**, *28*, 78-88.

[44] a) M.A. Carnahan, C. Middleton, J. Kim, T. Kim, M.W. Grinstaff, *J. Am. Chem. Soc.,* **2002**, *124*, 5291-5293 ; b) J.P. Berdhal, C.S. Johnson, A.D. Proia, M.W. Grinstaff, T. Kim, *AMA Arch. Ophthalmol.,* **2009**, *127*, 442-447 ; c) M. Wathier, P.J. Jung, M.A. Carnahan, T. Kim, M.W. Grinstadd, *J. Am. Chem. Soc*., **2004**, *126*, 12744-12745 ; d) M. Wathier, S.M. Johnson, T. Kim, M.W. Grinstaff, *Bioconjugate Chem.,* **2006**, *17*, 873-876.

[45] a) S. Söntjens, D.L. Nettles, M.A. Carnahan, L.A. Setton, M.W. Grinstaff, *Biomacromolecules,* **2006**, *7*, 310-316 ; b) L. Degoricija, P.N. Bansal, S.H.M. Söntjens, N.S. Joshi, M. Takahashi, B. Snyder, M.W. Grinstaff, *Biomacromolecules,* **2008**, 9, 2863-2872.

and release them. Ester bond is commonly used because it can be cleaved by a variety of esterase enzymes within the cell.[46] Acid labile hydrazone linkage is also widely utilized because the pH near tumor cells is more acid.[47]

Dendrimers for targeted drug delivery

In addition to linking groups, **targeting agents** can tremendously improve the delivery to specific tissue and reduce the side effects of treatment. For that purpose, the most widely employed targeting molecules are carbohydrates, folic acid, antibodies and peptides.[48]

Carbohydrate receptors are overexpressed on a great range of cancer cells. A large variety of biocompatible glycosylated dendrimers have been investigated and used for gene delivery,[49] imaging probe,[50] and drug delivery applications.[51] For example, a PEG-PAMAM dendron was modified by galactose for targeted gene delivery to cancer cells that overexpressed an asialoglycoprotein receptor.[52]

Folate receptor (FR), a 38 kDa glycosylphosphotidylinositol-anchored protein, exists in three major forms namely FR-α, FR-β and FR-γ. The FR-α form is overexpressed in many types of tumour cells including ovarian, endometrial, breast, and renal cell carcinomas.[53] The covalent attachment of folic acid to a molecule (i.e. proteins, liposome, dendrimer, etc) leads to a conjugate that can be endocytosed into folate receptor-bearing cells (Figure 7). Folic acid has been conjugated to polymers and dendrimers wearing with drugs or imaging moieties. In 1999, Fréchet *et al* conjugated folate residues to the chains ends of a hydrazide terminated polyether dendrimer to be potentially used as drug carrier. PEG-

[46] X. Bi, X. Shi, R. Shukla, I. Majoros, J.R. Baker Jr*, J. Comput. Theor. Nanosci.*, **2007**, *4*, 1179-1187.

[47] a) O. L. Padilla de Jesús, H.R. Ihre, L. Gagne, J.M.J. Fréchet, F.C. Szoka*, Bioconjugate Chem*., **2002**, *13*, 453−461; b) C.C. Lee, E.R. Gillies, M.E. Fox, S.J. Guillaudeu, J.M.J. Fréchet, F.C. Szoka*, PNAS U. S. A.,* **2006**, *103*, 16649-16654.

[48] Y. Cheng, L. Zhao, Y. Li, T. Xu*, Chem. Soc. Rev.,* **2011**, *40*, 2673-2703.

[49] a) H. Arima, Y. Chihara, M. Arizono, S. Yamashita, K. Wada, F. Hirayama, K. Uekama*, J. Control. Release,* **2006**, *116*, 64-74; b) K. Wada, H. Arima, T. Tsutsumi, Y. Chihara, K. Hattori, F. Hirayama, K. Uekama*, J. Control. Release,* **2005**, *104*, 397-413; c) K. Wada, H. Arima, T. Tsutsumi, F. Hirayama, K. Uekama*, Biol. Pharm. Bull.,* **2005**, *28*, 500-505.

[50] P. M. Nguyen, and P. Hammond*, Langmuir,* **2006**, *22*, 7825-7832.

[51] P. Agrawal, U. Gupta, N.K. Jain*, Biomaterials*, **2007**, *28*, 3349-3359.

[52] K. C. Wood, S.R. Little, R. Ranger, P.T. Hammond*, Angew. Chem., Int. Ed.,* **2005**, *44*, 6704-6708.

[53] B. S. Bloom, *Am. J. Med.,* **1998**, *84*, 20-24.

functionalized polyester boltorn® H40 was later conjugated with folic acid for tumour-targeted drug delivery.[54]

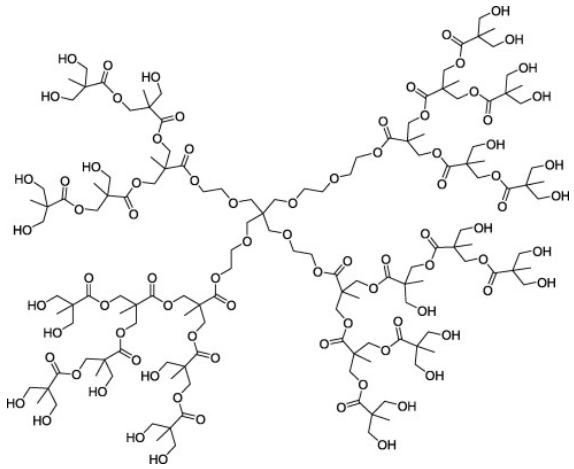

Figure 7: Structure of boltorn® hyperbranched polymer.

In 2011, Wang and co-workers achieved the targeted delivery of doxorubicin encapsulating it into a folic acid-dendrimer conjugate. The complexes were able to specifically target the drug to cells with high level of FR.[55]

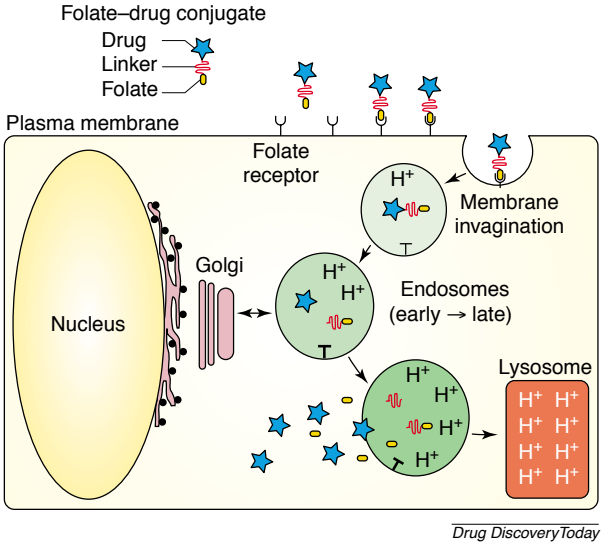

Figure 8 : Endocytosis of folate-drug conjugates. Adapted from C.P. Leamon et Al.[56]

[54] M. Pabaharan, J.J. Grailer, S. Pilla, D.A. Steeber, S. Gong, *Biomaterials,* **2009**, *30*, 3009-3019.
[55] Y. Wang, X. Cao, R. Guo, M. Shen, M. Zhang, M. Zhu, X. Shi, *Polym. Chem*., **2011**, *2*, 1754-1760.
[56] C.P. Leamon, P.S. Low, *Drug Discov. Today*, **2001**, *6*, 44-51.

Tumour-targeted drug delivery using monoclonal antibodies (mAbs) with specificity toward tumour markers has gained considerable attention in recent years. Attaching them to a drug reservoir such as nanoparticles, liposomes or polymers can significantly increase the drug loading capacity of antibodies. The advantage of such approach for cell-specific drug delivery is that higher payloads of the drug can be delivered without compromising the specificity and bonding efficacy of the antibody. All the work published about antibody-dendrimer conjugates for drug delivery has been carried out with PAMAM dendrimers. R. Shukla and co-workers have worked on the successful delivery of PAMAM dendrimers targeted by antibodies. *In vitro* and *in vivo* studies showed that anti-HER2 antibody targeted acetylated PAMAM dendrimer to HER2-overexpressing cell tumours.[57] Other antibodies including J591 and 60bca targeted dendrimers to prostate specific membrane antigen and CD14-expressing cells respectively.[58] In 2008, G5 PAMAM dendrimer was attached to an anti-HER2 antibody providing a general approach for the synthesis of Herceptin-targeted dendrimer-drug conjugates.[59] Some of the antibody-PAMAM complexes formed were prepared to be used as imaging probes for MRI.[60]

[57] R. Shukla, T.P. Thomas, J.L. Peters, A.M. Desai, J. Kukowska-Latallo, A.K. Patri, A. Kotlyar. J.R. Baker Jr*, Bioconjugate Chem.,* **2006**, *17*, 1109-1115.

[58] a) R. Shukla, T.P. Thomas, J. Peters, A. Kotlyar A. Myc, J.R. Baker Jr*, Chem. Comm.,* **2005**, 5739-5741 ; b) E. Hill, R. Shukla, S.S. Park, J.R. Baker Jr*, Bioconjugate Chem.,* **2007**, *18*, 1756-1762.

[59] R. Shukla, T.P. Thomas, A.M. Desai, A. Kotlyar, S.J. Park, J.R. Baker*, Nanotechnology,* **2008**, *19*, 295102-295118.

[60] a) K. Nwe, D.E. Gilenic, G.L. Ray, Y.S. Kim, M.W. Brechbiel*, Mol Pharm.,* **2012**, *9*, 374-381; b) H. Kobayashi, N. Sato, T. Saga, Y. Nakamoto, T. Ishimori, S. Toyama, K. Togashi, J. Konishi, M.W. Brechbiel*, Eur. J. Nucl. Med.,* **2000**, *27*, 1334-1339 ; c) C. Wu, M.W. Brechbiel, R.W. Kozak, O.A. Gansow*, Bioorg. Med. Chem. Lett.,* **1994**, *4*, 449-454.

Dendrimers based on *bis*-MPA

In the search for advantageous building blocks for drug delivery, we have focused our attention in polyester dendrimers based on 2,2-*bis*(hydroxymethyl)propionic acid (*bis*-MPA) monomers.

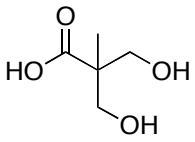

Figure 9: *bis*-MPA monomer molecule.

Dendrimers based on *bis*-MPA were first described in 1996 by Hult *et al.*[61] Dendrimers up to fourth generation were obtained by introducing the acetonide-protecting group and *N,N'*-dicyclohexylcarbodiimide (DCC) as the deshydratation agent.[62] Dendritic structures based on *bis*-MPA monomers are now commonly used and the core, the peripheral groups, and the synthetic pathway have been diverse.

A large range of cores has been used as starting point for the synthesis: aromatic,[63] aliphatic,[64] or porphirine ones.[65] The synthesis can be carried out either by the divergent or the convergent route. The choice of one or another depends of the steric impediment and the stability of the terminal groups.

The generation growth of the dendrimers can be achieved by Steglish esterification using DCC/DPTS as well as by anhydride esterification. In both cases the protection/deprotection of the hydroxyl groups can be obtained in several ways: benzylidene and acetonide being the protective groups. The use of

[61] A. Hult and E. Soderling, *J. Am. Chem. Soc.* **1996,** *118,* 6388-6395.
[62] H. Ihre, A. Hult, J.M.J. Fréchet, I. Gitsov*, Macromolecules,* **1998**, *31*, 4061-4068.
[63] a) J. K. Twibanire*,* H. Al-Mughaid, and T. B. Grindley*, Tetrahedron,* **2010**, *66*, 9602-9609 ; b) H. Ihre, A. Hult, J.M.J. Fréchet, and I. Gitsov *Macromolecules,* **1998**, *31*, 4061-468.
[64] a) D. G. Van Der Poll, H.M. Kieler-Ferguson, W.C. Floyd, S.J. Guillaudeu, K. Jerger, P.C. Szoka, J.M.J. Fréchet*, Bioconjugate Chem*. **2010**, *21*, 764–773 ; b) M. Malkoch, Hans Claesson, Peter Löwenhielm, E. Malmström, A. Hult*, J. Polym. Sci. A Polym. Chem.,* **2004**, *42*, 1758-1767.
[65] R. Vestberg, A.M. Nyström, M. Lindgren, E. Malmström, A. Hult*, Chem. Mater.,* **2004**, *16*, 2794-2804.

benzilidene-protected 2,2-*bis*(hydroxymethyl)propionic anhydride [66] offers various advantages such as an easy workup and very high yield. Moreover, the removal of protecting group obtained by hydrogenolysis between each generation is quantitative. The DCC/DPTS method requires column chromatography purification in every step, and the removal of the acetonide protective group is obtained by stirring in methanol with acidic DOWEX-50-X2 resin. This method is used when some functional groups present on the molecule can be sensitive to reduction by hydrogenation. Both methods are schematically resumed in Figure 10.

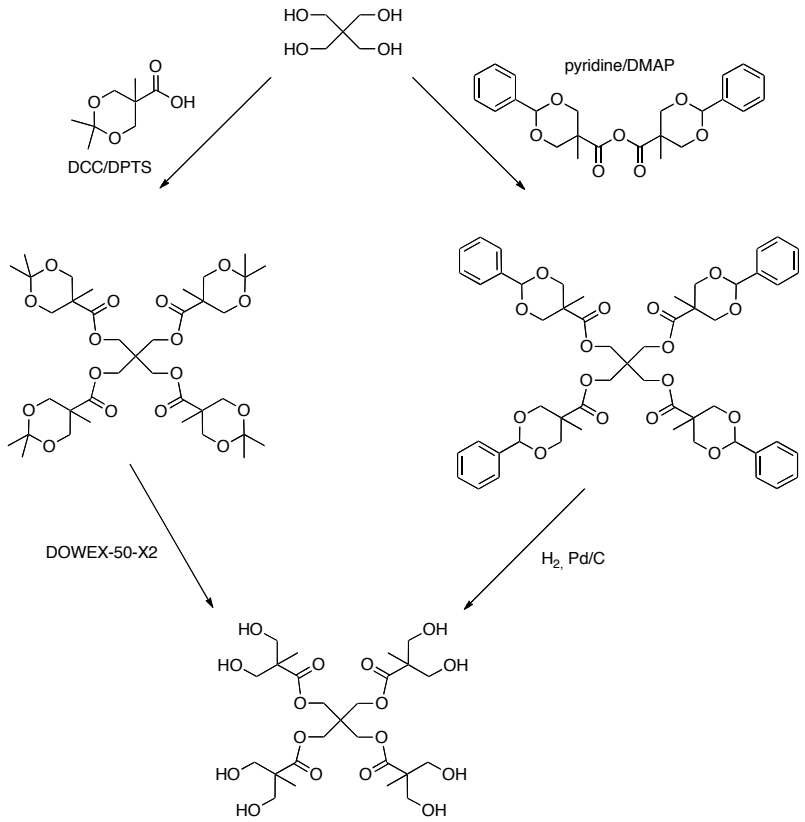

Figure 10: Synthesis of *bis*-MPA dendrimers.

Szoka and Fréchet collaboratively reported their pioneering work on the synthesis and biological evaluation of biodegradable *bis*-MPA dendrimers and

[66] a) H. Ihre, O.L. Padilla de Jesús and J.M.J. Fréchet*, J. Am. Chem. Soc.,* **2001**, *123*, 5908-5917 ; b) M. Malkoch, E. Malmstrom and A. Hult*, Macromolecules,* **2002**, *35*, 8307-8314

their PEO-hybrids.[67] The advantages of *bis*-MPA derivatives such as their biocompatibility *in vitro*[68] and *in vivo*, their solubility in biological environment, their ability to be degraded by a simple hydrolytic process and their ease of functionalization make them good candidates for drug delivery.

In 2002, Fréchet and co-workers[44c], prepared a dendrimer with a PEG chain as central core in order to improve biodistribution behaviour and decrease cytoxicity of the dendrimer. They observed that the PEG-core dendrimer showed much prolonged plasma circulation time compared to triphenol-cored polyester dendrimer. Moreover, due to the decreased spatial hindrance between adjacent surface functionalities, the dendrimer was easier to modify on its surface and doxorubicin was attached to the dendrimer via pH-sensitive spacer.

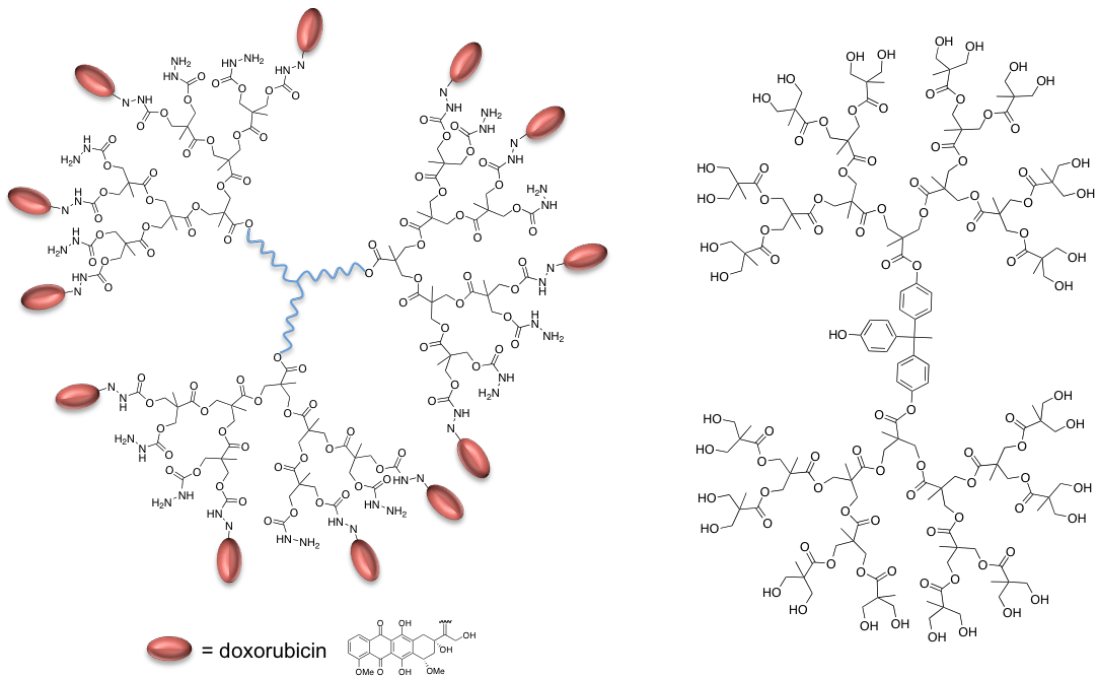

Figure 11: PEG-core *bis*-MPA dendrimer (left) and triphenol-core *bis*-MPA dendrimer (right).

[67] a) E.R. Gilliers, E. Dy, J.M.J. Fréchet and F.C. Szoka, *Mol. Pharm*., **2005**, *2*, 129-138 ; b) A.P. Goodwin, S.S. Lam and J.M.J. Fréchet, *J. Am. Chem. Soc.* **2007**, *129*, 6994-6995 ; c) L.P De Jesus, H.R. Ihre, L. Gagne, J.M.J. Fréchet, F.C. Szoka, *Bioconjugate Chem.* **2002**, *13*, 453-461 ; d) H. Ihre, O.L.P De Jesus, J.M.J. Fréchet, *J. Am. Chem. Soc.* **2001**, *123*, 5908-5917 ; e) E.R. Gillies and J.M.J. Fréchet, *J. Am. Chem. Soc.* **2002**, *124*, 14137-14146 ; f) H.R. Ihre, O.L.P De Jesus, F.C. Szoka and J.M.J. Fréchet, *Bioconj. Chem.*, **2002**, *13*, 443-452.

[68] N. Feliu, M.V. Walter, M.I. Montanez, A. Kunzmann, A. Hult, A. Nyström, M. Malkoch, B. Fadeel, *Biomaterials,* **2012,** *33*, 1970-1981.

Fréchet *et al.*, also designed a biocompatible "bow-tie" *bis*-MPA dendrimer to deliver anticancer drug doxorubicin to tumours for completely eradicate colon carcinoma in mice.[69] Later, they proposed a convenient approach for the synthesis of heterobifunctional polyester dendrimers derived from cyclic carbonate periphery to construct multifunctional dendrimers.[70]

Another product prepared by Szoka and Fréchet was a hybrid polyester-polyamide dendrimer wearing PEG chains and doxorubicin at its surface.[71] Nearly 90% of the surface functionalities of the dendrimer were conjugated with doxorubicin. The dendrimer was biodegradable and remained nontoxic for C26 cells at 5 mg/mL. The PEG-terminated polyester was modified with cypate, a near-infrared fluorescence probe, to image acidic tissues and the tumors in vivo.[72]

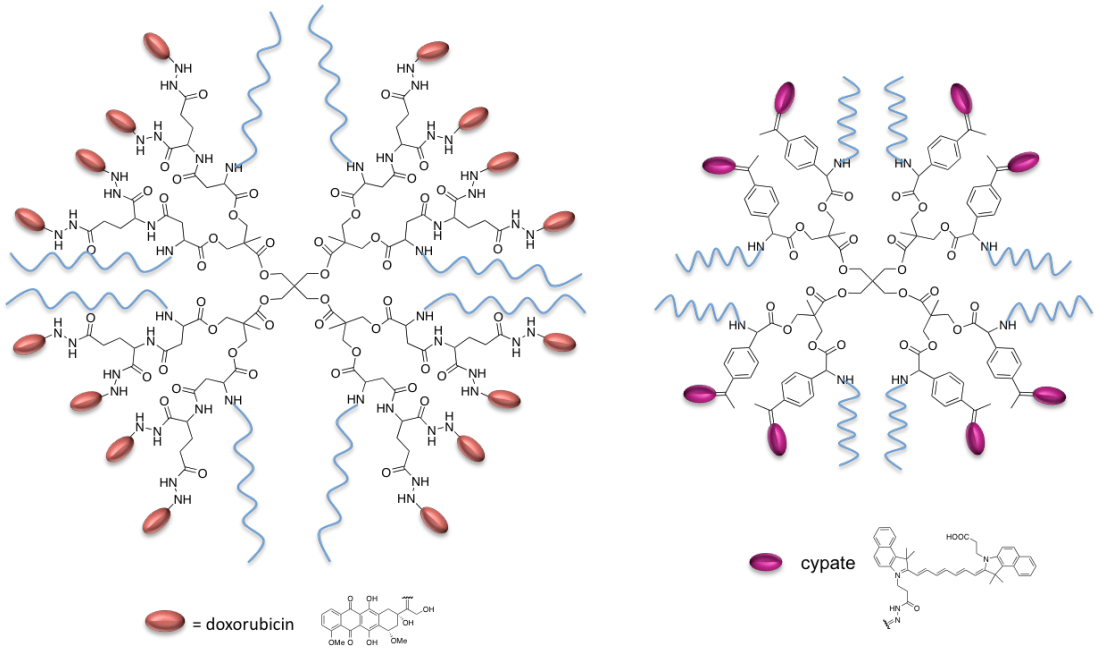

Figure 12: Hybrid polyester-polyamide dendrimer (left), PEG-terminated polyester modified with cypate (right).

[69] a) C.C. Lee, J.A. MacKay, J.M.J Fréchet and F.C. Szoka, *PNAS U. S. A.*, **2006**, *103*, 16649-16654; b) E.R. Gillies and J. M. J. Frechet, *J. Am. Chem. Soc.*, **2002**, *124*, 14137; c) C.C. Lee, J.A. MacKay, J.M.J. Fréchet and F.C. Szoka, *Nat. Biotechnol.*, **2005**, *23*, 1517-1526

[70] A.P. Goodwin, S.S. Lam and J.M.J Fréchet, *J. Am. Chem. Soc.*, **2007**, 129, 6994-6995.

[71] D.G. van der Poll, H.M. Kieler-Ferguson, W.C. Floyd, *Bioconjugate Chem.*, **2010**, *21*, 764-773.

[72] a) A. Almutairi, S.J. Guillaudeu, M.Y. Berezin, S. Achilefu, J.M.J. Fréchet, *J. Am. Chem. Soc.*, **2008**, *130*, 444-445 ; A. Almutairi, W.J. Akers, M.Y. Berezin, S. Achilefu, J.M.J. Fréchet, *Mol. Pharmaceutics*, **2008**, *5*, 1103-1110.

In 2010, J. del Barrio *et al.*, showed that PEG-poly(propionic acid) dendron with azobenzene surface assembled into core-shell structured nano-fibers, tubular micelles, and polymersomes in aqueous solution. The aggregated structures were photosensitive, indicating their use as intelligent vehicles with light-responsive properties for cancer therapy.[73]

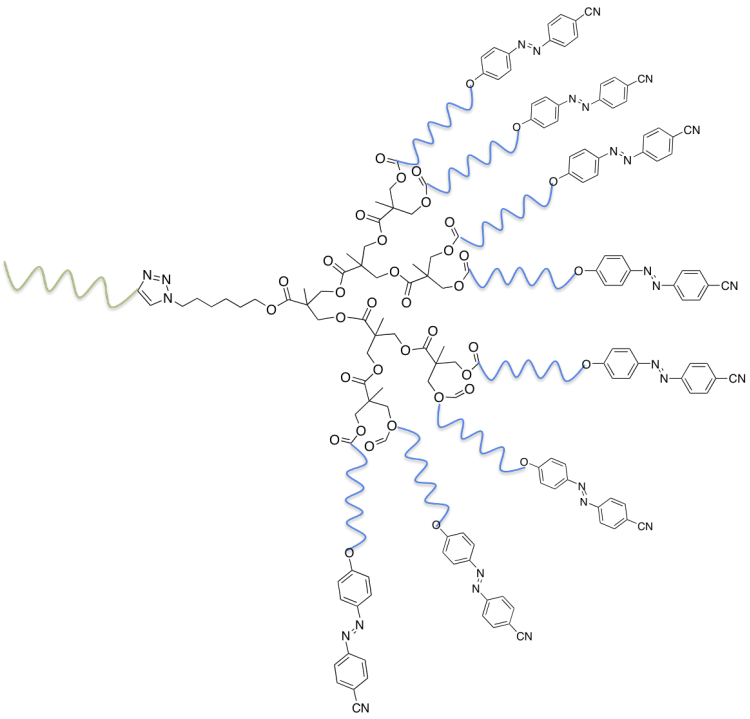

Figure 13: PEG-poly(propionic acid) dendron with azobenzene surface.

M. Prabaharan *et al.* conjugated PEG-functionalized polyester boltron® H40 with folic acid for tumour-targeted drug delivery.[74] The polymer exhibited no cytotoxicity against 4T1 cells, excellent biodegradable behaviour and high cellular uptake level mediated endocytosis.

As shown by these examples, *bis*-MPA dendritic derivatives are very interesting for the design of new drug delivery agents. They present excellent properties that deserve to be made the most of them.

[73] J. del Barrio, L. Oriol, C. Sánchez, J.L. Serrano, A. Di Cicco, P. Keller, M.-H. Li, *J. Am. Chem. Soc.,* **2010**, *132*, 3762-3769.
[74] M. Prabaharan, J.J. Grailer, S. Pilla, D.A. Steeber, S. Gong, *Biomaterials*, **2009**, *30*, 3009-3019.

CHAPTER 1:

DESIGN, SYNTHESIS AND EVALUATION OF BIS-MPA AND PAMAM DENDRITIC DERIVATIVES AS VECTORS FOR GENE DELIVERY

Introduction

Definitions

Gene Therapy may be defined as the treatment of human disease by the transfer of genetic material into specific cells of the patient in order to correct the overexpression or under-expression of a defective gene.[75] The concept of gene therapy was introduced in the late 1970's after the development of recombinant DNA technology. At this time, many approaches for gene therapy are being evaluated in animal models of human diseases and in clinical trials. While there have been no completely successful applications of gene therapy for human disease, considerable progress has been made. Compared to gene therapy, cell therapy is an older discipline, dating back to the first blood transfusions in the 1940's, and proceeding through organ and bone marrow transplantation in the 1960's and 70's, to the more modern adoptive transfer of lymphocytes to treat cancer and the potential to use stem cells to repair damaged organs in the future. Cell Therapy can be defined as the infusion or transplantation of whole cells into a patient for the treatment of an inherited or acquired disease. This technique can also be used for gene delivery; it is similarly called "cell-based delivery". Therapeutic approaches focus on the two delivery modes.[76] The gene therapy refers to the direct injection of genetic material into a localized body part, whereas the cell therapy involves harvesting targeted cells from the patient, transfecting them in vitro, and re-implanting them in the body (Figure 14).

The successful delivery of therapeutic genes to particular target sites is only possible by physical methods such as a gene gun, hydrostatic pressure, electroporation (permeabilization of the cells membrane by increasing the electrical conductivity), continuous infusion and sonication.[77] However, these techniques are not applicable to every cell line and often reduce cell viability. The

[75] R. C. Mulligan, *Science,* **1993**, *260*, 926-932.

[76] a) S. Pearson, H. Jia and K. Kandachi*, Nat. Biotechnol.*, **2004**, *22*, *3-4*; b) P. L. Chang and K. MacMillan Bowie, *Adv. Drug Delivery Rev.,* **1998**, *33*, 31.

[77] T. Niidome and L. Huang, *Gene Ther.,* **2002***, 9*, 1647-1652.

challenge that is being addressed today is the use of efficient vectors for nucleic acids delivery.

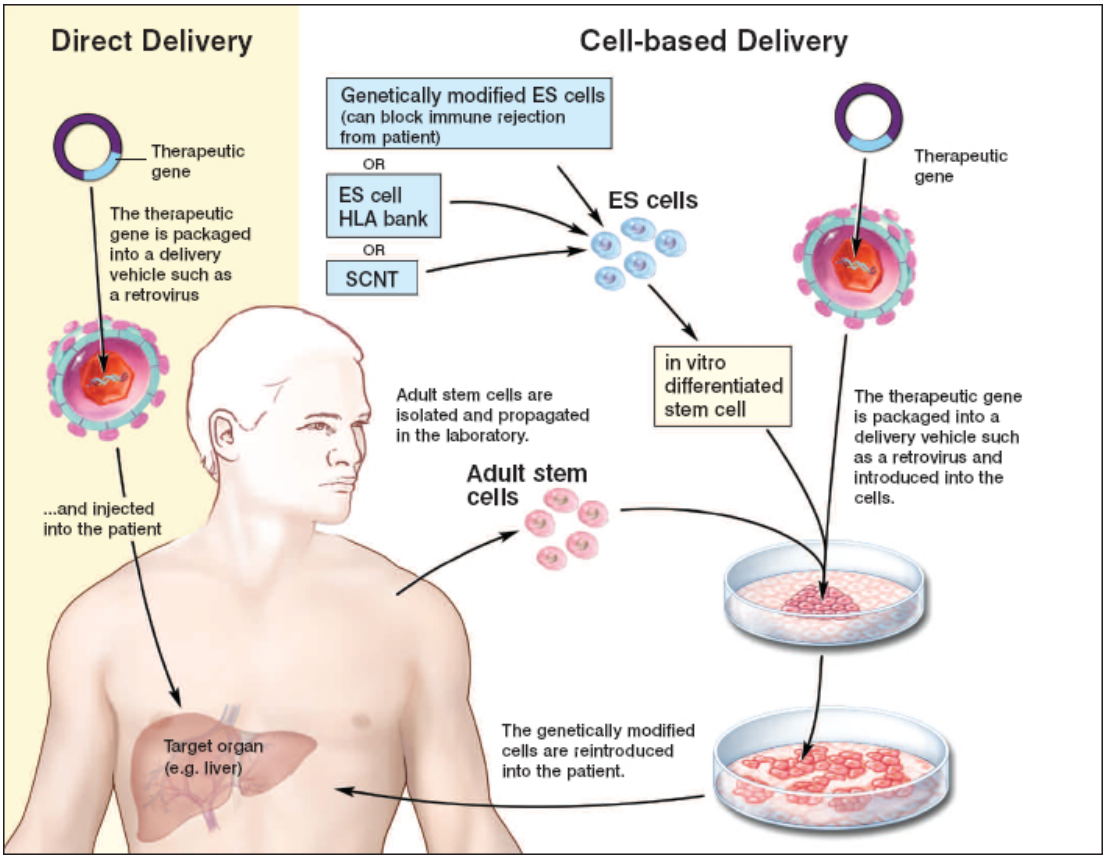

Figure 14: Schematic representation of direct delivery (gene therapy) and cell-based delivery (cell therapy). Adapted from M. Dekker.[78]

[78] M. Dekker, *Gene and cell therapy : therapeutic mechanisms and strategies*, ed. N. S. Templeton., **2004.**

Nucleic acids vectors

The efficacy of a drug is in a large part determined by its biodistribution, in other words, its interaction with the body. Drug targeting can be achieved by modifying the physicochemical properties of this drug with the help of delivery vectors. For low-molecular-weight drugs as well as for biologically active proteins, drug targeting has been achieved by controlling the properties of drug-vector complexes such as the particle size, molecular weight, surface charge, or by using a direct targeting part like an antibody or a folic acid molecule.

Nucleic acids can be delivered to target tissue or cells employing the same strategy. To improve the delivery of DNA into the cell, it must be protected from damage by enzymes and targeted to the cells by some vectors. They are various vector types including viral vectors, non-viral vectors and hybrids vectors (Figure 15).

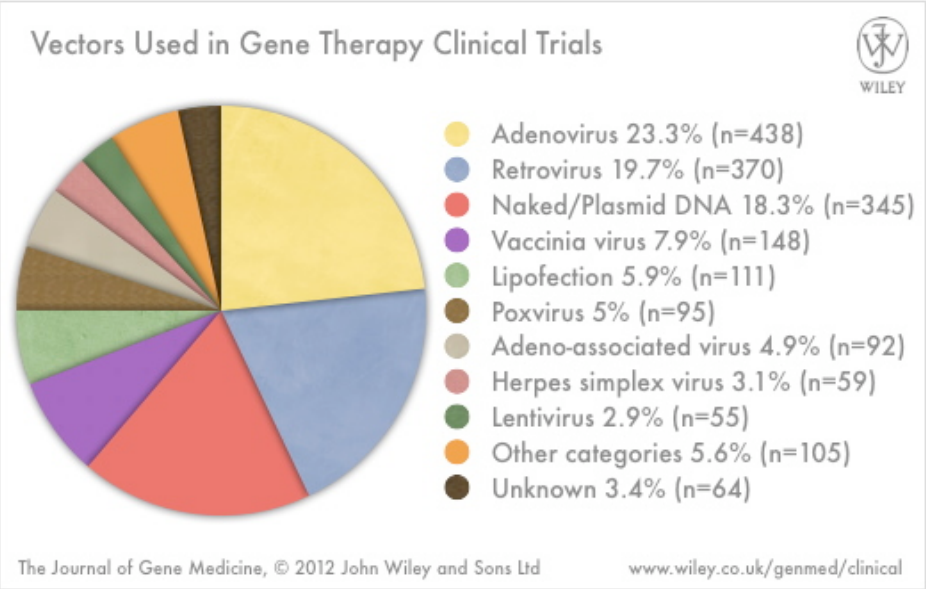

Figure 15: Vectors used in gene therapy clinical trials. Adapted from The Journal of Gene Medicine, 2012, Wiley.[79]

One possible way of targeting nucleic acids is using a ***viral vector***. In fact, the majority of DNA carriers used for clinical applications or first phase of clinical trials, are engineered viral or adenoviral vectors. Viruses can be transformed into

[79] *The Journal of Gene Medicine* **2012**, www.wiley.com/legacy/wileychi/genmed/clinical.

gene delivery vehicles by removing part of their genome and replacing it with a therapeutic gene. All viruses bind to their host and introduce their genetic material into the host cell as part of their replication cycle. The viruses are sophisticated gene delivery vehicles and such recombinant viral vectors are incredibly efficient. Nevertheless, despite the high efficiency of viral vectors *in vitro*, clinical trials are often limited by several concerns: toxicity, immunogenicity, high cost, packing problems. The limited space available in the viral genome combined with expensive production requirements and major safety issues related to over-reaction of the immune system have inspired the development of alternative non-viral strategies.[80]

Cellular vectors have been proposed as new vector systems because of their properties with regard to immune recognition and toxicity. Mesenchymal stem cells (MSCs) have been attractive cell therapy vehicles for the delivery of agents into tumor cells because of their capability of self-renewal, relative ease of isolation and expansion *in vitro*, and homing capacity allowing them to migrate toward and engraft into the sites of tumor.[81] To develop MSCs as therapeutic agents, efficient gene transfert to the cells is a prerequisite. The strategies for gene delivery into MSCs include using viral vectors and non-viral vectors. Several research groups have reported promising results following the injection of genetically engineered mesenchymal stem cells in animal models bearing different tumors.[82]

Synthetic vectors provide opportunities for improved safety, flexibility and more facile manufacturing. In general, synthetic vectors are materials positively charged that form electrostatic interactions with DNA or RNA, condensing the genetic material into nanometer-scale complexes that protect the

[80] a) J. Kaiser, *Science,* **2005**, *307*, 1544-1545; b) S. Lehrman, *Nature*, **1999**, *401*, 517-518.
[81] a) J.E. Dennis, N. Cohen, V.M. Goldberg, and A.I. Caplan, *J. Orthop. Res.,* **2004***, 22*, 735-741; b) Y.-L. Hu, Y.-H. FU, Y. Tabata and J.-Q. GAO, *J. Control. Release,* **2010***, 147*, 154-162.
[82] a) M. Studeny, F.C. Marini, J.L. Dembinski, C. Zompetta, M. Cabreira-Hansen, B. Nebiyou Bekele, R.E. Champlin, M. Andreeff*, J. Natl. Cancer. Inst.,* **2004***, 96*, 1593-1603; b) M. Studeny, F.C. Marini, R.E. Champlin, C. Zompetta, I.J. Fidler, M. Andreeff*, Cancer Res.,* **2002***, 62*, 3603-3608; c) M. Kassen, M. Kristiansen and B. M. Addallah, *Basic Clin. Pharmacol. Toxicol.,* **2004***, 95*, 209-214; d) J. Xiang, J. Tang, C. Song, Z. Yang, D.G. Hirst, Q.-J. Zheng, G. Li*, Cytotherapy,* **2009***, 11*, 516-526.

genes and allow them to enter into the cells. The electrostatic interactions occur between the negatively charged phosphates (P) of the nucleic acids and the nitrogen groups (N) of the synthetic vectors.

Non-viral vectors include cationic liposomes (lipoplexes) and cationic polymers (polyplexes).[83] Lipoplexes were first developed by Behr[84] and Felgner[85] and are extensively used for nucleic acid transfection, even *in vivo*. Many formulations of cationic lipids contain a zwitterionic or neutral co-lipid to enhance transfection. Chemists have successfully varied the structure of small cationic lipids leading to the establishment of numerous structure–activity relationships. Cationic polymers also vary widely in their structures, from linear to branched molecules that can be specifically tailored by choosing the appropriate molecular size or by adding targeting moieties. Among the best studies examples are polyethylenimine (PEI) and poly(L-lysine) polymers, which have high densities of protonable amines in their periphery and allows the efficient condensation of nucleic acids.

Due to every method of gene transfer having shortcomings, there have been also some hybrid methods that combine two or more techniques. Viral and synthetic components are combined to form ***hybrid vectors***. Polymers can replace the function of the viral envelope protein and interact with the target cell membrane, initiate cellular uptake and facilitate escape from endocytic vesicles. For instance, J. D. Ramsey and co-workers complexed non-infectious retrovirus-like particles, lacking a viral envelope protein, with poly-L-lysine (PLL) or polyethylenimine (PEI).[86] M. A. Kostiainen and colleagues have worked with various dendritic derivatives as PAMAM and Newkome-type dendrons with a

[83] T. Dutta, N.K. Jain, N.A.J. McMillan, H.S. Parekh*, Nanomedicine: Nanotechnology, Biology, and Medicine,* **2010**, *6*, 25-34.

[84] a) J.-P. Behr, *Tetrahedron Lett.,* **1986**, *27*, 5861-5864.; b) J.-P. Behr, *Bioconjugate Chem.,* **1994**, *5*, 382-389.

[85] P. L. Felgner, T.R. Gadek, M. Holm, R. Roman, H.W. Chan, M. Wenz, J.P. Northrop, G.M. Ringold, M. Danielsen, *PNAS U. S. A.,* **1987**, *84*, 7413-7417.

[86] J.D. Ramsey, A.N. Wu, D.W. Pack*, Journal of Controlled Release,* **2010**, *144*, 39–45.

spermine functionalized surface and shown that they can form electrostatic complexes with DNA.[87]

[87] M. A. Kostiainen, P. Hiekka-Taipale, J.A. Torre, R.J.M. Notle, J.J.L.M. Cornelisen*, J. Mater. Chem.,* **2011**, *21*, 2112–2117.

Dendrimers based gene therapy

Dendrimers with protonable amine groups can interact with all forms of nucleic acid by electrostatic interactions to form complexes commonly called « dendriplexes » which condense the nucleic acids. Whereas linear polymers often adopt random-coil structures, the 3D structure of a dendrimer is characterized by radial symmetry. For the purpose of gene delivery, functionalization and variation of the dendrimer structure is an important tool to manoeuvre through the many cellular obstacles.

Polyamidoamine dendrimers (PAMAM) were the first used for gene delivery by Szoka and co-workers. They performed the first transfection assays with dendritic vectors using a series of commercial PAMAM dendrimers in a broad range of cell lines.[88] The efficacy of the new vectors was found to be promising. PAMAM is now the most studied dendrimer for gene delivery with a considerable number of researches published.[89] This predominance can be linked to the fact that PAMAM dendrimers were one of the earliest dendritic systems synthesised at high generation numbers and commercialised. Despite these results, a major shortcoming of PAMAM dendrimers that limits their use both *in vitro* and *in vivo* has been undesirable toxicity associated with their high-surface cationic charge density and the excess of positive charge related with the high Nitrogen/Phosphate (N/P) ratios employed.[90] The N/P ratio is a measure of the ionic balance of the complexes. It refers to the number of nitrogen residues of the vector per DNA phosphate

To overcome this problem, PAMAM dendrimers have been modified and/or used at lower generations.[91] Szoka and colleagues covalently attached

[88] J. Haensler, F.C. Szoka Jr, *Bioconjugate Chem*., **1993**, *4*, 372-379.

[89] a) K. Sarkar, Kishor, P.P Kundu, *Int. J. Biol. Macromol*., **2012**, *51*, 859-867 ; b) Z. Yin, N. Liu, M. Ma, L. Wang, Y. Hao, X. Zhang, *Int. J. Nanomed.,* **2012***, 7*, 4625-4635 ; c) Z. Aydin, F. Akbas, M. Senel, S.N. Koc, *J. Bio. Mat. Res. A.,* **2012**, *100*, 2623-2628 ; d) Y. Tang, Y.-B. Li, B. Wang, R.-Y. Lin, M. van Dongen, D.M. Zurcher, X.-Y. Gu, M.M. Banaszak Holl, G. Liu, R. Qi, *Mol. Pharm*, **2012***, 9,* 1812-1821 ; e) B. Parker-Esquivel, K.J. Flores, D. Louiselle, M. Craig, L. Dong, R. Garrad, K. Ghosh, A.Wanekaya, G. Glaspell, R.K. DeLong, *Langmuir,* **2012**, *28*, 3860-3870 ; f) X. Liu, C. Lui, E. Laurini, P. Posocco, S. Pricl, F. Qu, P. Rocchi, L. Peng, *Mol. Pharm*., **2012**, *9*, 470-481.

[90] C.L. Gebbart and A.V. Kabanov*, J. Controlled Release,* **2001**, *73*, 401-416.

[91] a) N. Shah, R.J. Steptoe and H.S. Parekh*, J. Pept. Sci.,* **2011**; *17*, 470-478; b) T.L. Kaneshiro, X. Wang and Z.R. Lu*, Mol. Pharmaceutics,* **2007**, *4*, 759–768.

GALA (30 amino acid synthetic peptide with a glutamic acid-alanine-leucine-alanine repeat) to PAMAM dendrimers and observed that the transfection efficiency was enhanced.[92] In another approach, PAMAM dendrimers were covalently linked with cyclodextrin macrocycles to create a synergic effect between dendrimers and cyclodextrins.[93] To enhance PAMAM transport into cells, a series of artificial proteins was designed by grafting L-arginines, L-Lysine, Leucine, or phenylalaine residues to regular PAMAM dendrimers.[94] The surface of PAMAM was also modified with terminal hydroxyl groups instead of primary amines in order to reduce the toxicity by reducing the surface charge density; but the tranfection efficiency did not reach the levels obtained with PAMAM dendrimers without modifications.[95] PAMAM dendrimers were moreover modified with PEG chains, either at their core to form PAMAM-PEG-PAMAM derivatives,[96] or at their periphery.[97] The solubility was increased and the toxicity decreased but the transfection efficiency was not significantly improved compare to globular dendrimers.

PPI dendrimers were also investigated for transfection due to their structural similarities with PAMAM dendrimers, and their commercial availability. However, disappointing transfection and toxicity levels were obtained which disqualified the use of high generation PPI dendrimer a gene vector; but their use at lower generations, specifically G2, was found to be suitable.[98]

The search for an efficient and non-toxic gene transfection vector has led to the design and synthesis of a large variety of other dendritic structures; to cite just a few examples: poly(L-lysine) dendrimers[99] or dendritic-linear-dendritic

[92] J. Haensler and F. C. Szoka, Jr, *Bioconjugate Chem.,* **1993**, *4*, 372-379.

[93] a) H. Arima, F. Kihara, F. Hirayama, K. Uekama, *Bioconjugate Chem.,* **2001**, *12*, 476-484; b) F. Kihara, H. Arima, T. Tsutsumi, F. Hirayama, K. Uekama*, Bioconjugate Chem.,* **2003**, *14*, 342-350.

[94] a) J.S. Choi, K. Nam, J.-Y. Park *et Al., J. Controlled Release,* **2004**, *99*, 445-456; b) K. Kono, H. Akiyama, T. Takahashi, T. Takagishi, A. Harada*, Bioconjugate Chem.,* **2005**, *16,* 208-214.

[95] J.H. Lee, Y.-B. Lim, J.S. Choi, Y. Lee, T. Kim, H.J. Kim, J.K. Yoon, K. Kim, J.-S. Park*, Bioconjugate Chem.,* **2003**, *14*, 1214-1221.

[96] a) T.-I. Kim, H.J. Seo, J.S. Choi, H.-S. Jang, J.U. Baek, K. Kim, J.-S. Park*, Biomacromolecules*, **2004**, *5*, 2487-2492; b) J.-H. Fuhrhop and T. Wang, *Chem. Rev.,* **2004**, *104*, 2901-2937.

[97] D. Luo, K. Haverstick, N. Belcheva, E. Han, W.M. Saltzmann*, Macromolecules*, **2002**, *35*, 3456-3462.

[98] B.H. Zinselmeyer, S.P. Mackay, A.G. Shatzlein, I.F. Uchegbu*, Pharm. Res.*, **2002**, *19*, 960-967.

[99] J.S. Choi, D.K. Joo, C.H. Kim, K. Kim, J.S. Park, *J. Am. Chem. Soc.,* **2000**, *122,* 474-480.

derivatives, [100] polyethyleneimine (PEI), [101] phosphorous dendrimers, [102] guanidinylated dendrimers.[103] Generally, DNA binding ability was found to increase with the generation number, as measured by agarose gel electrophoresis and the best performing generation for cell transfection was dependent on the cell type. Chemical modification has been exploited for optimization toward a specific scientific goal.

The supposed mechanism of action of dendriplexes or polyplexes is represented in Figure 16.[104] First, the polymer forms a complex with nucleic acid. Then the complex is added to cells *in vitro* or is introduced into animals *in vivo* or *ex vivo*. After being delivered to their localization (e. g. by the blood flow), the cells internalize the complexes, and dendriplex-containing endosomes are formed. Deprotonation of dendrimer surface groups, dendrimer destruction, and nucleic acid release occurs when the pH changes from 7.4 (extracellular value) to 5.5 (intracellular value). Simultaneously, the endosomes undergo lysis and free nucleic acid is released into the cytoplasm.

[100] Y. Zhu, R. Sheng, T. Luo, H. Li, W. Sun, Y. Li, A. Cao, *Macromol. Biosci*., **2011**, *11*, 174-186.

[101] E. Pedziwiatr-Werbicka, M. Ferenc and M. Zaborski*, Colloids and Surfaces B: Biointerfaces,* **2011**, *83*, 360-366.

[102] D. Shcharbin, V. Dzmitruk, A. Shakhbazau, N. Goncharova, I. Seviaryn, S. Kosmacheva, M. Potapnev, E. Pedziwiatr-Werbicka, M. Bryszewska, M. Talabaev, A. Chernov, V. Kulchitsky, A.-M. Caminade, J.-P. Majoral*, Pharmaceutics,* **2011**, *3*, 458-473.

[103] a) S. Menuel, S. Fontanay, I. Clarot, R.E. Duval, L. Diez, A. Marsura*, Bioconjugate Chem*., **2008**, *19*, 2357–2362; b) T. A. Theodossiou, A. Pantos, I. Tsogas, C.M. Paleos*, ChemMedChem,* **2008**, *3*, 1635-1643.

[104] D. G. Shcharbin, B. Klajnert and M. Bryszewska*, Biochemistry (Moscow),* **2009**, *74*, 1070-1079.

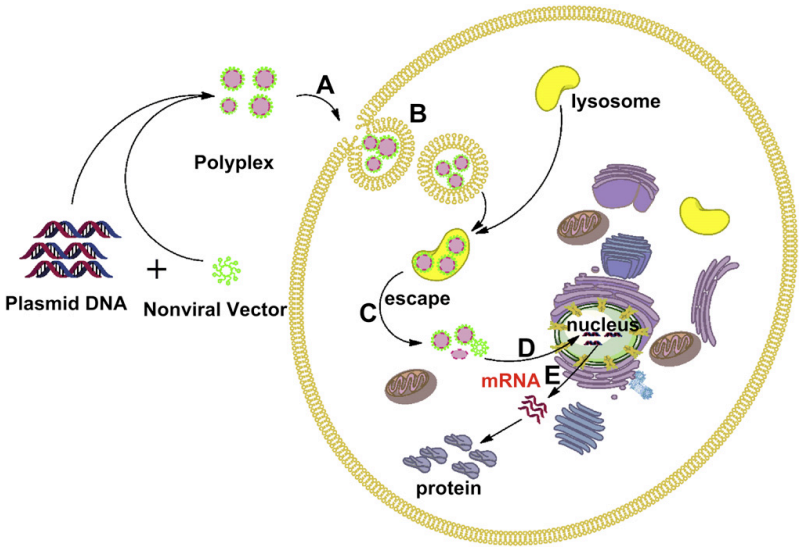

Figure 16: Possible way for transfecting cells using polymers. Adapted from Y. Shang *et Al.*[105]

[105] Y. Shang, T. Luo, C. Peng, R. Sheng, A. Cao, X. Cao, M. Shen, R. Guo, H. Tomás, X. Shi, *Biomaterials,* **2012**, *33,* 3025-3035.

Objectives and approach

The principal objective of this part of the thesis is to study the properties of dendritic molecules derived from *bis*-MPA and PAMAM dendrimers for their applications in gene delivery.

In this purpose, two kinds of molecules are studied: dendritic derivatives based on 2,2-*bis*(hydroxymethyl)propionic acid (*bis*-MPA) and ionic dendrimers based on polyamidoamine (PAMAM) and *bis*-MPA. Three *bis*-MPA derivatives *1*, *2*, *3* (Figure 17) and four ionic-PAMAM derivatives of different generations and different degree of amine substitution by 2-(2-(2-methoxyethoxy)ethoxy)acetic acid: *2G-IP-30, 2G-IP-16, 5G-IP-254, 5G-IP-128* (

Figure 18) were synthesized and studied. In order to complete the study, an ionic *bis*-MPA dendrimer, **I*bis*MPA**, was synthesized and its properties were compared with the previous derivatives.

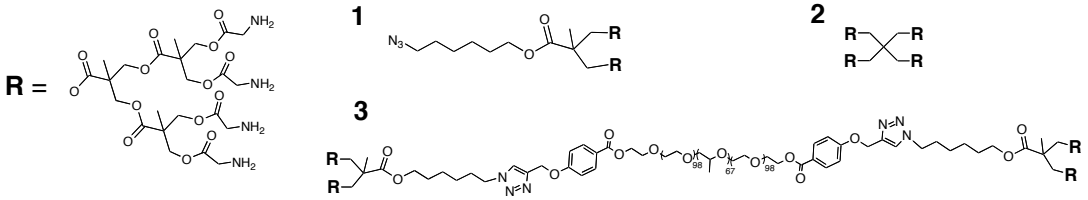

Figure 17: Structures of 3G *bis*-MPA dendron (1), 2G *bis*-MPA dendrimer (2) and pluronic-3G *bis*-MPA dendron copolymer (3), functionalized with amine groups.

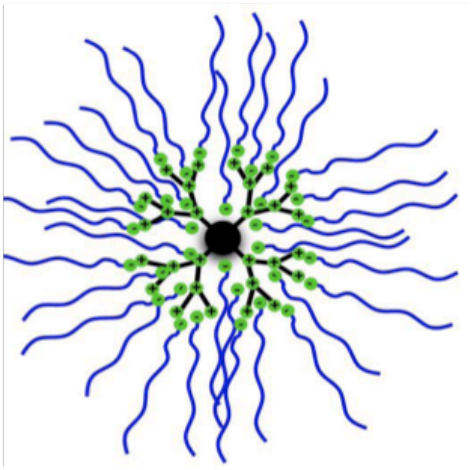

Figure 18: Scheme of ionic-PAMAM dendrimer functionalized by 2-(2-(2-methoxyethoxy)ethoxy)acetic acid.

In order to achieve these objectives, we propose to study plasmid DNA-dendrimers interactions between by these two kinds of dendritic derivatives. In this purpose, the following aspects will be developed:

1- Synthesis and structural characterization of the dendritic compounds,
2- Study of the cytotoxicity of the compounds: cell viability tests on U251MG cell line and mesenchymial cells,
3- Plasmid DNA complexion studies by agarose electrophoresis gel retardation assays.

Results and Discussion

bis-MPA dendrimers

As presented in the general introduction, *bis*-MPA dendrimers are very interesting for biomedical applications because of their unique properties. Here we propose to use them a nucleic acid vector to overcome the problems of toxicity found with other dendrimers. Moreover, *bis*-MPA derivatives are very easy to functionalize and although they do not contain protonable amine groups in their structure it is easy to introduce them in their periphery. No work was published about their use for transfection in spite of being interesting candidates as gene carriers. In this chapter, we intend to study three kinds of *bis*-MPA derivatives: a third generation dendron **[1]**, a second generation dendrimer **[2]** and a dendritic-linear-dendritic derivative **[3]**.

Ionic dendrimers

The use of non-covalent bonding to obtain compounds for materials or biological applications has considerably increased during the past years. The three principal types of non-covalent bonding are: hydrogen bonds, hydrophobic interaction, and ionic interactions. In this chapter, we will focus in the last one. The preparation of dendrimers by ionic interaction is a very convenient synthetic method due to its simplicity. The modification can be obtained in one step and does not need any purification. The variation of the functional groups can easily be carried out and permit to synthesize a large range of materials in a few time. In order to use this type of interactions, the functional groups have to be easily ionisable. To this end, dendrimers such as PAMAM, PPI or other kind functionalized with amine groups (-NH_2) are used with units possessing carboxylic groups (-COOH). The resulting materials are generated thanks to the exchange of the acid group proton to the amine base group, producing a salt: -$\boldsymbol{NH_3^+ \cdot OOC}$-. Few examples of ionically modified dendrimers have been described and used in applications such as liquid crystals,[106] dendrimer-dye assemblies,[107] and

[106] a) M. Marcos, R. Martín-Rapún, A. Omenat, J. Barberá, J.L. Serrano, *Chem. Mater.,* **2006**, *18,* 1206-1212; b) R. Martín-Rapún, M. Marcos, A. Omenat, J. Barberá, P. Romero, J.L. Serrano, *J. Am. Chem. Soc*.,

multilayer films.[108] The commercially available poly(amidoamine) (PAMAM) dendrimer is one of the most investigated families because of the chargeable amine groups on the surface of the dendrimers and its commercial availability.

From 1995, Crooks and co-workers[109] started to use this method to ionically functionalize PAMAM dendrimers. They described a non-covalent concept for organosoluble-inverted micelles that were prepared by self-assembly of PAMAM dendrimers modified with fatty acids, which relied on acid-base interaction. These micelles were capable of transporting hydrophilic guest molecules into organic solvents. Later, Frey and colleagues used the same idea with hyperbranched PEI polymer functionalized with dodecanoic or hexadodecanoic acids.[110] In spite of the interest of this subject, up to now, few work concerning the nanostructures formed in water by these simple ionic derivatives PAMAM dendrimers has been reported. In 2011, S. Hernández and collaborators published their work about nanoobjects coming from mesomorphic ionic PAMAM dendrimers.[111] They prepared a series of PAMAM dendrimers functionalized with fatty acids of different length and observed their capacity of forming nano-spheres in water and their possible use as hydrophobic or hydrophilic molecules carriers.

Here we propose to use this kind of ionically modified PAMAM dendrimers to form suitable dendriplexes for gene transfection applications. Instead of fatty chains, PAMAM dendrimers will be functionalized with 2-(2-(2-methoxyethoxy)ethoxy)acetic acid in order to lower their cytotoxicity. The efficiency of these compounds will be compared to commercial PAMAM and *bis*-MPA dendritic derivative previously mentioned in terms of cytotoxicity and dendriplexes formation.

2005, *127*, 7397-7403; c) S. Hernández, J. Barberá, M. Marcos, J.L. Serrano*, Macromolecules,* **2012**, *45*, 1006−1015; d) R. Martín-Rapún, M. Marcos, A. Omenat, J.L. Serrano, E. Taffin de Givenchy, F. Guittard, *Liquid Crystals* **2007**, *34*, 395-400.

[107] I. Willerich, Y. Li, and F. Grohn*, J. Phys. Chem. B,* **2010**, *114,* 15466-15476.

[108] J. L. Casson, J.L. Wang, H.L. Roberts, A.N. Parikh, J.M. Robinson, M.S. Johal*, J. Phys. Chem. B,* **2002**, *106,* 1697-1702.

[109] V. Chechik, M. Zhao, R. M. Crooks*, J. Am. Chem. Soc.,* **1999**, 121, 4910-4911.

[110] Y. Chen, Z. Shen, H. Frey, J. Pérez-Piero, S.-E. Stiriba*, Chem. Comm.,* **2005**, 755-757.

[111] S. Hernández, J. Barberá, M. Marcos, J.L. Serrano, *Soft Matter,* **2011**,7, 2560-2568.

Ionic bis-MPA dendrimer

To complete our library of dendritic derivatives for applications in gene delivery, we associated the properties of *bis*-MPA, such as its remarkable biocompatibility and its ability to be biodegraded, to the properties of ionic dendrimers that are more promising for the complexion of nucleic acids.

Design and synthesis

bis-MPA dendritic derivatives

For synthetic reasons, we chose to work with low generation derivatives: third generation dendron and second generation dendrimer. The third generation dendron was also used to prepare the dendritic-linear-dendritic derivative.

3rd generation *bis*-MPA dendron

In order to be eligible as nucleic acids vector, the dendron has to be functionalized by amine groups at least in its periphery. The amine groups were covalently attached with different spacers to the free hydroxyl groups of the dendron. Two dendrons were designed: the first one with a spacer of one carbon (2-aminoacetic acid: glycine) and the second one with a spacer of five carbons (6-aminohexanoic acid) to give more flexibility to the molecule. Each dendron was functionalized by a total of 8 amine groups. Moreover, the dendron was modified by an azide in its point in order to keep the possibility of further modifications (Figure 19).

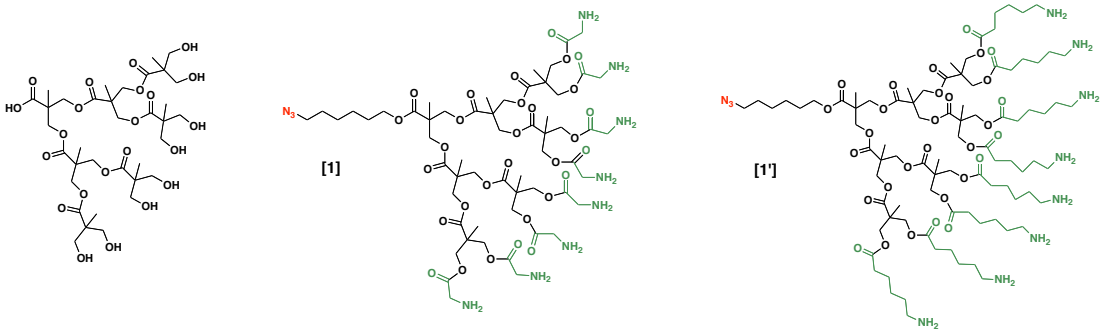

Figure 19: 3rd generation *bis*-MPA dendron (left), dendron modified with glycine and azide (centre), and dendron modified 6-aminohexanoic acid and azide (right).

The synthesis of the third generation *bis*-MPA dendrons was completed in nine steps, following a divergent strategy. The final dendron functionalized by glycine **[1]** was obtained as a yellowish solid in a 27% total yield from the commercial *bis*-MPA. The dendron with a five carbons spacer **[1']** was obtained in

a total yield of 7%. The crucial step was the addition of 6-aminohexanoic acid in which the pure product was obtained only in a 20% yield.

The synthetic process followed has been identical for both dendrons and is flowingly explained (synthetic scheme in Figure 20). As a first step (**i**), the hydroxyl groups of the *bis*-MPA monomer were protected by the formation of an acetal with 2,2-dimethoxypropane in presence of *p*-toluenesulfonic acid in acetone (**1-1**). Then, the dendron point was functionalized by an azide (6-azidohexan-1-ol) through a DCC/DPTS esterification in dichloromethane (**ii**, Steglish esterification, **1-2**). The 6-azidohexan-1-ol was previously obtained by a reaction of substitution between 6-chlorohexan-1-ol and sodium azide in dimethylformamide. As a third step (**iii**), the hydroxyl groups were deprotected using a DOWEX acid resin in methanol (**1-3**). The generation growth was obtained by esterification of the hydroxyl groups with the protected *bis*-MPA monomer (**1-1**) in presence of DCC and DPTS in dichloromethane (**iv**, **1-5**, **1-7**). After each esterification, the crude product was purified by column chromatography and the hydroxyl groups of the dendrons were deprotected. The following step (**v**) consisted on the formation of an ester bond between the hydroxyl groups of the dendron and the carboxyl group of a protected glycine (GlyBoc). The deprotection of the amine groups in acid environment (**vi**) offered the final product [**1**], which was obtained without need of further purification.

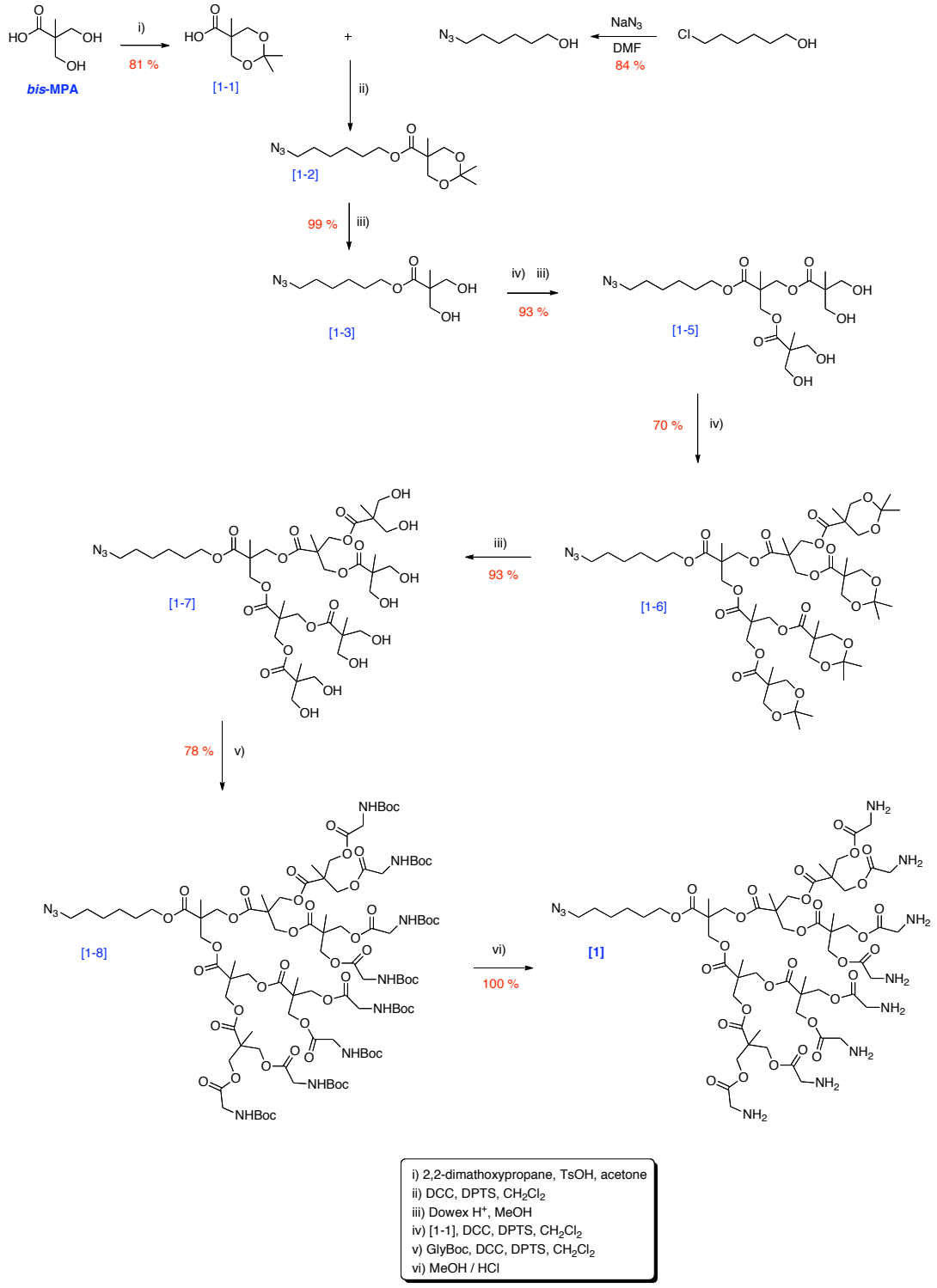

Figure 20: Synthetic scheme of third generation aminated *bis*-MPA dendron [1].

Both dendrons were synthesized and characterized by ^{1}H-NMR, ^{13}C-NMR, IR and mass spectroscopy (see experimental part). The complete functionalization of the third generation dendron by the aminated acid was confirmed in ^{1}H-NMR by

the peak corresponding to the -C**H**$_2$-NHBoc and integrating for 16H (3.87 ppm, d, *J* = 5.6 Hz in the case of **[1-8]** and 3.09, q, J_1 = 6.4 Hz, J_2 = 6.0 Hz in the case of **[1'-8]**). The correct functionalization of the dendrons by the azide a their point was revealed in IR by the band at approx. 2090 cm^{-1} in the products spectrums.

Unfortunately, the dendron **[1']** was found to be insoluble in water and its use as gene carrier was discarded.

The ^{1}H-NMR spectrum of the final compound **[1]** is represented in the following Figure 21. The protons of the methyl groups, **Hi**, **Hm**, and **Hp** appear at 1.34 ppm and 1.36 ppm as superposed singlets. The peaks corresponding to the C**H**$_2$ groups' protons **Hb**, **Hc**, **Hd** and **He** appear as quintuplets at 1.46 ppm, 1.60 ppm and 1.70 ppm. At 3.34 ppm, the peak corresponding to the C**H**$_2$ in α of the azide groups, **Ha**, is superposed with the solvent residual peak. The peak due the -C**H**$_2$-NH$_2$, **Ht**, is situated at 3.95 ppm as a singlet. At 4.18 ppm, is located the triplet corresponding to **Hf**. Finally, the peaks corresponding to the -C-C**H**$_2$-O- protons, **Hr,r'**, **Hj,j'**, **Hn,n'** appear in the 4.16 ppm to 4.86 ppm zone of the spectrum. These protons are diasteroisotopic, they are chemically identic but because of their space position they give different ^{1}H-NMR signals. They can appear as singlet, doublet or doublet of doublet depending of the arrangement of the *bis*-MPA molecules due to the different generations and the functional groups present in the broad part of the dendrons.

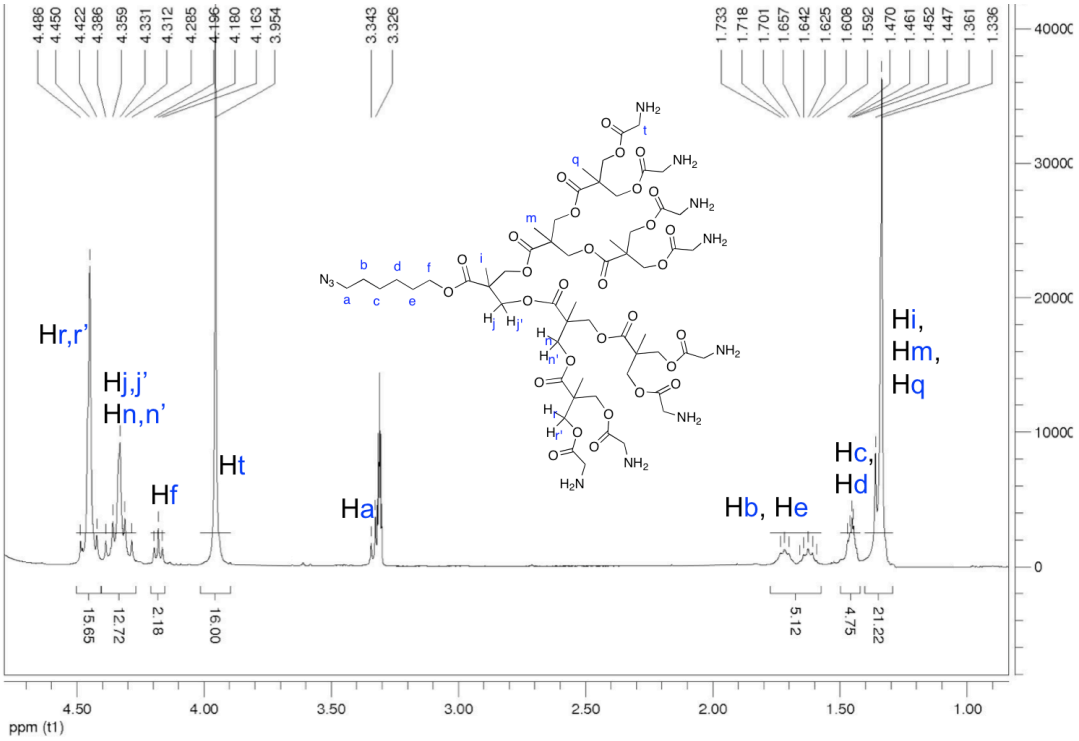

Figure 21: 1H-NMR spectrum of the compound [1], 400MHz, MeOD.

2nd generation *bis*-MPA dendrimer

The *bis*-MPA dendrimer [**2**] was designed to be comparable with the dendron. We selected the second generation *bis*-MPA dendrimer with a pentaerythritol group as core. The MW (2442) is approximately twice the one of the dendron (1412), and the number of external groups is 16, the double of the dendron ones.

The synthesis of the dendrimer (Figure 23) started from the commercial pentaerythritol and followed a divergent strategy (growth from the core). The first step of the synthesis consists on the formation of the *bis*-MPA anhydride that is highly reactive with nucleophiles such as alcohol or amines. In this purpose (Figure 22), the commercial *bis*-MPA monomer reacted with benzaldehyde dimethyl acetal and a catalytic amount of *p*-TsOH to form the benzylidene-protected derivative. Afterwards, the anhydride was formed by self-condensation of the protected derivative in presence of DCC (used as the dehydrated agent). The crude anhydride was purified from the DCU formed and the remaining DCC by precipitation into hexane.

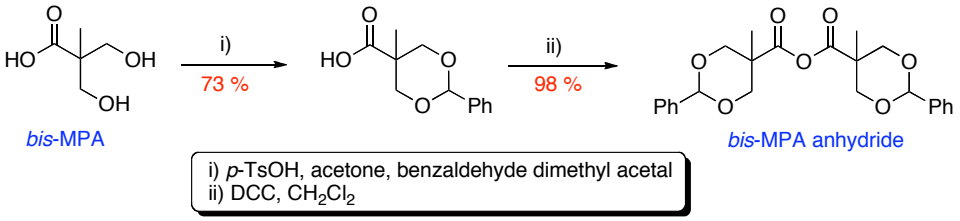

Figure 22: Synthetic scheme of *bis*-MPA anhydride.

The generation growth was obtained by esterification between the *bis*-MPA anhydride and the hydroxyl groups of pentaerythritol in presence of DMAP as acylating catalyst in a mixture 1:3 pyridine/dichloromethane (**i**). After reaction the excess of anhydride was quench by addition of water (stirring overnight). Pyridine, DMAP and the benzylidene protected acid formed as a by-product were removed by extractions with $NaHSO_4$ (1M), Na_2CO_3 (10% w/v) and brine. The removal of the benzylic groups was obtained by catalytic hydrogenation (**ii**). The esterification of the hydroxyl groups with protected glycine in presence of DCC and DPTS (**iii**) allowed obtaining the completely functionalized dendrimer with 16 amine groups. The crude was dissolved in EtOAc, filtrated to remove the DCU formed during the reaction, and concentrated. The resulting products were purified by dialysis (cellulose membrane MW 1000) against methanol during 24h. Finally, the deprotection of the amine groups (**iv**) in acidic environment gave the aminated product in a total yield of 84% without need of purification.

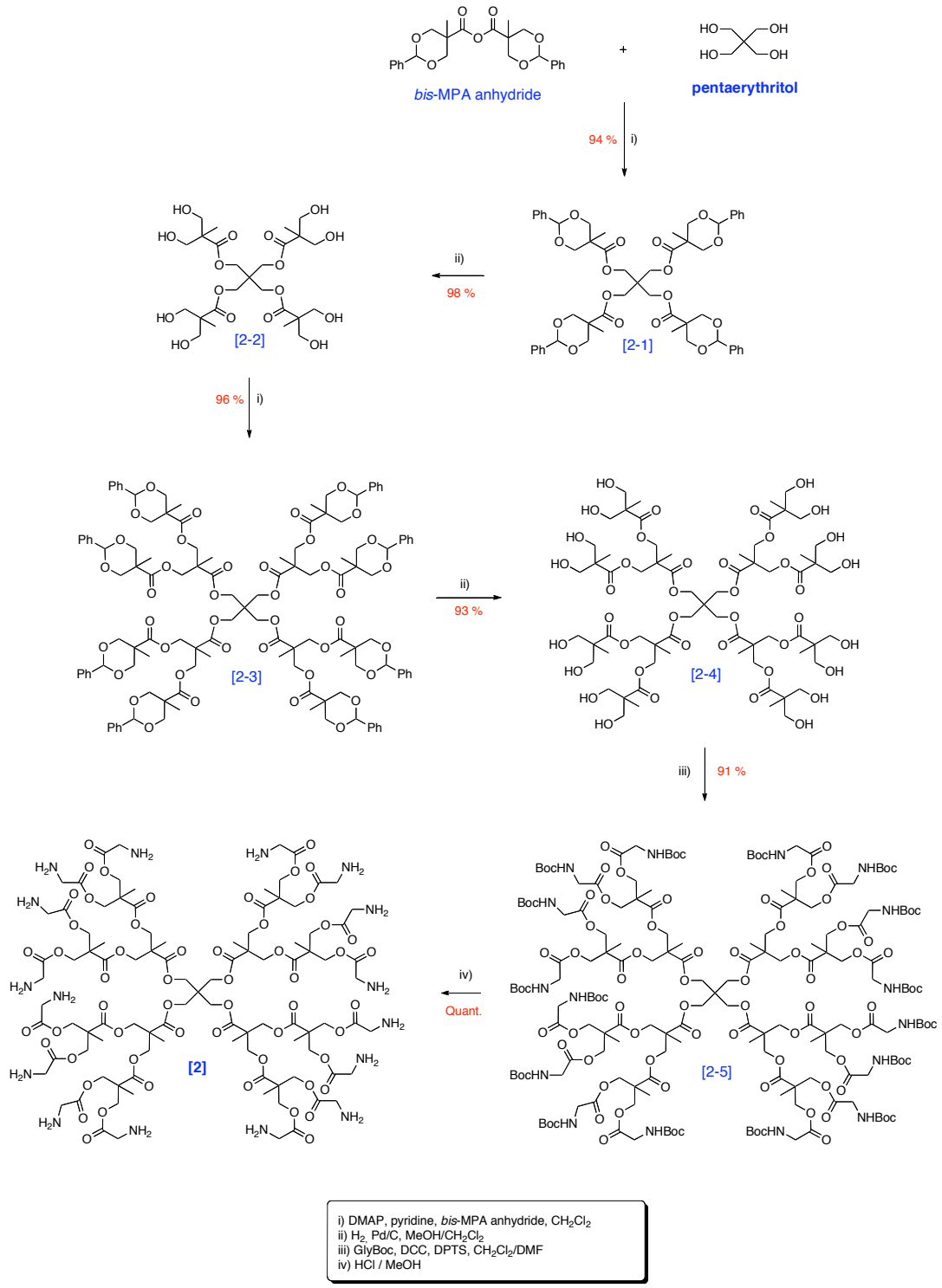

Figure 23: Synthetic scheme for the second generation aminated *bis*-MPA dendrimer [2].

The product growth was followed by NMR spectroscopy: the compound being symmetric, the NMR spectrums contain with few characteristic peaks. In the Figure 24, from the first **[2-2]** to the second generation **[2-4]** we can observe the

apparition of the peak due to the *bis*-MPA methyl group in green at 1.12 ppm in ^{1}H-NMR, and the shift of the methyl groups of the first generation to upper spectrum (1.18 pmm to 1.29 ppm). We can also observe in these spectrums the apparition of the peaks due to the second generation C**H**$_2$ at approx. 3.6 ppm in blue, and the shift of the first generation peaks to approx. 4.2 ppm.

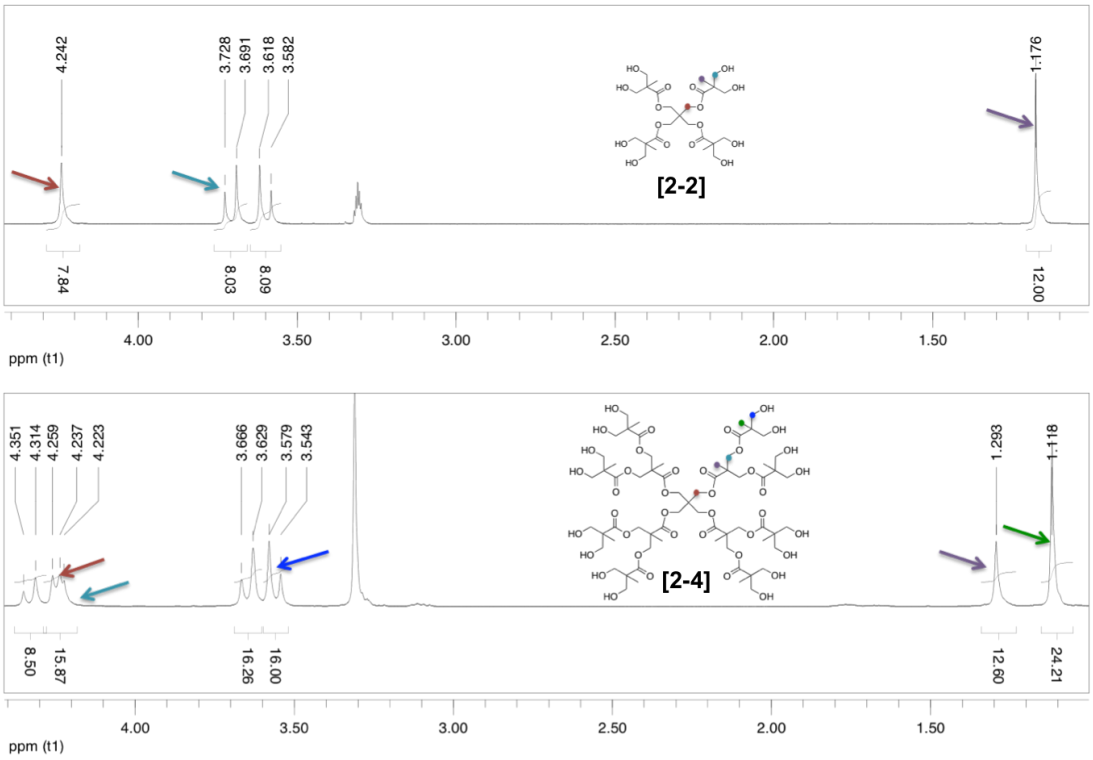

Figure 24: ^{1}H-NMR spectrums of first and second generations *bis*-MPA dendrimer.

The complete functionalization of the dendrimer by protected glycine was revealed in ^{1}H-NMR by the doublet (J = 5.4 Hz) corresponding to the –COO-C**H**$_2$-NHBoc at 3.86 ppm, integrating for 32 protons (16 C**H**$_2$) (see experimental part).

Dendritic-linear-dendritic dumbbell

As well as the third generation dendron and the second generation dendrimer, we chose to work with a dendritic-linear-dendritic derivative, also called a "dumbbell" derivative. In this regard, we decided to use the commercially available polymer F127 Pluronic®.

Pluronic® definition and history

Pluronics®, also known as poloxamers, are triblock ABA-type copolymers composed of a central hydrophobic chain of poly(propylene oxide) (**PPO**) and two hydrophilic chains of poly(ethylene oxide) (**PEO**) (Figure 25).

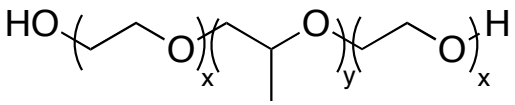

Figure 25: PEO-PPO-PEO copolymer structure.

Poloxamers are available in a large rank of molecular weights and PPO/PEO compositions. Their derivatives have been studied for various biomedical applications such as drug delivery, gene delivery or tissue engineering. F127 is a commercial pluronic® with a molecular weight of about 12600 Da, it contains approximately 67 PPO groups in its centre (**y**) and 99 PEO segments in its extremities (**x**). We chose to work with pluronic® because of its previous utilisation for biological applications. Pluronics® have been used to form micelles in order to solubilize hydrophobic drugs[112] and these polymers have also been used as hydrogels formed by photo-polymerisation capable of loading and releasing DNA.[113] Pluronic®-polycations conjugates are of interest in colloid science because of their self-assembly properties due to the presence of the PPO segments. Moreover, the hydrophobic PPO segments could facilitate membrane interactions and possibly act as a synthetic fusogen by incorporating into the membrane and thus improve the transport of the polyplexe (polymer-DNA complex). The polyplexe modified with Pluronic® can assemble into a core-shell structure with the shell consisting of PEO and polycations. The pluronic®-polycation conjugates have been demonstrated to enhance gene transfection efficiency and improve DNA biodistribution.[114] Fan and co-workers, by conjugating pluronic® to dendritic PEI, confirmed that the addition of the polymer can significantly facilitate intracellular trafficking and can change cellular

[112] a) E.S. Lee, Y.T. Oh, Y.S. Youn, M. Nam, B. Park, J. Yun, J.H. Kim, H.-T. Song, K.T. Oh, *Colloids Surfa. B,* **2011**, *82*, 190-195; b) W. Zhang, Y. Chi, Y. Shen, J. Ye, X. Sha, X. Fang, *Biomaterials,* **2011**, *32*, 2894-2906.
[113] K.W. Chun, J.B. Lee, S.H. Kim, T.G. Park, *Biomaterials,* **2005**, *26*, 3319-3326.
[114] L. Bromberg, V.Y. Alakhov and T.A. Hatton, *Current Opinion in Colloid & Interface Science,* **2006**, *11*, 217-223.

distribution.[115] J. Hao and colleagues investigated the modification of Pluronic P123 with dendritic PPI and observed a large increase of the transfection comparing with PPI dendrimer alone.[116] T. C. Lai and collaborators showed that the use of pluronic® could lead to higher transfection efficiency for DNA delivery systems.[117] Pre-treatment of cells with pluronic L64 was demonstrated to increase DNA transfection mediated by electrotransfer by L. Wasungu and co-workers. Pluronic® and pluronic® derivatives have been largely used in gene delivery.[118]

Here, we propose to functionalize pluronic® F127 with third generation *bis*-MPA dendrons wearing amine groups in the broad part.

Synthesis of dendritic-Pluronic® derivatives [3]

The final compound was obtained in three steps in a total yield of 38% (Figure 26). After the first and second steps, the product was purified by precipitation and filtration, inducing a lost of product and a decrease of the yield. The first step consists of the esterification of pluronic hydroxyls with 4-(prop-2-ynyloxy)benzoic acid in presence of DCC and DMAP in order to obtain the polymer functionalized by triple bonds in its extremities (**i**, **3-1**). This step allowed to directly add the third generation dendron previously synthetized (**1-8**) by coupling it by copper catalysed click-chemistry 1,3-dipolar cycloaddition in dimethylformamide. The copper(I) catalyst was generated *in situ* by reaction between copper sulphate and sodium ascorbate. The crude product was purified by dialysis against methanol (1000 MW cellulose membrane). Deprotection of the amine groups in acid environment (**iii**) gave the final product [**3**] without need of purification.

[115] W. Fan, X. Wu, B. Ding, Z. Cai, W. Zhang, D. Yin, X. Wang, Q. Zhu, J. Liu, X. Ding, S. Gao*, International Journal of Nanomedicine,* **2012**, *7*, 1127-1138.

[116] J. Hao, X. Sha, Y. Tang, Y. Jiang, Z. Zhang, W. Zhang, Y. Li, X. Fang*, Arch. Pharm. Res.,* **2009**, *32*, 1045-1054.

[117] T.C. Lai, K. Kataoka and G.S. Kwon*, Biomaterials,* **2011**, *32*, 4594-4603.

[118] a) P. Lemieux, N. Guerin, G. Paradis, R. Proulx, L. Chistyakova, A. Kabanov, V. Alakhov, *Gene Ther*., **2000**, *7*, 986–991; b) M. Bureau *et Al., Biochim. Biophys. Acta,* **2010**, *1800*, 537–543 ; c) B. Pitard, H. Pollard, O. Agbulut, O. Lambert, J.-T. Vilquin, Y. Cherel, J. Abadie, J.-L. Samuel, J.-L. Rigaud, S. Menoret, I. Anegon, D. Escande*, Hum. Gen. Ther.,* **2002***, 13*, 1767-1775; d) L. Desigaux, C. Gourden, M. Bello-Roufaï, P. Richard, N. Oudrhiri, P. Lehn, D. Escande, H. Pollard, B. Pitard*, Hum. Gene Ther.,* **2005**, *16*, 821-829; e) A.V. Kabanov, P. Lemieux, S. Vinogradov, V. Alakhov*, Adv. Drug Deliv. Rev.,* **2002**, *54*, 223-233; f) Z. Yang, J. Zhu, S. Sriadibhatla, C. Gebhart, V. Alakhov, A. Kabanov*, J. Control. Release*, **2005**, *108*, 496-512.

The copper catalysed 1,3-dipolar cycloaddition is a variant of the thermal Huisgen 1,3-dipolar cycloaddition that follows a different mechanism and provides huge rate acceleration compared to the uncatalysed reaction. The copper-catalysed reaction allows the synthesis of the 1,4-disubstituted regioisomers specifically. The copper catalyst, Cu(I), is generated *in situ* from the Cu(II) salts via reduction by sodium ascorbate.[119]

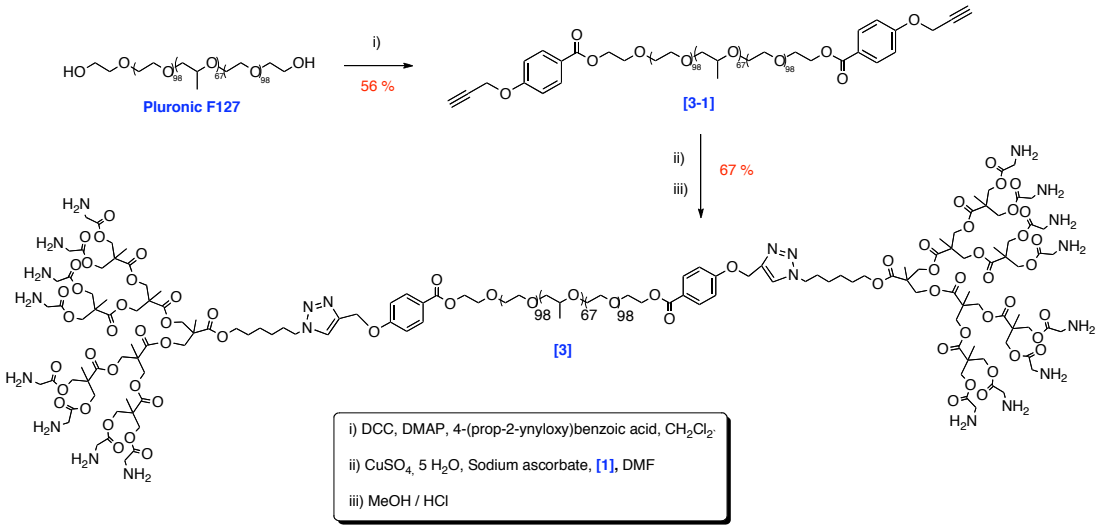

Figure 26: Synthetic scheme of pluronic dumbbell derivative.

The formation of compound **[3-1]** was shown in ^{1}H-NMR by the peaks corresponding to the aromatic protons at 6,97 ppm (d, 4H) and 7.99 ppm (d, 4H). The polymer functionalization by the aminated dendron (**1-8**) was revealed by the new peak corresponding to the methyl protons at 1.43 ppm (144H, 48CH_3, 16Boc groups), and the peaks due to the formation of the triazide cycle at 5.49 ppm (1H, -N=C**H**-C--) and 5.41 ppm (2H, -O-C**H$_2$**-C--). The formation of the final product [**3**] was confirmed in ^{1}H-NMR by the apparition of the singlet at approx. 5.3 ppm due to the proton of the triazine cycle formed. In the IR spectrum of [**3**], a band at 2970 cm^{-1} indicates the presence of protonated amines.

[119] F. Himo, T. Lovell, R. Hilgraf, V.V. Rostovtsev, L. Noodleman, K.B. Sharpless, V.V. Fokin, *J. Am. Chem. Soc.*, **2005**, *127*, 210-216.

Ionic-PAMAM dendrimers

In our case, the aim of using ionic PAMAM dendrimers is to decrease the toxicity of PAMAM dendrimers while maintaining their ability of forming electrostatical complexes with plasmid DNA. From this perspective, in order to obtain a simple system capable of self-assembling in water and form stable complexes with plasmid DNA, four ionic derivatives of PAMAM (**-NH_2**) modified by 2-(2-(2-methoxyethoxy)ethoxy)acetic acid (**-COOH**) were synthesized and studied (Figure 27).

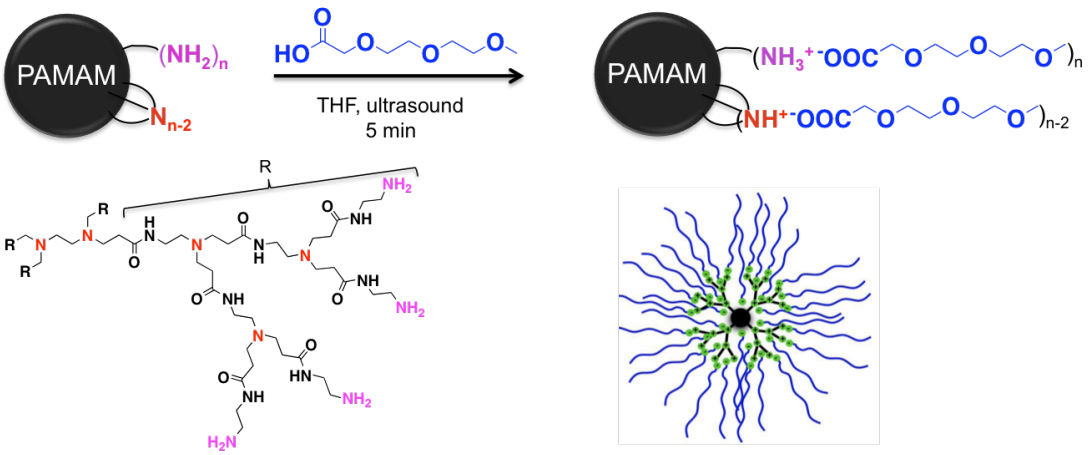

Figure 27: Synthesis of ionic-PAMAM dendrimers.

We chose to work with the second and fifth generations PAMAM dendrimers (Table 1) in order to compare the influence of the dendrimer size in the DNA condensation process. For each of the generations, two products were prepared: for one of them, only the surface primary groups were functionalized with 2-(2-(2-methoxyethoxy)ethoxy)acetic acid; for the other one, also the tertiary amine groups present in the inner part of the dendrimer (in red in Figure 27) were functionalized. These dendrimers are called **2G-IP-16**, **2G-IP-30**, **5G-IP-128** and **5G-IP-254**: 2G and 5G indicate the generation of the dendrimer, IP means ionic-PAMAM and 16-30-128-254 designate the theoretical number of amine groups functionalized by 2-(2-(2-methoxyethoxy)ethoxy)acetic acid.

	2G PAMAM	5G PAMAM
Molecular weight	3256	28826
Inside amine groups **N**	14	126
Surface amine groups NH_2	16	128
Total amine groups **N**+ NH_2	30	254

Table 1: Structural parameters of G2 and G5 PAMAM dendrimers.

The ionic compounds were synthesized by a procedure previously described,[120] following the method of Crooks.[121] The corresponding acid in the accurate stoichiometry was added to a solution of the appropriate PAMAM dendrimer. The mixture was ultrasonicated for 5 minutes. The solvent (THF) was slowly evaporated at room temperature and the products were dried under reduce pressure.

To confirm the formation of the ammonium-carboxylate salts in the materials, IR and NMR techniques were used.

IR spectrums analysis:

In the case of the compound **2G-IP-30**, the appearance of two bands due to the asymmetric and symmetric stretching modes of the carboxylate groups at 1550 and 1390 cm^{-1} confirmed the formation of the ionic salt (Figure 28). A small band at 1690 cm^{-1} suggests the presence of free acid.

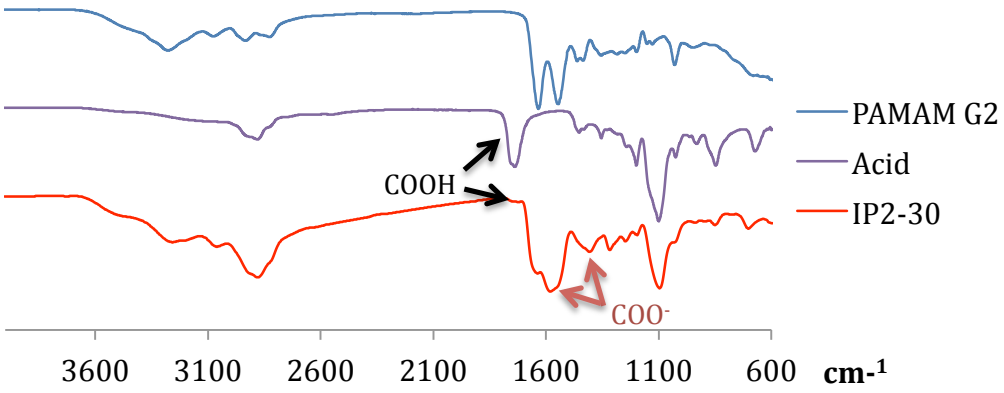

Figure 28: FT-IR spectrum of IP2G30 (red) compared to the one of the acid (violet) and PAMAM G2 (blue).

[120] R. Martin-Rapún, M. Marcos, A. Omenat, J. Barberá, P. Romero, J.L. Serrano, *J. Am. Chem. Soc.,* **2005**, *127*, 7397-7403.

[121] V. Chechik, M. Zhao, RM. Crooks, *J. Am. Chem. Soc.,* **1999**, *121*, 4910-4911.

NMR spectrums analysis:

As an example for all the compounds, the NMR spectrums of the second generation derivative **2G-IP-30** will be described. The peaks will be attributed with red letters for the PAMAM and with blue letters for the acid (Figure 29).

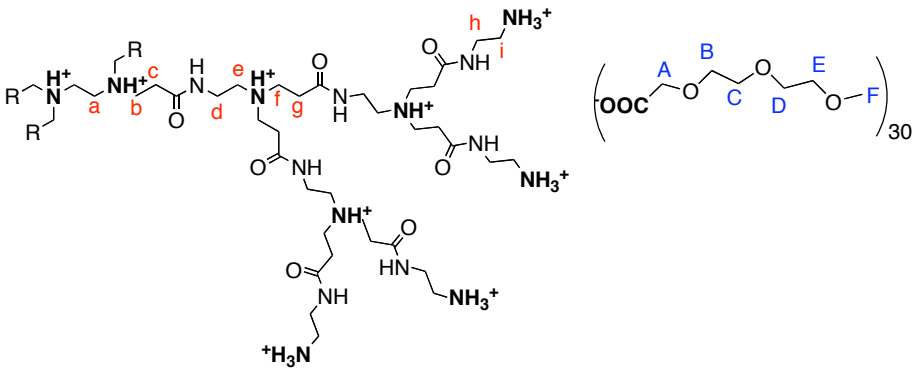

Figure 29: IP2-30 molecule, with characteristic peaks in ^{1}H NMR.

In ^{1}H-NMR spectrum, the shift of the signal from 3.26 ppm ($NHC\underline{\mathbf{H}}_2CH_2NH_2$) to 3.49 ppm ($NHC\underline{\mathbf{H}}_2CH_2NH_3^+$, H_h) and the displacement proton from 2.74 ppm ($NHCH_2C\underline{\mathbf{H}}_2NH_2$) to 3.08 ppm ($NHCH_2C\underline{\mathbf{H}}_2NH_3^+$, H_i) reveals the ammonium salt formation of the surface amine groups. Furthermore, signals corresponding to the protons attached to the carbonyl groups ($C\underline{\mathbf{H}}_2$-COOH) at 4.12 ppm are found at lower shift in the carboxylate groups, ($C\underline{\mathbf{H}}_2$-$COO^-$, H_A) at 3.97 ppm.

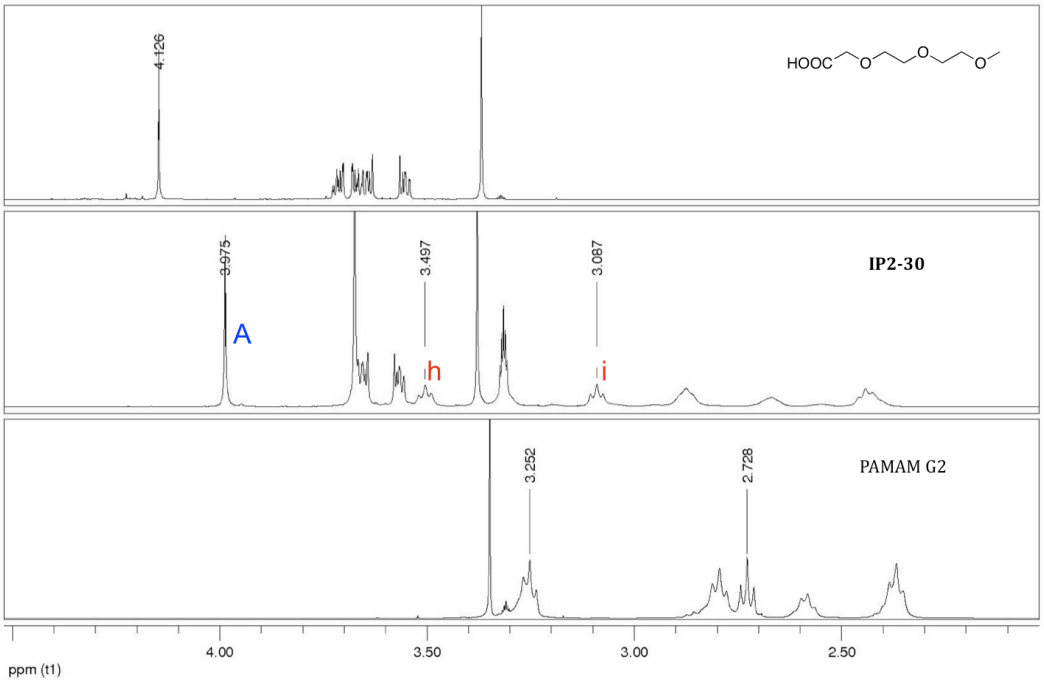

Figure 30: ^{1}H-NMR spectrums (400 MHz, MeOD) of acid (up), PAMAM G2 (down) and 2G-IP-30 (middle).

^{13}C-NMR experiments reveal the deprotonation of the carboxylic acid with the displacement of the signal corresponding to the C_{α} to carbonyl group in the acid (C**H$_2$**-COOH) from 69.0 ppm to 71.2 ppm in the dendrimer (C**H$_2$**-COO$^-$, C_A). Moreover, a shift of the signal of the carbon corresponding to the carbonyl can be observed: from 174.0 ppm for the carbon corresponding to the carboxylic acid (COOH) to 177.1 ppm for the carbon corresponding to the carboxylate (COO$^-$).

The protons and carbons were assigned using HSQC (Figure 30), HMBC and COSY experiments.

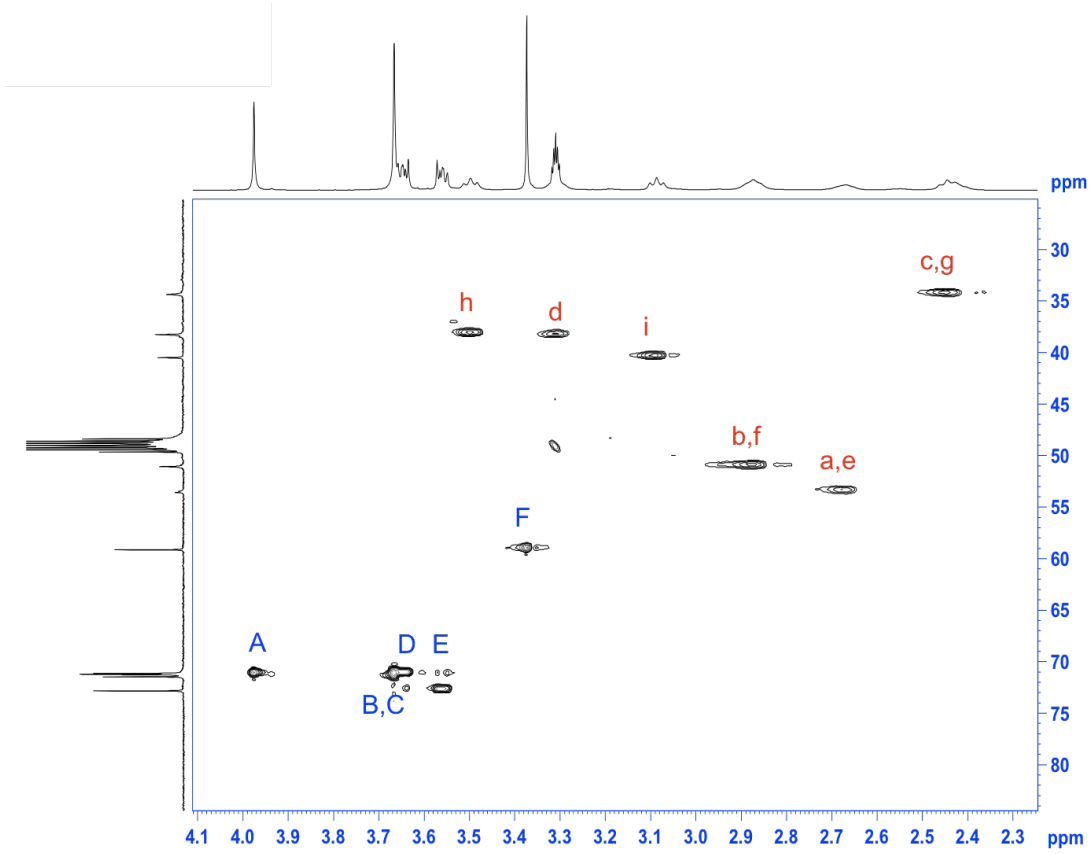

Figure 31: HSQC NMR spectrum of the compound 2G-IP-30.

Ionic bis-MPA dendrimer: IbisMPA

The second generation of *bis*-MPA dendrimer **[2]** was used as starting material and treated as previously explained to obtain the corresponding ionic dendritic derivative **I*bis*MPA** (Figure 32).

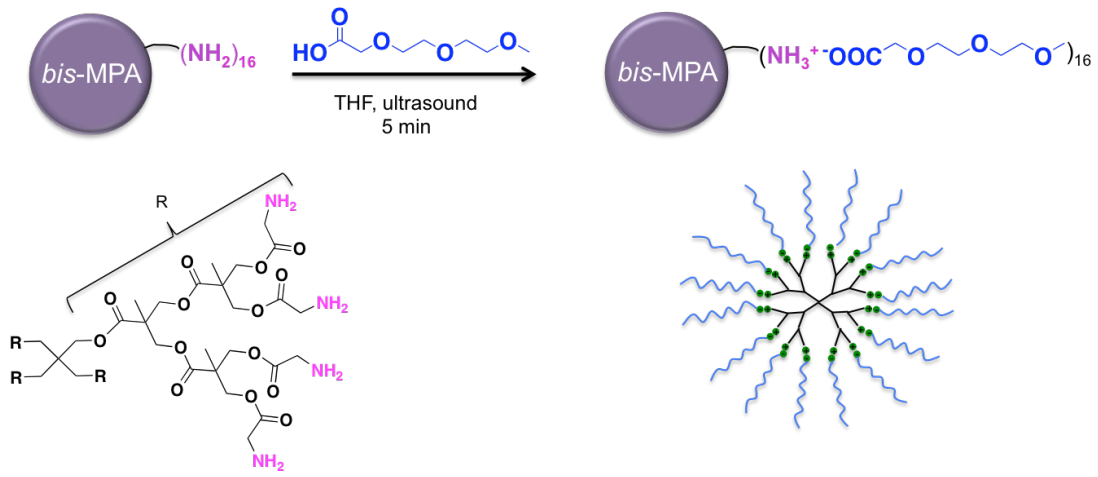

Figure 32: Synthesis of the ionic *bis*-MPA dendrimer (I*bis*MPA).

The comparison of the IR spectrums of the acid, the dendrimer **[3]** and the ionic dendrimer **I*bis*MPA** is shown in Figure 33. We can observe the apparition of a band at 1650 cm^{-1} corresponding to the carboxylate (υ OCO^-), and of a band at approx. 3450 cm^{-1} corresponding to the protonated amines (υ NH_3^+).

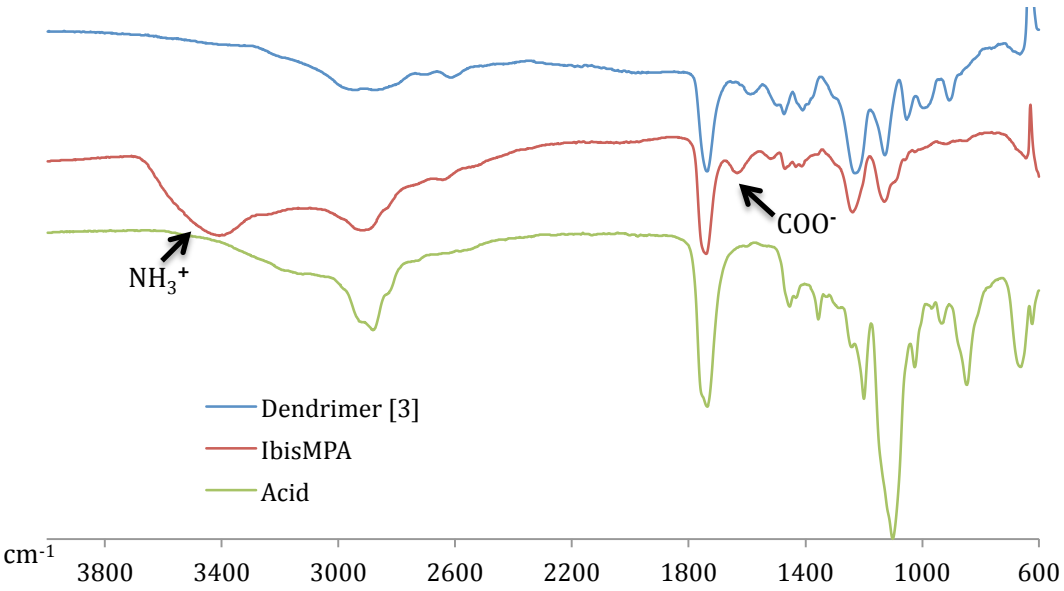

Figure 33: FT-IR of I*bis*MPA (in red), and its precursors (in blue and green).

The NMR study also gives us some evidence about the formation of the ionic compound (structure in Figure 34). The deprotonation of the carboxylic acid is demonstrated in ^{13}C-NMR, by the displacement of the signal du to the carbon in alpha of the carbonyl group of the acid (**C**H$_2$-COOH) from 69.1 ppm to 69.3 ppm for the dendrimer (**C**H$_2$-COO$^-$, C$_A$). Furthermore, a shift of the signal corresponding to the carbon of the carbonyl is observed from 174.0 for the acid (COOH) to 174.5 for the carboxylate (COO$^-$).

Although the displacements of the signals in NMR are minor, the modification of the dendrimer was confirmed by the great change in its properties (see Complexion studies).

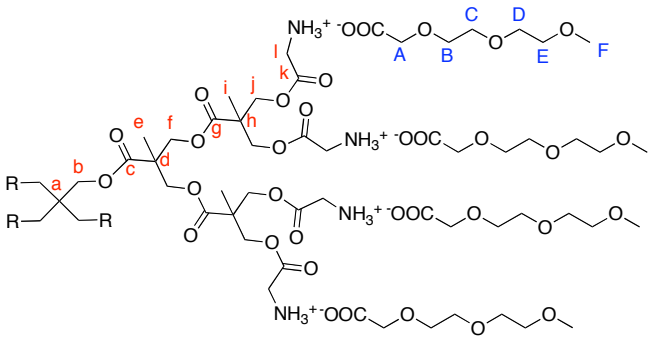

Figure 34: Structure of I*bis*MPA.

Biodegradation assays of *bis*-MPA derivatives

The degradations in aqueous media of the dendron **[1]** and of the dendrimer **[2]** were studied by mass spectroscopy following the method of Fadeel and co-worker.[122] Briefly, the products were dissolved in an aqueous buffer solution (0.1 M) at various pH: 3, 5, 7 and 9 and kept at 37°C. An aliquot of the dissolutions was taken at specific times for analysis by MALDI-TOF MS.

We observed that, as expected, the pH had a great influence on the degradation. At alkaline pH the ester bonds were hydrolysed much faster than at acidic pH. In all cases, the first degradation observed was a lost of glycine (-57 um), followed by the lost of all the glycine fragments. Then, the dendron was cleaved at the ester bonds of the *bis*-MPA (lost of 116 um) (Figure 35). The same process was observed for the dendron **[1]** and for the dendrimer **[2]**.

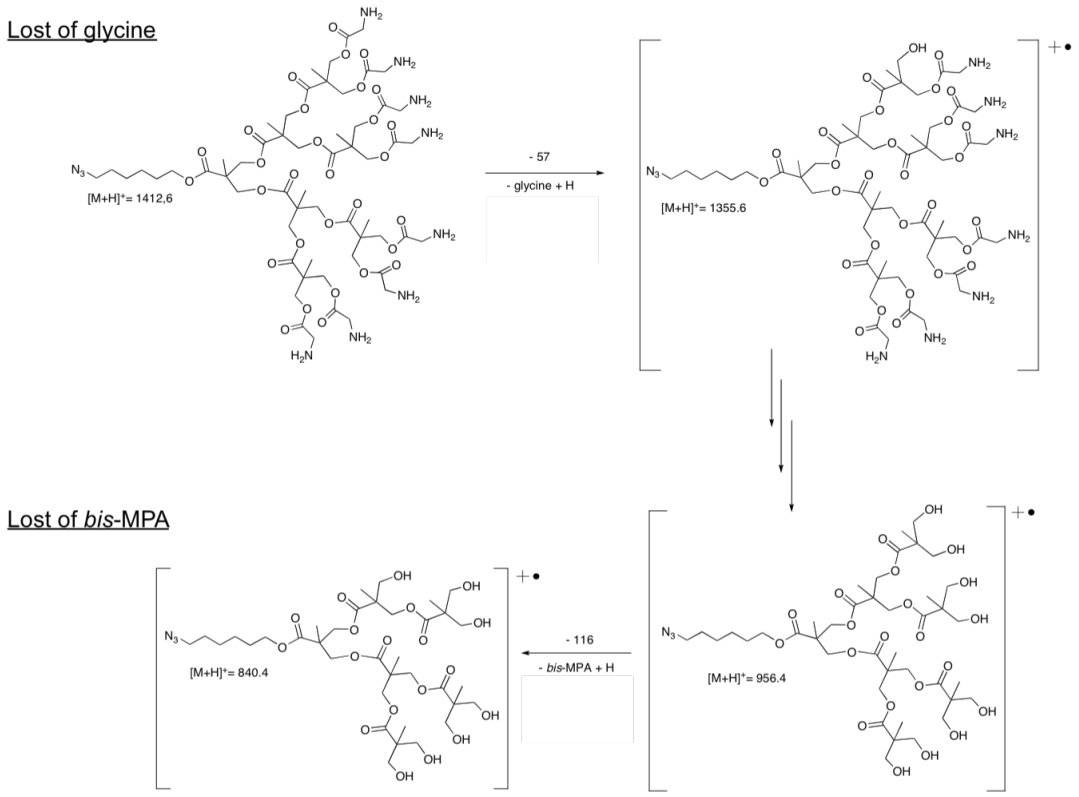

Figure 35: Scheme of dendron degradation.

[122] N. Feliu, M.V. Walter, M.I. Montañez, A. Kunzmann, A. Hult, A. Nyström, M. Malkoch, B. Fadeel, *Biomaterials*, **2012**, *33*, 1970-1981.

In the following Table 2 are reassembled the data of degradation: time of first lost of glycine, time of first lost of *bis*-MPA monomer.

Compound	pH[1]	Lost of glycine[2]	Lost of *bis*-MPA monomer[3]
Dendron [1]	3	1h	> 5 days
	5	1h	> 5 days
	7	1h	> 5 days
	9	1h	1 day
Dendrimer [2]	7	1h	> 5 days

Table 2: Summary of degradation results. [1]pH of the dissolution. [2]Time at which the beginning of the degradation could be observed by the lost of one glycine moiety. [3]Time at which the first lost of a *bis*-MPA monomer moiety was observed.

In the Figure 36, we can see an example of the degradation of the dendron **[1]** observed at pH 7 (100 mM). At t = 0 is represented the spectrum of the product immediately taken after dissolution, and then after different times at 37°C. After one hour, we can already observe a degradation of the dendron. The molecular peak has disappeared and we can see the appearance of the peaks corresponding to the lost of one or various glycine moieties (G). After 5 days, the degradation seems to have stopped to the "nude" dendron with hydroxyls groups.

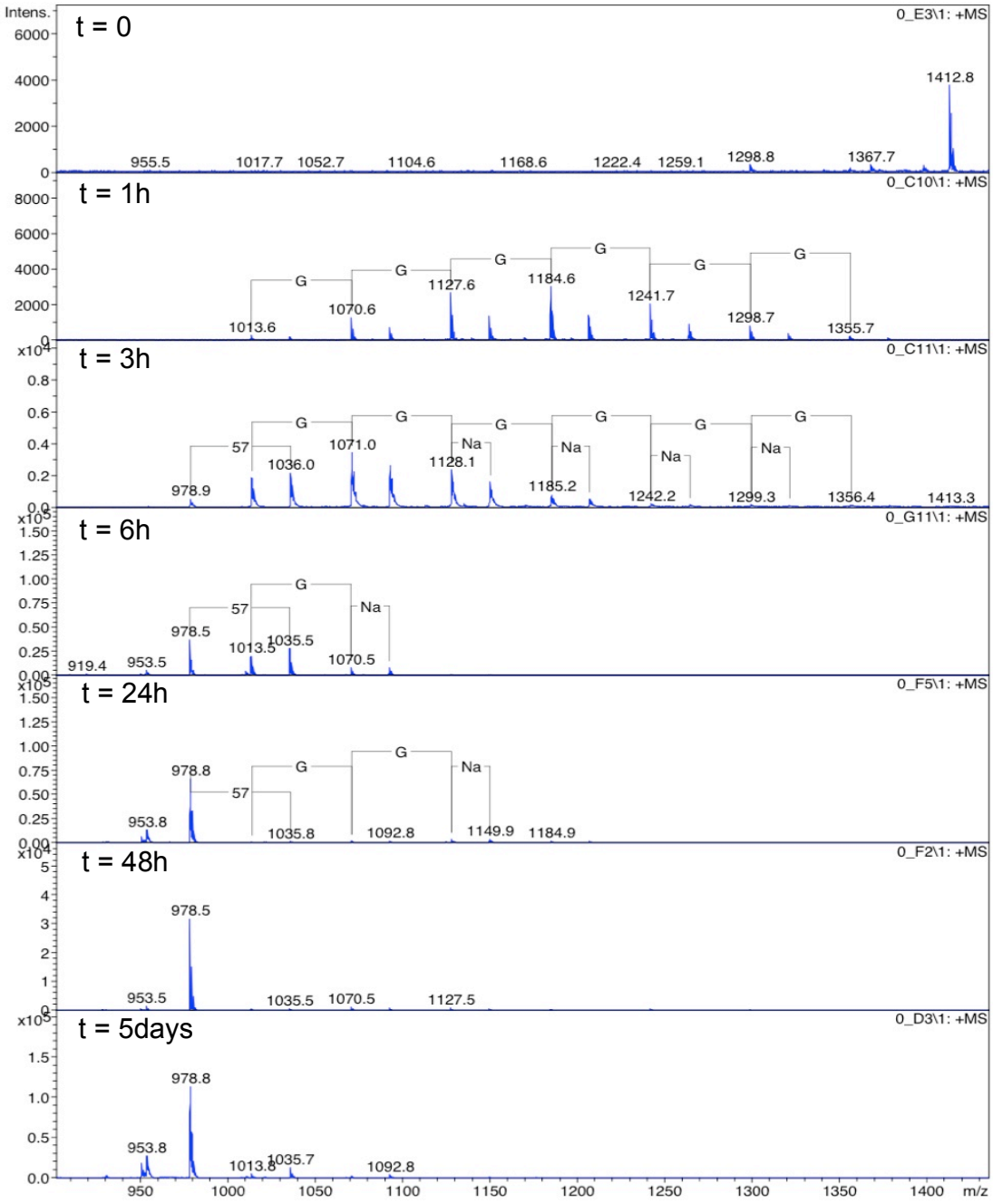

Figure 36: Mass spectrums of dendron [1] after different times of incubation at pH 7 (0.1M).

The results obtained have confirmed that dendritic derivatives composed of *bis*-MPA monomers assembled by ester bonds are sensitive to pH. These compounds result to be more stable in acid environment. Consequently, to work with these products is it important to take into account the pH (<7) and the temperature to limit the degradation. To avoid the degradation the best option is

to keep the products at the penultimate step of the synthesis, with the amines groups protected as -NHBoc, and carry out the last step just before using them.

Cell viability

There are various assay methods for evaluating the cytotoxic effects of chemical on cultured cells. The crystal violet staining (CVS) assay is a simple and reproducible assay of cytotoxicity.[123] This assay is based on the growth rate reduction reflected by the colorimetric determination of the stained cells.

The cell viability of *bis*-MPA derivatives and ionic-PAMAM dendrimers was tested on two cell lines, on mesenchymal stem cells (bMSCs mouse bone marrow stromal stem cells) and in a cancerous cell line (U251MG glioma cells). Mesenchymal stem cells or MSCs are multipotent stem cells that can differentiate into a variety of cell types. The cell viability was studied on these kinds of cells (cancerous and mesenchymial) because they are ones of the targets for gene delivery. For the treatment of cancers in the first case, and in the second case, because MSCs can be used as cellular vectors for cell therapy as explain briefly in the introduction.

[123] a) H. Itagaki, S. Hagino, S. Kato, M. Umeda*, Toxicol. in vitro,* **1991**, *5*, 139-143; b) K. Saotome, H. Morita, M. Umeda, *Toxicol. in vitro,* **1989**, *3*, 317-321.

bis-MPA derivatives [1], [2] and [3]

In the following graphics (Figure 37) are represented the cell viability results obtained with the ***bis*-MPA** dendritic derivatives at 1mM on U251MG cells and MSCs. The cell viability was tested after one to three days of incubations of the cells with the compounds.

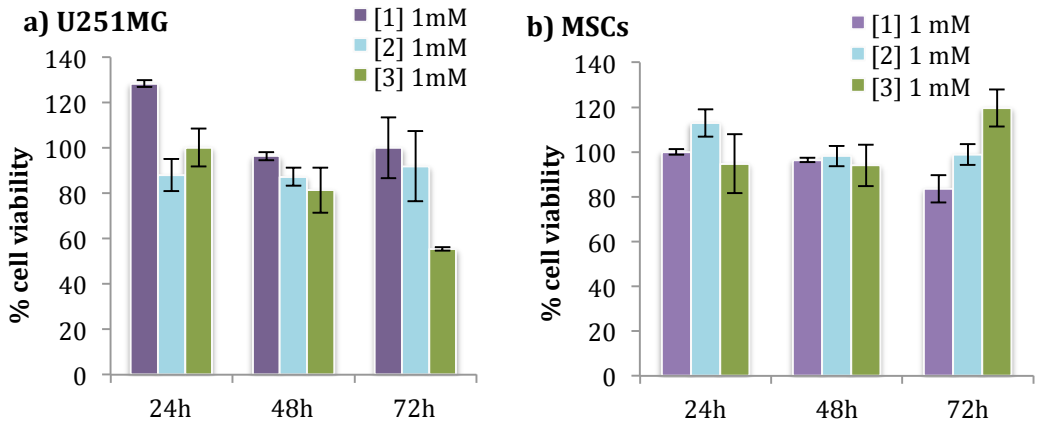

Figure 37: U251MG and MSCs cell viability at 1mM as a function of time for the dendritic derivatives [1] in purple, [2] in blue and [3] in green.

In the case of the dendron **[1]**, at 24h of incubation with the U251MG cells (Figure 37a), the cell viability was higher than 100 % (128%) meaning that the cells grow faster with the compound than without it. At 48h and 72h, no effect of the compound was observed; the cells were growing as the control. The dendrimer **[2]** had no significant cytotoxic effect on the cells. The dendritic-linear-dendritic derivative **[3]** presented toxicity after 3 days of incubation, with a cell viability under 60 %.

In the case of the MSCs, all the compounds presented cell viability higher than 80 % at 1mM, from 24h to 72h of incubation with the cells (Figure 37b).

The cell viability of **[3]** was tested at lower concentrations (Figure 38), and we could observe a decrease of the toxicity of the compound with the concentration until it was negligible at 0.125 mM.

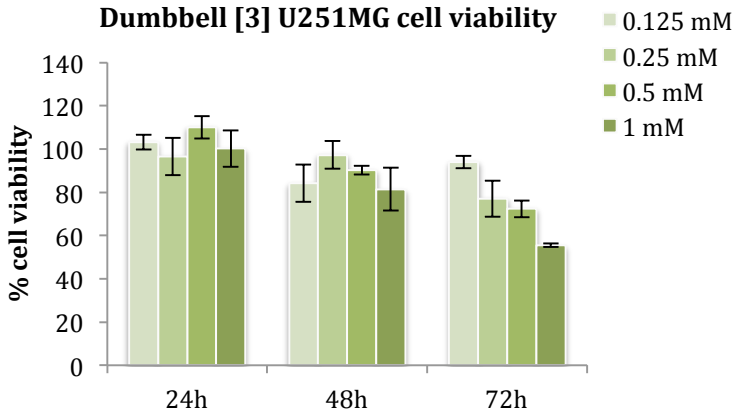

Figure 38: Cell viability of dendritic-linear-dendritic derivative [3] with U251MG cells at concentrations from 0.125 mM to 1 mM.

In the Table 3, the concentrations at which the dendritic derivatives presented no cytotoxicity for both cell type are converted in mg/mL.

Derivative	Dendron [1]	Dendrimer [2]	Dumbbell [3]
mM[a]	1	1	0.125
mg/mL[b]	1.70	3.02	2.04

Table 3: Concentrations of *bis*-MPA derivatives expressed in mg/mL and mM. [a]Concentration of the compounds in mM (µmol/mL). [b]Relative concentration of the compounds in mg/mL.

All the compounds presented good cell viability results at concentrations superior to 1 mg/mL (see Table 3).

Ionic derivatives 2G-IP-30, 2G-IP-16, 5G-IP-254, 5G-IP-128 and IbisMPA

The study was realized at concentrations of 0.5 mg/mL and below because the toxicity of the ionic PAMAM dendrimers was expected to be superior to the one of the previous *bis*-MPA derivatives. In the Table 4, the concentration of the products in mg/mL is converted in nmol/mL (µM) to facilitate the analysis of the results.

Compounds	0.5 mg/mL[a]
IP5-254	6.8 µM[b]
IP5-128	9.7 µM[b]
IP2-30	58.1 µM[b]
IP2-16	81.9 µM[b]
I*bis*MPA	94.4 µM[b]

Table 4: Concentrations of the ionic derivatives expressed in mg/mL and mM. [a]Concentration of the compounds in mg/mL. [b]Relative concentration of the compounds in µM (nmol/mL).

In the Figure 39 the results of cell viability obtained incubating the ionic derivatives of PAMAM dendrimers with MSCs and U251MG at a concentration of 0.5 mg/mL are represented.

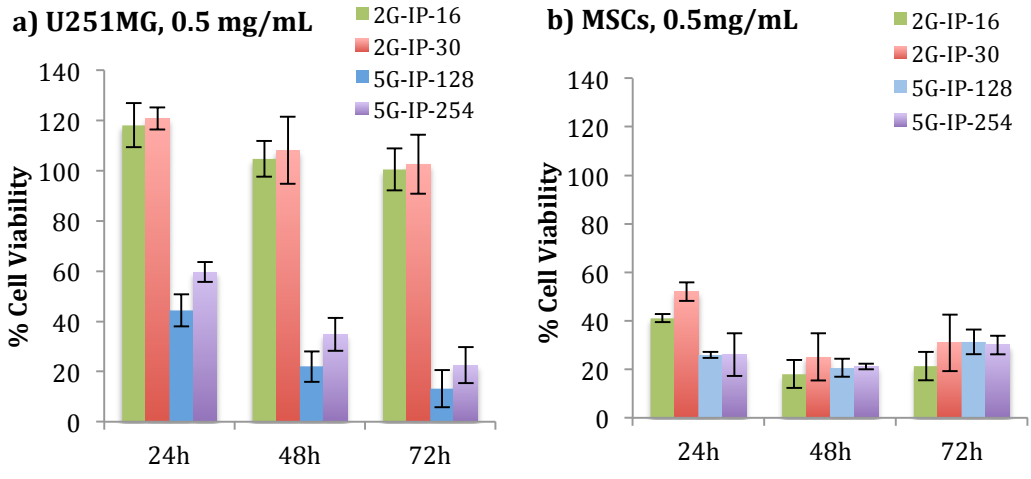

Figure 39: Cell viability with ionic-PAMAM derivatives incubated with U251MG cells and MSCs at 0.5 mg/mL for 24h to 72h.

These compounds were found to be more toxic than the derivatives of *bis*-MPA previously described. In the case of U251MG cells, only the G2 compounds were found to be non-toxic at 0.5 mg/mL. The G5 derivatives showed low cell viability after three days: between 20 % and 40 %. With mesenchymial cells, all the derivatives showed toxicity: between 20 % and 40 % of cell viability. The dendrimers of second generation were less toxic for U251MG cells (no toxicity found) than for mesenchymial cells (between 20 % and 30 % of cell viability).

The cell viability tests with the compounds of fifth generation were repeated at lower concentrations (Figure 40), from 62.5 µg/mL to 500 µg/mL. A difference of toxicity between the two products was observed; the dendrimer totally functionalized being the less toxic, especially at low concentrations. The difference of toxicity between the two cell lines is also remarkable; the compounds were less toxic for mesenchymial cells than for U251MG cells.

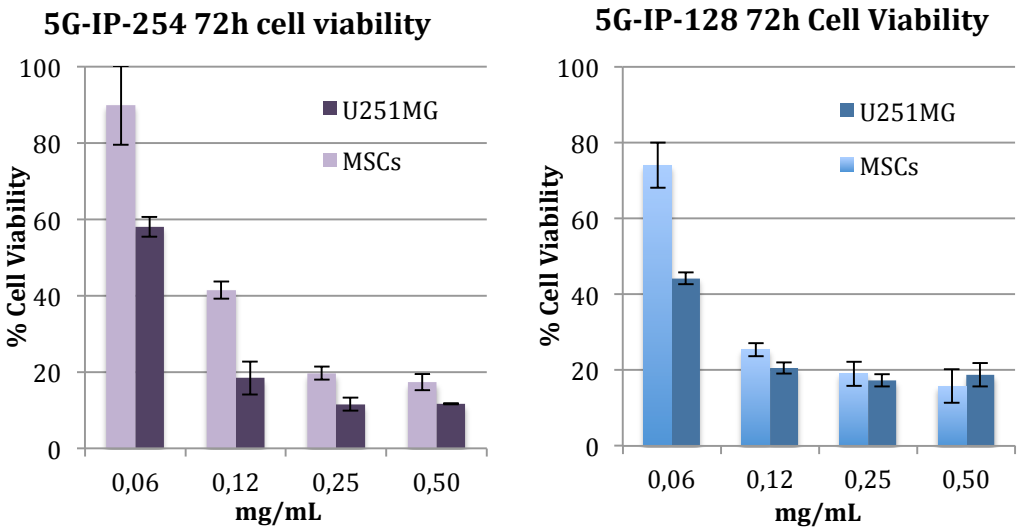

Figure 40: Cell viability results of U251MG cells and MSCs incubated with IP5-254 and IP5-128 during 72h.

The cell viability of **I*bis*MPA** was tested at concentrations up to 1 mg/mL (Figure 41).

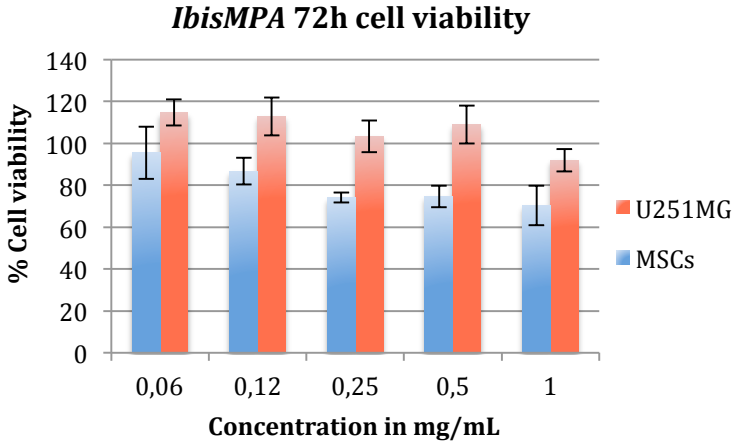

Figure 41: Cell viability results of MSCs and U251MG cells incubated with I*bis*MPA.

The ionic *bis*-MPA dendrimer was found to be less toxic than the ionic derivatives of PAMAM.

The first comment that we can make is that the ionic compounds of PAMAM are much more toxic than the derivatives of *bis*-MPA, even after their ionic functionalization by 2-(2-(2-methoxyethoxy)ethoxy)acetic acid. Both ionic compounds of PAMAM of fifth generation, **5G-IP-128** and **5G-IP-254**, presented poor cell viability from a concentration of 0.125 mg/mL in both cell lines, meanwhile the derivatives of second generation are less toxic, overall for U251MG cells.

The most interesting ionic compound in terms of cell viability is the derivative of *bis*-MPA: **I*bis*MPA**. Up to 1 mg/mL concentration (189 µM), its cell viability is superior to 60%.

For all the compounds, the cell viability varies considerably between the two cells (MSCs and U251MG). In the case of **I*bis*MPA**, we can observe a difference of approx. 20% of cell viability between the two cell lines, the compound being less toxic for U251MG cells. In the case of the ionic derivatives of PAMAM of second

generation, we can make the same comment: no toxicity observed with U251MG, and an important one in the case of the MSCs (20 % to 30 % cell viability).

A difference of cell viability at 0.5 mg/mL is observable between the derivatives of PAMAM totally functionalized (**5G-IP-254** and **2G-IP-30**) and the ones partially functionalized (**5G-IP-128** and **2G-IP-16**), the partially functionalized compounds presenting less toxicity.

For future studies of PAMAM ionic derivatives, it might be interesting to functionalize these compounds only at there periphery with a longer ethylene glycol chain in order to reduce their toxicity, but short enough to allow the amine groups of the dendrimers to interact with the phosphate groups of the nucleic acids.

Complexion studies

The complexion studies were carried out with two DNA plasmids (pDNA) of different sizes. The first one is a small plasmid of 4733 bp wearing green fluorescent protein: **pGFP**. The second one is a bigger plasmid, extracted from an adenovirus: **pAd**. We choose to work with these two plasmids to find out how the size could influence the complexion by our dendritic derivatives. Furthermore, the pGFP can be used easily for transfection assays as its presence is revealed by fluorescence.

The ability of the dendritic derivatives to form electrostatic complexes with DNA was verified by agarose gel electrophoresis retardation assays. Plasmid DNAs and the different compounds were incubated in TBE buffer during 30 minutes before running the gel. Derivatives/DNA interactions are shown by the lack of migration of DNA in the electrophoretic field. Ratios are expressed in weight of DNA/weight of dendritic derivatives.

The efficiency of the compounds to form complexes with pDNA will be compared in terms of N/P ratio at which all the pDNA is forming electrostatic interactions with the dendritic compounds. When no migration of pDNA is observed in the gels, the accurate ratio dendrimer/DNA is reached. The N/P ratio represents the molar ratio between the protonable amine groups present in the dendritic molecule and the anionic phosphate groups present in the pDNA.

bis-MPA derivatives

As we can see in the Figure 42 to Figure 44, electrostatic interactions between the nucleic acids phosphates and the amines of the derivatives occurs in all the cases.

In the first well of the gels free DNA is dropped off and its migration on the gel can be observed. When the ratio of dendrimer/DNA is increased, no more migration is observed: the gel retains the complex formed.

In the case of the dendron **[1]**, Figure 42, the accurate ratio is obtained when the quantity of dendron is 80000 times higher than the pGFP (in weight), and 1000 times higher than the pAd.

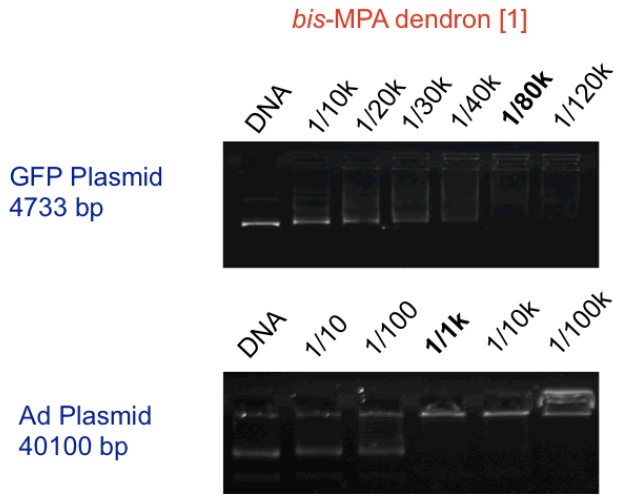

Figure 42: Picture of the agarose gel electrophoresis retardation assay realized with the *bis*-MPA dendron [1] incubated with pGFP and pAd.

In the case of the dendrimer **[2]**, Figure 43, the accurate ratio is obtained when using the same w/w ratios than for dendron **[1]**.

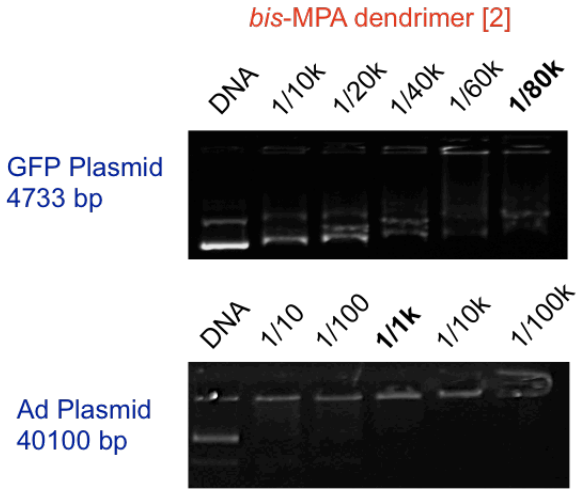

Figure 43: Picture of the agarose gel electrophoresis retardation assay realized with the *bis*-MPA dendrimer [2] incubated with pGFP and pAd.

Finally, in the case of the pluronic derivative **[3]**, Figure 44, the correct ratio is obtained when the quantity of compound is 6000 times higher than the pGFP, and 10000 times higher than the pAd.

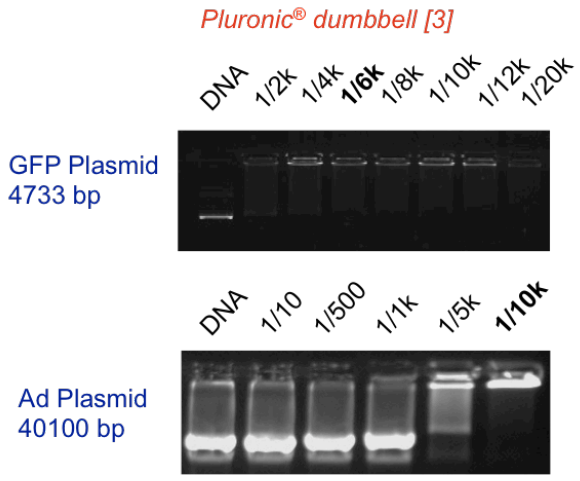

Figure 44: Picture of the agarose gel electrophoresis retardation assay realized with the *bis*-MPA derivative [3] incubated with pGFP and pAd.

In the following table, the w/w DNA/dendrimer results are resumed and expressed also in terms of N/P ratios.

	[1]	[2]	[3]
MW	1412 Da	2442 Da	16033 Da
pGFP	1:80k w/w **125196 N/P**	1:80k w/w **16161 N/P**	1:6k w/w **1975 N/P**
pAd	1:1k w/w **1568 N/P**	1:1k w/w **2222 N/P**	1:5k w/w **1616 N/P**

Table 5: Results obtained with the bis-MPA derivatives in terms of w/w DNA/dendrimers ratio, and in terms of N/P ratio. MW(pGFP)=3.12 10^6 Da, MW(pAd) = 24.06 10^6 Da.

In the case of the small plasmid, **pGFP**, the dumbbell derivative is the most efficient although the N/P ratio needed to complex all the pDNA is high. With **pAd**, the quantity of dendron **[1]** and dendrimer **[2]** needed is much lower. This reveals that this kind of small dendrimers would be more indicated as vectors of a "big" plasmid than as vectors of a "small" one. The dumbbell derivative **[3]** seems to have a similar efficiency with both pDNA.

As conclusion, all these three *bis*-MPA dendritic derivatives are able to form complexes with plasmid DNA of different sizes, at different ratios. However, the N/P ratios are not very satisfying.

Ionic-PAMAM derivatives

The second generation and fifth generation of ionic-PAMAM derivatives, fully functionalized or partially functionalized were studied. The dendrimers partially functionalized were modified only at their periphery. The results were compared with the ones obtained with commercial PAMAM dendrimer with terminal amine groups without modification (Figure 45).

Ratios DNA/dendrimer	O	A	B	C	D	E
	Free DNA	1/10 000	1/1 000	1/100	1/10	1/1

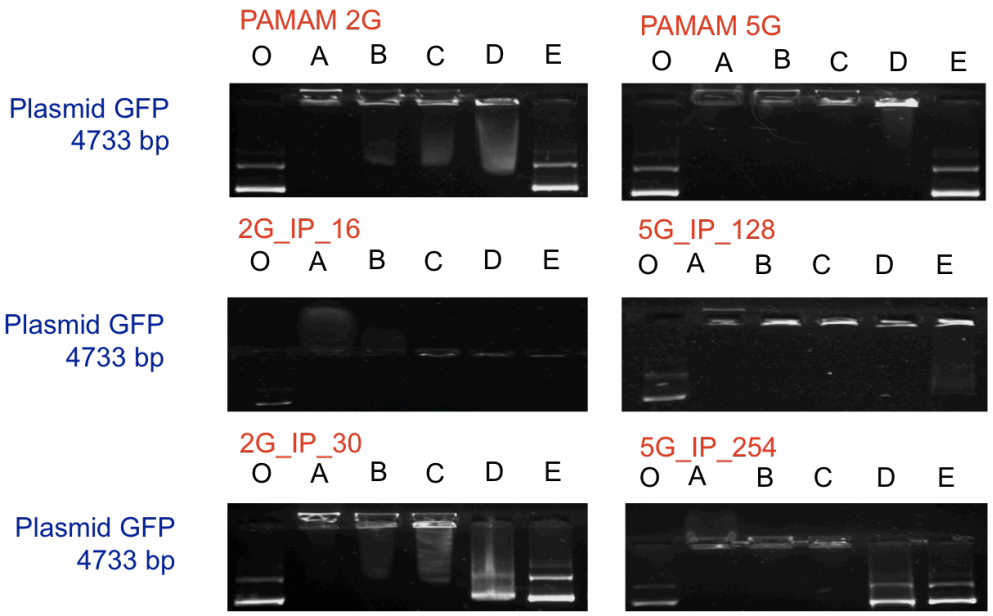

Figure 45: Agarose gel electrophoresis retardation assay DNA/Ionic-PAMAM dendrimers. Ratios are expressed in weight of DNA per weight of Ionic-PAMAM derivative.

As we can see in the Figure 45, ionic-PAMAM derivatives are good candidates for forming interactions with pGFP. In the case of the derivatives partially functionalized, the results obtained are even better that for PAMAM dendrimers of the same generation. In the case of the derivatives totally functionalized, they showed less complexion capability but still good results with ratios of about 1/10.

In the Figure 46, the pictures of the gel retardation assays carried out with the pAd are represented.

Ratios DNA/dendrimer	O	A	B	C	D	E
	Free DNA	1/10 000	1/1 000	1/100	1/10	1/1

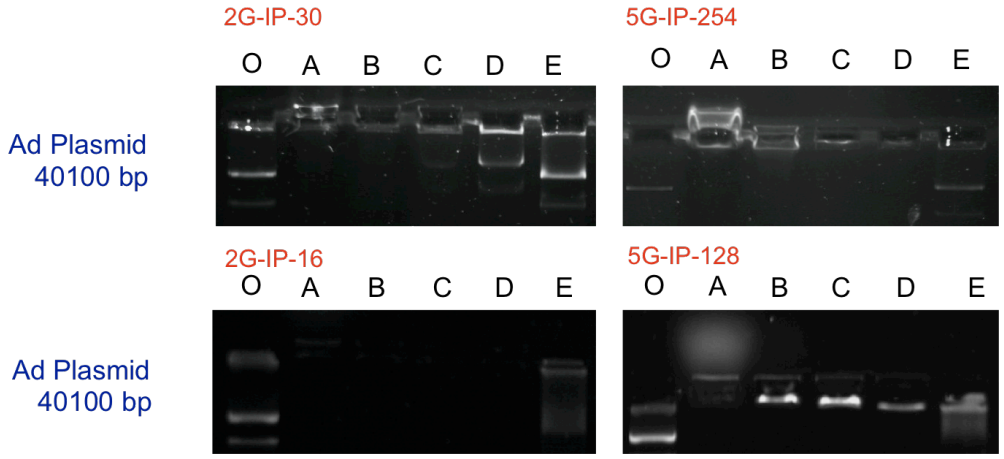

Figure 46: Gel retardation assays of ionic-Pamam dendrimers complexes with pAd.

In the Table 6, we can see that the compound of second generation **2G-IP-30** seems to be of equal efficiency with the pAd and pGFP. The compound of fifth generation **5G-IP-254** presented better results with the pAd, with a N/P ratio of 11. In the case of the dendrimer partially functionalized **2G-IP-16**, the results are better with pGFP, N/P ratio of 0.9, than with the pAd, N/P ratio of 8.7. The results obtained with the compound **5G-IP-128** are the same with both DNA plasmids, an N/P ratio of 8.3 is necessary to complex all the DNA. As with the GFP plasmid, the best results were obtained with the dendrimers partially functionalized 2G-IP-16 and 5G-IP-128.

	2G PAMAM	5G PAMAM	2G-IP-16	2G-IP-30	5G-IP-128	5G-IP-254
MW	3256 Da	28826 Da	6107 Da	8601 Da	51623 Da	74063 Da
pGFP	1:10 w/w **16 N/P**	1:10 w/w **13.3 N/P**	1:1 w/w **0.9 N/P**	1:100w/w **116 N/P**	1/10 w/w **8.3 N/P**	1/100 w/w **114 N/P**
pAd			1:10 w/w **8.7 N/P**	1:100w/w **116 N/P**	1:10 w/w **8.3 N/P**	1:10 w/w **11 N/P**

Table 6: Results obtained with the ionic-PAMAM derivatives in terms of w/w DNA/dendrimers ratio, and in terms of N/P ratio. MW(pGFP)=3.12 10^6 Da, MW(pAd) = 24.06 10^6 Da.

We observed that the partially functionalized dendrimers are more efficient than the fully functionalized ionic-PAMAM dendrimers to complex the DNA plasmids used. They resulted to be even more efficient that the commercial PAMAM dendrimers without being functionalized in the case of the pGFP. The N/P ratio results obtained with the dendrimers are similar working with the second generation or with the fifth generation in the case of the pGFP while with pAd better results were obtained working with the fifth generation, overall for the totally functionalized compounds.

Ionic bis-MPA dendrimer

The efficiency of **I*bis*MPA** dendrimer was compared to the one of the PAMAM ionic dendrimer **2G-IP-16** in Figure 47. The compound derived from PAMAM is able to form complexes with DNA at lower w/w ratios.

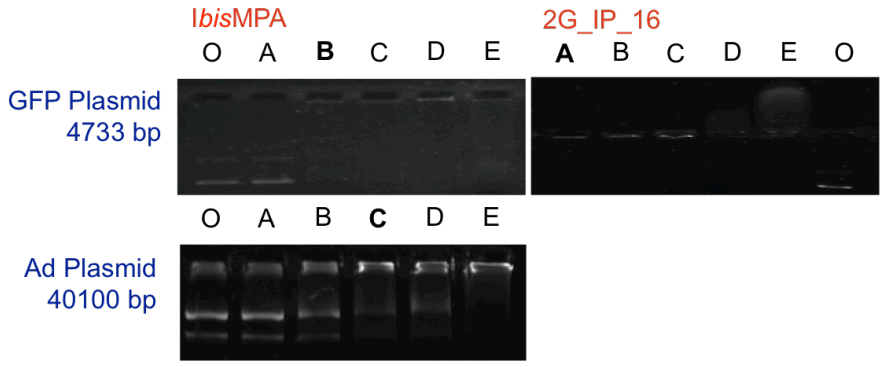

Ratio DNA/dendrimer w/w

O	A	B	C	D	E
Free DNA	1/1	1/10	1/100	1/1000	1/10 000

Figure 47: Gel retardation assays of ionic-bisMPA dendrimer complexes with Ad-Plamid and GFP-plasmid.

In the Table 6, the results in terms of DNA/dendrimer ratios were expressed. Functionalizing the dendrimer **[2]** to obtain the ionic dendrimer **I*bis*MPA** allowed to improve tremendously the interactions between the nucleic acids and the compound. The N/P ratios obtained with the **I*bis*MPA** dendrimer are approx. ten times higher than the one obtained for the **2G-IP-16** dendrimer, for the both DNA plasmids studied.

	[2]	I*bis*MPA	2G-IP-16
MW	2442 Da	5293 Da	6107 Da
pGFP	1:80k w/w **16161 N/P**	1:10 w/w **10 N/P**	1:1 w/w **0.9 N/P**
pAd	1:1k w/w **2222 N/P**	1:100 w/w **100 N/P**	1:10 w/w **8.7 N/P**

Table 7: Results obtained with the bis-MPA derivative [1], IbisMPA and 2G-IP-16 in terms of w/w DNA/dendrimers ratio, and in terms of N/P ratio. MW(pGFP)=3.12 10^6 Da, MW(pAd) = 24.06 10^6 Da.

This compound presents simultaneously interesting results in terms of DNA complexion and in terms of cell viability.

Conclusions

All the compounds synthesized, four *bis*-MPA dendritic derivatives and four ionic-PAMAM dendrimers, were able to form complexes with plasmid DNA of different sizes. Ionic-PAMAM dendrimers are promising compounds because of their ability to highly complex plasmid DNA and their lower toxicity than PAMAM dendrimers without modifications. Nevertheless, the **I*bis*MPA** compound was found to be the most interesting one because of its low cytotoxicity and its high ability to complex DNA.

Future Work:

To confirm the results obtained, *in vitro* nucleic acids transfection assays are necessary.

To follow this work, different generation of ionic dendrimers based on *bis*-MPA could be prepared to value the generational effect on the complexion of nucleic acids. Furthermore, *bis*-MPA derivatives could be used to form self-assembling macromolecules.

In the case of the ionic PAMAM derivatives, the cytotoxicity could be improved modifying the molecule wearing the acid, for instance with a larger polyethylene glycol part.

Experimental part

General methods

All the products except specifications were purchased from Aldrich.

^{1}H-NMR and ^{13}C-NMR experiments were performed using a Bruker AVANCE 400 or using a Bruker AMX300 operating at 400 or 300 MHz and 100 or 60 MHz respectively. $CDCl_3$, MeOD, and D_2O were used as solvents, chemical shifts are given in ppm relative to TMS, and the solvent residual peak was used as internal standard.

MS analyses were performed using an ESI-ion-TRAP Bruker Esquire3000 plus spectrometer or Bruker MicroFlex for MALDI ionization.

Analysis elemental data were obtained using a Perkin Elmer 2400 series II microanalyser.

The infrared spectra of all the complexes were obtained with a Mattson Genesis II FTIR and JACSO FT/IR-4100 apparatus in the 400-4000 cm^{-1} spectral range in ATR mode, using KBr, nuyol or over NaCl cells.

Gels for retardation assay were revealed using a Syngene Gene Genius Bioimaging system device.

Synthesis of *bis*-MPA derivatives

As the same synthetic processes have been used for the preparation of several different compounds, the general procedures will be described and each compound will be referred to the appropriate method.

Typical procedure for Steglish esterification (A):

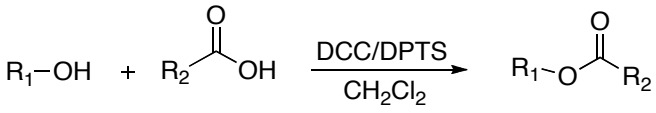

1 eq of the alcohol and 1.2 eq of the carboxylic acid were dissolved in dry dichloromethane with 0.4 eq of DPTS (per hydroxyl group to functionalize), under argon atmosphere. When the products were not totally soluble in dichloromethane, a few amount of dry dimethylformamide was added. After complete dissolution of the products, the flask was cooled to 0°C and 1.2 eq of DCC (per hydroxyl group to functionalize) in dry dichloromethane was added dropwise. The reaction mixture was stirred at room temperature and under argon atmosphere for 24 h. Then, the DCU formed was removed by filtration and the solvent evaporated to give the crude product, which was purified by column chromatography.

Typical procedure for deprotection of *bis*-MPA alcohol groups (B):

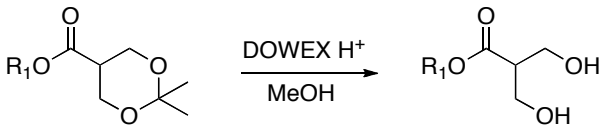

Before reaction, Dowex H^+ resin was washed with methanol and filtered. The protected product was dissolved in methanol and Dowex resin H^+ was added (dendron/Dowex 1:2 w/w). The reaction was allowed to stir at room temperature for 2 to 24 hours depending of the dendron generation. Then, the residue of Dowex

was filtered off and the solvent was evaporated under reduced pressure to give the pure product.

Typical procedure for deprotection of amine groups (C):

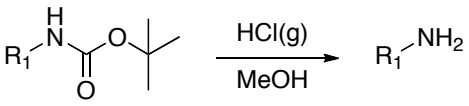

The product was dissolved in a solution of methanol or ethyl acetate saturated with hydrochloric acid (gaz) and was agitated for 10 minutes to 1 hour. The formation of a white precipitate was observed. The residue was concentrated and dried under reduce pressure to give the pure product as a pale yellow or white solid in a quantitative yield.

Typical procedure for dendrimer generation growth (D):

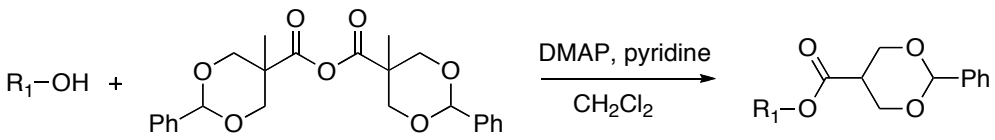

Pentaerythritol or G-1 dendrimer (1 eq) and DMAP (0.8 eq/OH) were dissolved in dry pyridine and then diluted with dry dichloromethane (1:3 v/v pyridine/dichloromethane). Solid *bis*-MPA anhydride (6 eq/OH) was added and the reaction mixture was allowed to stir at room temperature for 5 hours. The excess of anhydride was quenched by stirring the reaction mixture with 1:1 H_2O:pyridine solution overnight. The organic phase was diluted with 200 mL of CH_2Cl_2 and extracted with $NaHSO_4$ 1M (3 x 50 mL), Na_2CO_3 10% (3 x 50 mL) and brine (1 x 50 mL). The organic phase was dried over anhydrous $MgSO_4$ and the solvent evaporated to give the pure product as a white solid.

Typical procedure for deprotection of dendrimer OH groups (E):

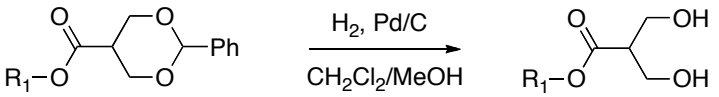

The protected dendrimer was dissolved in a few amount of dichloromethane and the solution was diluted with methanol. Pd/C 10% (20% in weight of dendrimer) was added to the solution and the reaction mixture was stirred under H_2 atmosphere (1 atm.) overnight. Then, the catalyst was filtered off over celite and washed with methanol. The solvent was evaporated to give the pure product as a white solid.

Isopropylidene-2,2-bis(methoxy)propionic acid (1-1)

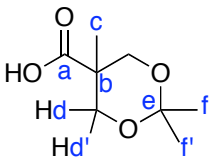

30.1 g (219.9 mmol) of commercial *bis*-MPA, 41.4 mL (330.0 mmol) of 2,2-dimethoxipropane and 2.30 g (11.9 mmol) of *p*-toluenesulfonic acid monohydrate were dissolved in 150 mL of dry acetone. The reaction mixture was stirred for 2 hours at room temperature. The catalyst was then neutralized using 3 mL of a NH_4OH (25 %)/EtOH (4:1) solution. The acetone was evaporated to give a white solid that was dissolved in 500 mL of EtOAc and extracted 3 times with 100 mL of water. The organic phase was dried over anhydrous $MgSO_4$ and the solvent was evaporated to give 30.9 g (177 mmol) of the pure product as a white solid in 81% yield.

NMR ^1H ($CDCl_3$, 400 MHz) δ (ppm): 1.21 (s, 3H, H_c), 1.42 (s, 3H, H_f), 1.45 (s, 3H, $H_{f'}$), 3.68 (d, *J* =12 Hz, 2H, H_d), 4.18 (d, *J* =12 Hz, 2H, $H_{d'}$).

NMR ^{13}C ($CDCl_3$, 400 MHz) δ (ppm): 18.4 (C_c), 21.8 (C_f), 25.3 ($C_{f'}$), 41.7 (C_b), 65.9 (C_d), 98.3 (C_e), 180.0 (C_a).

IR (cm^{-1}, Nujol): 3126 (COO-H st), 2854-2924 (C-H st), 1722 (C=O).

Calculated $[M]^+$ ($C_8H_{14}O_4$) m/z = 174.09. *Found:* ESI+: $[M+Na]^+$ m/z = 196.9.

6-azidohexan-1-ol

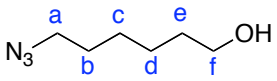

10.00 g (73 mmol) of 6-chlorohexan-1-ol were dissolved in 30 mL of DMF and 14.25 g (219 mmol) of NaN_3 were added. The reaction mixture was stirred at 140°C for 24 hours, and at room temperature for others 24 hours. 100 mL of Et_2O were added and the crude was extracted 3 times with 100 mL of water. The organic layer was dried over anhydrous $MgSO_4$ and the solvent was evaporated under reduced pressure. The crude product was purified by column chromatography eluting with Hexane/EtOAc 1:1 to give the pure product as a yellow liquid in a 84 % yield (8.79 g, 61 mmol).

NMR ^1H ($CDCl_3$, 300 MHz) δ (ppm): 1.35 (m, 4H, H_c, H_d), 1.56 (m, 4H, H_b, H_e), 1.96 (s, 1H, OH), 3.24 (t, J = 6.9 Hz, 2H, H_a), 3.6 (t, J = 6.6 Hz, 2H, H_f).

NMR ^{13}C ($CDCl_3$, 400 MHz) δ (ppm): 25.2 (C_d), 26.4 (C_c), 28.7 (C_b), 32.4 (C_e), 51.3 (C_a), 62.6 (C_f).

IR (cm^{-1}, KBr): 3339 (O-H st), 2861-2936 (C-H st), 2097 (N_3).

Calculated $[M]^+$ ($C_6H_{13}N_3O$) m/z = 143.11. *Found:* ESI+: $[M+Na]^+$ m/z = 166.0.

6-azidohexyl 2,2,5-trimethyl-1,3-dioxane-5-carboxylate (1-2)

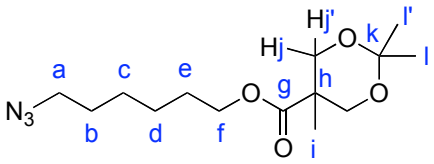

The product 1-2 was obtained by Steglish esterification (A) and purified by column chromatography eluting with dichloromethane. Yield: 66 %. Green oil.

NMR ^{1}H ($CDCl_3$, 400 MHz) δ (ppm): 1.17 (s, 3H, H_i), 1.37 (s, 3H, H_l), 1.39(m, 4H, H_c, H_d), 1.41 (s, 3H, $H_{l'}$), 1.60 (m, 4H, H_b, H_e), 3.25 (t, *J* = 6.9 Hz, 2H, H_a), 3.62 (d, *J* = 12 Hz, 2H, H_j), 4.13 (t, *J* = 6.3 Hz, 2H, H_f), 4.17 (d, *J* = 11.7 Hz, 2H, $H_{j'}$).

NMR ^{13}C ($CDCl_3$, 400 MHz) δ (ppm): 18.6 (C_i), 22.7 (C_l), 24.6 ($C_{l'}$), 25.4 (C_d), 26.3 (C_c), 28.4 (C_b), 28.7 (C_e), 41.8 (C_h), 51.3 (C_a), 64.6 (C_f), 66.0 (C_j), 98.0 (C_k), 174.2 (C_g).

IR (cm^{-1}, KBr): 2864-2939 (C-H st), 2096 (N_3 st), 1731 (C=O).

Calculated $[M]^+$ ($C_{14}H_{25}N_3O_4$) m/z = 299.18. *Found:* Maldi+: $[M+Na]^+$ m/z = 322.2.

(OH)$_2$-[G#1]-C$_6$H$_{12}$N$_3$ (1-3)

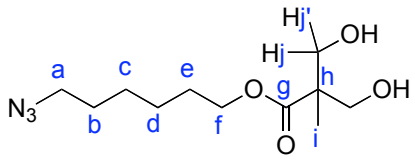

The product 1-3 was obtained by the deprotection method (B). Yield: 99 %. White solid.

NMR ^{1}H (CDCl$_3$, 400 MHz) δ (ppm): 1.05 (s, 3H, H$_i$), 1.40 (m, *J* = 3.6 Hz, 4H, H$_c$, H$_d$), 1.63 (m, 4H, H$_b$, H$_e$), 2.78 (s, 2H, OH), 3.27 (t, *J* = 6.6 Hz, 2H, H$_a$), 3.71 (d, *J* = 11.1 Hz, 2H, H$_j$), 3.89 (d, *J* = 11.2 Hz, 2H, H$_{j'}$), *4*.17 (t, *J* = 6.6 Hz, 2H, H$_f$).

NMR ^{13}C (CDCl$_3$, 400 MHz) δ (ppm): 17.1 (C$_i$), 25.3 (C$_d$), 26.2 (C$_c$), 28.3 (C$_e$), 28.6 (C$_b$), 49.1 (C$_h$), 51.2 (C$_a$), 64.8 (C$_f$), 67.8 (C$_j$), 175.9 (C$_g$).

IR (cm^{-1}, KBr): 3381 (O-H st), 2854-2924 (C-H st), 2097 (N$_3$ st), 1726 (C=O st).

Calculated [M]$^+$ (C$_{11}$H$_{21}$N$_3$O$_4$) m/z = 259.15. *Found:* MALDI+: [M+Na]$^+$ m/z = 282.2.

[G#2]-$C_6H_{12}N_3$ (1-4)

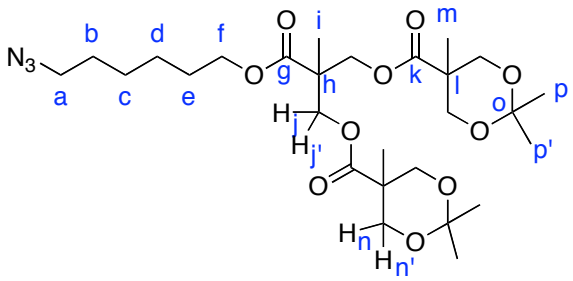

The product 1-4 was obtained by Steglish esterification method (A) and was purified by column chromatography eluting with dichloromethane. Yield: 19%. White solid.

NMR ^1H ($CDCl_3$, 300 MHz) δ (*ppm*): 1.15 (s, 6H, H_m), 1.28 (s, 3H, H_i), 1.35 (s, 6H, H_p), 1.38 (m, 4H, H_c, H_d), 1.41 (s, 6H, $H_{p'}$), 1.63 (m, *J* = 6.9 Hz, 4H, H_b, H_e), 3.27 (t, *J* = 6.6 Hz, 2H, H_a), 3.61 (d, *J* = 12 Hz, 4H, H_n), 4.11 (t, *J* = 6.6 Hz, 2H, H_f), 4.14 (d, *J* = 11.7 Hz, 4H, $H_{n'}$), 4.32 (s, 4H, $H_{j,j'}$).

NMR ^{13}C ($CDCl_3$, 400 MHz) δ (*ppm*): 17.7 (C_i), 18.5 (C_m), 22.1 (C_p), 24.9 (C_p), 25.4 (C_d), 26.3 (C_c), 28.3 (C_e), 28.6 (C_b), 42.0 (C_l), 46.7 (C_h), 51.2 (C_a), 65.1 (C_f), 65.2 (C_j), 65.6 (C_j), 65.8 (C_n), 65.9 (C_n), 98.0 (C_o), 172.5 (C_g), 173.5 (C_k).

IR (cm^{-1}, KBr): 2868-2939 (C-H st), 2097 (N_3 st), 1736 (C=O).

Calculated $[M]^+$ ($C_{27}H_{45}N_3O_{10}$) *m/z* = 571.31. Found: ESI+: $[M+H]^+$ *m/z* = 572.0.

(OH)$_4$-[G#2]-C$_6$H$_{12}$N$_3$ (1-5)

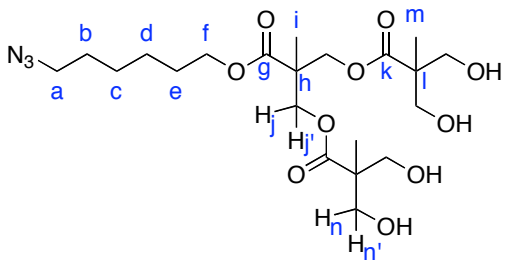

The product 1-5 was obtained following the synthetic method (B). Yield: 95 %. White solid.

NMR ^{1}H (MeOD, 300 MHz) δ (ppm): 1.14 (s, 6H, H$_m$), 1.29 (s, 3H, H$_i$), 1.43 (m, 4H, H$_c$, H$_d$), 1.61-1.71 (m, 4H, H$_b$, H$_e$), 3.31 (t, 2H, H$_a$), 3.61 (d, *J* = 10.8 Hz, 4H, H$_n$), 3.65 (d, *J* = 10.8 Hz, 4H, H$_{n'}$), 4.15 (t, *J* = 6.6 Hz, 2H, H$_f$), 4.25 (d, *J* = 11.1 Hz, 2H, H$_j$), 4.30 (d, *J* = 11.1 Hz, 2H, H$_{j'}$).

NMR ^{13}C (CDCl$_3$, 400 MHz) δ (ppm): 17.3 (C$_m$), 18.3 (C$_i$), 26.7 (C$_d$), 27.5 (C$_c$), 29.6 (C$_e$), 29.9 (C$_b$), 47.8 (C$_h$), 51.8 (C$_l$), 52.4 (C$_a$), 65.8 (C$_n$), 66.4 (C$_f$), 66.5 (C$_j$), 174.6 (C$_g$), 175.9 (C$_k$).

IR (cm^{-1}, KBr): 3283 (O-H st), 2923-2854 (C-H st), 2098 (N$_3$ st), 1731 (C=O st).

Calculated [M]$^+$ (C$_{21}$H$_{37}$N$_3$O$_{10}$) m/z = 491.25. *Found:* MALDI+: [M+Na]$^+$ m/z = 514.2.

[G#3]-$C_6H_{12}N_3$ (1-6)

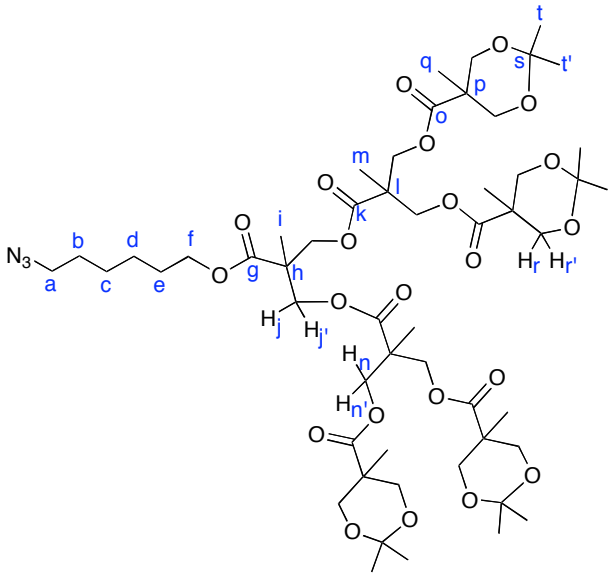

The product 1-6 was obtained by Steglish esterification (A). The crude product was purified by column chromatography eluting with a mixture 7:3 of Hexane:EtOAc. Yield: 75 %. Transparent oil.

NMR ^1H ($CDCl_3$, 400 MHz) δ (ppm): 1.13 (s, 12H, H_q), 1.25 (s, 3H, H_i), 1.26 (s, 6H, H_m), 1.34 (s, 12H, H_t), 1.40 (m, 16H, $H_{t'}$, H_c, H_d), 1.62 (m, 4H, H_b, H_e), 3.27 (t, J = 6.8 Hz, 2H, H_a), 3.61 (d, J = 12.8 Hz, 8H, H_n), 4.11 (m, 10H, H_r, H_f), 4.26 (d, J = 6.8 Hz, 4H, H_j), 4.29 (m, 8H, $H_{r'}$).

NMR ^{13}C ($CDCl_3$, 400 MHz) δ (ppm): 17.6 (C_i), 17.7 (C_m), 18.5 (C_q), 22.0 (C_t), 25.1 ($C_{t'}$), 25.4 (C_d), 26.3 (C_c), 28.4 (C_e), 28.7 (C_b), 42.0 (C_p), 46.6 (C_h), 46.8 (C_l), 51.3 (C_a), 64.9 (C_j), 65.4 (C_f), 65.8 (C_n), 65.9 (C_r), 98.1 (C_s), 171.8 (C_g), 172.0 (C_k), 173.4 (C_o).

IR (cm^{-1}, Nujol): 2990-2940-2876 (C-H), 2097 (N_3), 1739 (C=O).

Calculated $[M]^+$ ($C_{53}H_{85}N_3O_{22}$) m/z = 1115.56. *Found:* ESI+: $[M+Na]^+$ *m/z*=1138.4.

(OH)$_8$-[G#3]-C$_6$H$_{12}$N$_3$ (1-7)

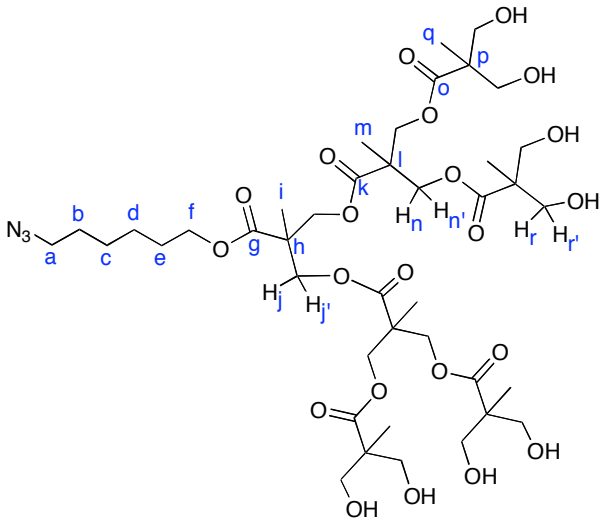

The product 1-7 was obtained following the procedure (B) and obtained in 93% yield as white solid.

NMR ^{1}H (MeOD, 400 MHz) δ (ppm): 1.15 (s, 12H, H$_q$), 1.29 (s, 6H, H$_m$), 1.30 (s, 3H, H$_i$), 1.44 (m, 4H, H$_c$, H$_d$), 1.61 (m, 2H, H$_b$), 1.70 (m, 2H, H$_e$), 3.32 (m, 2H, H$_a$), 3.59 (d, *J* = 6.8 Hz, 8H, H$_r$), 3.67 (m, 8H, H$_{j,j'}$, H$_n$), 4.16 (t, *J* = 7.2 Hz, 2H, H$_f$), 4.23 (m, 4H, H$_{n'}$), 4.30 (m, 8H, H$_{r'}$).

NMR ^{13}C (MeOD, 400 MHz) δ (ppm): 17.3 (C$_q$), 18.2 (C$_i$), 18.3 (C$_m$), 26.7 (C$_d$), 27.5 (C$_c$), 29.6 (C$_e$), 29.8 (C$_b$), 48.0 (C$_l$, C$_h$), 51.8 (C$_p$), 52.4 (C$_a$), 65.9 (C$_r$), 66.2 (C$_n$), 66.7 (C$_j$), 67.4 (C$_f$), 173.8 (C$_k$), 174.1 (C$_g$), 175.9 (C$_o$).

IR (cm^{-1}, KBr): 3288 (O-H st), 2923-2853 (C-H st), 2099 (N$_3$ st), 1732 (C=O st).

Calculated [M]$^+$ (C$_{41}$H$_{69}$N$_3$O$_{22}$) m/z = 955.44. *Found:* ESI+: [M+H]$^+$ m/z = 956.7.

(GlyBoc)$_8$-[G#3]-C$_6$H$_{12}$N$_3$ (1-8)

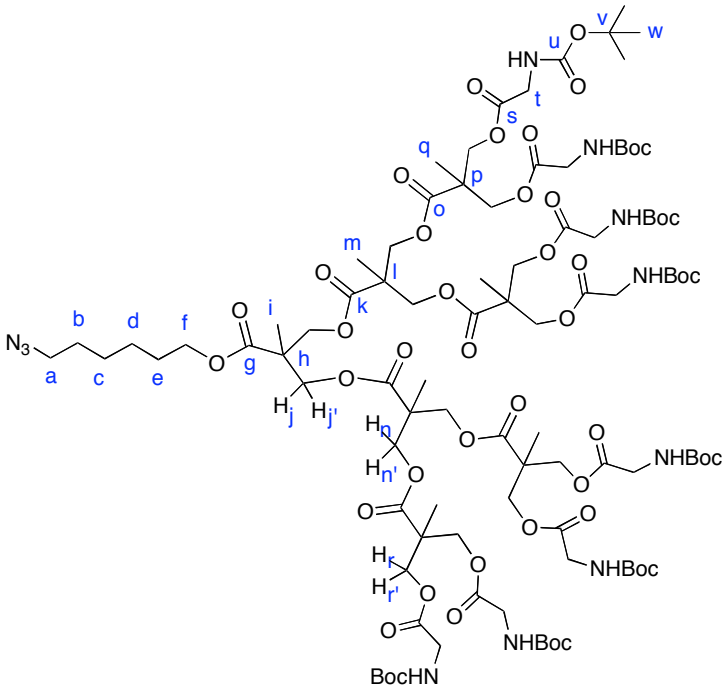

The product 1-8 was obtained by Steglish esterification (A). The crude product was purified by column chromatography eluting with a mixture 1:1 of Hexane:EtOAc. Yield: 78 %. White solid.

NMR ^{1}H ($CDCl_3$, 400 MHz) δ (ppm): 1.23-1.27 (m, 21H, H_i, H_m, H_q), 1.43 (m, 76H, H_c, H_d, H_w), 1.60 (m, 2H, H_b), 1.66 (m, 2H, H_e), 3.27 (t, *J* = 6.8 Hz, 2H, H_a), 3.88 (d, *J* = 5.6 Hz, 16H, H_t), 4.11 (t, *J* = 6.4 Hz, 2H, H_f), 4.27 (m, 28H, $H_{j,j'}$, $H_{n,n'}$, $H_{r,r'}$), 5.34 (s, 8H, NH).

NMR ^{13}C ($CDCl_3$, 400 MHz) δ (ppm): 17.6 (C_q), 17.8 (C_m, C_i), 25.4 (C_d), 26.3 (C_c), 28.3 (C_w, C_e), 28.6 (C_b), 42.2 (C_t), 46.3 (C_p), 46.4 (C_h), 46.6 (C_l), 51.2 (C_a), 65.3 (C_n), 65.5 (C_f), 65.6 (C_r), 66.1 (C_j), 79.9 (C_v), 155.8 (C_u), 170.0 (C_s), 171.5 (C_o), 171.8 (C_k), 172.0 (C_g).

IR (cm^{-1}, KBr): 3384 (N-H), 2978-2936 (C-H), 2098 (N_3), 1717-1734 (C=O).

Calculated $[M]^+$ ($C_{97}H_{157}N_{11}O_{46}$) *m/z* = 2212.03. Found: ESI+: $[M+Na]^+$ *m/z* = 2235.7.

$(C_3H_6NH_2)_8$-[G#3]-$C_6H_{12}N_3$ [1]

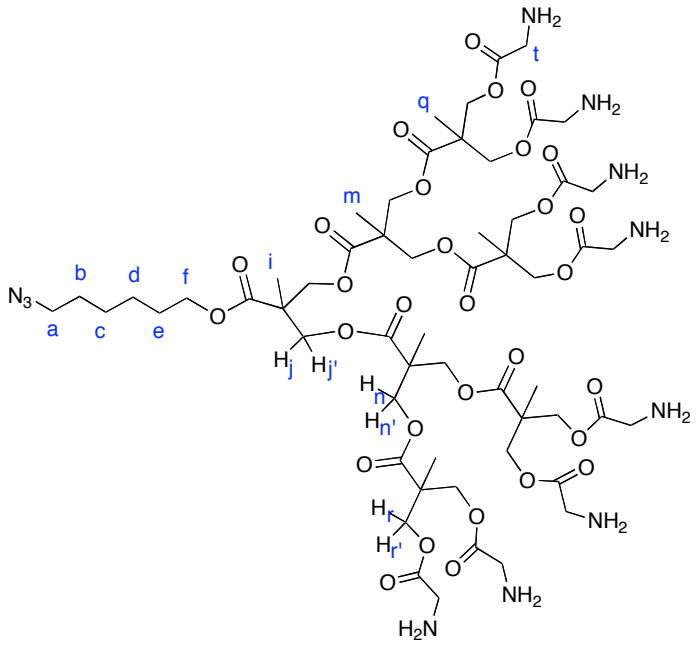

The product 1 was obtained following the synthetic method (C). Quantitative yield. Pale yellow solid.

NMR ^1H (MeOD, 400 MHz) δ (ppm): 1.35 (m, 21H, H_i, H_m, H_q), 1.47 (m, 4H, H_c, H_d), 1.64 (m, 2H, H_b), 1.73 (m, 2H, H_e), 3.27 (t, *J* = 6.8 Hz, 2H, H_a), 3.98 (s, 16H, H_t), 4.20 (t, *J* = 6.8 Hz, 2H, H_f), 4.28-4.50 (m, 28H, $H_{j,j'}$, $H_{n,n'}$, $H_{r,r'}$).

NMR ^{13}C ($CDCl_3$, 400 MHz) δ (ppm): 18.1 (C_i, C_m), 18.2 (C_q), 26.7 (C_d), 27.5 (C_c), 29.6 (C_e), 29.8 (C_b), 41.1 (C_t), 47.6 (C_p), 48.0 (C_h), 48.1 (C_l), 52.4 (C_a), 66.8 (C_n), 67.6 (C_n), 67.8 (C_j), 168.4 (C_s), 173.3 (C_o), 173.4 (C_k), 174.0 (C_g).

IR (cm^{-1}, KBr): 3354 (N-H), 2923-2848 (C-H), 2093 (N_3 st), 1731 (C=O st).

Calculated $[M]^+$ ($C_{57}H_{93}N_{11}O_{30}$) *m/z* = 1411.61. Found: MALDI+: $[M+H]^+$ *m/z* = 1412.9.

(C$_5$H$_{10}$NHBoc)$_8$-[G#3]-C$_6$H$_{12}$N$_3$ (1'-8)

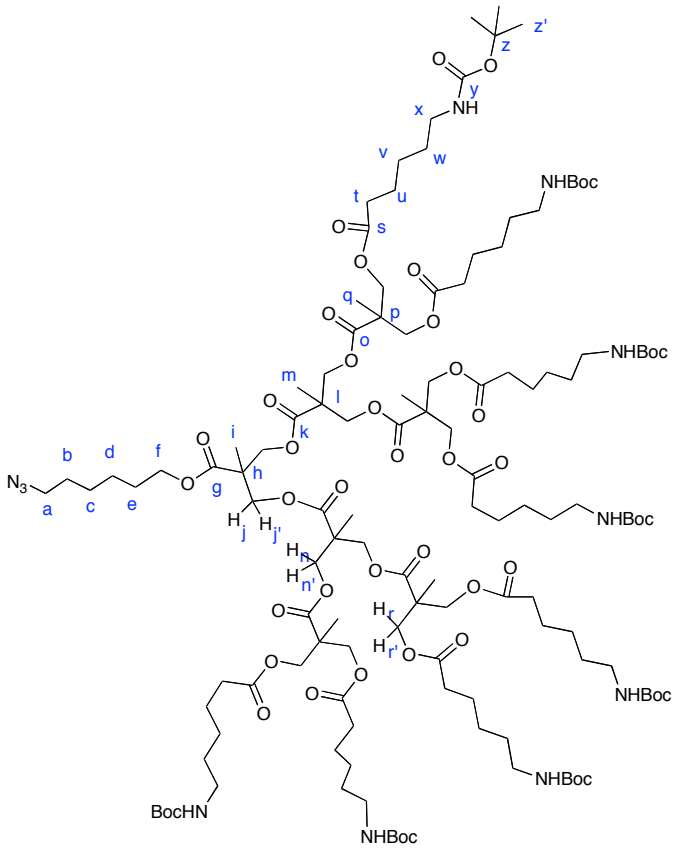

The product 1'-8 was obtained using the synthetic method (A). The crude product was purified by column chromatography eluting with a mixture 1:1 of Hexane:EtOAc.

The pure product was obtained in a 20% yield (201 mg, 76 µmol) as a white solid.

NMR ^{1}H ($CDCl_3$, 400 MHz) δ (ppm): 1.21 (s, 12H, H_q), 1.25 (s, 6H, H_m), 1.27 (s, 3H, H_i), 1.33 (m, 16H, H_v), 1.42 (s, 72H, $H_{z'}$), 1.48 (m, 20H, H_w, H_{c-d}), 1.60 (m, 20H, H_t, H_b, H_e), 2.30 (t, J = 7.2 Hz, 16H, H_a), 3.09 (q, J_1 = 6.4 Hz, J_2 = 6.0 Hz, 16H, H_x), 3.28 (t, J = 6.8 Hz, 2H, H_f), 4.10-4.28 (m, 28H, $H_{r,r'}$, $H_{n,n'}$, $H_{j,j'}$), 4.72 (s, 8H, 8NH).

NMR ^{13}C ($CDCl_3$, 400 MHz) δ (ppm): 17.5, 17.8, 24.4, 25.4, 26.2, 26.3, 28.4, 29.7, 33.8, 40.3, 46.3, 46.6, 51.2, 64.8, 79.0, 156.0, 172.0, 172.9.

IR (cm^{-1}, KBr): 3355 (N-H), 2975-2935-2865 (C-H), 2097 (N_3), 1741 (C=O).

Calculated $[M]^+$ ($C_{129}H_{221}N_{11}O_{46}$) m/z = 2660.53. Found: ESI+: $[M\text{-Boc}]^+$ m/z = 2562.3.

$(C_5H_{10}NH_2)_8$-[G#3]-$C_6H_{12}N_3$ [1']

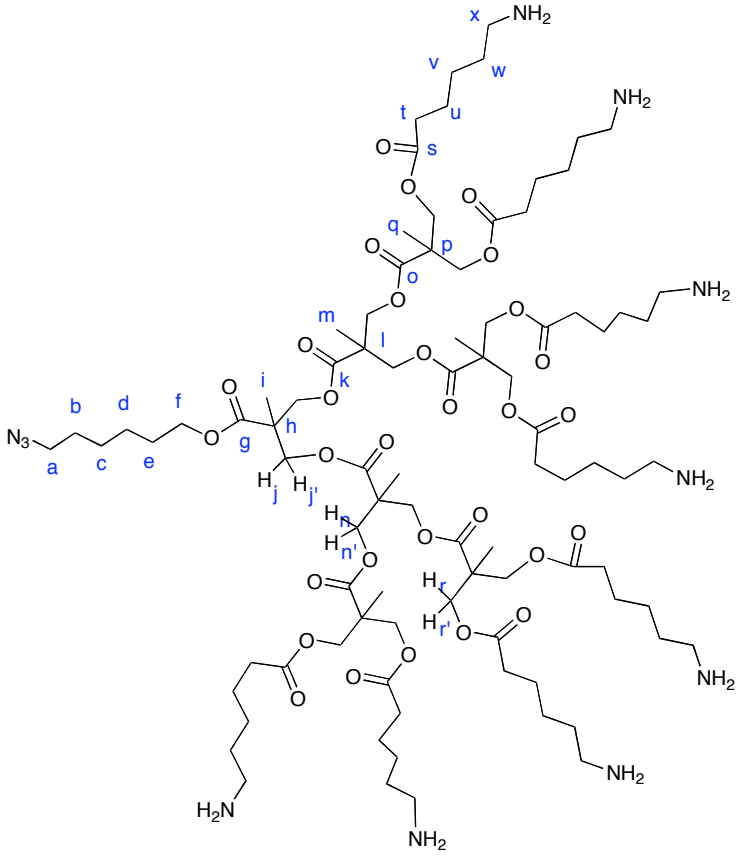

The product 1' was obtained by the synthetic method (C). Quantitative yield. Pale yellow translucent solid.

NMR ^1H (MeOD, 400 MHz) δ (ppm): 1.14 (s, 6H, H_q), 1.18 (s, 6H, H_q), 1.29 (m, 9H, H_m, H_i), 1.40-1.46 (m, 20H, H_c, H_d, H_v), 1.62-1.72 (m, 34H, H_u, H_w, H_e), 2.33-2.39 (m, 16H, H_t), 2.93 (t, *J* = 7.6 Hz, H_x), 3.60-3.69 (m, 16H, $H_{r,r'}$), 4.22-4.28 (m, 12H, $H_{j,j'}$, $H_{n,n'}$).

NMR ^{13}C (MeOD, 400 MHz) δ (ppm): 17.4, 17.8, 18.2, 25.4, 26.9, 28.2, 29.8, 34.4, 34.7, 40.6, 51.8, 52.1, 65.5, 65.8, 66.2, 66.6, 66.9, 67.3, 173.8, 174.8, 175.6, 175.9.

Calculated $[M]^+$ ($C_{89}H_{157}N_{11}O_{30}$) *m/z* = 1860.11. Found: MALDI+: $[M+Na]^+$ *m/z* = 1884.8.

IR (cm^{-1}, KBr): 3346 (N-H), 2920-2842 (C-H), 2096 (N_3), 1735 (C=O).

5-methyl-2-phenyl-1,3-dioxane-5-carboxylic acid (3-1)

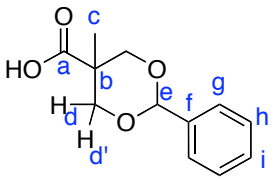

15 g (111.84 mmol) of commercial *bis*-MPA and 1.05 g (5.55 mmol) of *p*-TsOH were dissolved in 120 mL of acetone. 25.5 mL (166.62 mmol) of (dimethoxymethyl)benzene were added and the reaction mixture was stirred for 4 hours. Then, the reaction was cooled to 0°C during one night and the white precipitate was filtered and washed with cold acetone. After drying under vacuum, the product was obtained in a 73 % yield (18.10 g, 81.46 mmol) as a white solid.

NMR ^{1}H ($CDCl_3$, 400 MHz) δ (ppm): 0.95 (s, 3H, H_c), 3.67 (d, J = 11.2 Hz, 2H, H_d), 4.45 (d, J = 11.2 Hz, 2H, $H_{d'}$), 5.50 (s, 1H, H_e), 7.35 (m, 5H, H_g, H_h, H_i).

NMR ^{13}C ($CDCl_3$, 400 MHz) δ (ppm): 17.5 (C_c), 41.5 (C_b), 72.8 (C_d), 100.3 (C_e), 126.0 (C_g), 127.9 (C_i), 128.6 (C_h), 138.3 (C_f), 175.5 (C_a).

IR (cm^{-1}, KBr): 2924-2854 (C-H st), 1698 (C=O st).

Calculated $[M]^+$ ($C_{12}H_{14}O_4$) m/z = 222.09. Found: ESI+: $[M+Na]^+$ m/z = 245.1.

Elemental analysis calculated: C, 64.85; H, 6.35; O, 28.80; Found: C, 64.78; H, 6.26; O, 28.96.

5-methyl-2-phenyl-1,3-dioxane-5-carboxylic anhydride (3-2)

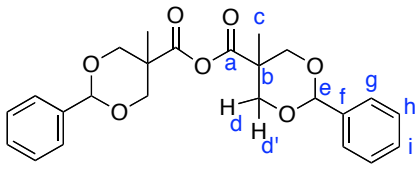

12.38 g (55.69 mmol) of (53) and 17.80 g (86.32 mmol) of DCC were dissolved in 70 mL of dry dichloromethane. The flask was flushed with argon and the reaction mixture was stirred overnight at room temperature. The precipitate was filtrated off and washed with 20 mL of dichloromethane. The filtrate was precipitated over 1 L of cold diethylic ether. The white precipitate was filtered and dry to give the pure product in a 98 % yield (11.67 g, 27.36 mmol).

NMR ^{1}H ($CDCl_3$, 400 MHz) δ (ppm): 1.12 (s, 6H, H_c), 3.68 (d, *J* = 12 Hz, 4H, H_d), 4.65 (d, *J* = 11.6 Hz, 4H, $H_{d'}$), 5.48 (s, 2H, H_e), 7.32 (m, 6H, H_h, H_i), 7.45 (m, 4H, H_g).

NMR ^{13}C ($CDCl_3$, 400 MHz) δ (ppm): 16.8 (C_c), 44.2 (C_b), 73.2 (C_d), 102.1 (C_e), 126.3 (C_g), 128.2 (C_i), 129.1 (C_h), 137.5 (C_f), 169.1 (C_a).

IR (cm^{-1}, KBr): 2923-2854 (C-H st), 1817 (C=O st sim).

Calculated $[M]^+$ ($C_{24}H_{26}O_7$) *m/z* = 426.17. Found: MALDI+: $[M+Na]^+$ *m/z* = 449.2.

Elemental analysis calculated: C, 67.59; H, 6.15; O, 26.26; Found: C, 67.60; H, 6.23; O, 26.17.

bis-MPA G2 (2-1)

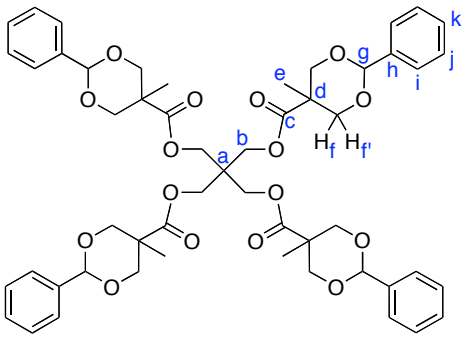

The product 2-1 was obtained following the synthesis method (D) as a white solid in a 94% yield.

NMR ^{1}H ($CDCl_3$, 300 MHz) δ (ppm): 0.87 (s, 12H, H_e), 3.58 (d, *J* = 11.4 Hz, 8H, H_f), 4.31 (s, 8H, H_b), 4.59 (d, *J* = 11.4 Hz, 8H, $H_{f'}$), 5.42 (s, 4H, H_g), 7.28-7.33 (m, H_j, H_k, 12H), 7.40-7.44 (m, 8H, H_i).

NMR ^{13}C ($CDCl_3$, 300 MHz) δ (ppm): 17.52 (C_e), 42.6 (C_d), 43.8 (C_a), 61.5 (C_b), 73.52 (C_f), 101.7 (C_g), 126.11 (C_i), 128.1 (C_j), 128.7 (C_k), 137.8 (C_h), 173.0 (C_c).

IR (cm^{-1}, KBr): 3039 (ArC-H), 2973-2930-2897-2864 (C-H), 1739 (C=O).

Calculated $[M]^+$ ($C_{53}H_{60}O_{16}$) m/z = 952.39. *Found:* MALDI+: $[M+Na]^+$ m/z = 975.3.

Elemental analysis calculated: C, 66.79; H, 6.35; O, 26.86. *Found:* C, 67.00; H, 6.18; O, 26.82.

bis-MPA G2 (OH)$_8$ (2-2)

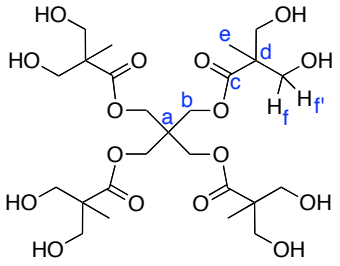

The product 2-2 was obtained following the synthesis by method (E). Yield: 98 %. White solid.

NMR ^{1}H (MeOD, 300 MHz) δ (ppm): 1.18 (s, 12, H$_e$), 3.59 (d, *J* = 10.8 Hz, 8H, H$_f$), 3.70 (d, *J* = 11.1 Hz, 8H, H$_{f'}$), 4.24 (s, 8H, H$_b$), 4.58 (br s, 8H, OH).

NMR ^{13}C (MeOD, 300 MHz) δ (ppm): 17.3 (C$_e$), 44.3 (C$_a$), 43.8 (C$_a$), 52.0 (C$_d$), 63.1 (C$_b$), 66.0 (C$_f$), 176.1 (C$_c$).

IR (cm^{-1}, KBr): 3333 (O-H), 2945 (C-H), 1737 (C=O).

Calculated [M]$^+$ (C$_{25}$H$_{44}$O$_{16}$) m/z =600.26. *Found:* ESI+: [M+Na]$^+$ m/z = 623.

Elemental analysis calculated: C, 49.99; H, 7.38; O, 42.62. *Found:* C, 50.24; H, 7.47; O, 42.29.

bis-MPA G3 (2-3)

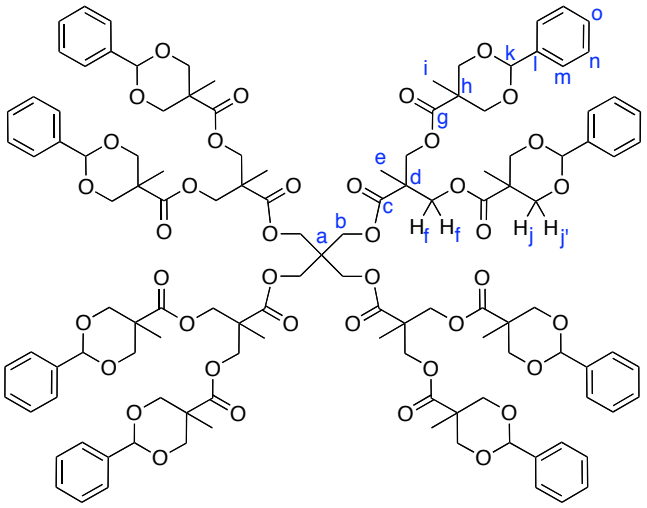

The product 2-3 was obtained following the procedure (D). Yield: 96 %. White solid.

NMR ^{1}H ($CDCl_3$, 300 MHz) δ (ppm): 0.90 (s, 24H, H_i), 1.17 (s, 12H, H_e), 3.52-3.57 (m, 16H, H_j), 3.91 (s, 8H, H_b), 4.34 (dd, J_1 = 6.6 Hz, J_2 = 11.1 Hz, 16H, $H_{f,f'}$), 4.55 (d, J = 11.7 Hz, 16H, $H_{j'}$), 5.38 (s, 8H, H_k), 7.28-7.33 (m, 24H H_n, H_o,), 7.40-7.44 (m, 12H, H_m).

NMR ^{13}C ($CDCl_3$, 400 MHz) δ (ppm): 17.6 (C_e, C_i), 42.5 (C_h), 43.0 (C_a), 46.9 (C_d), 61.3 (C_b), 64.9 (C_f), 73.38 (C_j), 101.6 (C_k), 126.2 (C_m), 128.1 (C_n), 128.8 (C_o), 137.9 (C_l), 171.7 (C_c), 173.0 (C_g).

IR (cm^{-1}, KBr): 3062-3036 (ArC-H), 2854-2934-2980 (C-H), 1740 (C=O).

Calculated $[M]^+$ ($C_{121}H_{140}O_{40}$) m/z = 2232.89. *Found:* MALDI+: $[M+Na]^+$ m/z = 2258.2.

Elemental analysis calculated: C, 65.04; H, 6.32; O, 28.64. *Found:* C, 65.03; H, 6.61; O, 28.36.

bis-MPA G3 (OH)$_{16}$ (2-4)

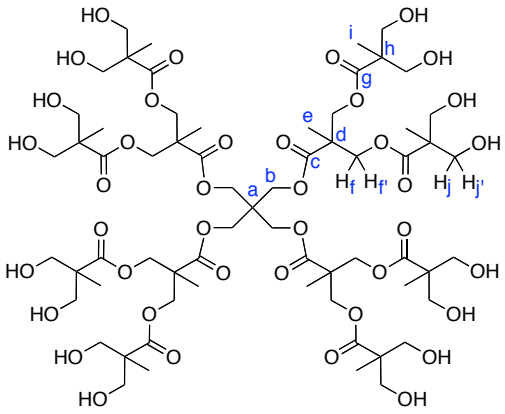

The product 2-4 was obtained following the procedure (E). Yield: 93 % (1.93 g, 1.26 mmol).

NMR ^{1}H (MeOD, 300 MHz) δ (ppm): 1.16 (s, 24H, H_i), 1.34 (s, 12H, H_e), 3.60 (d, *J* = 10.8 Hz, 16H, H_j), 3.69 (d, *J* = 11.1 Hz, $H_{j'}$), 4.26-4.30 (m, 16H, H_b, H_f), 4.37 (d, *J* = 12 Hz, 8H, $H_{f'}$).

NMR ^{13}C (MeOD, 300 MHz) δ (ppm): 17.4 (C_i), 18.3 (C_e), 44.3 (C_h), 45.8 (C_d), 48.2 (C_a), 63.7 (C_b), 65.9 (C_j), 66.1 (C_f), 173.8 (C_c), 176.0 (C_g).

IR (cm^{-1}, KBr): 3337 (O-H), 2948 (C-H), 1738 (C=O).

Calculated [M]$^{+}$ ($C_{65}H_{108}O_{40}$) m/z = 1528.64. *Found:* ESI+: $[M+Na]^{+}$ m/z = 1551.6.

Elemental analysis calculated: C, 51.04; H, 7.12; O, 41.84. *Found:* C, 51.23; H, 7.05; O, 41.92.

bis-MPA G2-GlyBoc$_{16}$ (2-5)

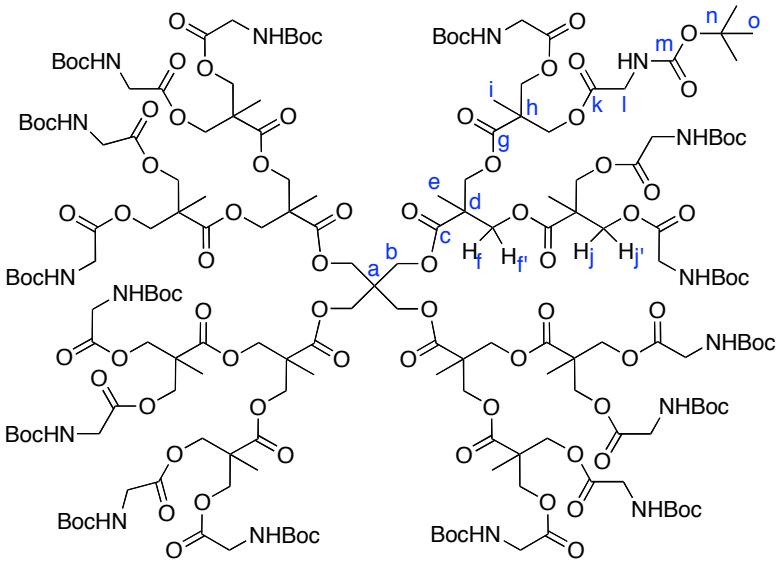

The product 2-5 was obtained following the procedure (A). The crude was dissolved in EtOAc, filtrated, and concentrated. The resulting product was dissolved in methanol and purify by dialysis (cellulose membrane MW 1000) against methanol during 24h, and the solvent evaporated. Yield: 91 %. White solid.

NMR ^{1}H ($CDCl_3$, 400 MHz) δ (ppm): 1.24 (s, 24H, H_i), 1.28 (s, 12H, H_e), 4.42 (s, 144H, H_o), 3.86 (d, J = 5.4 Hz, 32H, H_l), 4.21-4.33 (m, 56H, H_b, H_f, H_j), 5.49 (br s, 16H, NH).

NMR ^{13}C ($CDCl_3$, 400 MHz) δ (ppm): 17.4 (C_e), 17.8 (C_i), 28.2 (C_o), 42.2 (C_n), 46.4 (C_h), 46.9 (C_d), 65.6 (C_j), 79.9 (H_l), 155.9 (C_m), 170.1 (C_k), 171.8 (C_g), 171.9 (C_c).

IR (cm^{-1}, KBr): 3396 (N-H), 2980-2937 (C-H), 1746 (C=O).

Calculated $[M]^+$ ($C_{177}H_{284}N_{16}O_{88}$) m/z = 4041.82. *Found:* ESI+: $[M+Na]^+$ m/z = 4071.9.

Elemental analysis calculated: C, 52.57; H, 7.08; N, 5.54; O, 34.81. *Found:* C, 51.86; H, 7.12; N, 5.74; O, 35.28.

bis-MPA G2 [2]

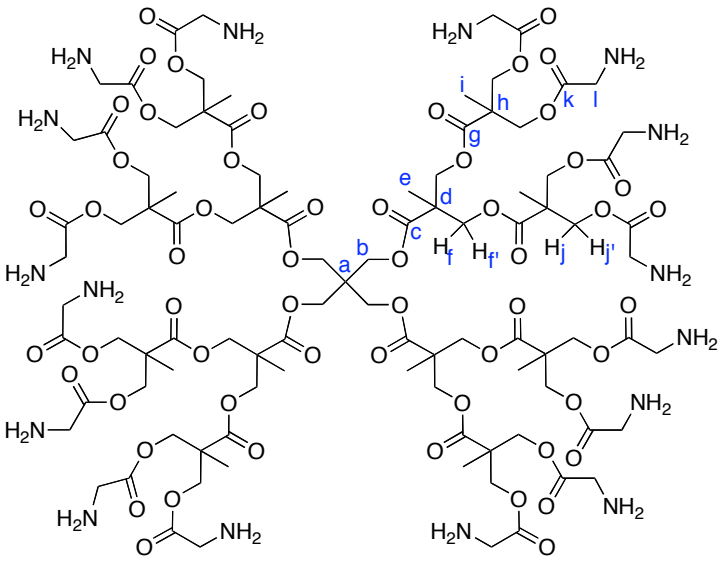

The product 2 was obtained by the procedure (C). Quantitative yield. White powder.

NMR ^{1}H (MeOD, 300 MHz) δ (ppm): 1.36 (s, 24H, H_i), 1.41 (s, 12H, H_e), 3.35 (s, 8H, H_b), 3.98 (s, 32H, H_l), 4.33-4.52 (m, 56H, H_f, H_j).

NMR ^{13}C (MeOD, 300 MHz) δ (ppm): 18.4 (m, C_e, C_i), 34.8 (C_a), 41.3 (m, C_d, C_h, C_l), 66.7 (C_b), 67.6 (m, C_f, C_j), 168.5 (C_k), 173.5 (C_g), 173.6 (C_c).

IR (cm^{-1}, KBr): 3421 (N-H), 2985 (C-H), 1750 (C=O).

Calculated $[M]^+$ ($C_{97}H_{156}N_{16}O_{56}$) m/z = 2242.35. *Found:* ESI+: $[M+H]^+$ m/z = 2443.5.

(HC≡CH$_2$OPh)-Pluronic-(PhOCH$_2$≡CH) (3-3)

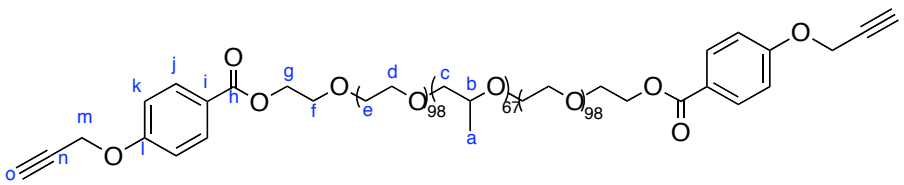

3.58 g (284 µmol) of F127 Pluronic were dried at 110°C under vacuum during 1 hour. The product was cooled at room temperature and dissolved in 10 mL of dry dichloromethane. 166 mg (1.13 mmol) of DMAP and 200 mg (1.13 mmol) of 4-(prop-2-ynyloxy)benzoic acid were added after dissolution, and the reaction mixture was cooled to 0°C. 234 mg (1.36 mmol) of DCC in dry dichloromethane were added. The reaction was allowed to stir at room temperature, under argon atmosphere, during 1 night. The crude product was then precipitated dropwise over 1 L of diethylic ether. The precipitate was filtrated after one night at 5°C, and washed with cold diethylic ether. The crude was then dissolved in methanol and dialysed with MW1000 cellulose membrane against methanol during 2 days. After evaporation under reduced pressure, the pure product was obtained in a 56 % yield (2.06 g, 150 µmol) as a pale yellow solid.

NMR ^{1}H ($CDCl_3$, 400 MHz) δ (ppm): 1.12 (m, 201 H, H_a), 3.36 (m, 67H, H_b), 3.26-3.80 (m, ≈1050, H_c, H_d, H_e, H_f, H_o), 4.41 (t, *J* = 4.4 Hz, 4H, H_g), 4.72 (d, *J* = 2.4 Hz, 4H, H_m), 6.97 (d, *J* = 8.8 Hz, 4H, H_j), 7.99 (d, *J* = 8.8 Hz, 4H, H_k).

NMR ^{13}C ($CDCl_3$, 400 MHz) δ (ppm): 17.3-17.4 (C_a), 55.8 (C_m), 63.9 (C_g), 70.6 (C_e, C_d), 72.9-73.3 (C_c), 75.1-75.5 (C_b), 114.5 (C_k), 131.6 (C_j).

IR (cm^{-1}, thin film over NaCl): 2985 (arC-H), 2881 (C-H), 2687 (C≡C), 1113 (C-O-O).

MALDI+: distribution with max at *m/z* = 4692.

(NHBoc)$_8$[G#3]Pluronic[G#3](NHBoc)$_8$ (3-4)

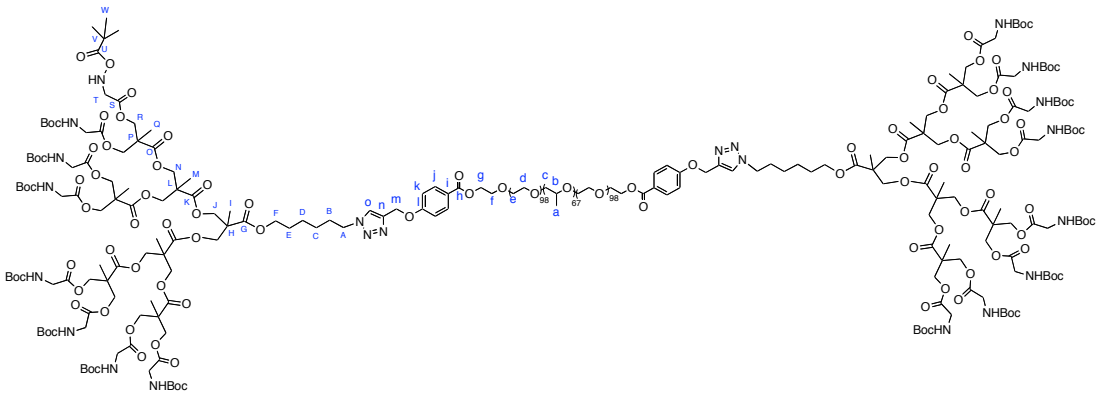

243 mg (18.8 µmol) of (3-3) and 100 mg (51.2 µmol) of (62) were dissolved in 3 mL of DMF. In another flask, 2.35 mg (9.4 µmol) of pentahydrated copper sulphate and 3.73 mg (18.8 µmol) of sodium ascorbate were mixed in 1 mL of DMF to give copper (I). After 10 minutes, both solutions were mixed and agitated over night under argon atmosphere. The resulting crude product was dialysed (cellulose membrane 12000) against methanol during 2 days. The pure product was obtained in a 76 % yield as a white solid.

NMR ^{1}H ($CDCl_3$, 400 MHz) δ (ppm): 1.12-1.14 (m, 201H, H_a), 1.24 (s, 36H, H_M, H_Q), 1.28 (s, 6H, H_I), 1.43 (m, 144H, H_W), 1.58-1.67 (m, 8H, H_C, H_D), 3.30-3.41 (m, 69H, H_b, H_A), 3.49-3.68 (m, ≈1050H, H_c, H_d, H_e, H_f), 3.88 (d, *J* = 5.2 Hz, 32H, H_T), 4.11 (m, 4H, H_g), 4.22-4.28 (m, 56H, H_J, H_N, H_R), 5.24 (s, 2H, H_o), 5.37 (br s, 16H, NH), 7.02 (m, 4H, H_i), 8.01 (m, 4H, H_j).

NMR ^{13}C ($CDCl_3$, 300 MHz) δ (ppm): 17.3, 17.4, 17.8, 28.3, 42.2, 46.4, 46.6, 65.3, 65.7, 70.5, 72.8, 72.9, 73.3, 75.0, 75.2, 75.6, 79.9, 114.3 (C_k), 123.0 (C_h), 131.7 (C_j), 143.1 (C_n), 155.9 (C_U), 162.0 (C_l), 166.1 (C_i), 170.0 (C_S), 171.5, 171.8.

IR (cm^{-1}, thin film over NaCl): 3360 (N-H), 2883 (C-H st), 1717-1743 (C=O), 1111 (C-O-C).

MALDI+: distribution with max at *m/z* = 15601 and m/z = 5179.

(NH$_2$)$_8$[G#3]Pluronic[G#3](NH$_2$)$_8$ [3]

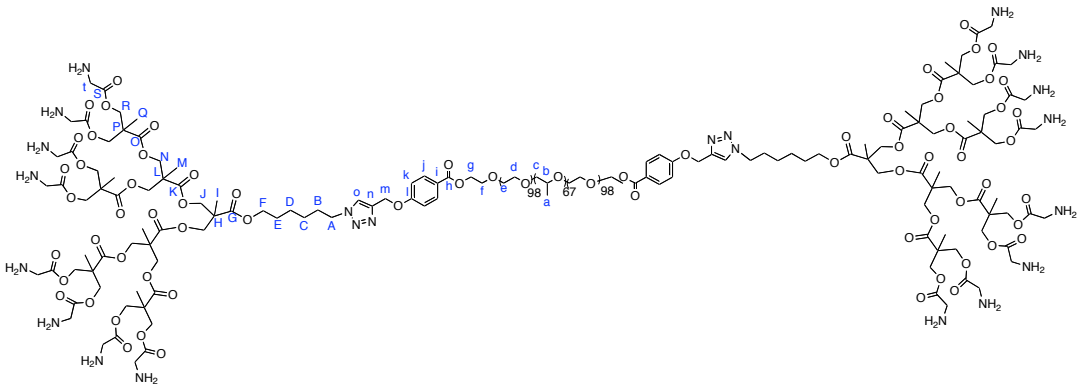

The product 3 was obtained following the synthesis method (C) in a quantitative yield, as a yellow solid.

NMR ^{1}H (MeOD, 400 MHz) δ (ppm): 1.13-1.15 (m, 201H, H_a), 1.29-1.34 (m, 36H, H_M, H_Q), 1.36-1.67 (m, 8H, H_C, H_D), 3.30-3.33 (m, 69H, H_b, H_A), 3.42-3.69 (m, ≈1080H, H_c, H_d, H_e, H_f), 4.02-4.06 (m, 18H, H_J, H_N), 4.11 (m, 4H, H_g), 4.33-4.35 (m, 32H, H_R), 4.96 (m, 32H, H_T), 5.32 (s, 4H, H_m), 5.49 (s, 2H, H_o), 7.02 (m, 4H, H_i), 8.01 (m, 4H, H_j).

NMR ^{13}C (MeOD, 400 MHz) δ (ppm): 17.7, 71.3-71.5, 74.1, 74.4, 76.6-76.8, 111.4.

IR (cm^{-1}, thin film over NaCl): 2970 (-NH^{3+}, st), 2880 (C-H st), 1742 (C=O), 1112 (C-O-C).

MALDI+: distribution with max at *m/z* = 4991.

Synthesis of the ionic dendrimers

Typical procedure for the synthesis of ionic-dendrimers

The ionic dendrimers were prepared by addition of a solution of dry tetrahydrofuran (THF) containing 2-[2-(2-methoxyethoxy)ethoxy]acetic acid to a solution of MeOH containing the dendrimer (approx. 10 mg). The acid was added in the stoichiometry necessary to functionalize only the surface amine groups “n”, or all the amine groups of the PAMAM, namely “2n-2”, being “n” the primary amine groups and “n-2” the tertiary amine groups (the values of “n” depend on the generation). The mixture was ultrasonicated for 5 min, and was slowly evaporated at room temperature and dried in vacuum at 40 °C to give an oily (2G) to waxy (5G) yellowish product. The resulting compounds present good solubility in water and chloroform.

2G-IP-16

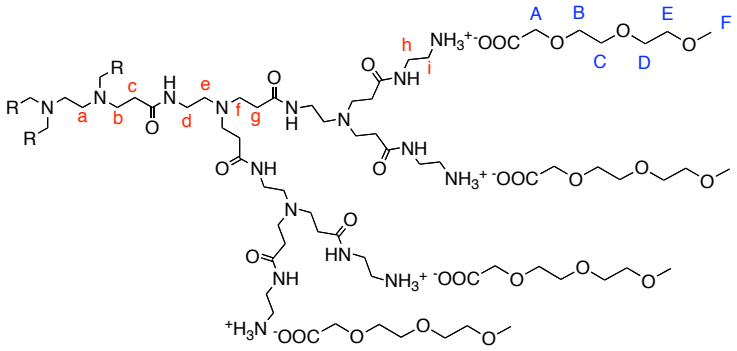

NMR ^{1}H ($CDCl_3$, 400 MHz) δ (ppm): 2.40 (m, H_c, H_f), 2.59 (m, H_e, H_a), 2.80 (m, H_b, H_f), 3.04 (m, H_i), 3.27 (m, H_d), 3.38 (s, H_F), 3.46 (m, H_h), 3.55 (m, H_E), 3.65 (m, H_B, H_C, H_D); 3.92 (s, H_A).

NMR ^{13}C (MeOD, 400 MHz) δ (ppm): 34.8 (C_c, C_g), 38.6 (C_d), 38.8 (C_h), 40.7 (C_i), 51.1 (C_b, C_f), 53.5 (C_a, C_e), 59.2 (C_F), 68.9 (C_A), 70.9-71.2-71.4 (C_B, C_C, C_D), 72.8 (C_E), 174.6 ($C{=}O_{GO}$), 174.7 ($C{=}O_{G1}$), 175.6 ($C{=}O_{G2}$), 178.1 (COO^-).

IR (cm^{-1}, KBr): 3240 (υNH), 3039 (υNH), 2869 (υCH_2), 1616 (υC=O amide), 1566 (υOCO^-), 1396 (∂OCO^-), 1311 (υC=O), 1091 (υO-C-O).

Elemental analysis: C, 45.21; H, 8.57; N, 12.56; O, 33.66.

2G-IP-30

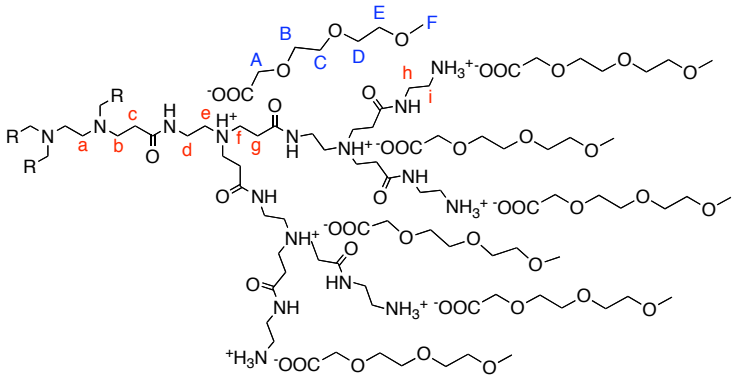

NMR ^{1}H (MeOD, 400 MHz) δ (ppm): 2.44 (m, H_c, H_g), 2.67 (m, H_e, H_a), 2.87 (m, H_b, H_f), 3.09 (m, H_i), 3.30 (H_d), 3.37 (s, H_F), 3.49 (m, H_h), 3.54-3.57 (m, H_E), 3.63-3.65 (m, H_D), 3.66 (m, H_B, H_C), 3.94 (s, H_A).

NMR ^{13}C (MeOD, 400 MHz) δ (ppm): 34.4 (C_c, C_g), 38.3 (C_d, C_h), 40.5 (C_i), 51.1 (C_b, C_f), 53.6 (C_a, C_e), 59.2 (C_F), 71.1-71.5 (C_B, C_C, C_D) 72.9 (C_E), 174.6 ($C{=}O_{G0}$), 175.4 ($C{=}O_{G1}$), 175.5 ($C{=}0_{G2}$), 177.1 (COO^-).

IR (cm^{-1}, KBr): 3239 (υNH), 3039 (υNH), 2866 (υCH_2), 1631 (υC=O amide), 1570-1547 (υOCO^-), 1400 (∂OCO^-), 1311 (υC=O), 1091 (υO-C-O).

Elemental analysis: C, 46.33; H, 8.66; N, 10.34; O, 34.67.

5G-IP-128

NMR ^{1}H (MeOD, 400 MHz) δ (ppm): 2.40 (m, H_c, H_g), 2.60 (m, H_e, H_a), 2.80 (m, H_b, H_f), 3.07 (m, H_i), 3.27 (H_d), 3.38 (s, H_F), 3.50 (m, H_h), 3.55-3.58 (m, H_E), 3.64-3.68 (m, H_D, H_B, H_C), 3.93 (s, H_A).
NMR ^{13}C (MeOD, 400 MHz) δ (ppm): 34.8 (C_c, C_g), 38.5 (C_d, C_h), 40.6 (C_i), 51.1 (C_b, C_f), 53.6 (C_a, C_e), 59.2 (C_F), 70.9-71.2-71.5 (C_B, C_C, C_D) 72.8 (C_E), 174.6 (C=O), 175.5 (C=O), 178.1 (COO^-).
IR (cm^{-1}, KBr): 3244 (υNH), 3029 (υNH), 2869 (υCH_2), 1631 (υC=O amide), 1554-15542 (υOCO^-), 1400 (∂OCO^-), 1311 (υC=O), 1090 (υO-C-O).
Elemental analysis: C, 46.50; H, 8.56; N, 11.47; O, 33.47.

5G-IP-254

NMR ^{1}H (MeOD, 400 MHz) δ (ppm): 2.53 (m, H_c, H_g), 2.84 (m, H_e, H_a), 3.03 (m, H_b, H_f), 3.09 (m, H_i), 3.37 (s, H_F), 3.41 (H_d), 3.54 (m, H_h), 3.55-3.58 (m, H_E), 3.63-3.66 (m, H_D, H_B, H_C), 3.93 (s, H_A).
NMR ^{13}C (MeOD, 400 MHz) δ (ppm): 33.4 (C_c, C_g), 37.7 (C_d), 38.3 (C_h), 40.4 (C_i), 51.0 (C_b, C_f), 53.6 (C_a, C_e), 59.2 (C_F), 70.2-71.3-71.5 (C_B, C_C, C_D) 72.9 (C_E), 174.1 (C=O), 174.7 (C=O), 175.5 (COO^-).
IR (cm^{-1}, KBr): 3464 (υNH), 3224 (υNH), 3029 (υNH), 2870 (υCH_2), 1655 (υC=O amide), 1554 (υOCO^-), 1400 (∂OCO^-), 1230 (υC=O), 1091 (υO-C-O).
Elemental analysis: C, 46.19; H, 8.25; N, 8.14; O, 37.42.

I*bis*MPA

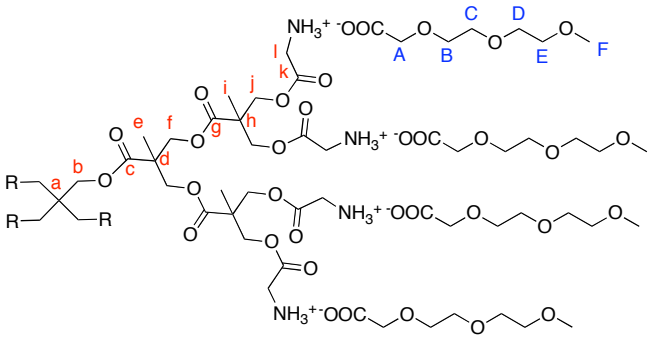

NMR ^{1}H (MeOD, 400 MHz) δ (ppm): 1.36 (H_i), 1.41 (H_e), 3.32 (H_b), 3.36 (H_F), 3.54-3.56 (H_E), 3.62-3.67 (H_D, H_C, H_B), 3.98 (H_l), 4.12 (H_A), 4.33-4.51 (H_f, H_j).

NMR ^{13}C (MeOD, 400 MHz) δ (ppm): 17.9 (C_e), 18.4 (C_i), 41.3 (C_l), 47.7 (C_b), 59.1 (C_F), 66.7 (C_f), 67.5 (C_j), 69.2 (C_A), 71.4-71.6-71.8 (C_B, C_C, C_D), 72.9 (C_E), 168.5 (C_k), 173.4 (C_g), 173.5 (C_c), 174.5 (COO^-).

IR (cm^{-1}, KBr): 3363 (υNH^{3+}), 1723 (υC=O), 1298 (υC-Oester), 1089-1081 (υC-O-C ester, υC-O-C ether).

bis-MPA derivatives Biodegradability assays

bis-MPA dendron and dendrimer were dissolved in aqueous buffers (pH 3, 5, 7, and 9) and characterized by mass spectrometry (MALDI-TOF-MS) at different times (1h, 3h, 6h, 24h, 48h, 5 days) until degradation.

Buffers preparation:

pH 3: citrate buffer

Citrate buffer at pH 3 was prepared mixing 46.5 mL of 0.1 M citric acid with 3.5 mL of 0.1 M sodium citrate. The final volume was adjusted to 100 mL with distillated water and the pH was verified and adjusts using a pH meter.

pH 5 and pH 7: citrate phosphate buffer

24.3 mL of 0.1 M citric acid was mixed with 25.7 mL of 0.2 M dibasic sodium phosphate for the preparation of pH5. 6.5 mL of 0.1 M citric acid was mixed with 43.6 mL of 0.2 M dibasic sodium phosphate for the preparation of pH5. The final volume was adjusted to 100 mL with distillated water and the pH was verified and adjusted using a pH meter.

pH 9: Tris-HCl buffer

50 ml of 0.1 M Tris(hydroxymethyl)aminomethane and 5 mL of 0.1 M hydrochloric acid were mixed and the final volume was adjusted to 200 ml with deionized water.

The buffers were used at 0.1 M. The dissolutions of dendrimers were prepared at 1 mg/mL, incubated at 37°C and aliquots were taken at specific times for analysis by MALDI-TOF.

Cell viability assays

U251MG epithelial cells and mesenchymal cells (MSCs) were seeded in a 96-well cell culture plate at a density of 2500 cells per well in 100µL of complete medium (DMEM for U251MG cells and Low Glucose DMEM for MSCs). The plates were incubated at 37°C with a 5 % CO_2 atmosphere during 24 hours. The next day, 50 µL of a solution of the dendritic derivatives dissolved in complete medium at the desired concentration (3 times the final concentration desired) was added. After 24h, 48h or 72h of incubation, the medium was removed and the cells were washed twice with PBS. Then, 100 µL of solution of 1 % gluteraldehyde were added and the plates were incubated 10 minutes at room temperature. Then, the gluteraldehyde was removed and 100 µL of PBS were added. When the experiment was over, PBS was removed and 50 µL of 1 % crystal violet was added. After 30 minutes of incubation at room temperature, the wells were watched with water until the water was uncoloured. When the wells were dried, 200 µL of 10 % acetic acid were added in the wells to dissolve the crystals formed. After homogenisation, absorbance measurements were carried out on a microplate reader (Biotek ELX800) at 570 nm. The relative cell viability (%) related to control wells containing cell culture medium was calculated by the formula Abs_{test} x 100 / $Abs_{control}$, where Abs_{test} is the absorption of the cells growth on the dendritic derivatives wells and $Abs_{control}$ is the absorption of the cells growth on the free wells. Each condition was tested at least in triplicates.

Gel retardation assays

Agarose gels were prepared at 0.5 % agarose in TBE buffer, with 2 µL/100 mL of GelRed. The quantity of plasmid DNA per well was 40 ng, and the amount of solution DNA/dendrimer injected in each well was 10 µL previously mixed with 1 µL of BlueBromophenol. Plasmid DNA and dendritic compounds were incubating in TBE for 30 minutes before running the gel. Gels were run at 90 V for 1 h and revelating with a bioimaging system device.

CHAPTER 2:

DESIGN, SYNTHESIS AND EVALUATION OF BIS-MPA DERIVATIVES AS CONTRAST AGENTS

Introduction and previous work

Magnetic Resonance Imaging

The field of biomedical imaging emerged from Röentgen's discovery of X-rays in 1985. The diagnosis and recognition of disease has evolved tremendously with the sophisticated imaging tools of today, such as the magnetic resonance imaging (MRI), computed tomography (CT) positron emission tomography (PET) and ultrasonography (US).[124] Over the past decades, nuclear magnetic resonance has been the most powerful method for the non-invasive investigation of human anatomy, physiology and pathophysiology. The rapidly emerging discipline of molecular imaging aims to probe fundamental molecular processes at the origin of the disease for early diagnosis and efficient therapy.[125] Thanks to the possibility to do early diagnosis, the need for exploratory surgery has been decreased improving patient care.

The advantages of MRI made this technique become one of the prominent non-invasive imaging techniques for disease diagnostic. They include high spatial resolution, a non-ionizing radiation source, and the ability to obtain physiological and anatomical information from soft tissue. Its major limitation being its low sensibility, scientists have developed non-toxic contrast agents over the last few decades.

The aim is to accumulate enough bioimaging probes in the area of interest and a minimum level in other organs and tissues. This can be achieved by binding functionalized low molecular weight paramagnetic metal complexes like, for instance, Gd(III)-DTPA and Gd(III)-DOTA (Figure 1) to polymer carriers (polysaccharides, synthetic polymers), which can be targeted to a particular site using antibodies or folic acid, for example. This would increase the contrast and reduce the required dosage of MRI agents.

[124] a) R. Weissleder, *Nat. Rev. Cancer*, **2002**, *2*, 11-18 ; b) T.F. Massoud and S.S. Gambhir, *Genes Dev.*, **2003**, *17*, 545-580.

[125] a) R. Weissleder, U. Mahmood, *Radiology,* **2001**, *219*, 316-333 ; b) D.J. Wagenaar, R. Weissleder and A.A. Hengerer, *Acad. Radiol*., **2001**, *8*, 409-420; c) H. R. Herschman, *Science,* **2003**, *302*, 605-608; d) R. Weissleder and V. Ntziachristos, *Nature Med*., **2003**, *9*, 123-128.

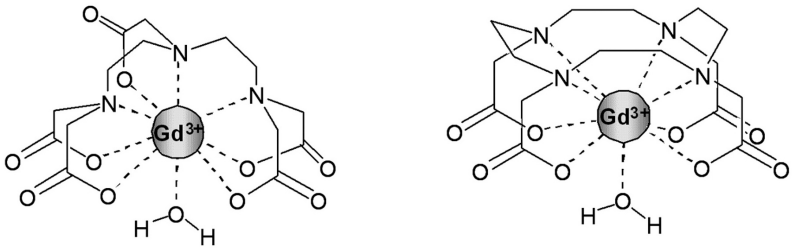

Figure 48: Chemical structures of Gd(III)DTPA and Gd(III)DOTA.

The efficiency of MRI contrast agents is often expressed in terms of their longitudinal relaxivity (r_1/mM^{-1}s^{-1}), which is their ability to shorten the longitudinal relaxation time of protons of water molecules (T_1/s).

$$\mathbf{(1/T_1)_{observed} = (1/T_1)_{diamagnetic} + r_1[Gd(III)]} \qquad \mathbf{(1)}$$

In the equation **(1)**, $(1/T_1)_{observed}$ is the observed longitudinal relaxation rate in the presence of contrast agent, [Gd(III)] is the concentration of Gd(III) and $(1/T_1)_{diamagnetic}$ is the diamagnetic longitudinal relaxation rate (in the absence of paramagnetic species). For Gd-DOTA, r_1 = 3.0 mM^{-1}s^{-1} and r_2 = 3.9 mM^{-1}s^{-1}; therefore, gram quantities of these agents must be administrated in order to obtain an adequate image contrast.[126]

[126] a) M Port, J.M. Idee, C. Medina, C. Robic, M. Sabatou, C. Corot*, Biometals,* **2008***, 21*, 469-490; b) J.L. Major, T.J. Meade, *Acc. Chem. Res.,* **2009***, 42*, 893-903 ; c) P. Caravan*, Acc. Chem. Res.* **2009***, 42*, 851-862; d) L.M. de Leon Rodriguez, A.J.M. Lubag, C.R. Maloy, G.V. Martinez, R.J. Gillies. A.D. Sherry*, Acc. Chem. Res*. **2009***, 42*, 948-957.

Dendrimers as MRI contrast agents

The multivalent character of dendrimers has positioned these well-defined, highly branched macromolecules at the forefront in the development of new contrast agents for biomedical magnetic resonance imaging.

The synthesis of different generations of Gd(III) DPTA-based PAMAM dendrimers was reported by Wiener and co-worker.[127] Bryant and colleagues investigated the relationship between r_1 and the molecular weight of the dendritic MRI contrast agent using different generations of Gd(III)DOTA-based PAMAM dendrimers.[128] In that case, a plateau value for r_1 of 36 $mM^{-1}s^{-1}$ (0.47 T, 20°C) was reached for the seventh generation of Gd(III)DOTA-based dendrimer (MW = 375 kDa). Gd(III)DTPA-functionalized PPI dendrimers were reported by Kobayashi *et al*[129], they demonstrated that the r_1 almost linearly increases with the molecular weight of these dendrimers. Later, new series of Gd(III)DTPA-based PPI dendrimers using different linker between Gd(III) complex and the dendrimer was described by Langereis and co-workers.[130] This study suggests that the linker between the Gd(III) complex and the dendrimer has a large effect on the overall relaxivity. Researchers at Schering AG (Berlin, Germany) developed another class of dendritic contrast agents: Gadomer-17® and Gd(III)DTPA-24-cascade-polymer.[131] These macromolecules are built from a trimesoytriamide central core

[127] E.C. Wiener, M.W. Brechbiel, H. Brothers, R.L. Magin, O.A. Gansow. D.A. Tomalia*, Magn. Reson. Med.,* **1994**, *31*, 1-8.

[128] L.H. Byant, M.W. Brechiel, C. Wu, R.L. Magin, O.A. Gansow, D.A. Tomalia, P.C. Lauterbur*, J. Magn. Reson. Imaging,* **1999**, *9*, 348-352.

[129] H. Kobayashi, S. Kawamoto, S.-K. Jo, H.L. Bryant Jr, M.W. Brechbiel, R.A. Star, *Bioconjugate Chem*., **2003**, *14*, 388-394.

[130] S. Langereis, Q.G. de Lussanet, M.H.P. van Genderen, W.H. Backes, E.W. Meijer*, Macromolecules,* **2004**, *37*, 3084-3091.

[131] a) C. Fink, F. Kiessling, M. Bock, M.P. Lichy, B. Misselwitz, P. Peschke, N.E. Fusenig, R. Grobholtz, S. Delorme*, J. Magn. Reson. Imaging,* **2003**, *18*, 59-65; b) G.M. Nicolle, E. Toth, H. Schmitt-Willich*,* B. Raduchel, A.E. Merbach*, Chem.-Eur. J.,* **2002**, *8*, 1040-1048; c) B. Misselwitz, H. Schmitt-Willich, M. Michaelis and J.J Oelin-ger*, Invest. Radiol*. **2002**, *37*, 146-151; d) B. Misselwitz, H. Schmitt-Willich, E. Wolfgang, T. Frenzel, H.J. Weinmann*, Magn. Reson. MAGMA,* **2001**, *12*, 128-134; e) H.E.D. Link, D.M. Shames, M. Wendland, A. Mülher, A. Grossman, W. Rosenau, R.C. Brasch*, Acad. Radiol.,* **2000**, *7*, 934-944; f) H.C. Roberts, A. Muhler and R.C. Brasch*, J. Magn. Reson. Imaging,* **1999**, *9*, 204-208; g) Q. Dong, D.R. Hurst, H.J. Weinmann, F.J. Londy, M.R. Prince*, Invest. Radiol.,* **1998**, *33,* 699-708; h) H.C. Roberts, M. Saeed, T.P. Roberts, A. Mülher, D.M. Shames, J.S. Mann, M. Stiskal, F. Demsar, R.C. Brasch*, J. Magn.*

to which 18 lysine amino acids residues are introduced. Gadomer-17® consist of 24 N-monosubstituted Gd(III)DO3A moieties, whereas Gd(III)DTPA-24-cascade-polymer contains 24 Gd(III)DTPA complexes.

Dendritic targeted contrast agents

Dendrimers have shown to be appropriate synthetic scaffolds for the incorporation of multiple Gd(III) moieties leading to an improved sensitivity of MRI as well as a prolonged blood circulation time of the MRI contrast agent. The development of target-specific MRI contrast agents, directed to defined molecular markers, could dramatically improve the imaging of a specific disease, due to the accumulation of agent at the region of interest.

Tumor-selective ligands have been used to construct novel drug conjugates. There is a continuing interest in the application of monoclonal antibodies (mAb) to develop targeted molecular MRI agents for both diagnostic and therapeutic purposes. The vitamin folic acid (FA) displays high affinity for the folate receptor (FR), which is a potentially useful biological target for the management of many human cancers. This membrane protein binds extracellular folates with very high affinity, and through an endocytic process, physically delivers them inside the cell for biological consumption. [132] There are now many examples of how this physiological system can be exploited for the targeted delivery of biologically active molecules to cancer.

So far, only a few examples of target-specific dendritic MRI contrast agents are known. Konda and colleagues reported the functionalization of Gd(III)DTPA-based PAMAM dendrimer with one or two folate moieties.[133] *In vivo* MR imaging in mice with ovarian tumors expressing the folate receptor resulted in a significant

---

Reson. Imaging, **1997**, *7*, 331-338; i) E.C. Wiener, F.P. Auteri, J.W. Chen, M.W. Brechbiel, O.A. Gansow, D.S. Schneider, R.L. Belford, R.B. Clarkson, P.C. Lauterbur*, J. Am. Chem. Soc.,* **1996**, *118*, 7774-7782; j) H.C. Schwickert, T.P. Roberts, A. Mühler, M. Stiskal, F. Demsar, R.C. Brasch*, Eur. J. Radiol*., **1995**, *20*, 144-150; k) G. Adam, J. Neuerburg, E. Spuntrup, A. Mülher, K.S. Vet Surg, R.W. Günther*, J. Magn. Reson. Imaging,* **1994**, *4*, 462-466; l) G. Adam, J. Neuerburd, E. Spuntrup*,* A. Mülher, K. Scherer, R.W. Günther*, Magn. Reson. Med.* **1994**, *32*, 622-628.

[132] I.R. Vlahov, C.P. Leamon, *Bioconj. Chem.,* **2012**, *23*, 1357-1369.

[133] S.D. Konda, M. Aref, S, Wang, M. Brechbiel, E.C. Wiener*, MAGMA,* **2001**, *12*, 104-113.

signal enhancement using folate-dendrimer Gd(III) chelate, while no enhancement was observed for mice with folate-receptor negative tumours.[134] Takahashi and colleagues proposed a different approach: Gd(III) was immobilized at the interior of the dendritic framework.[135] Dendritic wedges composed of one DTPA unit at the focal point and carbohydrates at the periphery, where associated through complexation with Gd(III).

Antibody-dendrimer conjugates have been explored for their use in radioimmunotherapy and imaging applications, including MRI, with promising outcomes.[136] Recently, New and co-workers reported the preparation along with the *in vivo* and *in vitro* MRI characterization of cystamine core dendrimers loaded with Gd(III)-DOTA; and the development and characterization of two dendrons conjugated to the $F(ab')_2$ fragment of the monoclonal antibody (mAb) panitumumab.[137] This study indicated that antibody based MRI contrast agents may be useful as pool agents and target specific delivery of the imaging agent. Other dendrimer-antibody derivatives were synthetized and studied for targeted cancer therapy, [138] for carbonyl metallo immunoassay (CMIA), [139] and as immunosensors for biological detection.[140]

---

[134] a) S.D. Konda, S. Wang, M. Brechbiel, E.C. Wiener*, Invest. Radiol*., **2002**, *37*, 199-204. ; b) S.D. Konda, M. Aref, M. Brechbiel, E.C. Wiener*, Invest. Radiol*., **2000**, *35*, 50-57; c) E.C. Wiener, S. Konda, A. Shadron, M. Briechbiel, O. Gansow*, Invest. Radiol*. **1997**, *32*, 748-754.

[135] M. Takahashi, Y. Hara, K. Aoshima, H. Kurihara, T. Oshikawa, M. Yamashita*, Tetrahedron Lett.,* **2000**, *41*, 8485-8488.

[136] a) C. Wu, M.W. Brechbiel, R.W. Kozak and O.A. Gansow*, Bioorg. Med. Chem. Lett*., **1994**, *4*, 449-454; b) G. Wu, R.F. Barth, W. Yang, S. Kawabata, L. Zhang, K. Green-Church*, Mol. Cancer Ther*., **2006**, *5*, 52-59; c) H. Kobayashi, N. Sato, T. Sago, Y. Nakamoto, T. Ishimori, S. Toyama, K. Togashi, J. Konishi, M.W. Briechbiel*, Eur. J. Nucl. Med.,* **2000**, *27*, 1334-1339; d) G. Wu, R.F. Barth, W. Yang, M. Chatterjee, W. Tjarks. M.J. Ciesielski, R.A. Fenstermaker*, Bioconjugate Chem.,* **2003**, *15*, 185-194.

[137] K. Nwe, D.E. Milenic, G.L. Ray, Y.-S. Kim, M.W. Brechbiel*, Mol. Pharm.* **2012**, *9*, 374-381.

[138] a) A. K. Patri, A. Myc, J. Beals, T.P. Thomas, N.H. Bander, J.R. Baker Jr.*, Bioconjugate Chem*., **2004**, *15*, 1174-1181; b) R. Shukla, T.P. Thomas, A.M. Desai, A. Kotlvar, S.J. Park, J.R. Baker Jr*, Nanotechnology,* **2008**, *19*, 295102; c) T.P. Thomas A.K. Patri, A. Myc, M.T. Myaing, J.Y. Ye, T.B. Norris, J.R. Baker Jr*, Biomacromol.,* **2004**, *5*, 2269-2274.

[139] N. Fischer-Durand, M. Salmain, B. Rudolf, A. Vessières, J. Zakrzewski, G. Jaouen*, ChemBioChem,* **2004**, *5*, 519-525.

[140] K. K. Ong, A.L. Jenkins, R. Cheng, D.A. Tomalia, H.D. Durst, J.L. Jensen, P.A. Emanuel, C.R. Swim, R. Yin*, Analytica Chimica Acta,* **2001**, *444*, 143-148.

Objectives and approach

The principal objective of this chapter of the thesis is to synthesize and characterize new *bis*-MPA dendritic derivatives incorporating Gd(III)DOTA moieties and evaluate their properties as contrast agents.

In order to achieve this purpose, the secondary objectives were defined as:

1) the synthesis of dendrons of first and second generations from the commercial *bis*-MPA monomer, followed by their characterization;
2) their attachment to DOTA moieties and the loading of gadolinium(III), their characterization and the relaxivity measurement of the compounds obtained;
3) the chemical conjugation of the dendrons to targeting units, a folic acid molecule and a monoclonal antibody (antiHER2), to allow the targeting of cancerous cells.

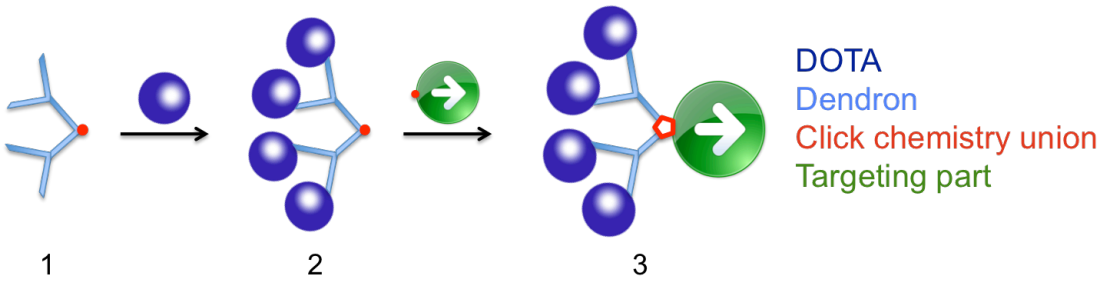

Figure 49: Synthesis of *bis*-MPA derivatives as targeted contrast agents.

Results and discussion

Design and synthesis

The synthesis of the final compounds was carried out in three different phases. The first one has been the synthesis and the functionalization of the *bis*-MPA dendrons by the contrast moiety: the DOTA ligands, which are used to sequester the Gd(III) ions. The second one consisted in the synthesis of the targeting part (folic acid or antibodies), and the third one in the conjugation of both parts to obtain targeted contrast agents.

Synthesis of dendron-DOTA conjugates

Two *bis*-MPA dendrons of first and second generation were synthetized, modified and couple to DOTA ligands. The dendrons were functionalized by an azide in their point in order to bind them by CuAAC to the targeting part (synthesis in Chapter 1).

In the broad part of the dendron, a spacer (6-aminohexanoic acid) was added in order to decrease the steric impediment when inserting the DOTA groups. This spacer was introduced by Steglish esterification (**i**, Figure 50) following the usual method, working with DCC/DPTS in dichloromethane and purifying by column chromatography. The ^{1}H-NMR spectrum of the products of first and second generation obtained showed the apparition of a signal at 1.4 ppm corresponding to the BOC methyls, also confirmed by ^{13}C-NMR and mass spectrometry (see experimental part).

After liberation of the amine groups in acid conditions (**ii**), the products were obtained in a yield of 99% for the first generation dendron (**N_3-G1-($C_5H_{10}NH_2$)$_2$**), and 75% in the case of the second-generation dendron (**N_3-G2-($C_5H_{10}NH_2$)$_4$**).

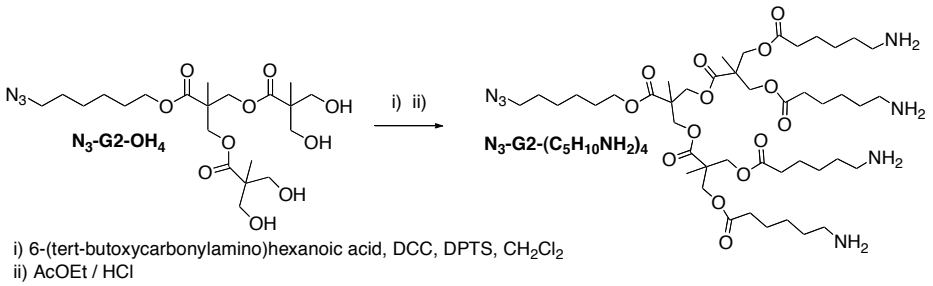

Figure 50: Synthesis of the second generation aminated *bis*-MPA dendron

Once the dendrons were modified, the following step was to functionalize them with the DOTA groups (**DOT3A *t*Bu ester**, Macrocyclics). The reaction between DOT3A-tBu-ester and the amine groups of the dendrons in the presence of carbodiimides (DCC, DCI and EDC) offered the desired product in a very low yield, stopping at the activated intermediate of DOT3A as confirmed by mass spectrometry (m/z = 778.56 in the case of DCC, Figure 51).

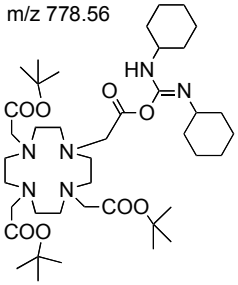

Figure 51: Activated intermediate of DOT3AtBu after reaction with DCC.

Another way of forming an amide bond is to use the combination of HATU (N-methylmethanaminium hexafluorophosphate) and HOAt (1-hydroxy-7-azabenzotriazole), both used for peptide coupling reactions. HOAt is reported to be an efficient additive that speeds up the coupling process, reduces racemization, and provides a visual indication (yellow to colorless) of the reaction end point. HATU appears to involve the formation of 7-azabenzotriazol-1-yl esters that are highly active probably because of intramolecular general base-catalysis. The combination of both compounds permits to enhance reactivity of the species and increase the yield of the reaction.

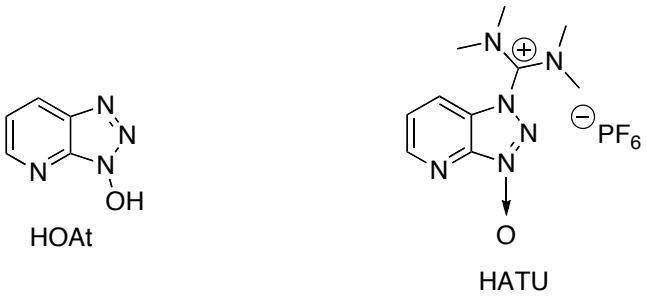

Figure 52: Chemical structures of HOAt and HATU.

In our case, the amide bond was formed using 1.2 eq of HATU and 1.2 eq of HOAt, in dry dichloromethane, stirring for 2 hours (Figure 54, **i**). In the Figure 53, the ^{1}H-NMR spectrum of the first generation dendron modified by DOT3AtBu is shown. We can observe the appearance of a broad peak integrating for 16H at 3.61 ppm corresponding to the 8 C**H**$_2$ **Hr, Hu** and **Hu'**. Moreover, the singlet corresponding to the BOC methyls (**Hz**) at 1.51 ppm and the multiplet corresponding to the R$_2$N-C**H**$_2$-C**H**$_2$-NR$_2$ (**Hs**, **Ht**, **Hv**, **Hw**) confirm the structure of the product obtained.

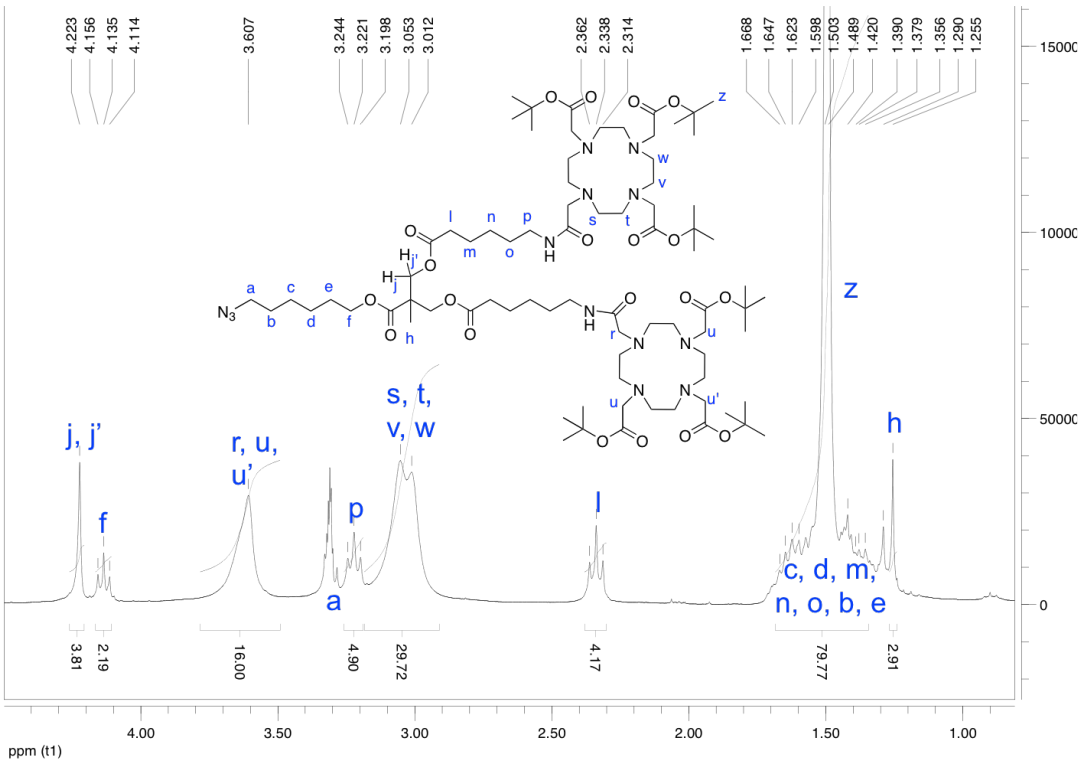

Figure 53: NMR spectrum of G1-DOT3A dendron.

The products were treated with trifluoroacetic acid in dichloromethane in order to deprotect the carboxylic acid groups (**ii**). The deprotection was confirmed in ^{1}H-NMR by the disappearance of the peak due to C**H$_3$**(tBu) at 1.5 ppm and in IR by the band at 3434 cm^{-1} corresponding to the carboxylic acids (O-H). The final compounds of first and second generation were recovered respectively in 57% and 74% yields.

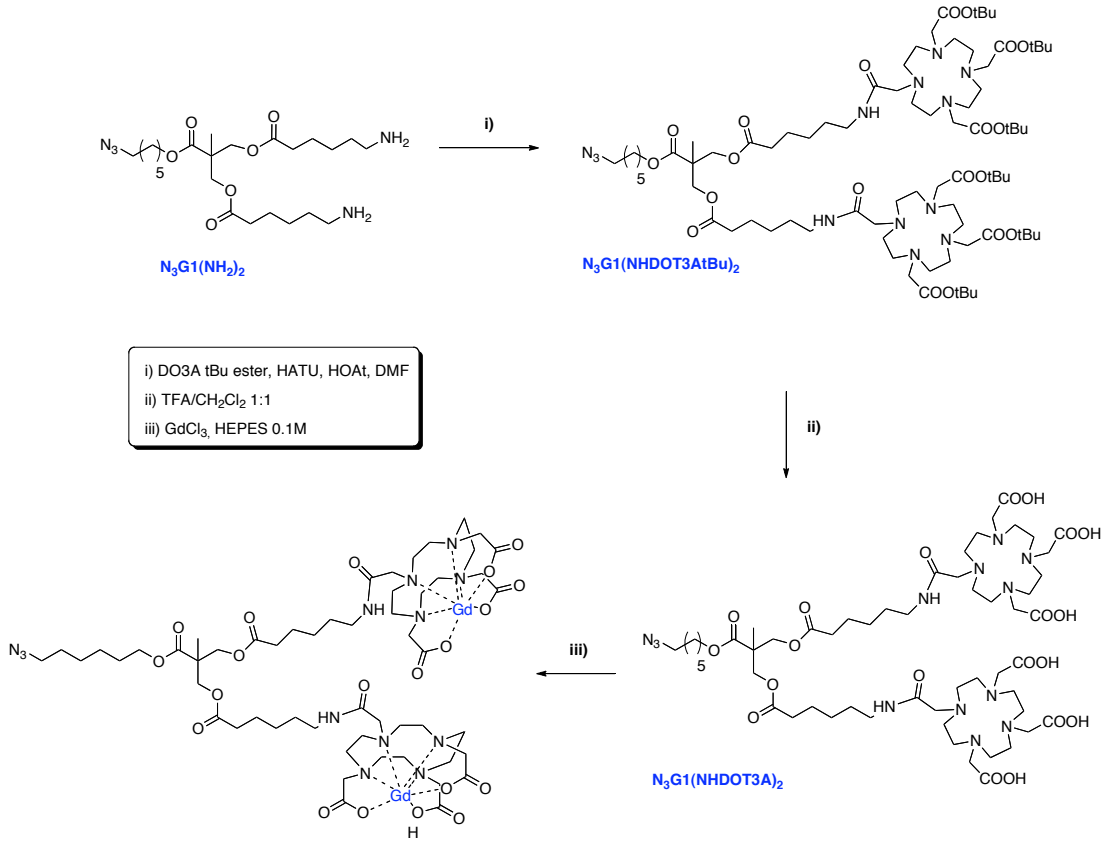

Figure 54: Formation of the DOTA-Gd(III) dendron of first generation N_3G1(NHDOT3A-Gd)$_2$.

The formation of the compounds was followed by the loading of the gadolinium ion inside the DOTA groups (Figure 54, **iii**), which was achieved by stirring the dendron and $GdCl_3$ in 0.1mM HEPES during 24 hours. Then, EDTA was added to complex the excess of gadolinium, and the resulting solution was purified by dialysis against deionized (miliQ) water (cellulose membrane, MW 1000) in order to remove the EDTA-Gd complexes.

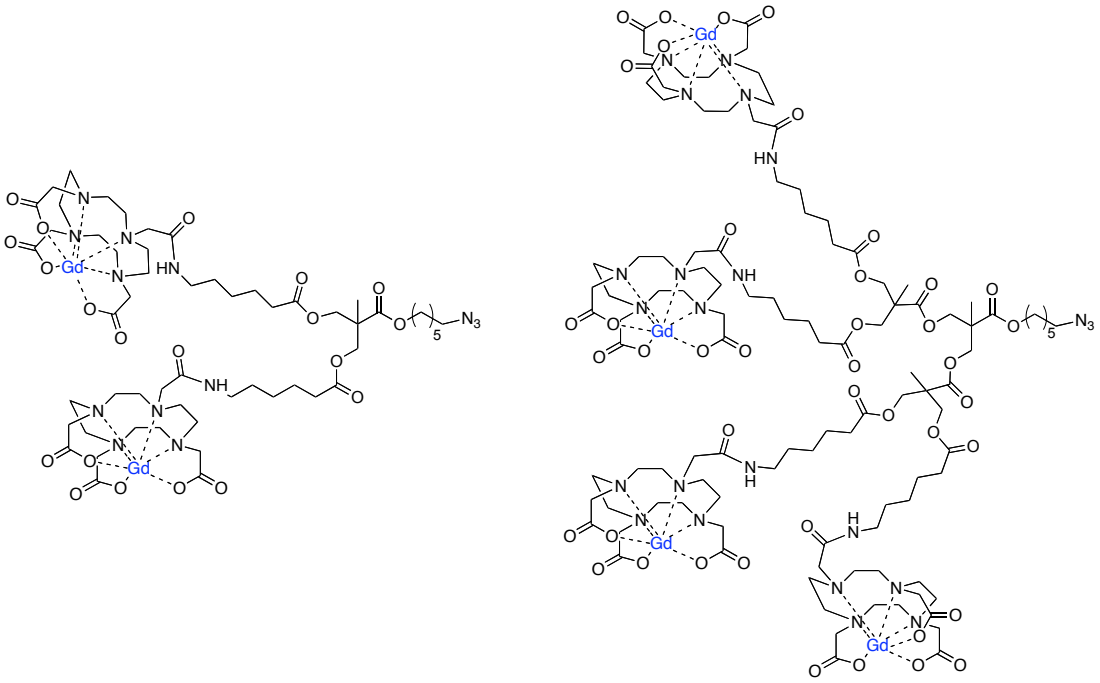

Figure 55: DOTA-dendrons loaded with Gd. Left: first generation dendron. Right: second generation dendron.

After freeze-drying, the relaxivity of the two dendrons in water was measured (Figure 56). The relaxivity measurements were carried out using a Bruker Mq60 NMR analyser Minispec (60MHz). 500 µL of sample at the appropriate concentration in deionized (miliQ) water were loaded in the device inside a glass tube. The measurements were carried out at 37°C, and the parameters of measurement, such as the gain, were adjusted for each compound.

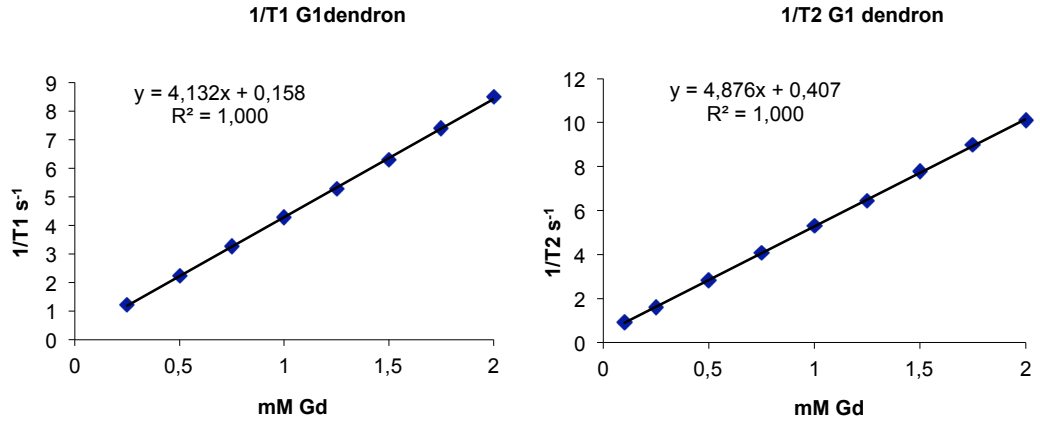

Figure 56: T1 and T2 measurements for the dendron of first generation in function of the concentration of Gd (mM). Gain$_{T1}$=55, gain$_{T2}$=53.

The relaxivity data r_1 and r_2 of the dendron of first generation were deduced from the gradient of the curves obtained. Supposing that both of the DOTA groups were loaded with gadolinium: r_1 = 4.13 $mM_{Gd}^{-1}.s^{-1}$, r_2 = 4.87 $mM_{Gd}^{-1}.s^{-1}$. The relaxivity is expressed in mM of gadolinium.

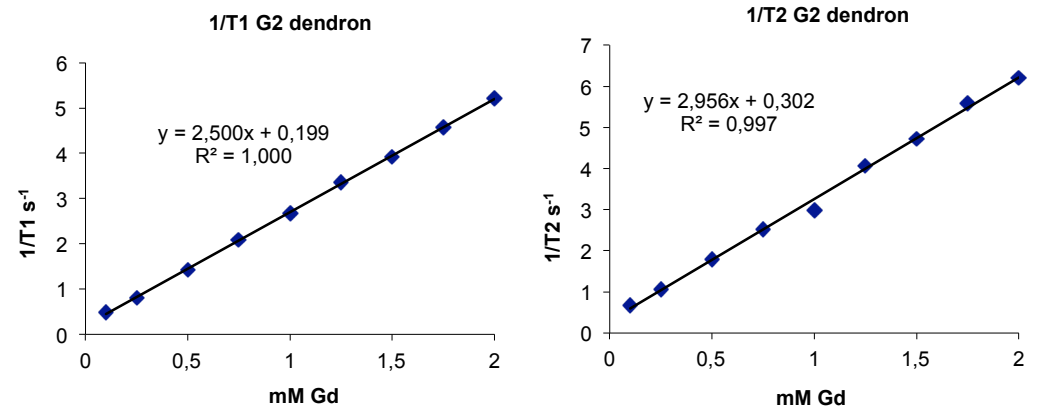

Figure 57: T1 and T2 measurements for the dendron of second generation in function of the concentration of Gd (mM). Gain$_{T1}$=54, gain$_{T2}$=54.

In the case of the second generation dendron, the values of relaxivity, $\boldsymbol{r_1}$ **= 2.50** $\mathbf{mM_{Gd}^{-1}.s^{-1}}$ and $\boldsymbol{r_2}$ **= 2.95** $\mathbf{mM_{Gd}^{-1}.s^{-1}}$ are lower. This could be due to the fact

the all the DOTA groups were not loaded with gadolinium (we considered a 100% loading efficiency for the calculation of the concentration).

If we compare the values obtained in both cases with the relaxivity values of **Gd(III)-DOTA** (Table 8), we can observe that they are very similar. We can conclude that the union of DOTA with our dendrons does not affect remarkably its efficiency.

	Gd(III)-DOTA	G1 dendron	G2 dendron	Unit
r_1	3.0	4.13	2.50	$mM^{-1}_{Gd}.s^{-1}$
r_1	/	*8.26*	*10.00*	$mM^{-1}_{dendron}.s^{-1}$
r_2	3.9	4.87	2.95	$mM^{-1}_{Gd}.s^{-1}$
r_2	/	*9.74*	*11.80*	$mM^{-1}_{dendron}.s^{-1}$

Table 8: Summary of the relaxivity data obtained for the first and second generation dendrons.

Although the relaxivity of the second generation dendron in terms of mM of gadolinium is less elevated than the one of the first generation dendron, its use is more interesting if we look at the global relaxivity in mM of dendron. For the first generation dendron we obtained a $r_{1(G1)}$ of about $\mathbf{8.3\ mM^{-1}_{dendron}.s^{-1}}$ which was improved to $r_{1(G2)} = \mathbf{10\ mM^{-1}_{dendron}.s^{-1}}$ when using the second generation dendron.

Synthesis and characterization of the targeting part

The main idea is to target the dendron-DOTA conjugates to cancerous cells in order to have an accurate view by MRI of the location of the tumor or metastatic cells. In order to do so, we decided to work with two different targeting moieties: folic acid and antiHER2 monoclonal antibody.

Folic acid, of which the receptor (**FR**) was shown to be overexpressed in various cancerous cell lines (Figure 58), is an interesting molecule for the

targeting of our contrast agents.[141] The utilization of the folate receptor for drug delivery can be compare to a Trojan horse since the drugs attached to the folate are shuttled inside the targeted FR-positive cells. The folic acid molecule has a very high affinity for the receptor and allows its effective targeting.

Cancers (solid tumors)	New cases per year in US	%FR	FR-expressing cancers/year
Breast	176 300	48	84 624
Lung	171 600	78	133 848
Uterus	37 400	90	33 660
Colon-rectum	129 400	32	41 408
Ovarian	25 200	90	22 680
Kidney	30 000	75	22 500
Head/neck	39 750	52	20 670
Brain and CNS	16 800	90	15 120
Gastric	26 700	38	10 146
Pancreatic	28 600	13	3718
Endocrine	19 800	14	2772
Testicular	7400	17	1258
Total	708 950		392 404

Figure 58: FR expression in selected solid tumors determined primarily by immunohistochemical analysis of cancer tissue microarrays using a monoclonal IgG to FR. Adapted from N. Parker et Al.[141]

The other strategy is to use **antibodies** directed toward a specific receptor. The HER2 receptor is a member of the epidermal growth factor receptor (EGFR, ErbB, Neu) family. Amplification or over-expression of this gene has been shown to play an important role in the pathogenesis and progression of certain aggressive types of breast cancer and, in recent years, it has evolved to become an important biomarker and target of therapy for the disease.[142] For these reasons it is interesting to use the monoclonal antibody **antiHER2** in targeting contrast agents to cancerous cells.

[141] a) N. Parker, M.J. Turk, E. Westrick, J.D. Lewis, P.S. Low, C.P. Leamon*, Anal. Biochem.,* **2005***, 338*, 284-293; b) P.S. Low and S.A. Kularatne, *Curr. Opin. Chem. Biol.,* **2009***, 13*, 256-262.

[142] a) S. Scholl, P. Beuzeboc, P. Pouillart, *Ann. Oncol.,* **2001***, 12*, S81-S87; b) S. Ménard, P. Casalini, M. Campiglio, S. Pupa, A. Agresti, E. Tigliabue, *Ann. Oncol.,* **2001***, 12,* S15-S19.

Conjugation with the folic acid molecule

Folic acid ((2S)-2-[(4-{[(2-amino-4-hydroxypteridin-6-yl)methyl]amino} phenyl)formamido]pentanedioic acid) was modified by reaction with propargyl amine in order to introduce the alkyne function that will allow the further conjugation by CuAAC. The propargyl folic acid was obtained in presence of DCC and DMAP with triethylamine. The successful synthesis of the product was confirmed by ^{1}H-NMR, ^{13}C-NMR, IR and mass analyses (see experimental part). In the ^{1}H-NMR spectrum, the presence of the N**H** of the amide bond was revealed by the triplet integrating for one proton at 8.28 ppm (Figure 59).

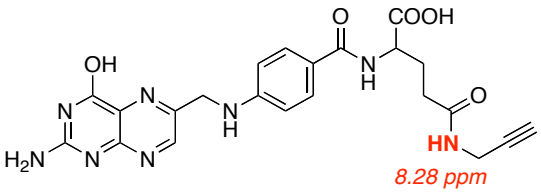

Figure 59: Modified folic acid molecule, NMR characteristic peak at 8.28 ppm (NH).

The union of the propargyl-FA and DOTA-dendrons was obtained by copper-catalyzed click-chemistry 1,3-dipolar cycloaddition. The reaction was carried out in dimethylformamide. The copper(I) catalyst was generated *in situ* by reaction between copper sulfate and sodium ascorbate as described in Chapter 1. In the IR spectrum (KBr), two broad bands at 3431 cm^{-1}, 1630 cm^{-1} and a band at 1405 cm^{-1} can be observed. The first one corresponds to the superposition of the bands due to the stretching modes of the O-H, N-H, COO-H bonds. The second one corresponds to the superposition of the bands due to the C=O stretching mode of the amide, acid, and carboxylate functions. The last band, at 1405 cm^{-1}, is due to the vibration of the O-C-O bonds of the carboxylate functions. Moreover, the formation of the triazide cycle was confirmed by the disappearance of the band corresponding to the azide function at approx. 2100 nm.

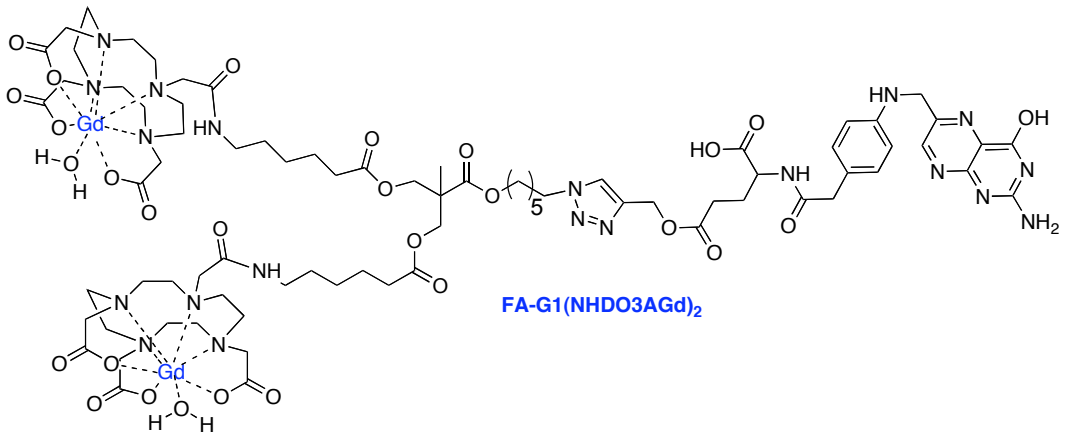

Figure 60: Folic acid-G1 DOTA dendron conjugate.

The relaxivity of the compounds was measured (Figure 61 and Figure 62, Table 2). In the case of the second generation dendron, after the click reaction low relaxivity values were obtained (r_1 = 0.65 $mM^{-1}s^{-1}$, r_2 = 0.77$mM^{-1}s^{-1}$) probably due to an exchange of the Gd ions with the Cu ions present in the reaction mixture. The dendron was reloaded with Gd ions ($GdCl_3$, 0.1M HEPES) and the measurement repeated.

	FA-G1	FA-G2	units
$\mathbf{r_1}$	1.97	2.78	$mM^{-1}{}_{Gd}.s^{-1}$
$\mathbf{r_2}$	2.34	2.73	$mM^{-1}{}_{Gd}.s^{-1}$
$\boldsymbol{r_1}$	*3.94*	*11.12*	$mM^{-1}{}_{FA\text{-}dendron}.s^{-1}$
$\boldsymbol{r_2}$	*4.68*	*10.88*	$mM^{-1}{}_{FA\text{-}dendron}.s^{-1}$

Table 9: Relaxivity of G1 and G2 compounds expressed in $mM^{-1}.s^{-1}$ of Gd and in $mM^{-1}.s^{-1}$ of compound.

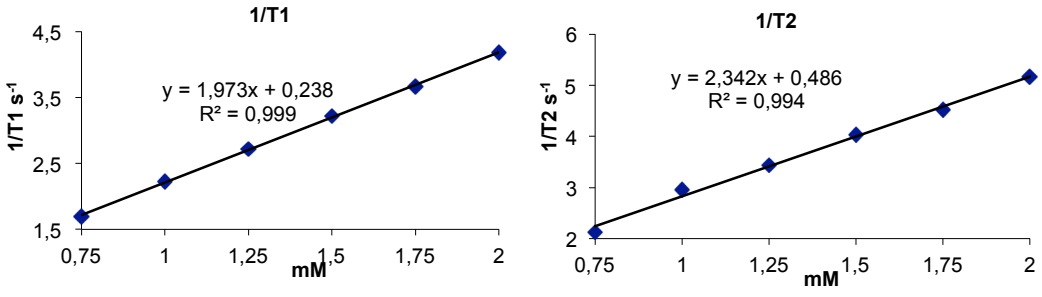

Figure 61: T1 and T2 measurements for the dendron of second generation modified by FA in function of the concentration of Gd (mM). $Gain_{T1}$=54, $gain_{T2}$=53.

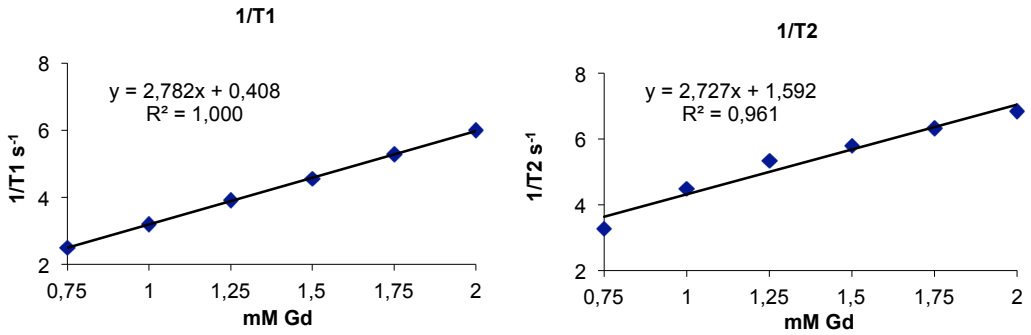

Figure 62: T1 and T2 measurements for the dendron of second generation modified by FA in function of the concentration of Gd (mM). $Gain_{T1}$=54, $gain_{T2}$=53.

In the case of the second generation dendron, the relaxivity values are almost three times better than the one of the Gd(III)-DOTA contrast agents. The improvement of the contrast agents activity combined with the targeting ability of the folic acid molecule make the second generation dendron an interesting compound for future *in vitro* and *in vivo* tests.

Conjugation with anti-bodies

The structural characteristics of the antibody molecules offer us various options for their modification and their conjugation. Nevertheless, it is important to take into account the possible affectation of the antigen binding activity. In the Figure 63, a schematic illustration of an antibody structure is represented.[143] The most basic immunoglobulin G molecule is composed of two light chains and two heavy chains that are linked by disulfide-bridges. Depending on the class of immunoglobulin, the molecular weight of the heavy chains ranges from about 50 kDa to around 75 kDa and the weight of the light chains is about 25 kDa. The two light chains and the two heavy chains of a same molecule are identical. For IgG molecules the global molecular weight representing all four parts is comprised between 150 kDa and 200 kDa.

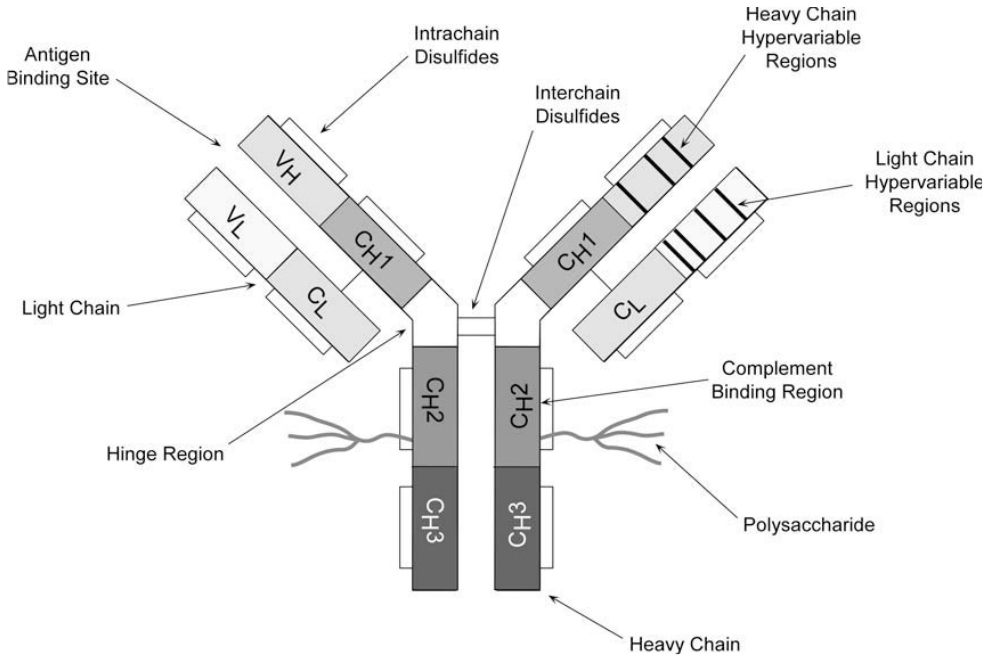

Figure 63: Illustration of an antibody structure. Adapted from Hermanson.[143]

Different functional groups are suitable for modification or conjugation purposes. Amine and carboxylate groups are abundant in antibodies. Favor site-directed reactions is very important to preserve the activity of the antibody. One of

[143] G.T. Hermanson, *Bionconjugate techniques,* **2008**, Elsevier.

the methods is to take advantage of the carbohydrate chains typically attached to the C_H2 domain within the Fc region. In this purpose, the oxidation of the polysaccharide sugar residues with sodium periodate generating aldehyde groups is necessary (Figure 64). Direct conjugation though the antibody carbohydrate chains avoids the modification of the antigen binding regions while allowing the use of intact antibody molecules.

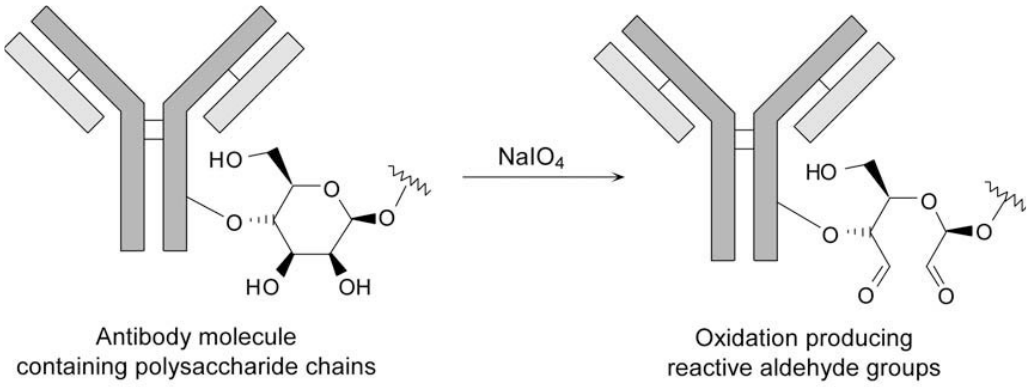

Figure 64: Antibody carbohydrates oxidation with sodium periodate. Adapted from Hermanson.[143]

After the oxidation of the carbohydrates, the antibody is ready to be modified with aminated compounds by forming a Schiff base (RCH=NR').

We chose to work with the human epidermal growth factor receptor-2 (also known as Neu, HER-2 or ErbB2), which is a member of the epidermal growth factor receptor subfamily and is considered to be one of the most promising targets in cancer immunotherapy.[144] The **HER2** protein (185 kDa) has been shown to be overexpressed in a variety of tumors, including breast[145] and ovarian cancers,[146] and has been associated with more aggressive tumor growth and poorer clinical outcomes. The overexpression of HER2 receptors in tumor cells as well as their presence in the extracellular domain makes it an ideal target for

[144] H.S. Cho, K. Masen, K.X. Ramyar, A.M. Stanley, S.B. Gabelli, D.W. Denney, D.J. Leahy, *Nature,* **2003**, *421*, 756-760.

[145] D.J. Slamon, G.M. Clark, S.G. Wong, W.J. Levin, A. Ullrich, W.L. McGuire, *Science,* **1987**, *235*, 177-182.

[146] M.A. Olayioye, R.M. Neve, H.A. Lane, N.E. Hynes, *Embo. J.,* **2000**, *19*, 3159-3167.

receptor-mediated drug delivery to tumors. Monoclonal antibodies directed against HER2 offer a potential strategy for HER2-targeted delivery.

Before starting to work with the antiHER2 antibody and the Gd(III)DOTA-dendron derivatives, the reaction was optimized using a similar dendrimer modified by a fluorescent dye and an polyclonal antibody (horseradish, Sigma). Rhodamine B was chosen as fluorescent moiety because of its facility of use and modification. The fluorescence allows following the reaction in an easier way. The use of polyclonal antibodies is motivated by the high price of the monoclonal antibodies.

Rhodamine-dendron synthesis and characterization:

The commercial rhodamine B base reacted with propargyl alcohol to give the clickable derivative **rhodamine-alkyne** (**i**). Then, copper catalyzed 1,3-dipolar cycloaddition in dimethylformadide (**ii**) followed by the deprotection of the amine groups in acid environment (**iii**) gave the desired product in 50 % total yield (Figure 65).

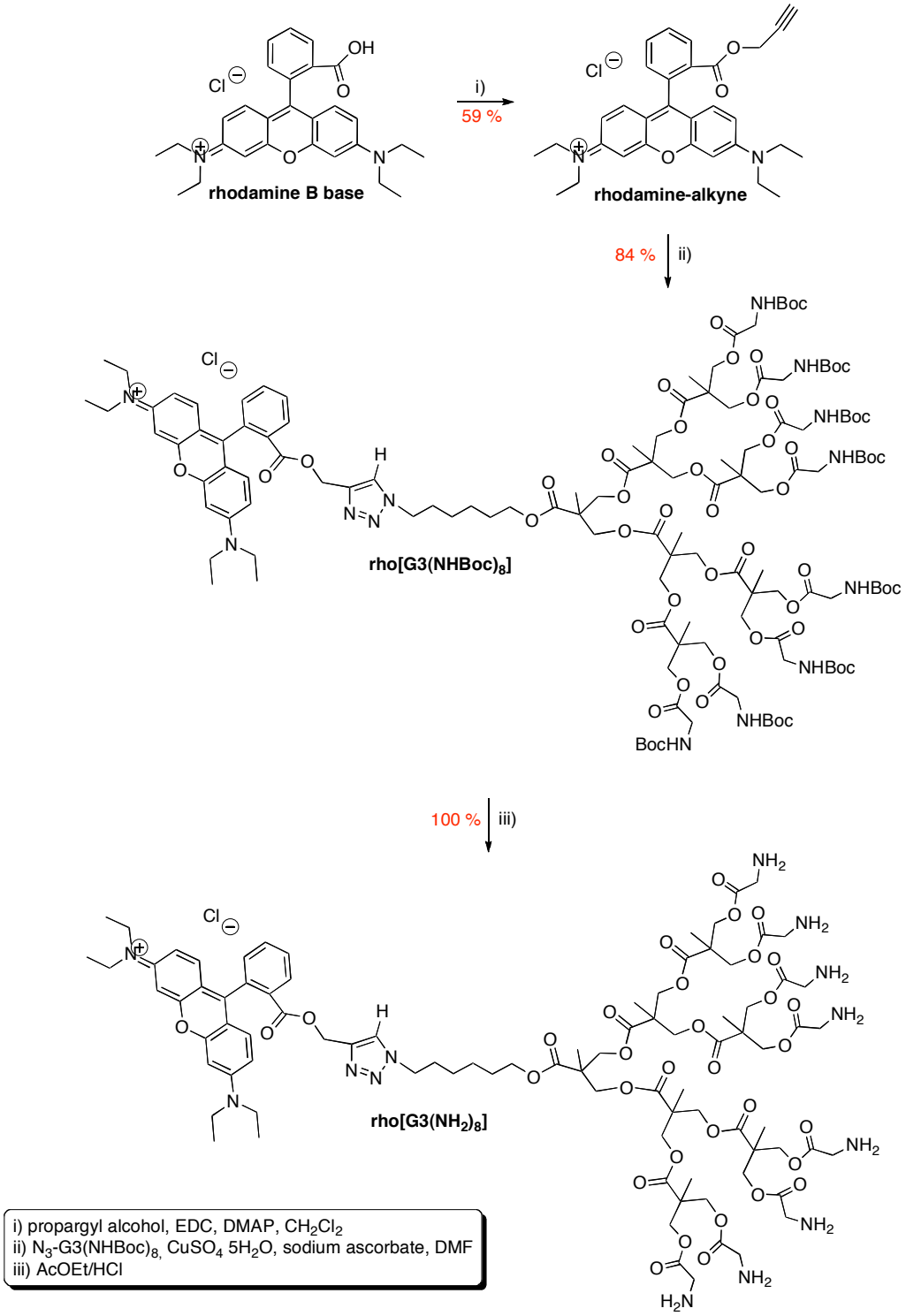

Figure 65: Synthesis of the rhodamine-dendron derivative.

The ^{1}H-NMR spectrum of the alkyne-rhodamine compound is shown in Figure 66: ^{1}H-NMR spectrum of alkyne-rhodamine. 300MHz, CDCl3 (7.26ppm). The alkyne modification of rhodamine B base was demonstrated by the presence

of the triplet integrating for 1H at 2.42 ppm due to the -C≡C**H**, **Ha**, and of the doublet integrating for 2H at 4.62 ppm due to the –C**H**$_2$-C≡CH, **Hb**. The peaks corresponding to the =N-C**H**$_2$-CH$_3$ (**Hj**), and to the =N-CH$_2$-C**H**$_3$ (**Hk**), appear respectively at 3.65 ppm (q, J = 7 Hz, 8H) and at 1.33 ppm (t, J = 7 Hz, 12H). The four aromatic protons of the C-**Ph**-COO- are situated at 8.33 ppm (**Hc**, dd, J_{ortho} = 7.8 Hz, J_{meta} = 0.9 Hz, 1H), 7.75 ppm (**Hd**, td, J_{ortho} = 7.8 Hz, J_{meta} = 1.2 Hz, 1H), 7.85 ppm (**He**, td, J_{ortho} = 7.5 Hz, J_{meta} = 1.2 Hz, 1H) and 7.36 ppm (**Hf**, dd, J_{ortho} = 7.8 Hz, J_{meta} = 1.2 Hz, 1H). The signals corresponding to the aromatic protons on the cycle in α of –N(CH$_2$-CH$_3$)$_2$ appear at 7.06 ppm (**Hg**, d, J_{ortho} = 9.6 Hz, 2H), 6.92 ppm (**Hh**, dd, J_{ortho} = 9.3 Hz, J_{meta} = 2.4 Hz, 2H) and 6.84 ppm (**Hi**, d, J_{meta} = 2.1 Hz, 2H).

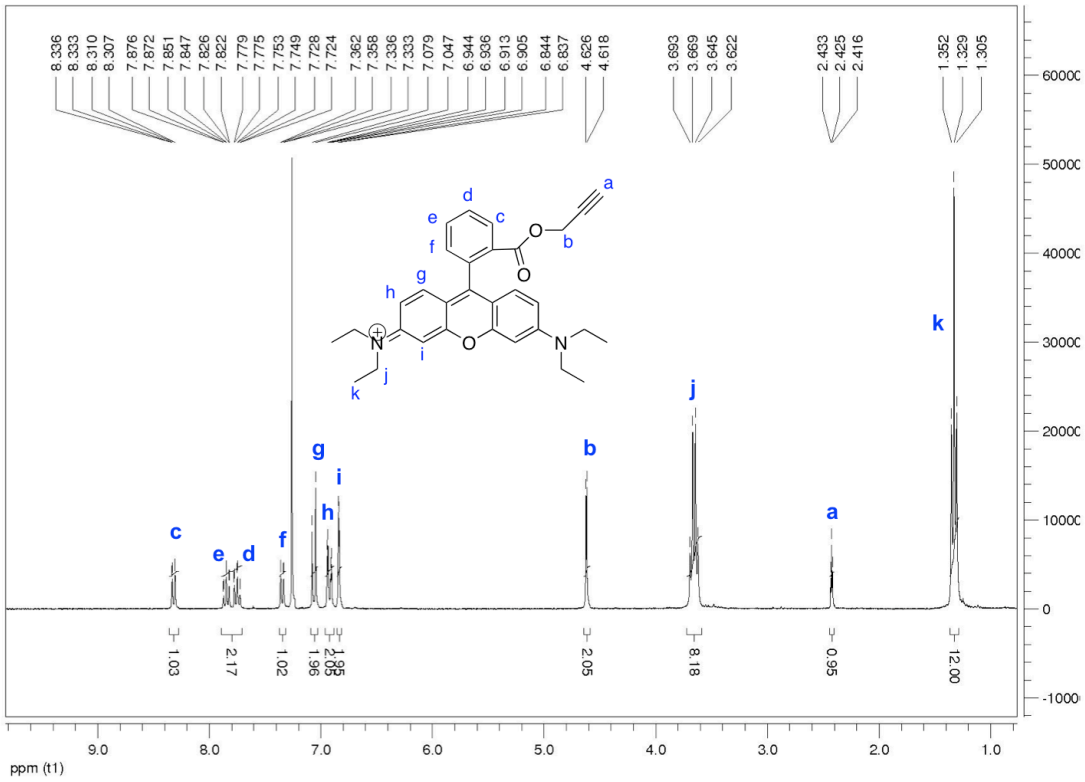

Figure 66: ^{1}H-NMR spectrum of alkyne-rhodamine. 300MHz, CDCl3 (7.26ppm).

In the case of the compound formed at the next reaction step (**ii**, **rho[G3(NHBoc)$_8$]**), the formation of the triazide cycle was confirmed by the disappearance of the -C≡C**H** triplet at 2.42 ppm, and the shift of the doublet from 4.62 ppm (–C**H**$_2$-C≡CH) to 5.23 ppm (–C**H**$_2$-C=C-N). Besides, the apparition of the singlet peak due to the proton on the triazide cycle at 7.85 ppm was observed.

The fluorescence emission intensity of the final compound, **rho[G3(NH$_2$)$_8$]**, was studied in function of its concentration. The maximum of emission was found at 580 nm (Figure 67).

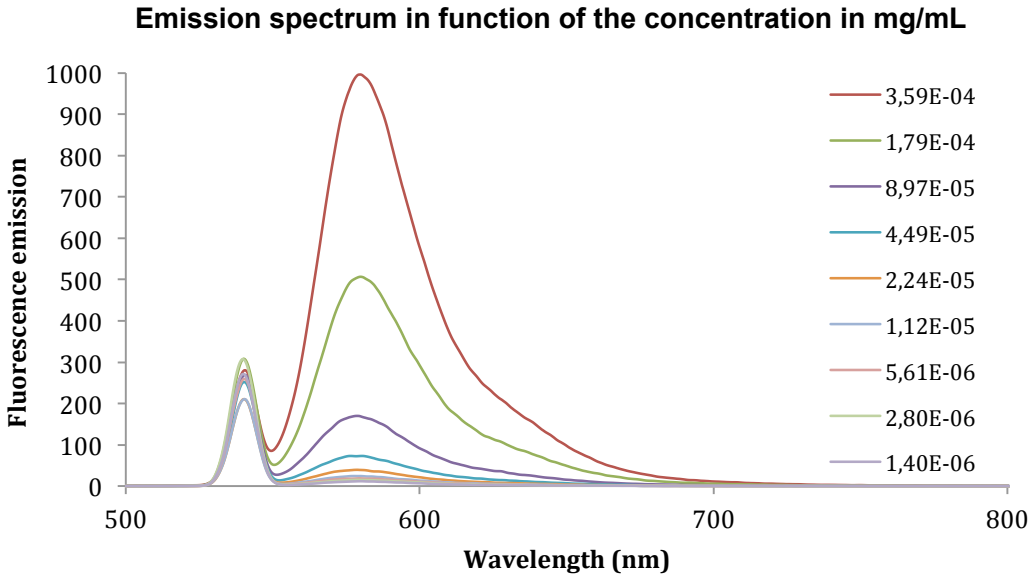

Figure 67: Emission spectrum of rho[G3(NH$_2$)$_8$] in function of its concentration in mg/mL. The peak of excitation appears at 540 nm.

Optimization of antibody-dendron reaction:

The fluorescent derivative was bound first to a polyclonal antibody (horseradish, Sigma P7899), in order to optimize the reaction. The procedure was adapted from Bioconjugate techniques 2008.[147] Briefly, the covalent bonding was obtained by the formation of Schiff bases that are produced from an amine and a carbonyl group (aldehyde or ketone) by nucleophile addition forming a heminaminal. This reaction is followed by deshydratation to generate an imine (Figure 68).

In order to form the desired aldehyde, the antibody (AB) sugars were oxidated using sodium periodate ($NaIO_4$, 1000eq). After purification by gel exclusion chromatography (Sephadex column, GE Healthcare), the dendron was added and the mixture agitated for 2 hours. Then, cyanoborohydride was added as

[147] G.T. Hermanson, *Bioconjugate techniques* **2008**, Elsevier.

a reductive agent for the stabilization of the Schiff bases formed. Finally, the unreacted aldehyde groups were blocked using ethanolamine. The final product was purified by exclusion chromatography in order to eliminate the excess of rhodamine dendron, other reagents, and salts.

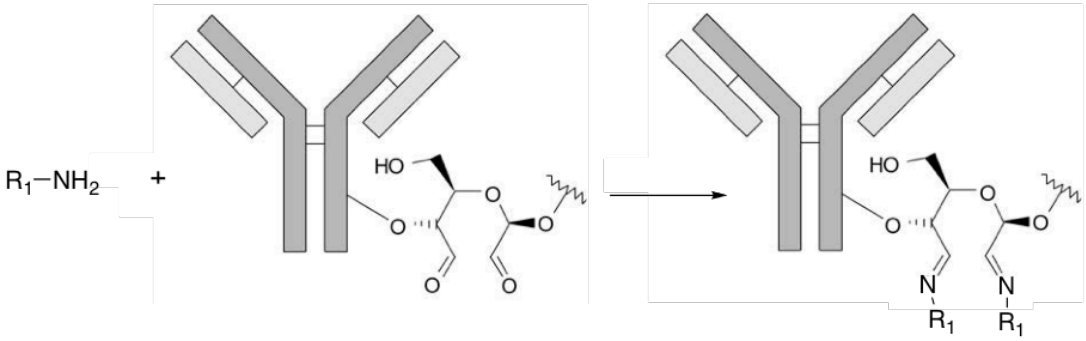

Figure 68: Formation of the Schiff bases by reaction between the compound amines and the aldehyde groups generated by previous oxidation of the antibody.

If the coupling of the dendron with the antibody were efficient, the antibody would wear a fluorescent labeling that could be seen by fluorescence emission spectroscopy. In the case of the antiHER2 mAb, it would also allow the visualization of the marking in HER2 receptor positive cells by fluorescent microscopy.

The different steps of the coupling were realized at various pH in order to optimize the reaction (Table 10). In the literature,[24] the reaction is realized at pH 9.6. However, as we could see in the Chapter 1, our dendritic compounds are easily degraded in alkaline conditions. This is the reason why we needed to adapt the protocol to our particular case, and see if the reaction could be carried out in acid condition.

	Oxidation	Schiff base Formation	Max Fluorescence intensity
A	pH 8	pH 8	75
B	pH 5	pH 8	66
C	*pH 5*	*pH 5*	*189*

Table 10: Conditions of reaction and maximum fluorescence intensity.

As we can observe in the Figure 69, the best condition was found at pH 5, where more fluorescence intensity was obtained, meaning that more dendron was attached to the antibody. This result confirms the possibility of modifying the antibody without degrading the dendritic unit.

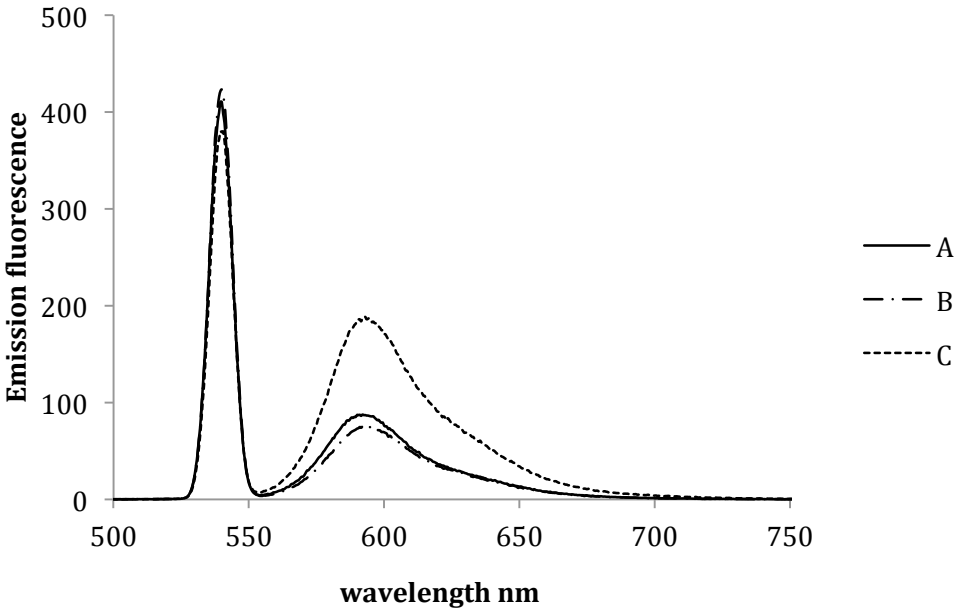

Figure 69: Fluorescence emission spectrum of the products of the AB-dendron reaction realized in the conditions A (all the steps at pH 8), B (oxidation of the AB at pH 5, reaction with the rho[G3(NH_2)$_8$] at pH 8), and C (all the steps at pH 5). The peak of excitation appears at 540 nm.

The rhodamine-modified antibody, obtained with the reaction condition **C**, was characterized by **SDS-PAGE**. SDS-PAGE, Sodium Dodecyl Sulphate PolyAcrylamide Gel Electrophoresis, is used to separate proteins according to their

electrophoretic mobility (a function of the length of a polypeptide chain and its charge). In most proteins, the binding of SDS to the polypeptide chain imparts an even distribution of charge per unit mass, thereby resulting in a fractionation by approximate size during electrophoresis. The protein to be analyzed is mixed with SDS, an anionic detergent that denatures secondary and non–disulphide–linked tertiary structures, and applies a negative charge to each protein in proportion to its mass. Blue bromophenol is added as a tracking dye. The samples are boiled to promote protein denaturation, helping SDS to bind.

The gel is made of polyacrylamide and SDS and its concentration varies from 4% to 24%. An electric field is applied across the gel, causing the negatively charged proteins to migrate across the gel towards the positive (+) electrode (anode). Depending on their size, each protein will move differently through the gel matrix: short proteins will more easily fit through the pores in the gel, while larger ones will have more difficulty (finding more resistance).

Following the electrophoresis, the gel has to be stained, in our case using a silver staining.

In the Figure 70, a picture of the gel obtained is presented. It compares the AB without modification (AB), the AB after all the reaction steps except the addition of rho[G3(NH_2)$_8$] (AB-) and the AB modified by rho[G3(NH_2)$_8$] (ABrho). A prestained protein standard was used as reference (Spectra Multicolor Broad Range Protein Ladder, Thermoscientific), each band correspond to a protein of known molecular weight. In all the cases, we can observe the presence of a band corresponding to the heavy chains of the antibody at approx. 50 kDa and a band corresponding to the light chains at approx. 25 kDa.

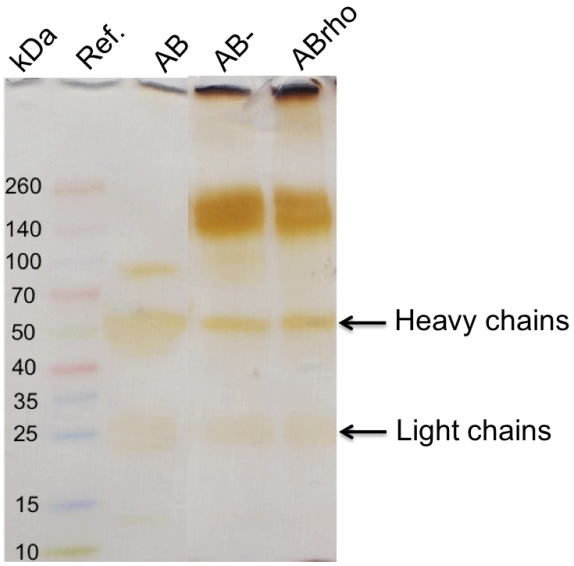

Figure 70: SDS-PAGE of the modified antibody. AB = antibody control without modifications, AB- = antibody after all reaction steps except the addition of rhodamine dendron, ABrho = antibody modified by rhodamine dendron. The scale is given in kDa.

Polyclonal antibodies are a combination of immunoglobulin molecules, consequently there is a slight difference between the molecular weight of the different parts, and the bands observed are wide. A difference between the bands observed for the AB control and for the AB that followed all the reaction steps, AB- and ABrho, was observed. It seems that the oxidation of the AB sugars leads to an aggregation of the molecules (band at approx. 140 MDa). No clear difference was observed between the ABrho and the AB- (without dendron), probably due to the width of the bands. However, the binding of the dendron to the antibody was confirmed by fluorescence emission spectroscopy in Figure 69. This is the reason why we decided to continue with this reaction method using the **mAB antiHER2**.

Confirmation of the biological activity of anti-HER2 after modification:

The operation was repeated with the monoclonal antibody antiHER2 following the process described previously. The reaction was carried out using 0.5 mL of antiHER2 at 200 µg/mL. After all the reaction steps and the two gel filtrations (80 % yield), 2 mL of the modified antiHER2 were obtained at a theoretical concentration of 30 µg/mL. The concentration of antibody after the reaction cannot be deduced using conventional methods such as the coomasie staining and the Lowry assay because of the interference of the rhodamine in the absorption measurements.

The union of the dendron to the antibody was confirmed by fluorescence emission spectroscopy. The maximum of emission was observed at 580 nm (Figure 71).

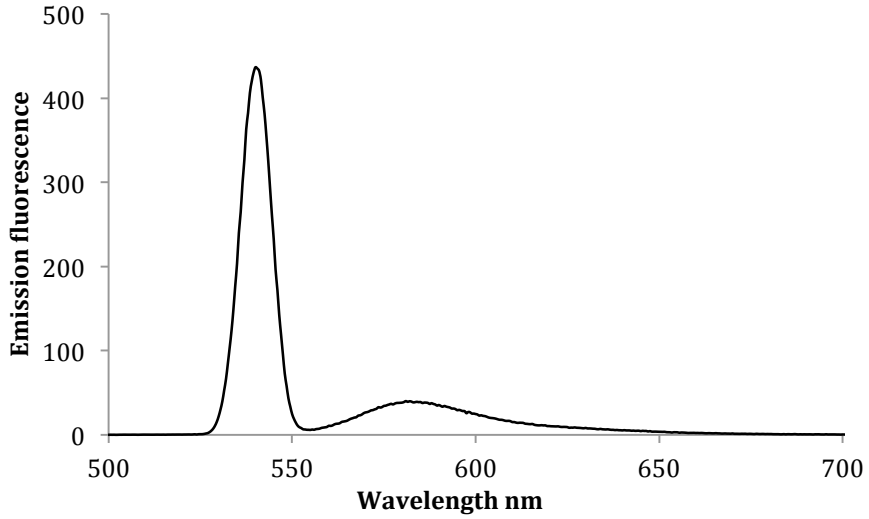

Figure 71: Emission spectrum of modified anti-HER2. The peak of excitation appears at 540 nm.

The modified mAB was characterized by SDS-PAGE and isoelectric focusing (**IEF**) (Figure 72). The isoelectric point (**pI**) is the pH at which a particular molecule carries no net electrical charge. Biological amphoteric molecules such as proteins contain both acid and basic functional groups. Amino acids that make up proteins may be positive, negative, or neutral, and together give a protein its

overall charge. At pH below their pI, proteins carry a net positive charge; at pH above their pI they carry a net negative charge. Proteins can, thus, be separated according to their isoelectric point (overall charge) on a polyacrylamide gel using a technique called isoelectric focusing (IEF), which uses a pH gradient to separate the proteins.

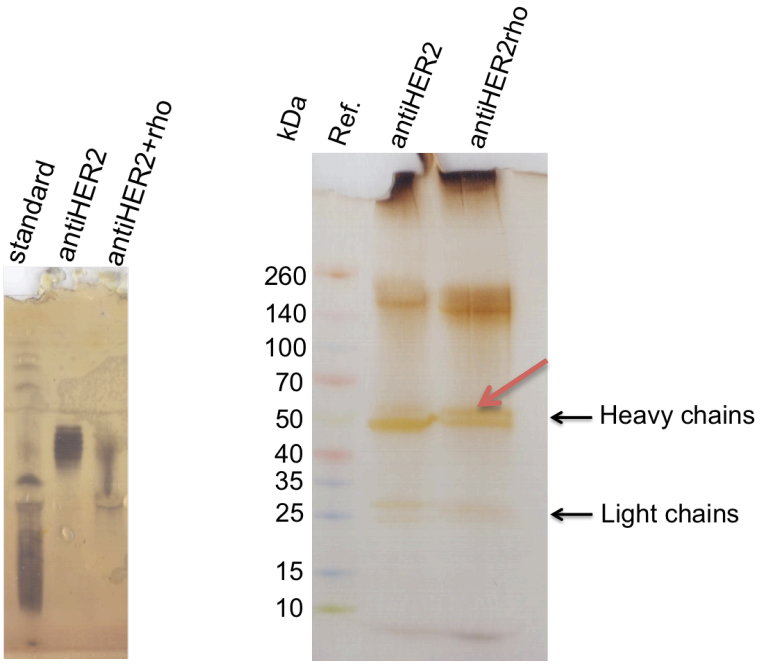

Figure 72: IEF (left) and SDS-PAGE (right) of the antiHER2 before and after reaction with the rhodamine dendron. AntiHER2 = antibody without modification, antiHER2rho = antiHER2 modified with the rhodamine dendron.

In the Figure 72, we can observe that the modification of the antiHER2 structure by the rhodamine dendron provoked a slight difference between the isoelectric points of the proteins. In the SDS-PAGE gel, a new band just above the heavy chain band (red arrow) at approx. 50 kDa is observed. This band could correspond to the modification of the heavy chains by our dendron. The band situated between 140 kDa and 260 kDa also seems to be more intense.

In vitro characterization:

After characterization, the **antiHER2-rho** was incubated with cells that express the HER2 receptor: **MCF-7** (breast cancer cells) as positive control, and cells that express the receptor in a very low amount: **COS-7** (fibroblast cells) as negative control.

In a first assay, our modified antiHER2 AB was incubated at 37°C during 30 min with both cell lines after fixation. Unexpectedly, no red fluorescence emission was detected in the case of the MCF-7. To find out if the problem was due to an issue with the membrane receptor or because the MCF-7 cells were not a good positive control for HER2 receptor, a second assay was realized. In this experiment, before incubating the cells with the AB, the membrane of the cells was permeabilized to open the access to the intracellular receptors to the AB. During this assay red fluorescence emission was seen when the MCF-7 cells were permeabilized and no fluorescence when the membrane was intact. After looking for literature, we found out and confirmed that an important condition for this experiment is the way of dissociating the cells before using them. Indeed, using trypsin induced a disappearance of HER2 receptor from the cell membrane.[148] For the following experiment, EDTA was used instead of trypsin for cell dissociation.

To confirm the activity of the antibody a 4-points experiment was carried out:

- a) Incubation with the **commercial antiHER2** (Santa Cruz Biotechnology), followed by the incubation with a **secondary antibody** (anti-mouse, Alexa Fluor 488, Invitrogen) for detection;
- b) Incubation with **rhodamine-modified antiHER2**, followed by the incubation with the **secondary antibody**;
- c) Incubation with **rhodamine-modified antiHER2**;
- d) Incubation only with the **secondary antibody**.

[148] M.A. Molina, J. Codony-Servat, J. Albanell, F. Rojo, J. Arribas, J. Baselga*, Cancer Research,* **2001**, *61*, 4744-4749.

The secondary antibody was used for detection purpose. This antibody is conjugated to a fluorescent dye (in our case Alexa Fluor 488, green fluorescence) and by recognizing the primary antibody it allows to detect its presence on the cells as illustrated in Figure 73.

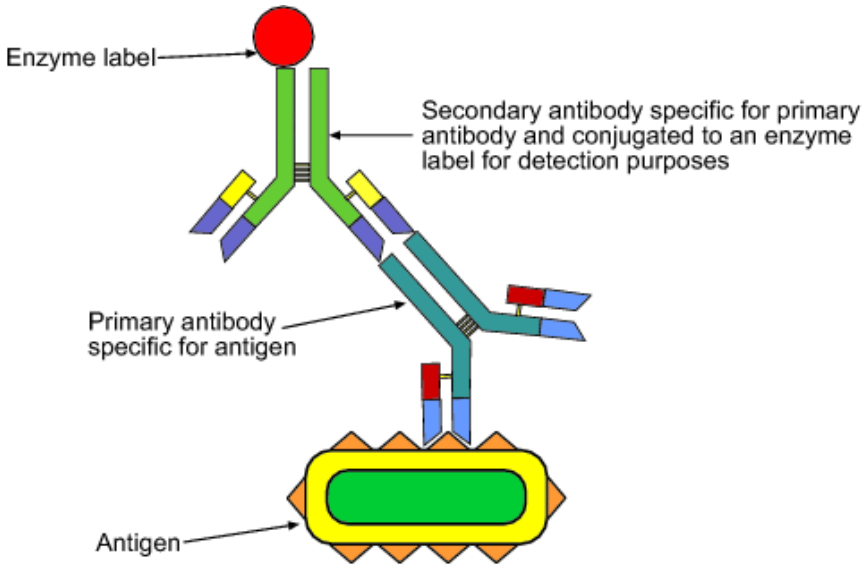

Figure 73: Schematic illustration of the role of the secondary antibody.

In the Figure 74, the results with **MCF-7** cells, used as positive control for the HER2 receptor, are shown. The fluorescence of the cells was visualized using an inverted microscope system (Nikon Eclipse Ti).

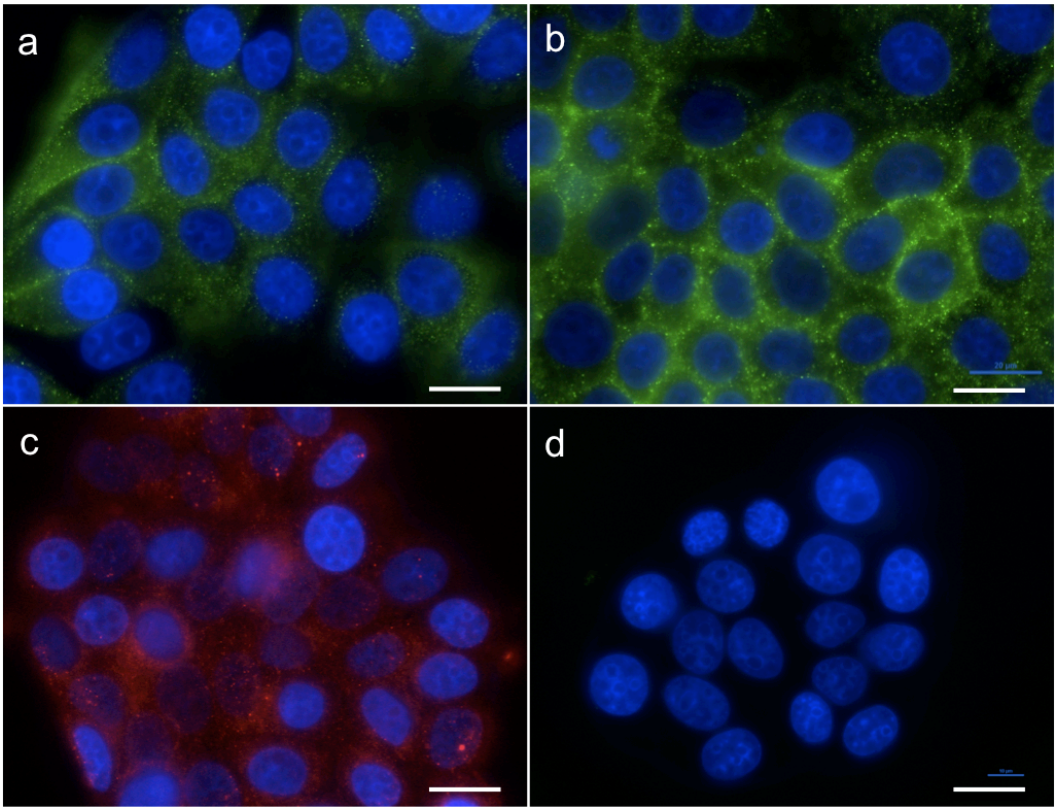

Figure 74: Fluorescence microscopy pictures of MCF7 cells. Nuclei were marked with DAPI (blue), the secondary antibody is represented in green (Alexa Fluor 488) and our antiHER2 modified with rhodamine is represented in red. Primary antibodies were used at 3 µg/mL and secondary antibody at 6µg/mL. a: MCF7 cells incubated with commercial antiHER2, followed by secondary antibody incubation; b: MCF7 cells incubated with our rhodamine modified antiHER2, followed by secondary antibody incubation; c: MCF7 cells incubated with our rhodamine modified antiHER2; d: MCF7 cells incubated only with the secondary antibody. Scale bar: 20 µm.

The results obtained in the picture **a,** green marking of the cells, confirm that MCF-7 cells present the HER2 receptor, and that the commercial antiHER2 can be used to target them. The presence of marking in the experiment **b** confirms that our modified antibody is also able to recognize the receptor after chemical modification. The red marking in the picture **c** shows that our modified AB antiHER2-rho can be detected using the rhodamine fluorescence, without the need

of a secondary antibody. Finally, in picture **d** we can see that there is no marking of the cells when they are incubated only with the secondary antibody, confirming that the signal in **a** and **b** is exclusively due to the presence of the antiHER2 antibodies.

To ensure that the modified antibody keep its specificity for the antiHER2 receptor, the same experiment was carried out using **COS-7** cells (Figure 75). COS-7 cells were used as negative control because they present a very low amount of HER2 receptors.

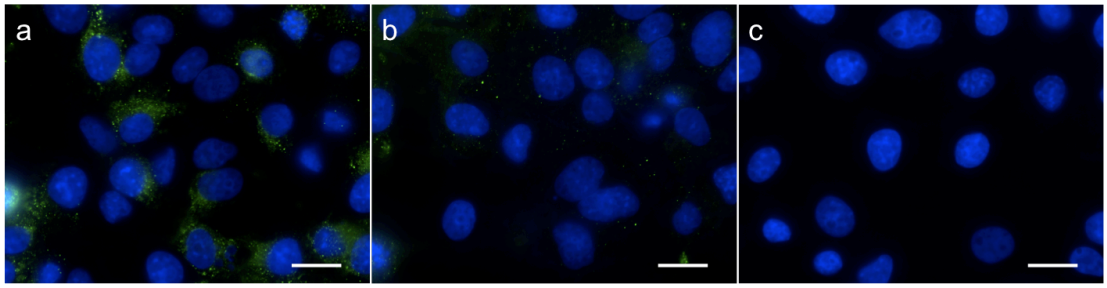

Figure 75: Fluorescence microscopy pictures of COS7 cells. Nuclei were marked with DAPI (blue), the secondary antibody is represented in green (Alexa Fluor 488) and our antiHER2 modified with rhodamine is represented in red (Rhodamine). Primary antibodies were used at 3 µg/mL and secondary antibody at 6µg/mL. a: COS7 cells incubated with commercial antiHER2, followed by secondary antibody incubation; b: COS7 cells incubated with our rhodamine modified antiHER2, followed by secondary antibody incubation; c: COS7 cells incubated with our rhodamine modified antiHER2. Scale bar: 20 µm.

No or very low marking of the cells by the commercial antiHER2 (**a**), and the antiHER2-rho (**b** and **c**) was seen. This observation confirms that the modification of the antibody did not spoil its specificity to HER2 receptor.

Taken all together, the results confirm that after chemical modification and attachment of dendritic compounds to the heavy chain of the AB, its biological activity and specificity is preserved. Our modified antiHER2, antiHER-rho, is a good system for targeting cells expressing HER2 receptor. AntiHER2 modified by rhodamine can be used to mark HER2 expressing cells without the need of secondary antibody detection.

Having this confirmation, antiHER2/dendron-DOTA conjugates were prepared following the same methodology.

Dendrimer synthesis and antiHER2 coupling:

First, the DOTA dendron was bound by copper-catalyzed click chemistry 1,3-dipolar cycloaddition to a third generation *bis*-MPA dendron functionalized with primary amines at its surface. This step permits us to have eight amine groups on the surface of our dendrimers and improve the attachment to the antibody. Then, the whole dendrimer was attached to the antibody by forming a Schiff base (RCH=NR') (Figure 76).

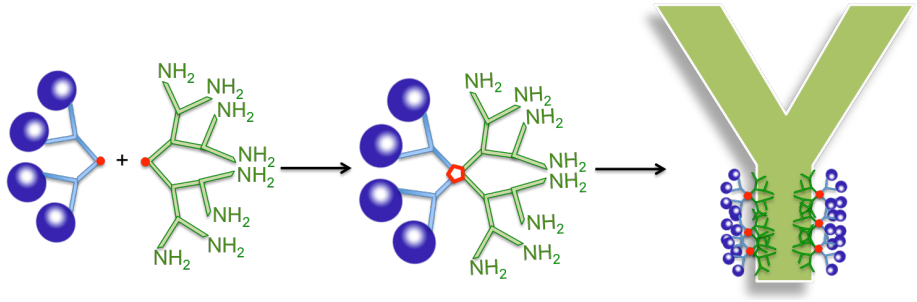

Figure 76: Simplified scheme of dendron-antibody union.

The first step was to synthesize a third generation dendron functionalized at its point by a triple bond and at his broad part with amine groups. The synthesis was carried out from the commercial *bis*-MPA monomer following the same method than in Chapter 1 for the synthesis of the dendron **[1]** (Steglish esterifications followed by the hydroxyl groups deprotection). The final dendron was obtained in 9 steps in a global yield of 15 % (Figure 77).

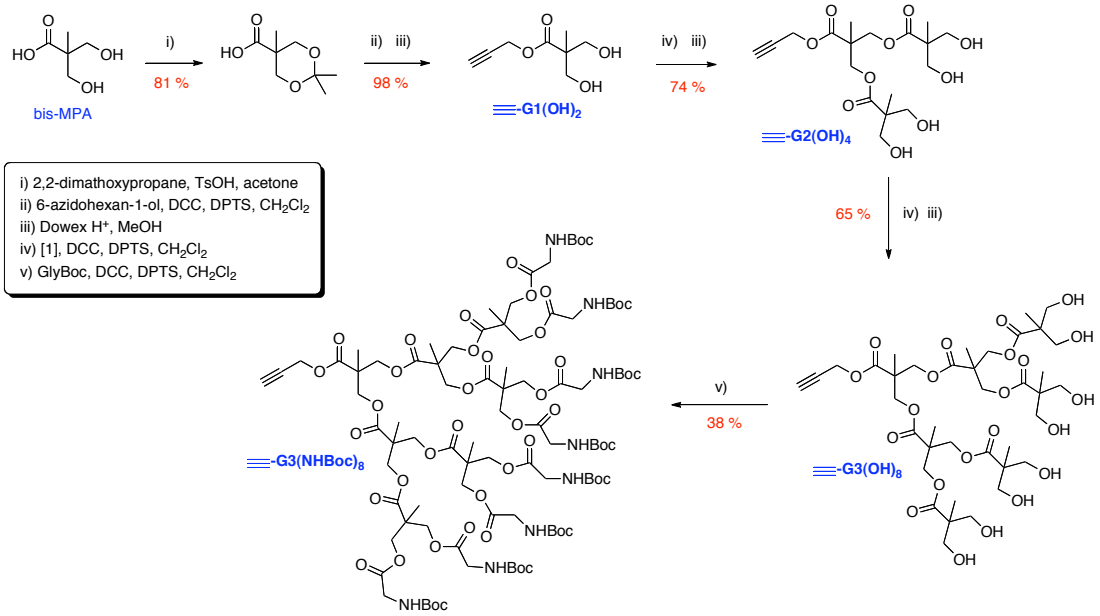

Figure 77: 3rd generation *bis*-MPA dendron functionalized by glycine at its surface and alkyne at its point.

The correct functionalization by the alkyne of **≡-G1(OH)$_2$** (**ii**) was confirmed by the presence of the triplet peak due to the proton **H**-C≡C- at 2.46 ppm in ^{1}H NMR. In the case of the final compound, the singlet peak at 1.46 ppm corresponding to the -Boc methyls and integrating for 72H and the doublet peak corresponding to the –CO-C**H**$_2$-NHBoc protons at 3.90 ppm integrating for 16H revealed the correct functionalization.

The protected third generation dendron **≡-G3(NHBoc)$_8$** was then attached to the DOTA dendron by copper-catalyzed click chemistry 1,3-dipolar cycloaddition, in dimethylformamide. The copper(I) catalyst was generated *in situ* by reaction between copper sulfate and sodium ascorbate. This step was carried out after the loading of gadolinium inside the DOTA groups. The product was purified by extractions and dialysis against deionized (miliQ) water. The reaction was followed by the deprotection of the amine groups in acid environment (Figure 78).

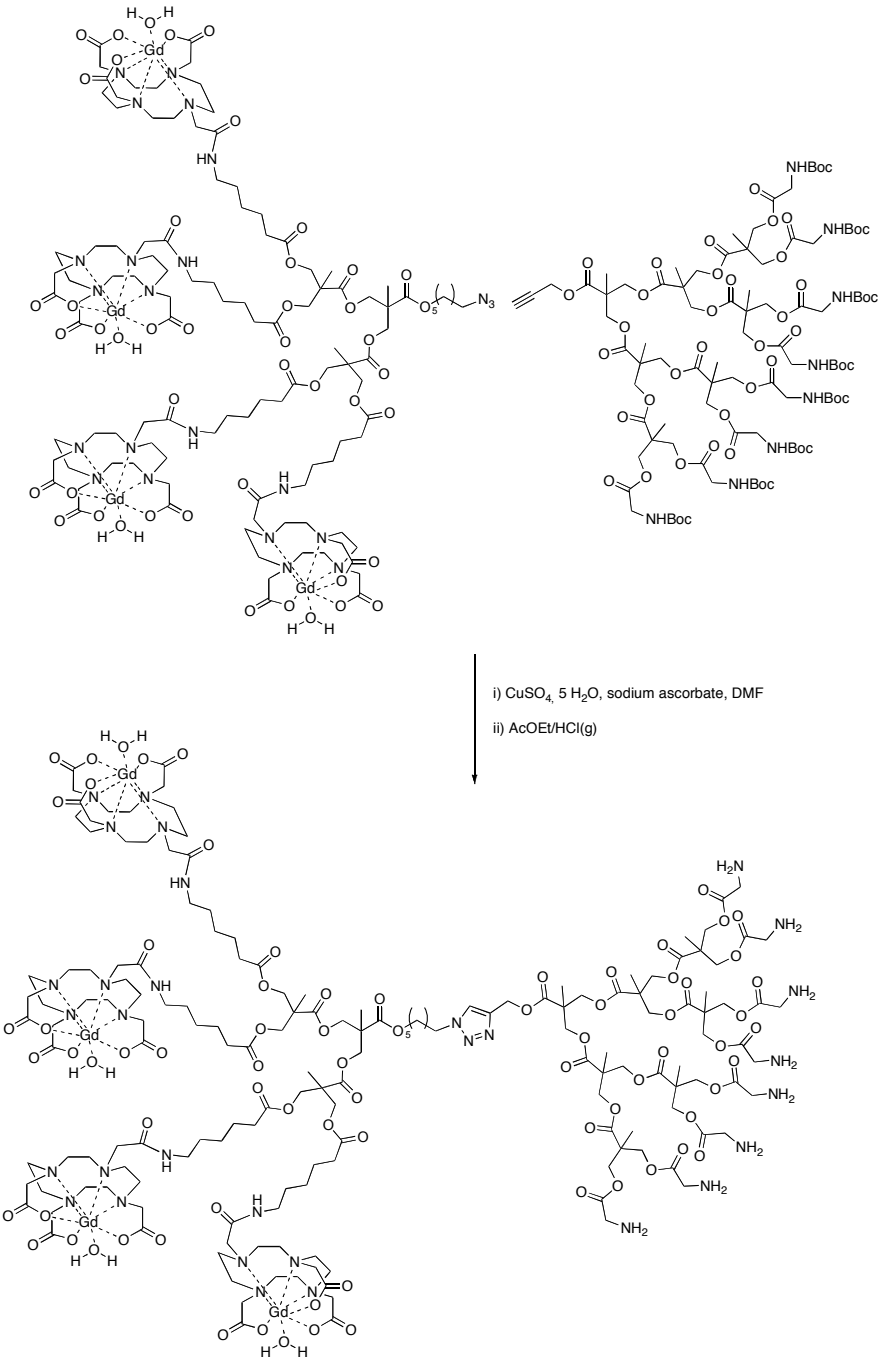

Figure 78: Union of 2nd generation DOTA-dendron and aminated-dendron by CuAAC ($G2(DOTA\text{-}Gd)_4$-$G3(NH_2)_8$).

The presence of metal ions in the molecule hinders the possibility of characterization of the molecule by ^{1}H-NMR or ^{13}C-NMR. However, the IR spectrum confirmed the formation of the desired product with the appearance of new bands at 2851 cm^{-1} and 2919 cm^{-1} corresponding to the CH_2 (υC-H), and the

band at 1734 cm^{-1} (υC=O) corresponding to the esters of the *bis*-MPA aminated dendron.

After the CuAAC reaction, no relaxivity signal was detected; as we saw in the case of the folic acid, this could be due to an exchange of the gadolinium ions with the copper ions present in the reaction mixture. After purification of the product, the compound was dissolved in HEPES and stirred during one night in presence of $GdCl_3$. EDTA was then added to the solution in order to capture the excess of gadolinium and copper ions. The solution was dialyzed against deionized (miliQ) water. The resulting solution was freeze-dried, and the relaxivity of the compound was measured (Figure 79, Table 11).

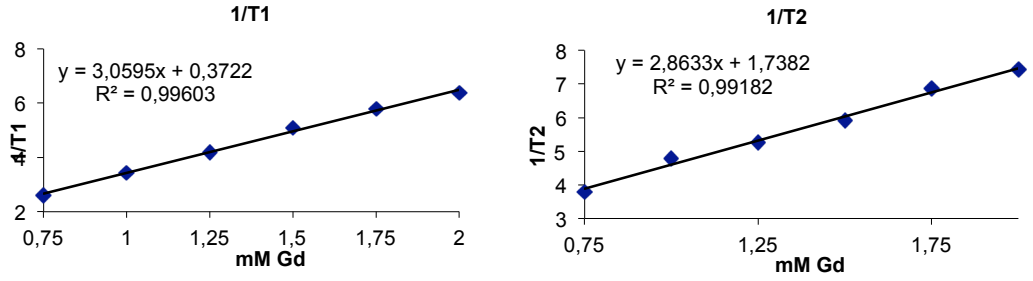

Figure 79: T1 and T2 measurements for the G2(DOTA-Gd)$_4$-G3(NH$_2$)$_8$ dendrimer in function of the concentration of Gd (mM). Gain$_{T1}$=55, gain$_{T2}$=53.

r_1 $mM^{-1}{}_{Gd}.s^{-1}$	3.06
r_2 $mM^{-1}{}_{Gd}.s^{-1}$	2.86
r_1 $mM^{-1}{}_{dendrimer}.s^{-1}$	*12.24*
r_1 $mM^{-1}{}_{dendrimer}.s^{-1}$	*11.44*

Table 11: Relaxivity values obtained for G2(DOTA-Gd)$_4$-G3(NH$_2$)$_8$.

The dendrimer was then covalently united to the modified anti-HER2 by the process described previously (formation of Shiff bases). After purification of the $AB_{DOTA\text{-}Gd}$ by exclusion chromatography, the AB was characterized by IEF and SDS-PAGE (Figure 80).

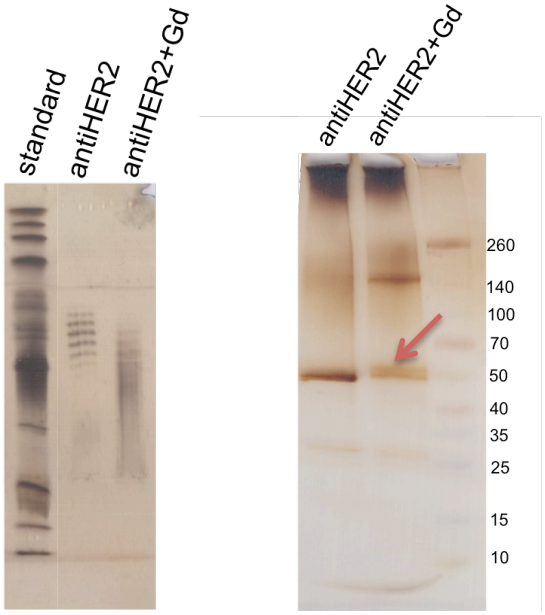

Figure 80: IEF (left) and SDS-PAGE (right) of the anti-HER2 before and after reaction with the G2(DOTA-Gd)$_4$-G3(NH$_2$)$_8$ dendrimer. AntiHER2=antibody without modification, antiHER2+Gd = antiHER2 modified with the G2(DOTA-Gd)$_4$-G3(NH$_2$)$_8$ dendrimer.

In the IEF gel, a difference was observed between the bands due to the commercial antiHER2 and the bands due to the antiHER2(DOTA-Gd), characterizing the structural modification of the antibody. In SDS-PAGE, the appearance of a strong band between 140 and 260 kDa probably due to an agglomeration was observed. At approx. 50 kDa, we can observe that the band corresponding to the heavy chains decreased in intensity and a new band appeared just above (red arrow). This new band is characteristic of the heavy chains modification by our dendritic compound. The intensity of the band corresponding to the light chains at approx. 25 kDa remained constant.

Due to the low amount of antiHER2(DOTA-Gd) prepared, the relaxivity could not be measured with the equipment available in our laboratories. However, *in vitro* experiments are programmed in collaboration with the Nanoimage unit of the BIONAND center in Málaga.

Conclusions

Dendrons modified by Gd(III)DOTA contrast agents present interesting relaxivity data. The use of the second generation dendron permit to increase the relaxivity up to 3 times compared to Gd(III)DOTA ligands.

The covalent attachment of the Gd(III)DOTA dendrons to targeting molecules such as the folic acid molecule is possible conserving the contrast agent activity.

The chemical modification of an antiHER2 monoclonal antibody by dendritic derivatives affected neither its biological activity nor its selectivity for the HER2 receptor.

Future work:

In vitro studies of the FA-[G2-Gd(III)DOTA] and antiHER2-DOTAGd(III) compounds needs to be carried out to confirm the efficiency of the targeting moiety.

Higher generations of *bis*-MPA-DOTA dendron could be investigated, and their effect compared.

Experimental part

General methods

All the reagents except specifications were purchased from Sigma-Aldrich.

^{1}H-NMR and ^{13}C-NMR experiments were performed on a Bruker AVANCE 400 spectrometer operating at 400 MHz or 100 MHz or on a Bruker 300 operating at 300 MHz and 60 MHz. $CDCl_3$, MeOD, and D_2O were used as solvents and chemical shifts are given in ppm relative to TMS. The solvent residual peak was used as internal standard.

MS analyses were performed using an ESI-ion-TRAP Bruker Esquire3000 plus spectrometer or a Bruker MicroFlex for Maldi analysis. The infrared spectra of all the complexes were obtained with a Mattson Genesis II FTIR or JASCO FT/IR-4100 in the 400-4000 cm^{-1} spectral range directly or over NaCl cells. Relaxivity measurements were carried out using a Bruker Mq60 NMR analyser Minispec. The fluorescence data were obtained with a Perkin Elmer LS55 Fluorescence spectrometer device. The absorbance measurements were carried out using a Varian Cary50 Probe UV-visible spectrophotometer. The isoelectric point of the antibody was measured using a PhastSystem device.

Synthesis and characterization

The typical procedure for Steglish esterification (A), typical procedure for deprotection of *bis*-MPA alcohol groups (B), typical procedure for deprotection of amine groups (C), typical procedure for dendrimer generation growth (D), and typical procedure for deprotection of dendrimer OH groups (E) are describe in Chapter 1.

$N_3C_6H_{12}$-[G#1]-$(C_5H_{10}NHBoc)_2$

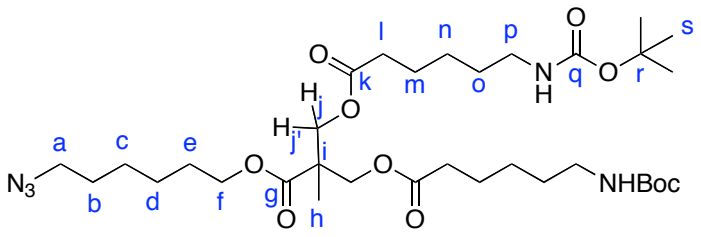

The product was obtained following the Steglish esterification procedure (A). The crude product was purified by column chromatography eluting with a mixture 1:1 of Hexane:EtOAc, after 24 h of reaction. The pure product was obtained in a 99 % yield (1.31 g, 1.90 mmol) as a yellow oil.

NMR ^1H ($CDCl_3$, 300 MHz) δ (ppm): 1.30 (s, 3H, H_h), 1.32-1.50 (m, 8H, H_c, H_d, H_n, H_o), 1.43 (s, 18H, H_s), 1.56-1.66 (m, 8H, H_b, H_e, H_m), 2.29 (t, J =7.5 Hz, 4H, H_l), 3.08 (m, 4H, H_p), 3.27 (t, J = 6.6 Hz, 2H, H_a), 4.11 (t, J = 6.6 Hz, 2H, H_f), 4.18 (d, J = 14.4 Hz, 2H, H_j), 4.23 (d, J = 11.1 Hz, 2H, $H_{j'}$), 4.59 (br s, 2H, NH).

NMR ^{13}C ($CDCl_3$, 300 MHz) δ (ppm): 17.8 (C_h), 24.4 (C_m), 25.4 (C_d), 26.2 (C_n), 26.3 (C_c), 28.3 (C_s), 28.4 (C_o), 28.7 (C_b), 29.7 (C_e), 33.9 (C_l), 40.3 (C_i), 46.3 (C_p), 51.3 (C_a), 65.0 (C_f), 65.2 (C_j), 79.9 (C_r), 155.9 (C_q), 172.7 (C_g), 172.9 (C_k).

IR (KBr, cm^{-1}): 3379 (N-H), 2936-2864 (C-H), 2097 (N=N=N), 1740-1714 (C=O).

Calculated $[M]^+$ ($C_{97}H_{157}N_{11}O_{46}$) m/z = 685.43. Found: ESI+: $[M+Na]^+$ m/z = 708.4.

$N_3C_6H_{12}$-[G#1]-$(C_5H_{10}NH_2)_2$

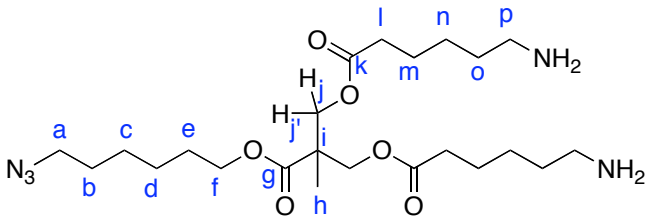

The compound was obtained following the deprotection procedure (C) as transparent oil in a quantitative yield.

NMR ^1H ($CDCl_3$, 400 MHz) δ (ppm): 1.17 (s, 3H, H_h), 1.32-1.35 (m, 8H, H_c, H_d, H_n, H_o), 1.54-1.60 (m, 8H, H_b, H_e, H_m), 2.29 (t, *J* =7.5 Hz, 4H, H_l), 2.98 (m, 4H, H_p), 3.27 (t, *J* = 6.6 Hz, 2H, H_a), 4.10 (m, 4H, H_f, H_j), 4.23 (d, *J* = 11.1 Hz, 2H, $H_{j'}$), 7.94 (br s, 4H, NH).

NMR ^{13}C ($CDCl_3$, 400 MHz) δ (ppm): 18.2 (C_h), 24.1 (C_m), 25.2 (C_d), 25.6 (C_n), 26.1 (C_c), 26.9 (C_o), 28.2 (C_b), 28.6 (C_e), 33.5 (C_l), 39.7 (C_i), 45.9 (C_p), 51.1 (C_a), 64.6 (C_f), 64.9 (C_j), 172.7 (C_g), 172.9 (C_k).

IR (KBr, cm^{-1}): 3417 (N-H), 2939 (C-H), 2097 (N=N=N), 1738 (C=O).

$N_3C_6H_{12}$-[G#1]-(C_5H_{10}NH-DO3A tBu ester)$_2$

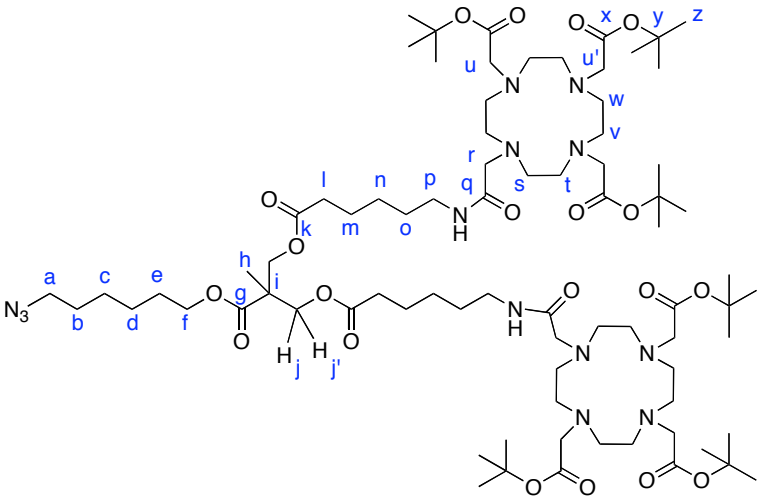

To a suspension of 100 mg (174 µmol) of (tBuO)$_3$-DOTA-OH, 78 mg (204 µmol) of HATU and 28 mg (204 µmol) of HOAt in 5 mL of dry dichloromethane was added 47 mg (85 µmol) of $N_3C_6H_{12}$-[G#1]-($C_5H_{10}NH_2$)$_2$ and the mixture was allowed to stir overnight. The crude was diluted with $CHCl_3$ (15 mL) and washed 4 times with H_2O. The organic phase was concentrated, diluted with EtOAc and washed 4 times with H_2O. The organic phase was concentrated, diluted in MeOH and dialyzed against MeOH (cellulose membrane MW 1000) for 1 day. Evaporation of the solvent gave the pure product as an off-white solid. Yield 56 % (39 mg, 24µmol).

NMR ^{1}H (MeOD, 300 MHz) δ (ppm): 1.25 (s, 3H, H_h), 1.29-1.66 (m, 74H, H_c, H_d, H_m, H_n, H_o, H_z, H_b, H_e), 2.33 (t, J =7.2 Hz, 4H, H_l), 3.01-3.05 (br m, 32H, H_s, H_t, H_v, H_w), 3.22 (t, J = 6.9 Hz, 4H, H_p), 3.27 (t, J = 6.6 Hz, 2H, H_a), 3.61 (br m, 16H, H_r, H_u, $H_{u'}$), 4.11 (t, J = 6.6 Hz, 2H, H_f), 4.22 (s, 4H, $H_{j,j'}$).

NMR ^{13}C (MeOD, 300 MHz) δ (ppm): 18.2 (C_h), 25.6 (C_m), 26.6 (C_d), 27.4 (C_n), 28.5 (C_z, C_o), 29.5 (C_c), 29.8 (C_b), 30.1 (C_e), 34.8 (C_l), 40.2 (C_i), 47.7 (C_p), 51.3-53.0 (m, C_a, C_s, C_t, C_v, C_w), 56.9 (m, C_r, C_u, $C_{u'}$), 66.3 (C_f), 66.6 (C_j), 83.3 (C_y), 171.1-171.2 (m, C_x, C_q), 174.4 (C_g), 174.5 (C_k).

IR (KBr, cm^{-1}): 3420 (NH amide), 2099 (N_3), 1733 (C=O ester).

Calculated $[M]^+$ ($C_{97}H_{157}N_{11}O_{46}$) m/z = 1594.06. Found: MALDI+: $[M+Na]^+$ m/z = 1617.2.

$N_3C_6H_{12}$-[G#1]-(C_5H_{10}NH-DO3A)$_2$

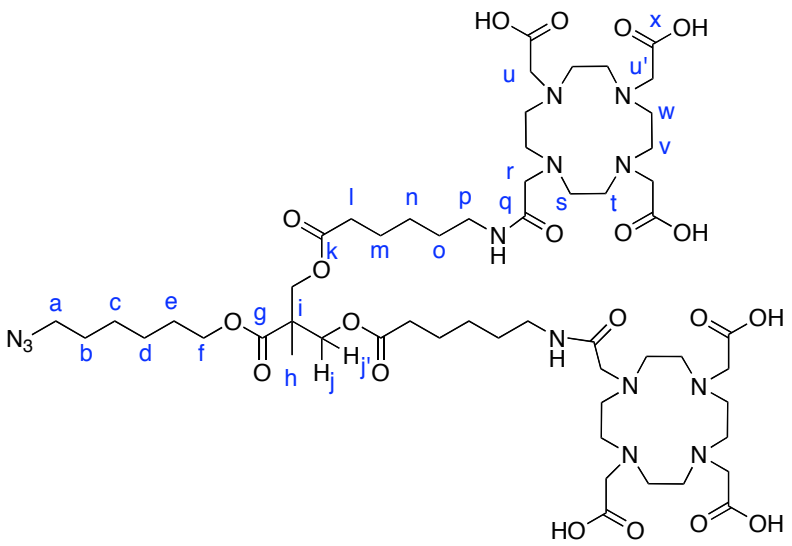

50 mg of the protected product $N_3C_6H_{12}$-[G#1]-(C_5H_{10}NH-DO3A tBu ester)$_2$ were dissolved in 1 mL of 1:1 TFA/CH_2Cl_2 dissolution. The reaction mixture was agitated overnight under argon atmosphere. Then, the solvent was evaporated to give a brown oil which was dissolved in the smallest quantity of MeOH and precipitated in Et_2O as a pale yellow solid. The solid was recovered by centrifugation (5 min, 3000 rpm), washed several times with ether and centrifuged. The pure product was obtained in a quantitative yield after drying the solid in reduced pressure.

NMR ^1H ($CDCl_3$, 300 MHz) δ (ppm): 1.26 (s, 3H, H_h), 1.29-1.70 (m, 20H, $H_{b\text{-}e}$, $H_{m\text{-}o}$), 2.34 (t, *J* = 7.2 Hz, 4H, H_l), 3.20 (t, *J* = 6.9 Hz, 4H, H_p), 3.30 (br s, 32H, $H_{s\text{-}t}$), 3.74-3.80 (m, 16H, H_r, $H_{u\text{-}u'}$), 4.14 (t, *J* = 6.3 Hz, 2H, H_f), 4.22 (m, 4H, $H_{j,j'}$).

NMR ^{13}C ($CDCl_3$, 300 MHz) δ (ppm): 25.6, 26.6, 27.0, 27.2, 27.5, 29.5, 30.0, 33.6, 34.8, 40.4, 47.7, 50.2, 51.0-51.5, 55.4-55.8, 56.2-56.3, 66.2, 66.5-66.6, 174.5, 174.8.

IR (KBr, cm^{-1}): 3433 (O-O-H carboxylic acid), 3097 (N-H amide), 2919-2850 (C-H), 2101 (N_3), 1733 (C=O ester), 1683 (C=O amide).

$N_3C_6H_{12}$-[G#1]-(C_5H_{10}NH-DO3AGd)$_2$

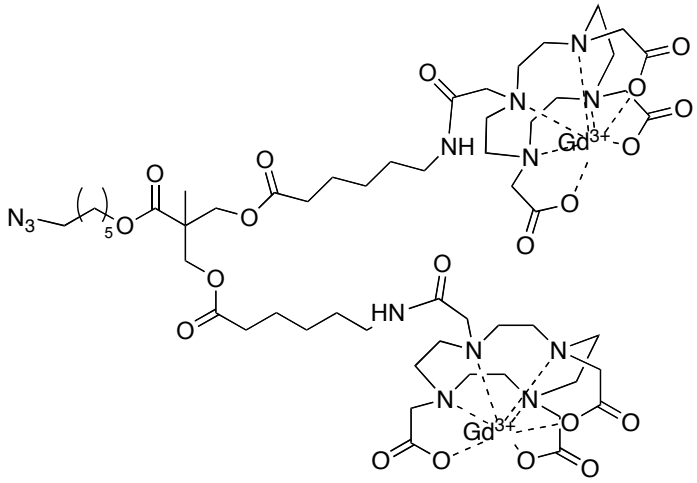

The product was dissolved in HEPES 1mM and 3eq/DOTA of $GdCl_3$ was added, the reaction was allowed to stir overnight. Then, EDTA 0.2 M was added (1.2 eq/$GdCl_3$) in order to complex the excess of Gd remaining in the solution and the solution was stirred for 2 hours. The solution was then dialyzed against miliQ water (cellulose membrane MW 1000), and the pure product was freeze-dried. White solid.

Relaxivity measurements: r_1 = 4.13 $mM^{-1}{}_{Gd}.s^{-1}$, r_2 = 4.87 $mM^{-1}{}_{Gd}.s^{-1}$.

IR (KBr, cm^{-1}): 3433 (OO-H carboxylic acid), 3097 (N-H amide), 2919-2850 (C-H), 2101 (N_3), 1733 (C=O ester), 1683 (C=O amide).

$N_3C_6H_{12}$-[G#2]-(C_5H_{10}NHBoc)$_4$

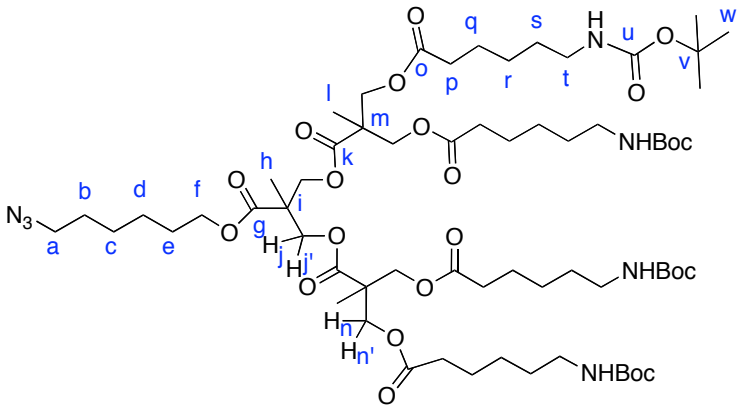

The compound was obtained following the procedure for Steglish estirification (A). The crude product was purified by column chromatography eluting with a mixture 7:3 of Hexane:EtOAc. The pure product was obtained in a 75% yield (1.03 g, 0.766 mmol) as yellow oil.

NMR ^1H ($CDCl_3$, 300 MHz) δ (ppm): 1.21-1.44 (m, 73H, 2H_c, 2H_d, 3H_h, 6H_l, 8H_r, 8H_s, 36H_w), 1.47-1.65 (m, 12H, H_b, H_e, H_q), 2.29 (t, *J* = 7.5 Hz, 8H, H_p), 3.08 (q, *J* = 6.6 Hz, 8H, H_t), 3.27 (t, *J* = 6.9 Hz, 2H, H_a), 4.07-4.24 (m, 12H, $H_{j,j'}$, $H_{n,n'}$), 4.66 (br s, 4H, NH).

NMR ^{13}C ($CDCl_3$, 300 MHz) δ (ppm): 14.2 (C_j), 17.8 (C_l), 24.4 (C_q), 25.4 (C_d), 26.2 (C_c, C_n), 28.4 (C_w, C_b), 28.7 (C_e), 29.7 (C_s), 33.8 (C_p), 40.3 (C_t), 46.4 (C_m), 46.6 (C_i), 51.3 (C_a), 65.3 (C_n), 65.6 (C_k), 65.7 (C_f), 79.0 (C_v), 155.9 (C_u), 172.0 (C_g, C_k), 172.9 (C_o).

IR (KBr, cm^{-1}): 3390 (N-H), 2939-2860 (C-H), 2096 (N=N=N), 1741(C=O).

Calculated $[M]^+$ ($C_{65}H_{113}N_7O_{22}$) *m/z* = 1343.79. Found: MALDI+: $[M+Na]^+$ *m/z* = 1366.7.

$N_3C_6H_{12}$-[G#2]-($C_5H_{10}NH_2$)$_4$

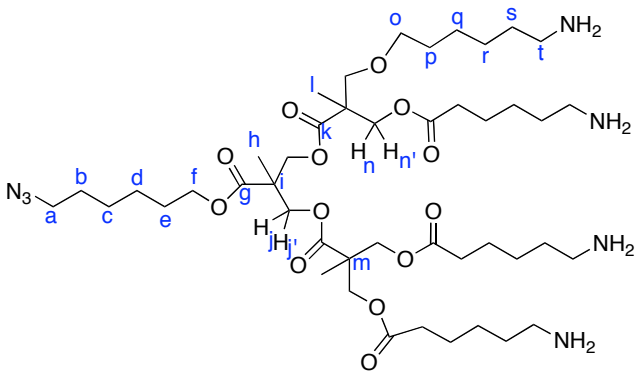

The compound was obtained following the method of deprotection of amines (C), as pale yellow solid in quantitative yield.

NMR ^1H ($CDCl_3$, 300 MHz) δ (ppm): 1.26 (s, 6H, H_l), 1.29 (s, 3H, H_h), 1.42-1.48 (m, 12H, H_b, H_e, H_r), 1.60-1.71 (m, 20H, H_c, H_d, H_q, H_s), 2.38 (t, *J* = 7.2 Hz, 8H, H_p), 2.94 (t, *J* = 7.5 Hz, 8H, H_t), 4.15 (t, *J* = 6.3 Hz, 2H, H_f), 4.21 (s, 8H, $H_{n,n'}$), 4.28 (d, *J* = 2.4 Hz, 4H, $H_{j,j'}$).

NMR ^{13}C ($CDCl_3$, 300 MHz) δ (ppm): 18.2, 20.8, 25.4, 26.7, 26.9, 27.4, 28.3, 29.6, 28.3, 34.5, 40.7, 47.8, 47.9, 52.4, 66.4, 66.5, 67.0, 173.7, 173.9, 174.4, 175.2.

IR (KBr, cm^{-1}): 3430 (N-H), 2935-2862 (C-H), 2097 (N=N=N), 1739(C=O).

Calculated $[M]^+$ ($C_{45}H_{81}N_7O_{14}$) *m/z* = 944.16. Found: MALDI+: $[M+H]^+$ *m/z* = 945.12.

$N_3C_6H_{12}$-[G#2]-(C_5H_{10}NH-DO3A tBu ester)$_4$

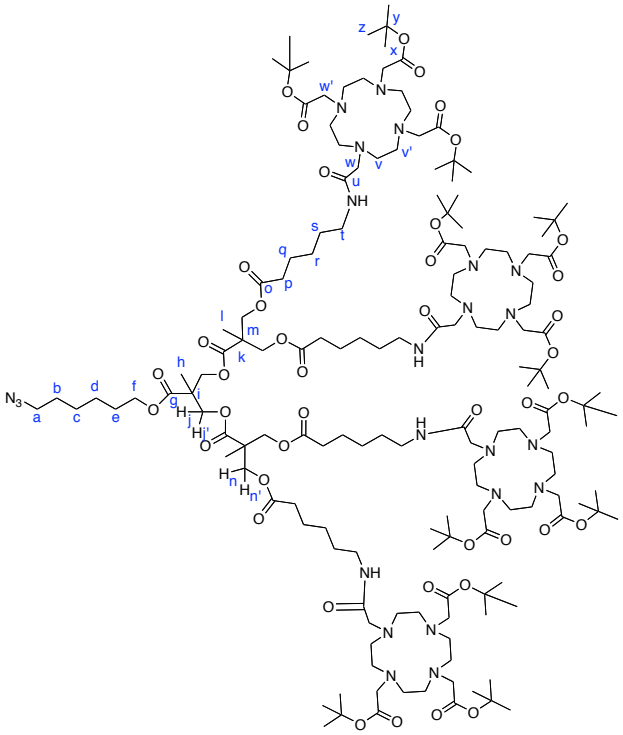

To a suspension of 100 mg (174 µmol) of (tBuO)$_3$-DOTA-OH, 78 mg (204 µmol) of HATU and 28 mg (204 µmol) of HOAt in 5 mL of dry dichloromethane was added 46 mg (43 µmol) of ***$N_3C_6H_{12}$-[G#2]-($C_5H_{10}NH_2$)$_4$*** and the mixture was left to stir overnight. The crude was diluted with $CHCl_3$ (15 mL) and washed 4 times with H_2O. The organic phase was concentrated, diluted with EtOAc and washed 4 times with H_2O. The organic phase was concentrated, diluted in MeOH and dialyzed against MeOH (cellulose membrane MW 1000) for 1 day. Evaporation of the solvent gave the pure product as an off-white solid. Yield: 74 %.

NMR ^{1}H (MeOD, 300 MHz) δ (ppm): 1.25 (s, 6H, H_l), 1.29 (s, 3H, H_h), 1.36-1.70 (m, 136H, 2H_c, 2H_d, 8H_q, 8H_r, 8H_s, 108H_z), 2.35 (t, J = 7.5 Hz, 8H, H_p), 3.00-3.05 (m, 64H, $H_{v,v'}$), 3.22 (t, 8H, H_t), 3.27 (t, 2H, H_a), 3.61 (m, 24H, H_w), 4.13 (t, J = 6.3 Hz, 2H, H_f), 4.26 (s, 8H, $H_{n,n'}$), 4.28 (m, 4H, $H_{j,j'}$).

NMR ^{13}C (MeOD, 300 MHz) δ (ppm): 18.3 (C_h, C_l), 25.7 (C_q), 26.7 (C_d), 27.5 (C_n), 28.6 (C_z), 29.6 (C_c), 29.9 (C_b), 30.1 (C_s), 34.8 (C_p), 40.3, 47.9, 48.0, 52.7, 56.8, 66.4 (m, C_n, C_k, C_f), 82.8-83.5 (m, C_y), 173.7, 174.6.

IR (KBr, cm^{-1}): 3420 (NH amide), 2099 (N_3), 1733 (C=O ester).

Calculated [M]$^+$ ($C_{157}H_{281}N_{23}O_{42}$) m/z = 3163.04. Found: MALDI+: [M+Na]$^+$ m/z = 3186.6.

$N_3C_6H_{12}$-[G#2]-(C_5H_{10}NH-DO3A)$_4$

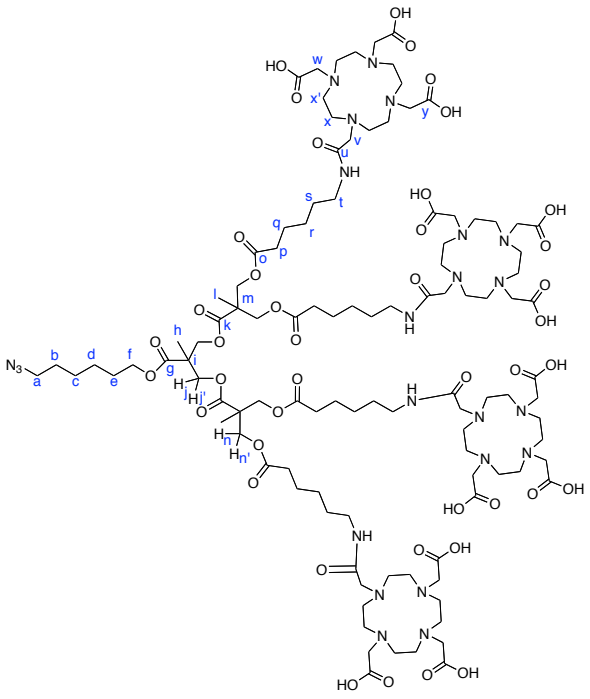

50 mg of the protected product ***$N_3C_6H_{12}$-[G#2]-(C_5H_{10}NH-DO3A tBu ester)$_4$*** were dissolved in 1 mL of 1:1 TFA/CH_2Cl_2 dissolution. The reaction mixture was agitated overnight under argon atmosphere. Then, the solvent was evaporated to give a brown oil which was dissolved in the smallest quantity of MeOH and precipitated in Et_2O as a pale yellow solid. The solid was recovered by centrifugation (5 min, 3000 rpm), washed several times with ether and centrifuged. The pure product was obtained in a quantitative yield after drying the solid in reduced pressure.

NMR ^1H ($CDCl_3$, 300 MHz) δ (ppm): 1.25 (s, 6H, H_l), 1.28 (s, 3H, H_h), 1.30-1.71 (m, 36H, H_{c-d}, H_{q-s}), 2.36 (t, J = 7.2 Hz, 8H, H_p), 3.0 (t, *J* = 7.8 Hz, 2H, H_a), 3.2 (t, *J* = 6.9 Hz, 8H, H_t), 3.30 (m, 64H, H_x), 3.80 (br s, 32H, H_{v-w}), 4.14 (t, *J* = 6.3 Hz, 2H, H_f), 4.20 (s, 8H, $H_{n,n'}$), 4.28 (m, 4H, $H_{j,j'}$).

NMR ^{13}C ($CDCl_3$, 300 MHz) δ (ppm): 18.2 (C_l), 18.3 (C_h), 25.6 (C_q), 26.6 (C_d), 27.0 (C_c), 27.2 (C_b), 27.5 (C_r), 29.5 (C_e), 30.0 (C_s), 34.8 (C_p), 40.3-40.6 (m, C_i, C_m), 47.8 (C_t), 50.2 (C_a), 50.9-51.5 (m, C_y), 55.2-55.6 (m, C_w), 56.1-56.3 (C_v), 66.4 (C_j, C_n), 67.0 (C_f), 171.9-172.3 (C_u), 173.7 (C_o), 174.0 (C_k), 174.8 (C_w).

IR (KBr, cm^{-1}): 3434 (O-O-H carboxylic acid), 3097 (N-H amide), 2918-2849 (C-H), 2101 (N_3), 1730 (C=O ester), 1679 (C=O amide).

$N_3C_6H_{12}$-[G#2]-(C_5H_{10}NH-DO3AGd)$_4$

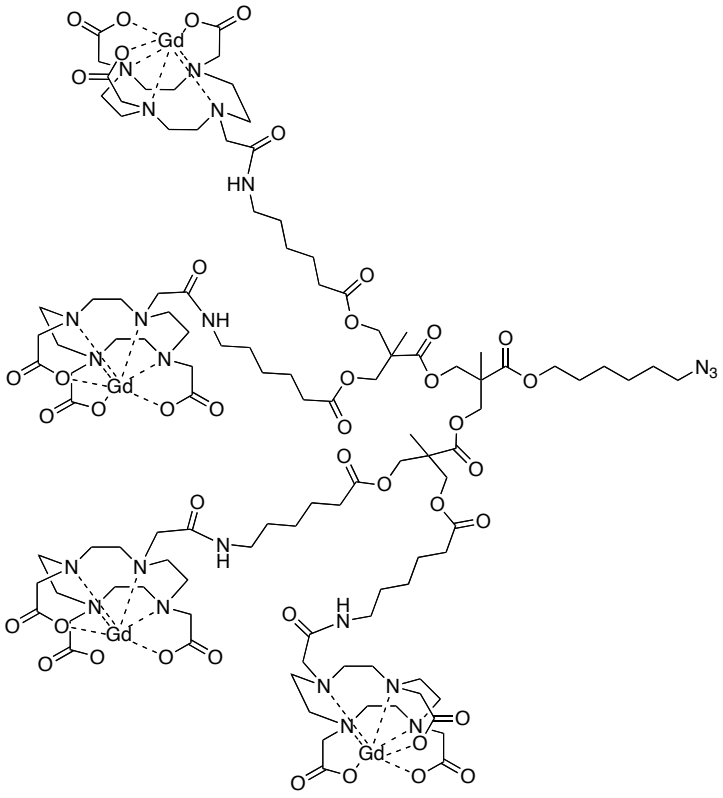

The product was dissolved in HEPES 0.1mM and 3eq/DOTA of $GdCl_3$ was added, the reaction was allowed to stir overnight. Then, EDTA 0.2 M was added (1.2 eq/$GdCl_3$) in order to complex the excess of Gd remaining in the solution and the solution was stirred for 2 hours. The solution was then dialyzed against miliQ water (cellulose membrane MW 1000), and the pure product was freeze-dried. White solid.

Relaxivity measurements: r_1 = 2.50 $mM^{-1}{}_{Gd}.s^{-1}$, r_2 = 2.95 $mM^{-1}{}_{Gd}.s^{-1}$.

FTIR (KBr, cm^{-1}): 3275 (υNH, υOH), 3064-2929 (υCH_2), 2140 (υN_3), 1652-1635 (υC=O), 1558-1540 (O-C-O^- carboxylates).

Propargyl folic acid

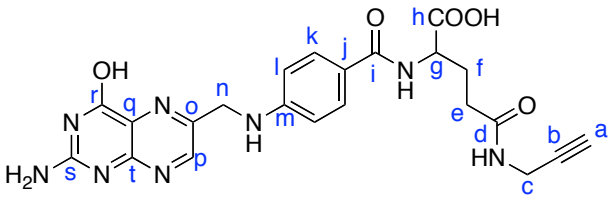

Folic acid (500 mg, 1.13 mmol) was dissolved en 20 mL of DMSO and 0.25 mL of triethylamine. DCC (257 mg, 1.25 mmol) and DMAP (28 mg, 0.23 mmol) were added and the reaction mixture was stirred at room temperature, in the darkness for 24 h. Then, propagilic amine (127 mg, 2.26 mmol) was added and the mixture was stirred for other 24 hours. Afterwards, the formed DCU was removed by filtration and the crude was precipitate in EtOAc. The yellow precipitated was recovered by filtration, dissolved in 1M NaOH and precipitated by the addition of 1M HCl. The orange solid was recovered by filtration and washed with 1:1 EtOH/H_2O in 78% yield.

NMR ^{13}C ($CDCl_3$, 300 MHz) δ (ppm): 1.87-2.02 (m, 2H, H_f), 2.15-2.30 (m, 2H, H_e), 2.46 (t, *J* = 1.8 Hz, 1H, NH), 3.00 (t, *J* = 2.1 Hz, 1H, H_a), 3.79 (t, *J* = 2.7 Hz, 2H, H_c), 4.26-4.30 (m, 1H, H_g), 4.52 (s, 2H, H_n), 6.62 (d, *J* = 8.7 Hz, 2H, H_l), 7.62 (d, *J* = 7.5 Hz, 2H, H_k), 8.09-8.16 (dd, *J* = 7.5 Hz, *J'* = 13.2 Hz, 1H, NH), 8.26-8.30 (t, *J*= 5.7 Hz, 1H, NH), 8.40 (br s, 2H, NH_2), 8.71 (s, 1H, H_p).

NMR ^{1}H ($CDCl_3$, 300 MHz) δ (ppm): 26.3 (C_f), 27.7 (C_c), 30.3 (C_f), 45.6 (C_n), 72.6 (C_a), 81.1 (C_b), 111.2 (C_l), 121.4 (C_j), 127.9 (C_k), 147.6 (C_m), 147.7 (C_p), 150.5 (C_o), 151.5 (C_q), 152.7 (C_t), 158.6 (C_s), 166.2 (C_i), 171.3 (C_r), 173.5 (C_d), 173.8 (C_h).

IR (cm-^{1}, KBr): 3378 (N-H, O-H, COO-H), 1684-1716 (C=O amide, acid, carboxylate), 1405 (O-C-O carboxylate).

Calculated $[M]^+$ ($C_{22}H_{22}N_8O_5$) *m/z* = 478.46. Found: MALDI+: $[M+H]^+$ *m/z* = 479.0.

prop-2-ynyl 2,2,5-trimethyl-1,3-dioxane-5-carboxylate

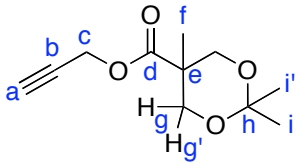

5 g (28.70 mmol) of isopropylidene-2,2-*bis*(methoxy)propionic acid (synthesis in Chapter 1, 1-1), 1.75 mL (30.14 mmol) of propargyl alcohol and 3.38 g (11.48 mmol) of DPTS were dissolved in 50 mL of dry dichloromethane. The flask was flushed with argon, cooled to 0°C, and a solution of 8.88 g (43.05 mmol) of DCC in 10 mL of dichloromethane was added dropwise. The reaction was allowed to stir at room temperature, under argon atmosphere for 24 hours. The reaction mixture was then filtrated and the solvent was evaporated. The oil/solid mixture obtained was stirred with hexane, and the solid filtered off. The product was then purified by column chromatography eluting with dichloromethane to obtain 4.70 g (22.14 mmol, 77 %) of the pure product as a green oil.

NMR ^{1}H ($CDCl_3$, 300 MHz) δ (ppm): 1.21 (s, 3H, H_f), 1.38 (s, 3H, H_i), 1.42 (s, 3H, $H_{i'}$), 2.46 (t, *J* = 2.4 Hz, 1H, H_a), 3.65 (d, *J* = 11.7 Hz, 2H, H_g), 4.20 (d, *J* = 12 Hz, 2H, $H_{g'}$), 4.73 (d, *J* = 2.4 Hz, 2H, H_c).

NMR ^{13}C ($CDCl_3$, 400 MHz) δ (ppm): 18.3 (C_f), 22.5 (C_i), 24.5 ($C_{i'}$), 41.8 (C_e), 52.3 (C_c), 65.8 (C_g), 74.9 (C_a), 77.4 (C_b), 98.0 (C_h), 173.3 (C_d).

IR (KBr, cm^{-1}): 3273 (≡C-H), 2876-2941-2992 (C-H), 2129 (C≡C), 1739 (C=O).

Calculated $[M]^+$ ($C_{11}H_{16}O_4$) *m/z* = 212.10. Found: Maldi: $[M+Na]^+$ *m/z* = 225.1.

≡-G1(OH)$_2$

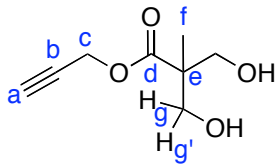

The product was obtained following the synthetic method (B) of deprotection the hydroxyl groups. White solid. 98 % yield.

NMR ^{1}H ($CDCl_3$, 300 MHz) δ (ppm): 1.09 (s, 3H, H_f), 2.49 (t, J = 2.7 Hz, H_a), 2.76 (br s, OH), 3.72 (d, J = 11.4 Hz, H_g), 3.92 (d, J = 11.4 Hz, $H_{g'}$), 4.75 (d, J = 2.4 Hz, 2H, H_c).

NMR ^{13}C ($CDCl_3$, 400 MHz) δ (ppm): 16.9 (C_f), 49.3 (C_e), 52.4 (C_c), 67.0 (C_g), 75.2 (C_a), 77.3 (C_b), 174.9 (C_d).

IR (KBr, cm^{-1}): 3396 (O-H), 3293 (≡C-H), 2945-2885 (C-H), 2127 (C≡C), 1729 (C=O).

Calculated $[M]^+$ ($C_8H_{12}O_4$) *m/z* = 172.18. Found: ESI+: $[M+H]^+$ *m/z*=173.0, $[M+Na]^+$ m/z=195.0.

≡-G2

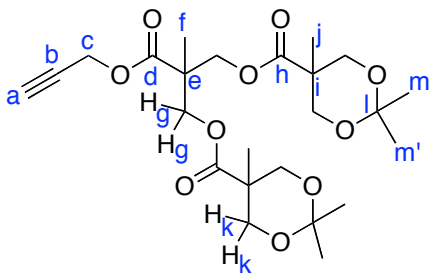

The product was obtained following the synthetic method (A) for Steglish esterification. The crude product was purified by column chromatography eluting gradually with a mixture of 4:1 Hexane:EtOAc to a mixture of 1:1 Hexane:EtOAc. The pure product was obtained as yellow oil in a 79 % yield (4.03 g, 8.37 mmol).

NMR ^{1}H ($CDCl_3$, 300 MHz) δ (ppm): 1.16 (s, 6H, H_j), 1.31 (s, 3H, H_f), 1.36 (s, 6H, H_m), 1.41 (s, 6H, $H_{m'}$), 2.46 (t, *J* = 2.4 Hz, 1H, H_a), 3.61 (d, *J* = 12 Hz, 4H, $H_{k'}$), 4.15 (d, *J* = 12 Hz, 4H, $H_{k'}$), 4.33 (s, 4H, $H_{g,g'}$), 4.71 (d, *J* = 2.4 Hz, 2H, H_c).

NMR ^{13}C ($CDCl_3$, 400 MHz) δ (ppm): 17.5 (C_f), 18.4 (C_j), 21.6 (C_m), 25.4 ($C_{m'}$), 43.6 (C_e), 46.7 (C_i), 52.6 (C_c), 65.2 (C_g), 65.9 (C_k), 75.3 (C_a), 77.1 (C_b), 98.0 (C_l), 171.8 (C_d), 173.4 (C_n).

IR (KBr, cm^{-1}): 3249 (≡C-H), 2993-2923-2857 (C-H), 2121 (C≡C), 1733 (C=O).

Calculated $[M]^+$ ($C_{24}H_{36}O_{10}$) *m/z* = 484.54. Found: MALDI+: $[M+Na]^+$ *m/z*=507.2.

≡-G2(OH)₄

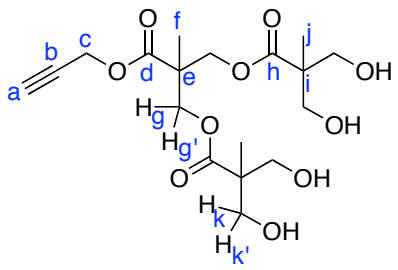

The product was obtained following the synthetic method (B) of deprotection of the *bis*-MPA hydroxyl groups. The pure product was obtained in a 94 % yield (3.02 g, 7.46 mmol).

NMR ^{1}H ($CDCl_3$, 300 MHz) δ (ppm): 1.05 (s, 6H, H_j), 1.34 (s, 3H, H_f), 2.49 (t, *J* = 2.4 Hz, 1H, H_a), 3.71 (dd, *J* = 6 Hz, *J* = 11.4 Hz, 4H, H_k), 3.87 (dd, *J* = 5.1 Hz, *J* = 10.5 Hz, 4H, $H_{k'}$), 4.30 (d, *J* = 11.1 Hz, 2H, H_g), 4.47 (d, *J* = 11.1 Hz, 2H, $H_{g'}$), 4.74 (d, *J* = 2.4 Hz, 2H, H_c).

NMR ^{13}C (MeOD, 400 MHz) δ (ppm): 17.3 (C_f), 18.1 (C_j), 40.5 (C_e), 47.9 (C_i), 51.8, 53.6 (C_c), 65.8 (C_k), 66.3 (C_g), 76.7 (C_a), 78.5 (C_b), 173.7 (C_d), 175.9 (C_h).

IR (KBr, cm^{-1}): 3310-3402 (O-H), 3258 (≡C-H), 2923-2853 (C-H), 2125 (C≡C), 1731 (C=O).

Calculated $[M]^+$ ($C_{18}H_{28}O_{10}$) *m/z* = 404.41. Found: MALDI+: $[M+Na]^+$ *m/z*=427.2.

≡-G3

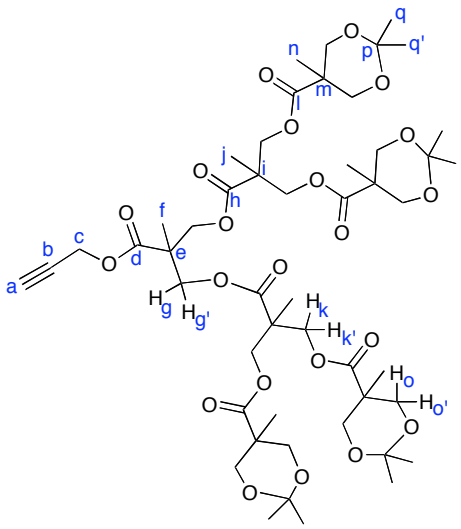

The product was obtained following the synthetic method (A) for esterification. The crude product was purified by column chromatography eluting with a mixture 1:1 of Hexane:EtOAc. The pure product was obtained in a 73 % yield (1.86 g, 1.80 mmol) as a white solid.

NMR ^{1}H ($CDCl_3$, 400 MHz) δ (ppm): 1.13 (s, 12H, H_n), 1.27 (s, 6H, H_j), 1.29 (s, 3H, H_f), 1.34 (s, 12H, H_q), 1.40 (s, 12H, $H_{q'}$), 2.54 (t, *J* = 2.4 Hz, 1H, H_a), 3.61 (d, *J* = 12.4 Hz, 8H, H_o), 4.14 (d, *J* = 12 Hz, 8H, $H_{o'}$), 4.30 (m, 12H, $H_{k,k'}$, $H_{g,g'}$), 4.73 (d, J = 2.4 Hz, 2H, H_b).

NMR ^{13}C ($CDCl_3$, 400 MHz) δ (ppm): 17.5, 17.6, 18.4, 25.2, 42.0, 46.6, 46.8, 52.8, 64.9, 65.6, 65.9, 66.0, 66.1, 75.7, 98.1, 171.8, 173.5.

IR (KBr, cm^{-1}): 3269 (≡C-H), 2992-2853 (C-H), 2128 (C≡C), 1733 (C=O).

Calculated $[M]^+$ ($C_{50}H_{76}O_{22}$) *m/z* = 1128.48. Found: ESI+: $[M+H]^+$ *m/z*=1129.2.

Elemental analysis calculated: C, 58.35; H, 7.44; O, 34.20. *Found:* C, 58.20; H, 7.58; O, 34.22.

≡-G3(OH)$_8$

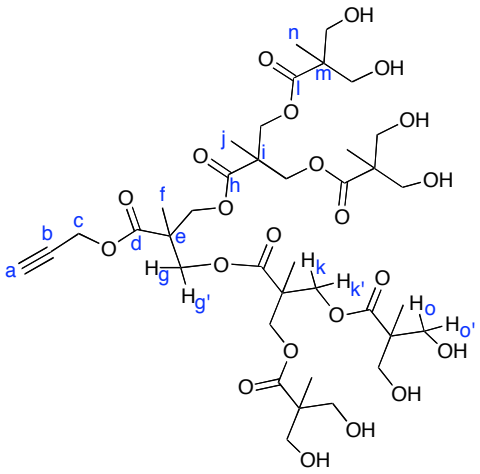

The product was obtained following the synthetic method (B). The pure product was obtained in 89 % yield (1.35 g, 1.55 mmol) as a white solid.

NMR ^{1}H (MeOD, 400 MHz) δ (ppm): 1.15 (s, 12H, H_n), 1.30 (s, 6H, H_j), 1.32 (s, 3H, H_f), 2.99 (t, *J* = 2.4 Hz, 1H, H_a), 3.58-3.69 (m, 16H, $H_{o,o'}$), 4.23-4.35 (m, 12H, $H_{k,k'}$, $H_{g,g'}$), 4.78 (d, *J* = 2.4 Hz, 2H, H_c).

NMR ^{13}C (CDCl$_3$, 400 MHz) δ (ppm): 17.3, 18.0, 18.3, 48.0, 51.8, 53.8, 65.8, 66.2, 67.0, 67.2, 77.0, 78.6, 173.3, 173.8, 175.9.

IR (KBr, cm^{-1}): 3378 (O-H), 2942-2885 (C-H), 2224 (C≡C), 1729 (C=O).

Calculated $[M]^+$ ($C_{38}H_{60}O_{22}$) *m/z* = 868.36. Found: ESI+: $[M+H]^+$ *m/z* = 869.1.

≡-G3(NHBoc)$_8$

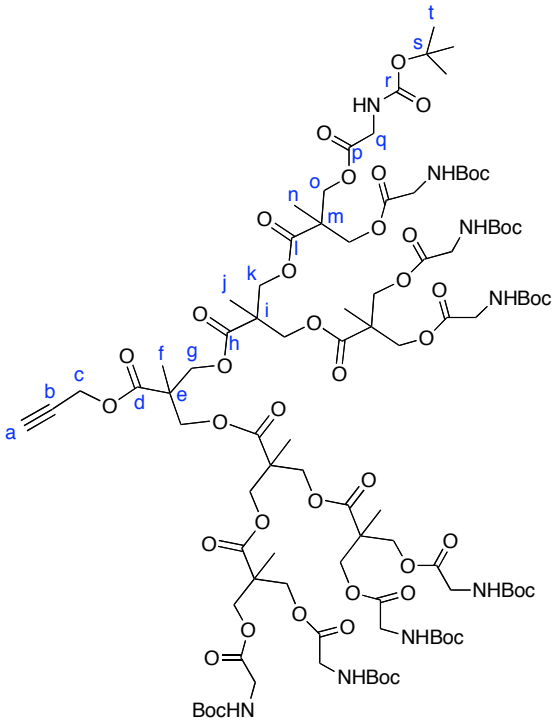

The compound was obtained following the Steglish esterification procedure (A). The crude product was purified by column chromatography eluting with a mixture 7:3 of Hexane:EtOAc. The pure product was obtained in a 38% yield (886 mg, 0.42 mmol) as a white solid.

NMR ^{1}H ($CDCl_3$, 400 MHz) δ (*ppm):* 1.25 (s, 12H, H_n), 1.26 (s, 6H, H_j), 1.33 (s, 3H, H_f), 1.46 (s, 72H, H_t), 2.59 (t, J = 2.4 Hz, 1H, H_a), 3.90 (s, 16H, H_q), 4.25 (m, 28H, H_g, H_k, H_o), 4.75 (d, J = 2.4 Hz, 2H, H_c).

NMR ^{13}C ($CDCl_3$, 400 MHz) δ (*ppm):* 17.5-17.9 (m, C_n, C_j, C_f), 28.3 (C_t), 42.2 (C_q), 46.4 (C_m), 46.6 (C_e), 46.7 (C_i), 52.9 (C_c), 65.4-65.7 (m, C_g, C_k, C_o), 75.8 (C_a), 77.2 (C_b), 80.0 (C_s), 155.8 (C_r), 170.1 (C_p), 171.4 (C_l), 171.6 (C_h), 171.8 (C_d).

IR (KBr, cm^{-1}): 3402 (N-H), 2980 (C-H), 1748-1717 (C=O).

Calculated $[M]^+$ ($C_{94}H_{148}N_8O_{46}$) *m/z* = 2124.95. Found: ESI+: $[M+Na]^+$ *m/z* = 2148.6.

≡-G3(NH$_2$)$_8$

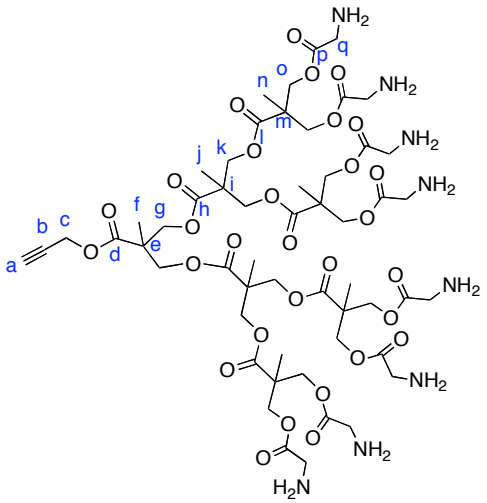

The product was obtained following the method for the deprotection of amine groups (C), as a yellow solid in a quantitative yield.

NMR ^{1}H (MeOD, 300 MHz) δ (ppm): 1.34 (s, 12H, H$_n$), 1.35 (s, 6H, H$_j$), 1.39 (s, 3H, H$_f$), 3.06 (t, *J* = 2.1 Hz, 1H, H$_a$), 3.95 (m, 16H, H$_q$), 4.32-4.38 (m, 12H, H$_g$, H$_k$), 4.42-4.45 (m, 16H, H$_o$), 4.82 (d, *J* = 2.4 Hz, 2H, H$_c$).

NMR ^{13}C (MeOD, 300 MHz) δ (ppm): 18.1 (m, C$_f$, C$_j$, C$_n$), 41.2 (C$_q$), 47.7 (C$_e$, C$_j$, C$_m$), 54.0 (C$_c$), 66.9 (C$_g$), 67.7 (C$_k$, C$_n$), 77.34 (C$_a$), 78.68 (C$_b$), 168.4 (C$_p$), 173.3 (m, C$_d$, C$_h$, C$_l$).

IR (KBr, cm^{-1}): 3433 (N-H), 2983 (C-H), 2222 (C≡C), 1746 (C=O).

Calculated [M]$^+$ (C$_{54}$H$_{84}$N$_8$O$_{30}$) *m/z* = 1325.28. Found: MALDI+: [M+Na]$^+$ *m/z* = 1347.5.

Propargyll rhodamine

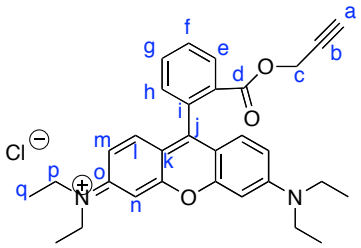

Rhodamine B base (479 mg, 1 mmol), propargyl alcohol (62 mg, 1.1 mmol), EDC (211 mg, 1.1 mmol) and DMAP (24 mg, 0.2 mmol) were dissolved in 5 mL of dry dichloromethane. The reaction was flushed with argon, protected from the light and stirred overnight. Then, 10 mL of dichloromethane were added and washed with water (2 x 10 mL), 0.1 M HCl (10 mL) and brine (NaCl). The organic phase was dried over anhydrous $MgSO_4$ and concentrated under reduced pressure. The crude was purified by column chromatography eluting with 1:10 MeOH/$CHCl_3$ and obtained in 59 % yield as a dark fuchsia solid.

NMR ^1H ($CDCl_3$, 300 MHz) δ (ppm): 1.33 (t, *J* = 6.9 Hz, 12H, H_p), 2.42 (t, *J* = 2.4 Hz, 1H, H_a), 3.65 (q, *J* = 7.2 Hz, 8H, H_o), 4.62 (d, *J* = 2.4 Hz, 2H, H_c), 6.84 (d, *J* = 2.1 Hz, 2H, H_n), 6.95 (dd, *J* = 2.4 Hz, 9.3 Hz, 3H, H_m), 7.05 (d, *J* = 9.6 Hz, 2H, H_l), 7.35 (dd, *J* = 1.2 Hz, 7.8 Hz, 1H, H_h), 7.75 (dt, *J* = 1.2 Hz, 7.5 Hz, 1H, H_f), 7.85 (dt, *J* = 1.2 Hz, 7.5 Hz, 1H, H_g), 8.32 (dd, *J* = 0.9 Hz, 7.8 Hz, 1H, H_e).

NMR ^{13}C ($CDCl_3$, 300 MHz) δ (ppm): 12.6 (C_p), 46.1 (C_q), 52.9 (C_c), 75.5 (C_a), 77.2 (C_b), 96.5 (C_n), 113.5 (C_m), 114.3 ($C_{m'}$), 129.2 (C_h), 130.3 (C_f), 131.1 (C_l), 131.5 (C_e), 133.5 (C_g), 133.8 (C_j), 155.6 (C_k), 157.8 (C_o), 158.1 (C_i), 164.2 (C_d).

Calculated $[M]^+$ ($C_{31}H_{33}N_2O_3$) *m/z* = 481.60. Found: MALDI+: $[M]^+$ *m/z* = 481.3.

rho[G3(NHBoc)$_8$]

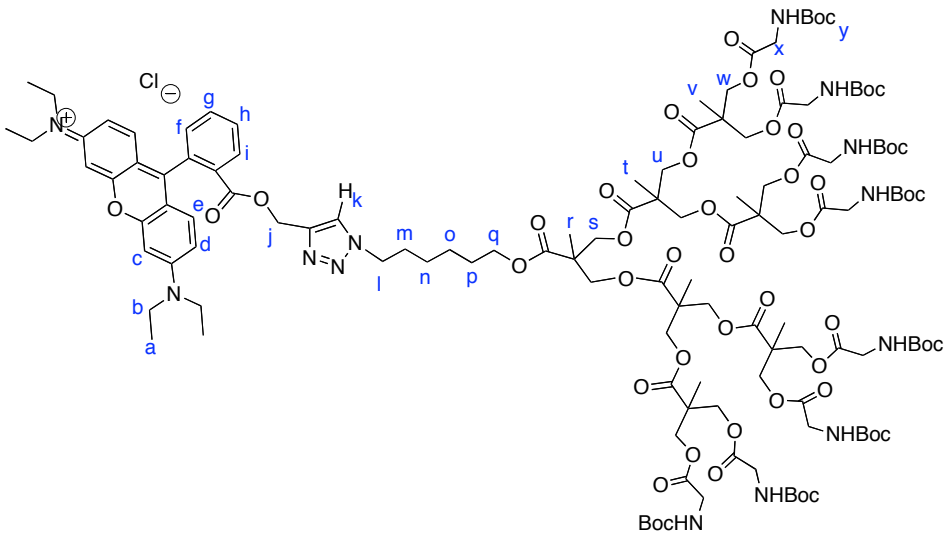

In one hand, the azide functionalized 3rd generation aminated dendron (synthesis in Chapter 1, 1-8) (184 mg, 83 µmol) and alkyne functionalized rhodamine (50 mg, 100 µmol) were dissolved in DMF. In the other hand, copper sulphate pentahydrated (2.5 mg, 10 µmol) and sodium ascorbate (4 mg, 21 µmol) were stirred in DMF for one hour. When the Cu(I) was formed, the solution containing rhodamine and dendron was added and the reaction mixture was agitated for 1 days, at room temperature, under argon atmosphere. After this time, 10 mL of dichloromethane were added and the crude was washed with brine (1 x 5 mL) and with water (3 x 5 mL). The organic phase was dried over anhydrous $MgSO_4$ and concentrated under reduced pressure to give the pure product as a dark purple solid in 84 % yield.

NMR ^{1}H ($CDCl_3$, 300 MHz) δ (ppm): 1.22-1.43 (m, 105H, H_r, H_t, H_v, H_y, H_a), 1.63-1.65 (m, 4H, H_o, H_n), 1.83-1.87 (m, 4H, H_m, H_p), 3.60-3.67 (q, *J* = 6.9 Hz, 8H, H_b), 3.87 (d, *J* = 5.7 Hz, 16H, H_x), 4.08 (t, *J* = 6.6 Hz, 2H, H_q), 4.12-4.29 (m, 28H, H_s, H_u, H_w), 4.39 (t, *J* = 6.9 Hz, 2H, H_l), 5.12 (s, 2H, H_j), 5.41 (br s, 8H), 6.88 (m, 4H, H_c, H_d), 7.05 (d, *J* = 9.3 Hz, 2H, H_e), 7.35 (m, 1H, H_f), 7.69-7.84 (m, 2H, H_g, H_h), 8.29 (d, *J* = 7.5 Hz, 1H, H_i).

NMR ^{13}C ($CDCl_3$, 300 MHz) δ (ppm): 12.7, 17.5, 17.8, 28.3, 42.2, 46.1, 46.4, 46.7, 58.7 (C_a), 65.4, 65.5, 65.6, 79.8, 96.4, 113.6, 114.2, 123.1, 129.9, 130.0, 130.4, 131.3, 132.9, 133.5, 155.6, 155.9, 157.7, 162.5, 164.8, 170.0, 171.6, 171.8, 172.0.

Calculated $[M]^+$ ($C_{128}H_{190}N_{13}O_{49}$) *m/z* = 2694.94. Found: MALDI+: $[M]^+$ *m/z* = 2694.6.

rho[G3(NH$_2$)$_8$]

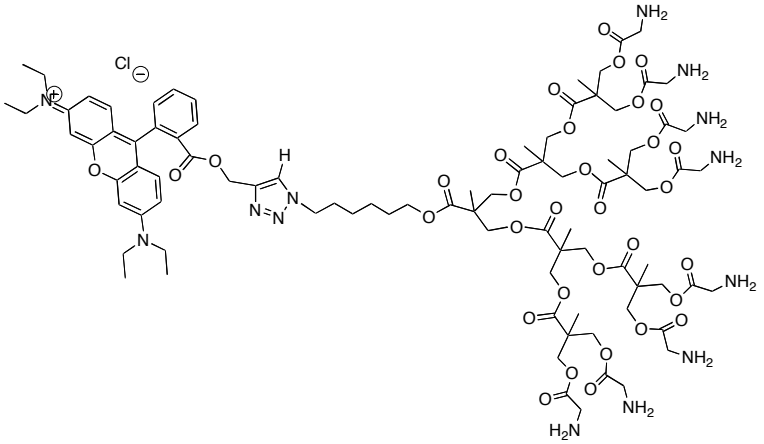

The pure product was obtained as a dark purple solid, in a quantitative yield, following the method (C) for the deprotection of amine groups.

NMR ^{1}H (MeOD, 300 MHz) δ (ppm): 1.26-1.32 (m, 37H, CH_3, CH_2), 1.67 (m, 2H, CH_2), 1.97 (m, 2H, CH_2), 3.68-3.70 (m, 8H, CH_3-C$\underline{H}_2$-N-), 3.94 (m, 16H, C$\underline{H}_2$-NH_2), 4.14 (m, 4H, CH_2), 4.32 (m, 12H, CH_2), 4.44 (m, 16H, CH_2), 6.95-7.08 (m, 5H), 7.41 (d, *J* = 6.9 Hz, 1H), 7.81-7.86 (m, 2H), 8.18-8.34 (m, 3H).

NMR ^{13}C ($CDCl_3$, 300 MHz) δ (ppm): 13.0, 18.4, 26.6, 27.3, 27.5, 29.6, 30.7, 31.1, 31.8, 34.8, 37.1, 41.4, 47.0, 47.7, 66.8, 67.0, 67.8, 97.4, 114.8, 115.6, 131.2, 131.6, 131.8, 132.4, 134.4, 135.1, 157.2, 158.2, 159.8, 166.4, 168.4, 173.3, 173.4, 174.0.

IR (KBr, cm^{-1}): 3426 (N-H), 2976 (C-H), 1746 (C=O), 1648 (C=N).

Calculated $[M]^+$ ($C_{128}H_{190}N_{13}O_{49}$) *m/z* = 1892.9. Found: MALDI+: $[M-456]^+$ *m/z* = 1436.9 (-8 Glycine groups of 57 um).

Folate-[G#1]-(DOT3AGd)$_2$

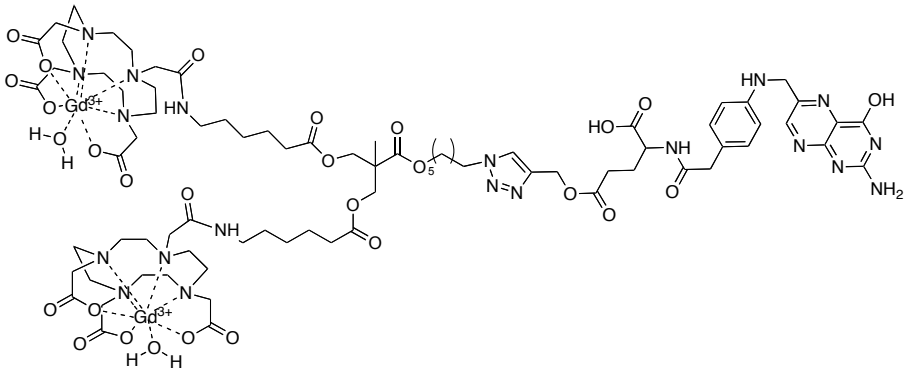

Pentahydrated copper sulfate (64 µg, 0.26 µmol) and sodium ascorbate (93 µg, 0.47 µmol) were dissolved and stirred in deionized water for one hour. Then, the alkyne modified folic acid (2.5 mg, 5.2 µmol) previously dissolved in dimethylformamide and the $N_3C_6H_{12}$-[G#1]-(C_5H_{10}NH-DO3AGd)$_2$ dendron (7.4 mg, 4.7 µmol) were added. The reaction mixture was stirred under argon atmosphere for 24h. EDTA 0.1M was added to the reaction to complex the copper ions and the solution was stirred for 2h. Finally, a dialysis againt deionized water during 24h allowed to recover to pure product in a 76% yield as a pale yellow solid.

Relaxivity measurements: r_1 = 1.97 $mM^{-1}{}_{Gd}.s^{-1}$, r_2 = 2.34 $mM^{-1}{}_{Gd}.s^{-1}$

IR (KBr, cm^{-1}): 3431 (N-H, O-H), *disapearence* of the band at 2099 cm^{-1} (N_3), 1615-1683 (C=O, O=CO^- carboxylates, N-H amide), 1405 (O-C-O carboxylates).

Folate-[G#2]-(DOT3AGd)$_4$

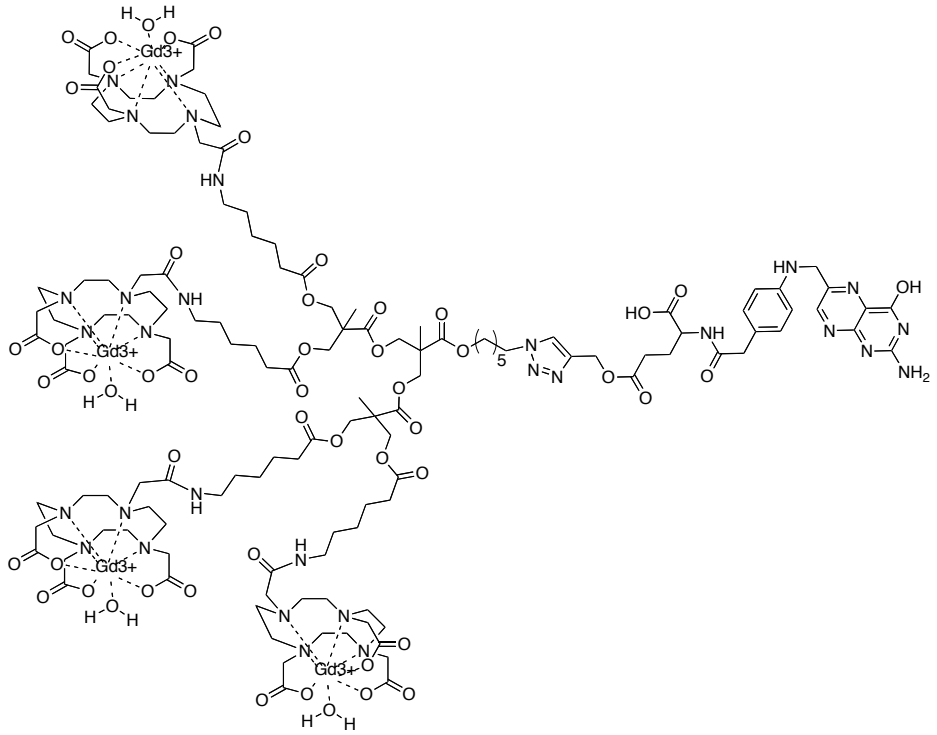

The product was synthesized in the same conditions than Folate-[G#1]-(DOT3AGd)$_2$ and recovered in a 68% yield as a pale yellow solid.

Relaxivity measurements: r_1 = 2.78 $mM^{-1}{}_{Gd}.s^{-1}$, r_2 = 2.73 $mM^{-1}{}_{Gd}.s^{-1}$.

IR (KBr, cm^{-1}): 3430 (N-H, O-H), disapearence of the band at 2099 cm^{-1} (N_3), 1617-1683 (C=O, O=CO^- carboxylates, N-H amide), 1405 (OC-O carboxylates).

(GlyBoc)$_8$[G#3]-[G#2]-DOT3A

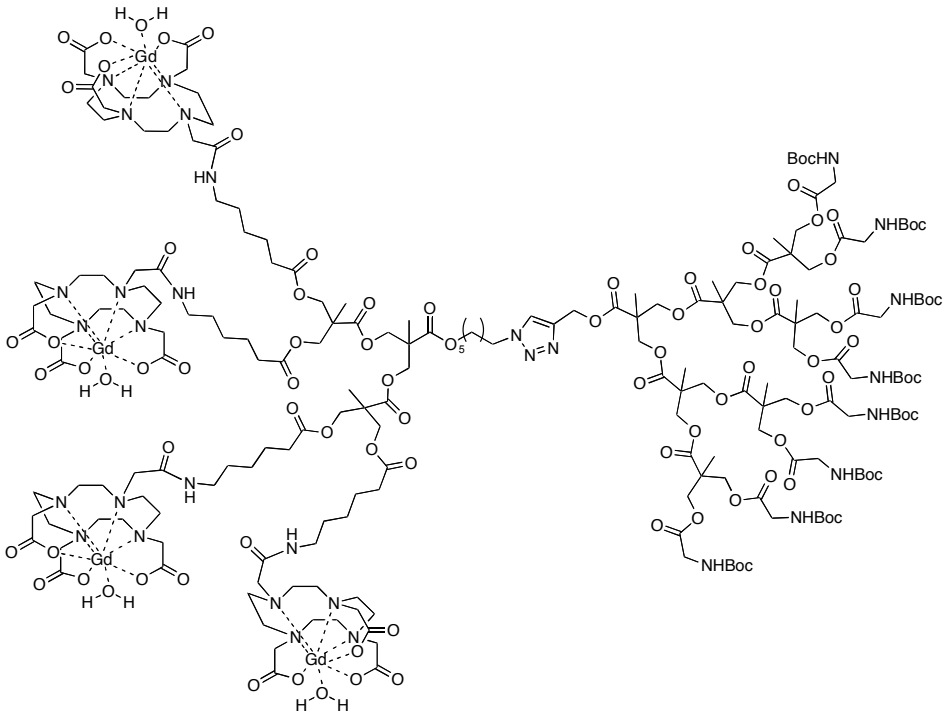

First, copper sulphate pentahydrated (1.6 mg, 6 μmol) and sodium ascorbate (2.5 mg, 12 μmol) were stirred in DMF for one hour. When the Cu(I) was formed, (GlyBoc)$_8$[G#3]-$CH_2CC{\equiv}H$ (80 mg, 38 μmol) and $N_3C_6H_{12}$-[G#2]-($C_5H_{10}NH$ - DO3AGd)$_4$ (50 mg, 31 μmol) were added and the reaction mixture was agitated for 1 days, at room temperature, under argon atmosphere. After this time, 10 mL of dichloromethane were added and the crude was washed with brine (1 x 5 mL) and with water (3 x 5 mL). The organic phase was concentrated under reduced pressure and dissolved in a few amount of methanol. The solution was dialyzed against methanol (cellulose membrane, MW 2000) and the solvent evaporated to give the pure product as a white solid in a 54% yield.

IR (KBr, cm^{-1}): 3403 (N-H), 2980-2934 (C-H), 1746-1723 (C=O).

(Gly)$_8$[G#3]-[G#2]-DOT3A

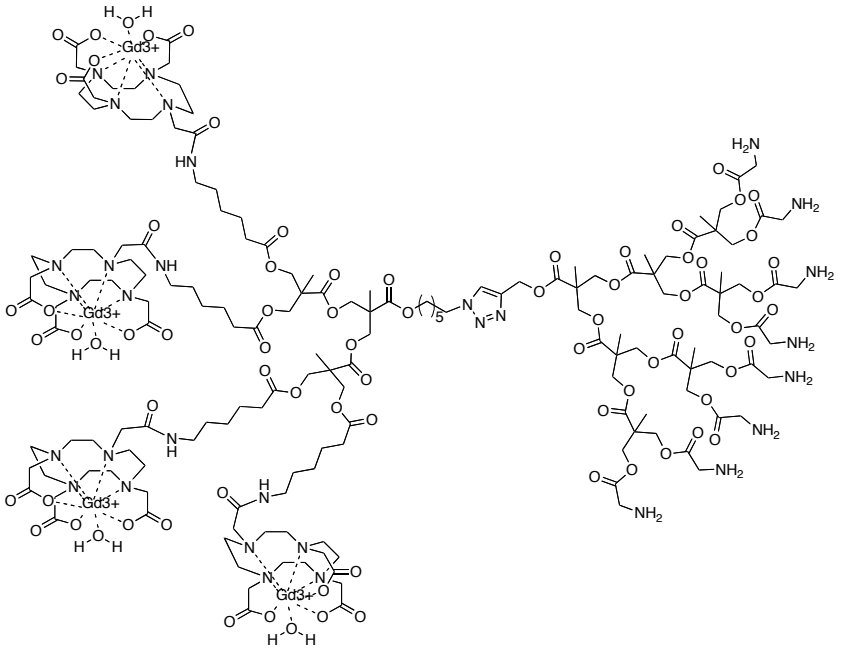

The pure product was obtained as a white solid, in a quantitative yield, following the method (C) for the deprotection of amine groups.

Relaxivity measurements: r_1 = 3.06 $mM^{-1}{}_{Gd}.s^{-1}$, r_2 = 2.86 $mM^{-1}{}_{Gd}.s^{-1}$

IR (KBr, cm^{-1}): 3430 (N-H, O-H), 2919-2851 (C-H), disapearence of the band at 2099 cm^{-1} (N_3), 1734 (C=O esters), 1615-1652 (C=O, O-C-O^- carboxylates, N-H amide).

Reaction with antibodies

1 mL of antibody at 2.5 mg/mL in 10 mM phosphate buffer pH5 was oxidated by sodium periodate (1500eq) during 2h a 37°C, in darkness and under agitation. The antibody was purified by gel filtration (Sephadex) at pH 5 10mM to eliminate the salts. The column of gel was previously equilibrated with the phosphate buffer pH 5, 10mM. The antibody was recovered and 100 eq of the dendrimer was added. The reaction mixture was agitated during 2h at 37°C. After this time, a solution of $NaCNBH_3$ at 0.1M in NaOH was added (370 eq) and the mixture was agitated in darkness at room temperature. Then, the unreacted aldehydes were blocked by the addition of 50µL of 1M ethanolamine, pH 9.6, and the stirring of the solution during 30 minutes at room temperature. Finally, the excess of dendron and salt was removed by gel filtration with a Sephadex column in phosphate buffer 10mM pH 7. The resulting modified antibody was characterized by fluorescence emission spectroscopy, SDS-page, and isoelectric point.

Immunofluorescence antiHER2/rhodamine

COS-7 and MCF-7 cells were seeded in a 24-wells plate at 100 000 cells per well, in 1 mL of medium. After 48h, the medium was removed and the cells were washed twice with PBS containing calcium. Then, the cells were fixed with 4 % formaldehyde in PBS during 20 minutes at 4°C. Afterwards, the cells were washed 3 times with PBS containing calcium and were incubated 1 hour with PBS-BSA. Then, the cells were incubated 5 minutes with 1 mL of 0.2 % (v/v) Triton solution in Ca PBS to permeabilize the cell membrane when it is the case. The cells were washed twice 5 minutes with Ca PBS, and they were incubated twice 5 minutes with PBS-BSA (0.2 % w/v in Ca PBS). The cells were then incubated with the antiHER2 wearing rhodamine (20µL at approx. 3µg/mL) during 1 hour at room temperature. The cells were washed once 5 minutes with PBS-BSA and 4 times 5 minutes with Ca PBS. The cells were incubated 1 hour with the secondary antibody (antimouse alexa 488) at room temperature if needed and the washing steps were repeated. The samples were finally mounted with Mowiol (Calbiochem, Merk Chemicals) containing DAPI following standard protocols. The samples were kept at 4°C before microscope analysis.

CHAPTER 3:

DESIGN, SYNTHESIS AND EVALUATION OF BIS-MPA DENDRITIC COMPOUNDS AS ANTIMALARIAL DRUGS VEHICLES

Introduction and previous work

Malaria

Malaria, the most prevalent parasitic disease in the world, is an infection caused by the apicomplex protozoan of the *Plasmodium* genus. It is mostly present in the tropics where the four species that cohabit (*P. falciparum, P. viviax, P. malariae y P. ovale*) are transmitted to humans by the bites of the female mosquito vector of the *Anopheles* genus. Owing to its geographical localization, malaria is still a forgotten disease that suffers of a lack of research and an insufficient development of therapies and vaccine, which results in the lost of million of lives (Figure 81).[149]

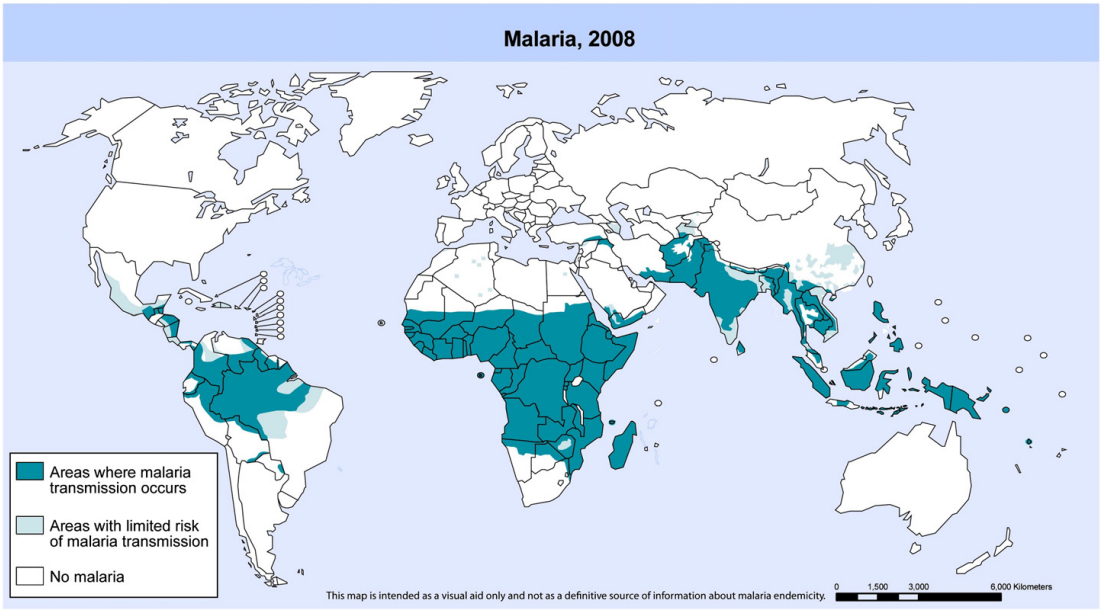

Figure 81: Areas where malaria transmission occurs, with limited risk, and without malaria. Adapted from WHO 2011.[149]

The proper characteristics of the disease, related with the particularity of the transmission way and the control difficulty of its extension, augment the difficulties for finding a cure or an effective way of prevention.

[149] WHO Global Malaria Programme, *World Malaria Report,* **2011.**

In the life cycle of *Plasmodium* parasites[150] the female *Anopheles* mosquito inoculates *Plasmodium* sporozoites that bind to and infect hepatocytes in the liver and proliferate into thousands of merozoites. The merozoites rupture from the hepatocytes and invade red blood cells (RBCs) where they develop into rings, trophozoites, and then into schizonts (Figure 82) that burst and release more merozoites, which start the blood cycle again.

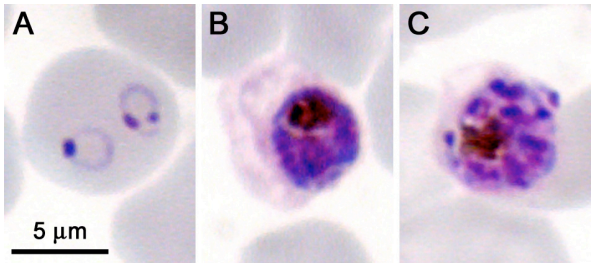

Figure 82: Giemsa staining of Plasmodium-infected RBCs. At the ring (A), trophozoite (B), and schizont (C) stages of *P. falciparum*. Adapted from P. Urban et Al.[151]

Because of the long duration of the intra-erythrocytic stage and the sheer numbers of parasites in this phase at any time, *Plasmodium*-infected RBCs (pRBCs) are the main target for chemotherapeutic approaches.[152] A variety of factors such as the localisation of the disease, the conditions of transmission, the complexity of the parasite life cycle, the drug resistance and HIV co-infections, reduce the success of chemotherapy.[1] Furthermore, drugs used for the treatment of malaria cause severe side effects. Depending on the *Plasmodium* specie responsible for the infection, and on other factors such as the seriousness of the disease, the existence of the pre-infection exposure, and the determination of the clinical status of the patient and drug susceptibility, the appropriate treatment can be chosen.

Other strategies are employed to prevent malaria infection like the elimination of the mosquito vector of the parasites using long-lasting insecticidal nets and indoor residual spraying of insecticides. Additionally, in the case of

[150] R. Tuteja, *FEBS J.,* **2007***, 274*, 4670-4679.
[151] P. Urban, A. Estelrich, A. Adeva, A. Cortés, X. Fernàndez-Busquets*, NRL,* **2011***, 6*, 620-628.
[152] K.S. Griffith, L.S. Lewis, S. Mali, M.E. Parise, *JAMA,* **2007***, 297*, 2264-2277.

pregnant women, intermittent preventive treatment with antimalarial drug has been used to reduce the impact of the infection on the fetus during pregnancy.

Nevertheless extrinsic factors such as the poor distribution of medicines in different countries, drug interactions, socio-economic conditions of affected populations and resistance of the vector to insecticides increase the difficulties for the eradication of malaria in the world. The best solution in terms of efficiency and cost to fight against the disease would be the vaccination of the endemic population but until now there is not a commercially available vaccine to control malarial infection. However, two vaccines, known as RTS,S/AS01B and RTS,S/AS02B,[153] are undergoing phase I and II clinical trials.

To prevent drug-resistance mechanisms in malaria therapy and numerous side effects due to prolonged conventional therapy, new strategies for intracellular antimalarial drug delivery are urgently needed. Nanotechnology could be converted in a good therapeutic weapon targeting existing drugs, increasing their efficiency and avoiding drug-resistance. For instance, drugs encapsulated in nano-systems able to pass through the digestive vacuole membrane by different mechanisms could be used in order to bypass chloroquine (one of the currently used antimalarial drugs) transporters. One of the most important properties of a nano-carrier in the context of malaria is the ability to remain in the blood stream for a long period of time in order to improve the interaction with infected red blood cells (pRBCs) and parasite membranes.

[153] K.E. Kester, J.F. Cummings, O. Ofori-Anyinam, C.F. Ockenhouse, U. Krzych, P. Moris, R. Schwenk, Z. Debebe, E. Pinelis, L. Juompam, J. Williams, M. Dowler, V.A. Stewart, R.A. Wirtz, M.-C. Dubois, M. Lievens, J. Cohen, W.R. Ballou, D.G. Heppner Jr*, J. Infect. Dis.,* **2009**, *200*, 337-346.

Amphiphilic molecules and supramolecular objects

Amphiphilic molecules as polymers and dendrimers have been used as vehicles for low molecular weight molecules in order to dissolve, stabilize and target them. In addition to their application in the design of nano-delivery systems, amphiphilic molecules are shown to have biological effects themselves.[154]

The formation of vesicles is a two-step process in which the amphiphile molecule first forms a bi-layer and then closes to form a vesicle. The shape of self-assemble amphiphilic structures is determined by the size of the hydrophobic moiety relative to the hydrophilic part, and the curvature is related to the packing parameter.[155] The packing parameter (p) relates in a direct manner the structure of the molecule with its packing form.[156] Concretely, the packing parameter (p) is directly proportional to the volume of the hydrophobic part (v), and inversely proportional to the product of the transversal surface of the hydrophilic part (a) per the molecule length (l) (Figure 83).

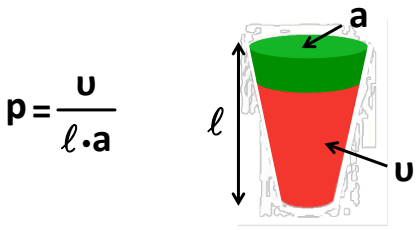

Figure 83: Packing parameter. Adapted from S. Hernández.[157]

For p<1/3, the molecules adopt a conic form and organize themselves in spherical micelles. When 1/3≤p≤1/2, the molecules adopt a truncated cone form and arrange themselves in a cylindrical micelle. For 1/2≤p<1, the molecules also adopt a truncated

[154] a) A.V. Kabanov, E. Batrakova and D. Miller, *Adv. Drug Deliv. Rev.*, **2003**, *55*, 151-164 ; b) J. Zastre, J. Jackson, H. Burt, *Pharm. Res.*, **2004**, *21*, 1489-1497 ; c) C.W. Todd, M. Balusubramanian, M.J. Newman, *Adv. Drug Deliv. Rev.*, **1998**, *32*, 199-223.

[155] S.T. Hyde, *J. Phys. (Paris)*, **1990**, *51*, C7209.

[156] J. N. Israelachvili, D.J. Mitchel and B.W. Nimham, *J. Chem. Soc. Faraday Trans. T.2*, **1976**, *72*, 1525-1568.

[157] S.M. Hernandez Ainsa, PhD disertation: Nuevos materiales funcionales basados en dendrímeros cristales líquidos íonicos, Universidad de Zaragoza, **2010**.

cone arrangement but with dimensions similar to a cylinder, they assemble in a flexible bilayer that can curve and generate a vesicle. When p ≈ 1, the molecules adopt a cylindrical shape and the bilayer formed by supramolecular organization is plane, avoiding the formation of vesicles. When p>1, the molecules adopt an inverted truncated cone shape and arrange themselves in inverted micelles, with the hydrophobic part in contact with the external environment[158] (Figure 84).

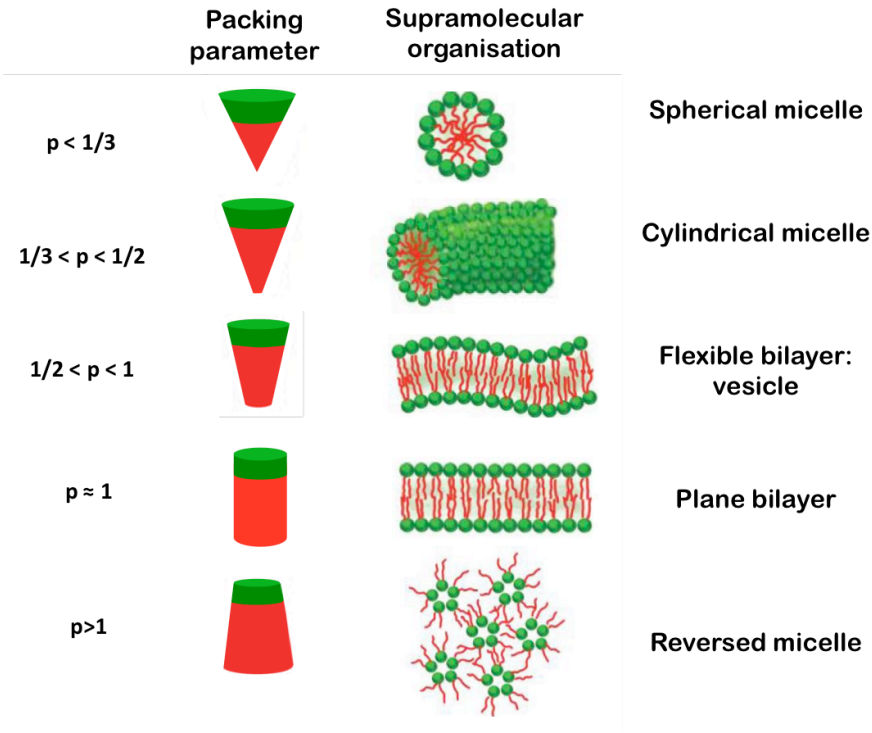

Figure 84: Relationship between an amphiphilic molecule structure and its supramolecular organization in function of the packing parameter. Adapted from S. Hernández.[157]

Spherical or cylindrical micelles, vesicles and bilayers are the most common nano-objects formed with amphiphilic molecules in water.[159] Polymer vesicles can exhibit shapes that are unknown for liposomes vesicles: stable high genus vesicles

[158] a) P.C. Hiemenz, R. Rajagopalan, *Principles of colloid and surfaces chemistry. New York: Marcel. Dekker, Inc.* **1997** ; b) J. N. Israelachvili, *Intermolecular and Surface Forces, 2nd. Ed. Acaddemic Press Ltd., London,* **1991**. ; c) M. Antonietti and S. Föster, *Adv. Mater.*, **2003**, 15, 1323-1333. ; d) S. Šegota, Đ. Težak, *Adv. Coll. Interf. Sci.,* **2006**, *121*, 51-75.

[159] a) B.L.S. Mui, H.G. Döbereiner, T.D. Madden, P.R. Cullis, *Biophys. J.,* **1995**, *69*, 930-941; b) T. Shimizu, M. Masuda, H. Minamikawa, *Chem. Rev.,* **2005**, *105*, 1401-1443.

(e.g. doughnut-like vesicles).[160] Besides, other types of supramolecular structures can be found like nano-spheres and nano-capsules.[161] Nano-capsules are formed when a third hydrophobic component, like oil, is added. In this case; the molecules form a mono-layer that envelop the hydrophobic component. The main difference between nano-spheres and vesicles is that the inner part of nano-spheres is not empty: it is full of the molecules themselves (Figure 85).

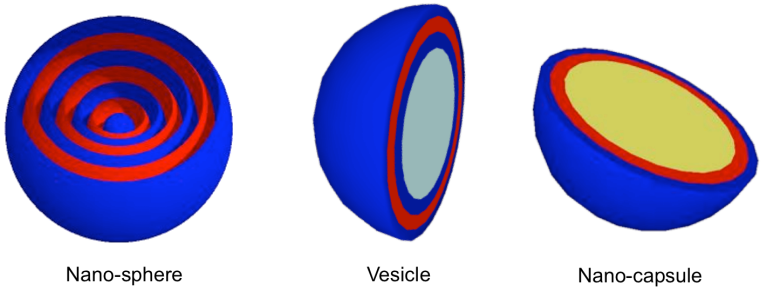

Figure 85: Representation of nano-sphere, vesicle and nano-capsule. In blue is represented the hydrophilic part, in red the hydrophobic part. In clear blue in represented the water inside of the vesicle. In yellow is represented the oil inside the nano-capsule. Adapted from S. Hernández.[157]

A great number of studies have been published about the influence of factors like temperature,[162] addition of another solvent,[163] change of salt concentration or pH,[164] influence of light,[165] on the formation or the modification of nano-objects.

[160] C.K. Haluska, W.T. Gózdz, H.-G. Döbereiner, S. Förster, G. Grompper, *Phys. Rev. Lett.,* **2002**, *89,* 238302-238305.

[161] a) K. Letchford, H. Burt, Eur. *J. Pharm. Biopharm*., **2007**, *65*, 259-269 ; b) C. Prego, D. Torres, E. Fernandez-Megia, R. Novoa-Carballal, E. Quinoa, M.J. Alonso, *J. Control. Release,* **2006**, *111*, 299-308 ; c) T. Ameller, V. Marsaud, P. Legrand, R. Gref, G. Barratt, J.M. Renoir, *Pharm. Res.,* **2003**, *20*, 1063-1070 ; d) K.S. Soppimath, T.M. Aminabhavi, A.R. Kulkarni, W.E. Rudzinski, *J. Control. Release,* **2001**, *70*, 1-20 ; e) A. F. Thünemann, J. Beyermann, H. Löwen, *Langmuir,* **2000**, *16*, 850-857.

[162] a) P. Bhargava, Y. Tu, J.X. Zheng, H. Xiong, R.P. Quirk, S.Z.D. Cheng, *J. Am. Chem. Soc.,* **2007**, *129*, 1113-1121 ; b) J.E. Chung, M. Yokoyama, T. Okano, *J. Control. Release,* **2000**, *65*, 93-103.

[163] C. Liu, M.A. Hillmyer, T.P. Lodge, *Langmuir,* **2008**, *24*, 12001-12009.

[164] A. Choucair, C. Lavigueur, A. Eisenberg, *Langmuir,* **2004**, *20*, 3894-3900.

[165] a) J.Q. Jiang, B. Qi, M. Lepage, *Macromolecules,* **2007**, *40*, 790-792; b) H.I. Lee, W. Wu and J.W. Oh, *Angew. Chem. Int. Ed.,* **2007**, *46*, 2453-2457 ; c) E. Mabrouk, D. Cuvelier and F. Brochard-Wyart, *PNAS U.S.A.,* **2009**, *106* , 7294-7298.

Block copolymers have been one of the most studied systems because of the possibility of controlling the structures of the hydrophobic and hydrophilic parts during their synthesis. Vesicles are promising system for the encapsulation and delivery of hydrophobic or hydrophilic molecules. Hydrophobic compounds can be solubilized into the vesicle bilayer by stirring together with the vesicle solution or by dissolving the vesicle forming polymer and the compound in an organic co-solvent with subsequent transfer to water. Hydrophilic molecules can be encapsulated by dissolving the block copolymer in the aqueous drug solution. A continuous loss of encapsulated substance occurs via permeation through the vesicle bilayer. The larger thickness of polymer bilayers (5-20 nm) compared to lipid bilayer (3-5 nm) induces a much slower permeation of molecules.[166]

Amphiphilic dendrimers

Amphiphilic dendrimers is a family of dendrimers comprising: amphiphilic layered dendrimers, amphiphilic segmented dendrimers, also called Janus dendrimers when the dendrimer has two segments, and amphiphilic dendritic homopolymers. Amphiphilic linear dendritic hybrids are the major class of dendritic amphiphiles. They are formed by linear-dendritic amphiphiles as linear-dendritic hybrids and amphiphilic dendritic-liner-dendritic "dumbbells" (Figure 86).

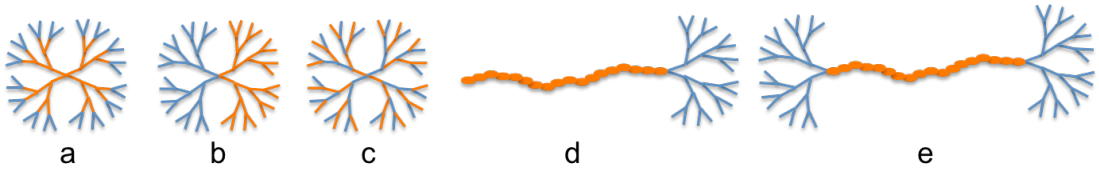

Figure 86: Structures of amphiphilic dendrimers and amphiphilic linear dendritic hybrids.[167] From left to right: a) layered dendrimers, b) segmented dendrimers, c) dendritic homopolymers, d) linear-dendritic hybrids and e) dendritic-linear-dendritic "dumbbells".

Amphiphilic dendrimers, in addition to their characteristic dendritic properties, include regions of contrasting polarity. Compared to linear

[166] M. Antonietti and S. Föster, *Adv. Mater.*, **2003**, *15*, 1323-1333.
[167] Y. Wang and S.M. Grayson, *Adv. Drug Deliv. Rev.*, **2012**, *64*, 852–865.

amphiphiles, dendritic amphiphiles can exhibit more stable micellar aggregates, and for large, highly branched structures, can even generate unimolecular micelles. The small hydrodynamic volumes exhibited by dendrimers are also appealing for many drug delivery applications, because they are typically large enough to slow renal filtration yet small enough to prevent accumulation in the spleen, liver and elsewhere.[168] Because of their specific properties, the use of dendrimers has been studied for a wide range of applications, including drug delivery, gene transfection, biosensors, and catalytic nanoreactors.[169]

Polymersomes, or polymeric vesicles, are polymeric capsules with a bilayer membrane formed by amphiphilic block copolymers. Depending on the ratio between the hydrophobic and hydrophilic part of the polymers, spherical micelles, rods and vesicles form spontaneously.[170] **Dendrimersomes**, or dendritic vesicles, are stable, monodisperse and unilamellar vesicles self-assembled in water from amphiphilic dendrimers.

Compared to other drugs, just few studies were published about the delivery of antimalarial drugs using dendrimers. D. Bhadra and co-workers studied dendrimers formed from lysine as vehicle for Artemether[171,172] but in spite of encouraging results, no experimental work was done about the efficiency of nano-carriers based of dendrimers against malaria.

---

[168] a) F. Yuan, D. Fukumura, M. Leunig, D.A. Berk, V.P. Torchilin, R.K. Jain, *Cancer Res.,* **1995**, *55*, 3752-3756 ; b) H.R. Ihre, O.L.P. De Jesus, F.C. Szoka, J.M.J. Fréchet*, Bioconjugate Ch*em., **2002**, *13*, 433-452.

[169] a) R. Esfand and D.A. Tomalia*, Drug. Discov. Today,* **2001**, *6*, 427-436 ; b) E.R. Gillies and J.M.J. Fréchet*, Drug Discov. Today,* **2005**, *10*, 35-43 ; c) P.M. Heegaard, U. Boas*, Chem Soc. Rev.,* **2004***, 33*, 43-63 ; d) S. Svenson, D.A. Tomalia*, Adv. Drug Deliv. Rev.,* **2005**, *57*, 2106-2129 ; e) A. D'Emanuele, D. Attwood*, Adv. Drug Deliv. Rev.,* **2005**, *57*, 2147-2162 ; f) L. Twyman, A. Beezer, R. Esfand, M.J. Hardy, J.C. Mitchell*, Tetrahedron Lett.,* **1999**, *40*, 1743-1746 ; g) M. Liu, K. Kono and J.M.J. Fréchet*, J. Control. Release,* **2000**, *65*, 121-131; h) C. Kojima, K. Kono, K. Maruyama, T. Takagishi*, Bioconjugate Chem.,* **2000**, *11*, 910-917 ; i) E.R. Gillies and J.M.J. Fréchet*, J. Am. Chem. Soc*., **2002**, *124*, 14137-14146 ; j) I.J. Majoros, A. Myc, T. Thomas, C.B. Mehta, J.R. Baker Jr, *Biomacromolecules* **2006**, *7*, 572-579.

[170] D.E. Discher, A. Eisenberg, *Science*, **2002**, *297*, 967-973.

[171] D. Bhadra, S. Bhadra, N.K. Jain*, J. Drug Deliv. Sci. Technol*., **2005**, *15*, 65-73.

[172] D. Bhadra, S. Bhadra, N.K. Jain, *Pharm. Res*., **2006**, *23*, 623-633.

Antecedents

Interesting results were obtained with an aminated dendron of *bis*-MPA of third generation, **[G3-*bis*MPA]**, in terms of cell viability and growth inhibition of the *Plasmodium* parasite. This dendron was functionalized by amine groups in its periphery and by an azide in its point to allow further modifications by copper catalyzed azide-alkyne cycloaddition (Figure 87, see synthesis in Chapter 1). This compound was chosen for the first growth inhibition assay because it is a possible precursor for the synthesis of amphiphilic dendritic compounds that could be used to form nano-objects.

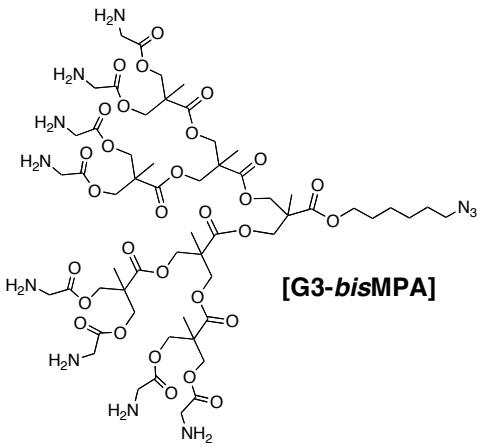

Figure 87: Molecular structure of [G3-*bis*MPA] dendron.

To value the specific toxicity of the compound against *Plasmodium*, cytotoxicity tests were carried out at concentrations from 39 µg/mL to 10 mg/mL. The toxicity of the compound was evaluated by a cell viability assay on Human Umbilical Vein Endothelial (HUVEC) cells using WST-1 as labeling reagent (Figure 88) after 48h of incubation of the cells with the compound. WST-1 cell viability test is based on the mitochondrial activity of the cells.

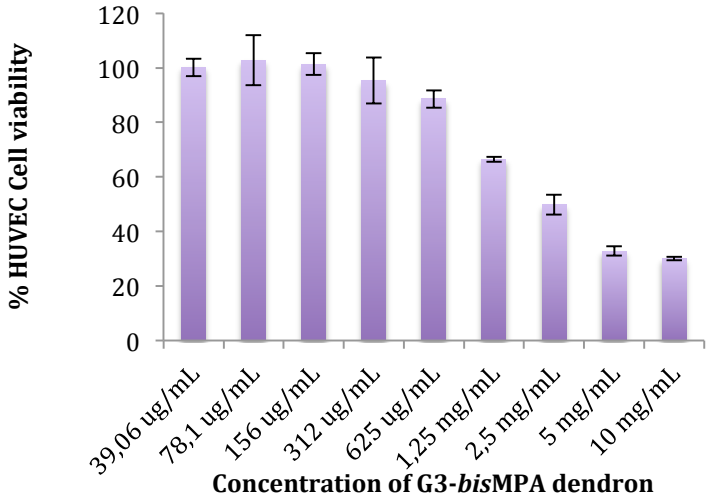

Figure 88: Cell viability of HUVEC cells incubated 48h with the compound [G3-*bis*MPA].

Although some toxicity has been observed, high concentrations, such as 1.25 mg/mL, were needed for an appreciable effect. The IC_{50} value was calculated by non-linear regression with an inhibitory dose-response model using GraphPad Prism5 software.[173] The results indicate that the compound present significant cytotoxicity, with an IC_{50} value of 2 mg/mL. The compound did not present hemolytic activity at these concentrations.[174]

The growth inhibition (GI) of the *Plasmodium* parasite at ring stage generated by the compound was evaluated. The GI was calculated by the difference between the number of parasite-infected red blood cells (pRBCs) in the control, and the number of infected RBCs after 48h of incubation with the derivative. The number of pRBCs was determined by fluorescence-assisted cell sorting (FACS) analysis (Figure 89).

[173] http://www.graphpad.com/scientific-software/prism/.

[174] To realize the haemolysis assay, the RBCs are incubated with the compound and then centrifuged to separate the cells and the floating part. If there is haemolysis, haemoglobin has been liberated in the floating part and can be quantified by spectrophotometry.

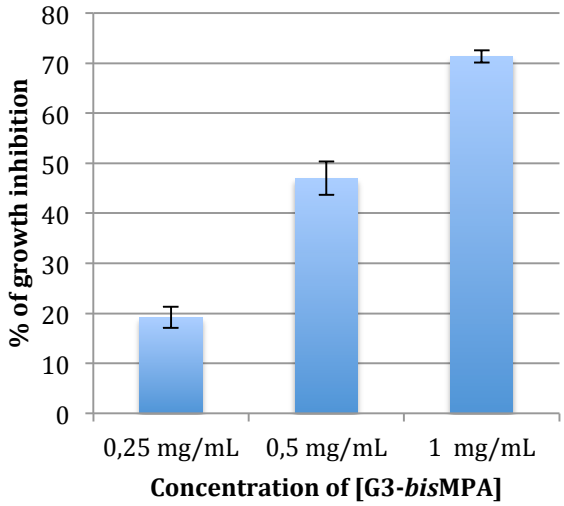

Figure 89: Percentage of growth inhibition induced by [G3-*bis*MPA] at different concentrations. pRBCs were incubated 48h with the compound before FACS analysis (50000 cells, 3 repetitions).

From a concentration of 0.25mg/mL, an effect on the growth of the parasite can be appreciated. This effect increases with the concentration and reaches a maximum of 71% of growth inhibition at 1mg/mL.

These first assays indicate that the compound **[G3-*bis*MPA]** is an interesting precursor for the preparation of amphiphilic derivatives in the objective to form nano-objects encapsulating antimalarial drugs. This compound presented low cytotoxicity *in vitro* on HUVEC cells, **IC_{50}=2mg/mL**, and "an **intrinsic toxicity for the plasmodium** from **0.25 mg/mL**.

Objectives and approach

The principal objectives of this chapter of the thesis are the preparation of nano-carriers of antimalarial drugs formed from *bis*-MPA dendrimers and pluronic® derivatives followed by their *in vitro* study. In this purpose different aspects of the work will be developed:

1)- Design and synthesis of amphiphilic dendritic derivatives,
2)- Encapsulation of hydrophilic antimalarial drugs inside the nano-carriers,
3)- Characterization of the complexes obtained,
4)- *In vitro* study of their activity against the *Plasmodium* parasite, cytotoxicity tests and internalization assays.

This work has been realized in collaboration with the NanoMalaria group of Xavier Fernández Busquets at the CRESIB (Barcelona). Dendrimers have been synthesized and characterized at the INA (Zaragoza). The biological studies of dendrimers in terms of unspecific toxicity, antimalarial activity and interaction with pRBCs were performed by Julie Movellan and Patricia Urbán in the CRESIB laboratories.

Design and synthesis

Design

On the basis of the antecedents with the compound **[G3-*bis*MPA]**, four products were designed as vectors of antimalarial drugs combining the toxicity of the dendron itself and the liberation of the drug. The compounds were designed to contain a **polar** and an **apolar** part that should allow them to self-organize into nano-objects able to encapsulate small molecules.

Two products were formed from **[G3-*bis*MPA]** dendron: **A** and **B** (Figure 90). They both contain a polar part formed by a *bis*-MPA dendron of second or third generation functionalized by amine groups, and an apolar part formed by a *bis*-MPA dendron of second generation functionalized with apolar chains ($C_{17}H_{35}$; from stearic acid). In this case both dendrons were synthetized separately and then coupled by copper-catalyzed azide-alkyne cycloaddition (CuAAC).

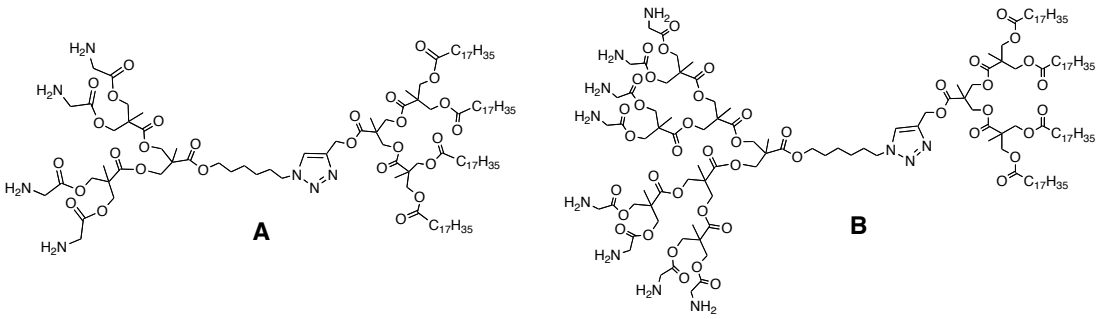

Figure 90: Molecular structures of compounds A (left) and B (right).

As an alternative to the previously presented dendrimers, a second family of compounds was selected. Pluronics®, also known as poloxamer, are triblock ABA-type copolymers composed of a central hydrophobic block of poly(propylene oxide) (PPO) and two hydrophilic chains of poly(ethylene oxide) (PEO). It has been shown that pluronic® increases cellular internalization[175] and forms micelles.[176]

[175] G. Pembouong, N. Morellet, T. Kral, M. Hof, D. Scherman, M.-F. Bureau, N. Mignet, *J. Control. Release,* **2011**, *151*, 57-64.

Previous work with Pluronic® without modifications has been realized recently by S.J. Surana and co-workers.[177] They explored the formulation and evaluation of *in situ* gel for the nasal delivery of Artemether (an hydrophobic antimalarial drug) by a temperature induced gelation technique using Pluronic® with a muco-adhesive polymer of hydroxypropylmethyl cellulose (HPMC) in different ratios.

Two products composed by Pluronic® F127 modified by *bis*-MPA dendrons were synthesized: **C** and **D** (Figure 91). In the case of the compound **C**, Pluronic® was functionalized with a first generation of aminated-*bis*-MPA dendron, and in the case of the compound **D** by the **[G3-*bis*MPA]** dendron.

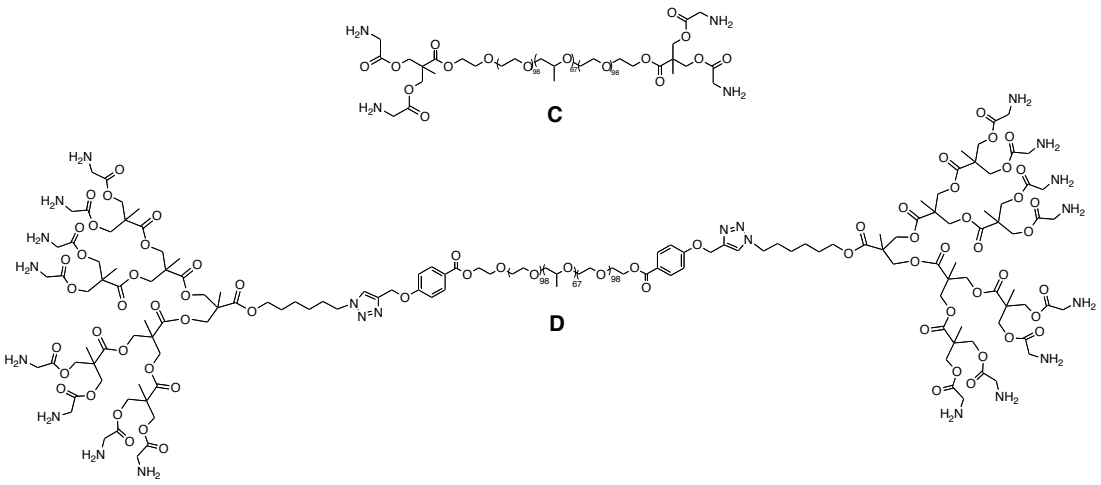

Figure 91: Molecular structure of polymers C and D

[176] E.S. Lee, Y.T. Oh, Y.S. Youn, M. Nam, B. Park, J. Yun, J.H. Kim, H.-T. Song, K.T. Oh*, Colloid Surf. B,* **2011**, *82*, 190-195.

[177] H.S. Mahajan, S.K. Shah, S.J. Surana, *J. Inclusion Phenom. Macrocyclic Chem.,* **2011***, 70*, 49-58.

The hydrophobic content of these molecules was calculated as following: ***Hc = (MW hydrophobic part / MW molecule) x 100***. It varies from 24 % for product **D** to 44 % for product **A** (Table 12).

Product	Apolar part	Polar part	Hc
A	Apolar dendron 2G	Polar dendron G2	44
B	Apolar dendron 2G	Polar dendron G3	33
C	PPO pluronic	PEO pluronic + polar dendron G1	29
D	PPO pluronic	PEO pluronic + polar dendron G3	24

Table 12: Hydrophobic content of derivatives A, B, C and D

Synthesis of the compounds A, B, C and D

Synthesis of A and B

The synthesis of the products **A** and **B** begun with the preparation of two *bis*-MPA dendrons by Steglich esterification, both of them functionalized by an azide group or an alkyne in order to be coupled by CuAAC. The dendrons were synthesized from the commercial *bis*-MPA monomer as described in the Chapter 1. One of the dendron was functionalized by stearic acid to form the apolar part and the other by protected-glycine to form the polar part of the molecule. In the Figure 92 the synthetic scheme is represented for the compound **B**.

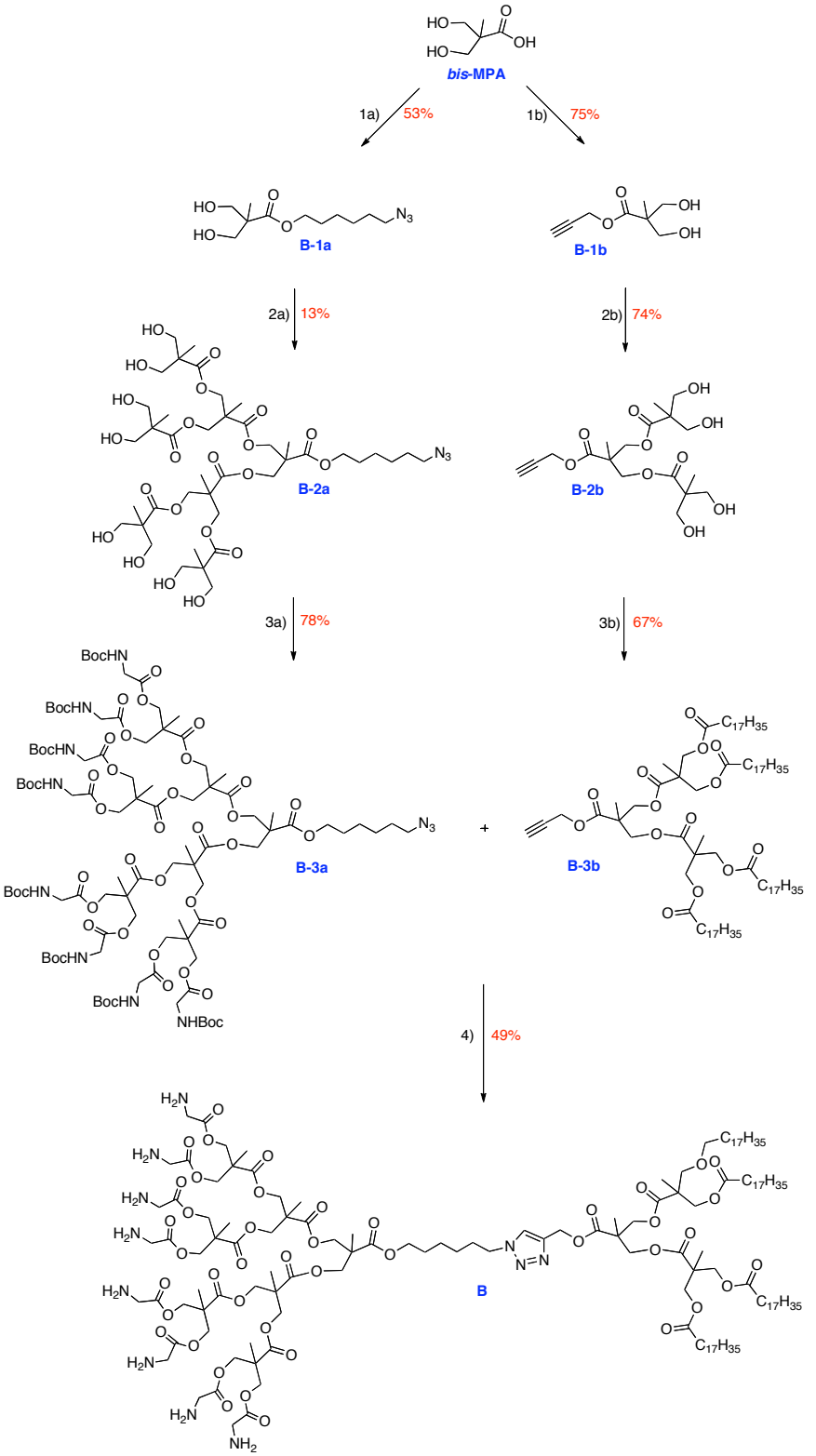

1a) 2,2-dimethoxypropane, *p*-TsOH, Acetone (81%); 6-azidohexan-1-ol, DCC, DPTS, CH_2Cl_2 (66%); DOWEX H^+, MeOH (99%).
1b) Propargyl alcohol, DCC, DPTS, CH_2Cl_2 (77%); DOWEX H^+, MeOH (98%).
2) Isopropylidene *bis*-MPA, DCC, DPTS, CH_2Cl_2; DOWEX H^+, MeOH; (2a: 13%; 2b: 74%).
3a) GlyBoc, DCC, DPTS, CH_2Cl_2 (78%).
3b) Stearic acid, DMAP, CH_2Cl_2 (67%).
4) $CuSO_4$ $5H_2O$, sodium ascorbate, DMF (49%); MeOH/HCl (Quant.).

Figure 92: Synthetic scheme for the product B.

As a first step, the *bis*-MPA carboxylic acid was functionalized by an azide (**1a**) or by a triple bond (**1b**). In order to do so, the hydroxyl groups of the *bis*-MPA monomer were protected by the formation of an acetal with 2,2-dimethoxypropane in presence of *p*-toluenesulfonic acid in acetone. Then, the esterification of the carboxylic acid with 6-azidohexan-1-ol (**1a**, 53%) or propargyl alcohol (**1b**, 75%) in presence of DCC and DPTS in dichloromethane gave the functionalized products. The crudes were purified by filtration to eliminate the DCU formed and by column chromatography for the removal of the alcohols excess. The hydroxyl groups of the dendrons were deprotected in acid environment using a DOWEX H^+ resin in methanol.

The generation growth was obtained by esterification of the hydroxyl groups with the protected *bis*-MPA monomer in presence of DCC and DPTS in dichloromethane (**2a, 2b**). After each esterification, the crudes were purified by column chromatography and the hydroxyl groups of the dendrons were deprotected in acid environment.

The next step consists in the functionalization of the dendrons surface. The azido-modified dendron (**B-2a**, 13%) was functionalized by protected glycine in order to obtain an aminated derivative **B-3a** (see Chapter 1). The alkyne-modified dendron (**B-2b**, 74%) was functionalized by stearic acid in order to form the apolar part of the dendron. The reaction of esterification was carried out in dichloromethane in presence of DMAP as acylation catalyst and was purified by filtration (removal of DCU) and precipitation in cold acetone (elimination of the excess of stearic acid) to give the pure product (**B-3b**) in a 67% yield.

The last step of the synthesis (**4**, 49%) consists in the copper-catalyzed 1,3-dipolarcycloaddition between the azido-dendron (**B-3a**) and the alkyno-dendron (**B-3b**). The copper (I) catalyst was generated *in situ* by the reduction of the copper (II) salt ($CuSO_4$, $5H_2O$) with sodium ascorbate in dimethylformamide. Then, the dendrons were added and the reaction mixture was stirred during two days. The crude product was purified by precipitation in acetone. Finally, the amine groups were deprotected in acid environment to give the final product in a quantitative yield.

The products **A** and **B** were obtained in **total yields** of **16%** and **3%** respectively, from the *bis*-MPA monomer. The final compounds were characterized by ^{1}H-NMR, ^{13}C-NMR, IR, mass spectroscopy and elemental analysis (see experimental part).

The ^{1}H-NMR spectrum of the compound **A** is represented in the Figure 93. The singlet peak at 7.67 ppm integrating for one proton (**Hl**) confirmed the formation of the triazide cycle resulting from the CuAAC reaction. Between 4.10 ppm and 4.55 ppm are situated the peaks corresponding to the C**H**$_2$ of the *bis*-MPA dendrons (12 CH_2, **Hb,b', Hd,d', Ho,o', Hq,q'**), with the -C**H**$_2$-NH_2 (4 CH_2, **Ha**) and the -C**H**$_2$-O- **Hf**. At 5.24 ppm is located the peak due to the CH_2 in α of the triazide cycle **Hk**. The peaks corresponding to the methyl groups of the *bis*-MPA appear at approx. 1.2 ppm (**Hc, He, Hn, Hq**) with the peak due to the -C**H**$_2$- groups from the apolar chains **Hs**. The peak corresponding to the -C**H**$_2$**-** groups in α of the C=O, **Hr**, is situated at 2.28 ppm.

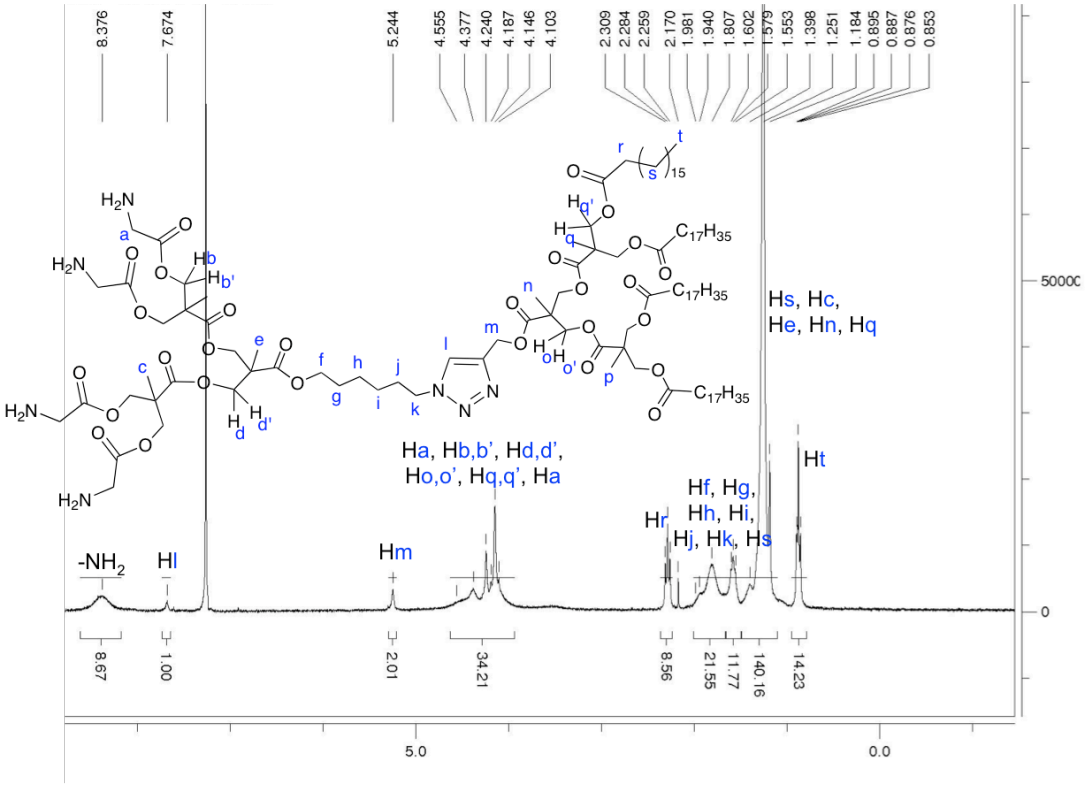

Figure 93: ^{1}H-NMR spectrum of the compound A. 300 MHz, $CDCl_3$, shift in ppm.

Synthesis of C and D

The product **C** was obtained in 3 principal steps: synthesis of *bis*-MPA anhydride (**C1-C2**), reaction with Pluronic® (**C3-C4**) and, finally, functionalization by glycine (**C5-C**)(Figure 94).

The first step consists in protecting the *bis*-MPA hydroxyl groups to form the benzylidene-protected derivative (**C1**, 73%) followed by the corresponding anhydride (**C2**, 98%) as first described by Fréchet and co-worker in 2001.[178] Then, the reaction between the commercial F127 Pluronic® and *bis*-MPA anhydride in presence of DMAP in dichloromethane (**C3**, 84%) followed by the deprotection of the hydroxyl groups by palladium hydrogenation gave the *bis*-MPA-functionalized pluronic® (**C4**, 92%). Subsequently, the Steglish esterification with protected glycine in presence of DCC and DMAP in dichloromethane gave **C5** (95%). The amine groups deprotection in acid environment offers the final product **C** in a total yield of 53%. All the products were purified by precipitation except in the case of the product **C5** that was purified by dialysis against methanol (cellulose membrane 1000MW).

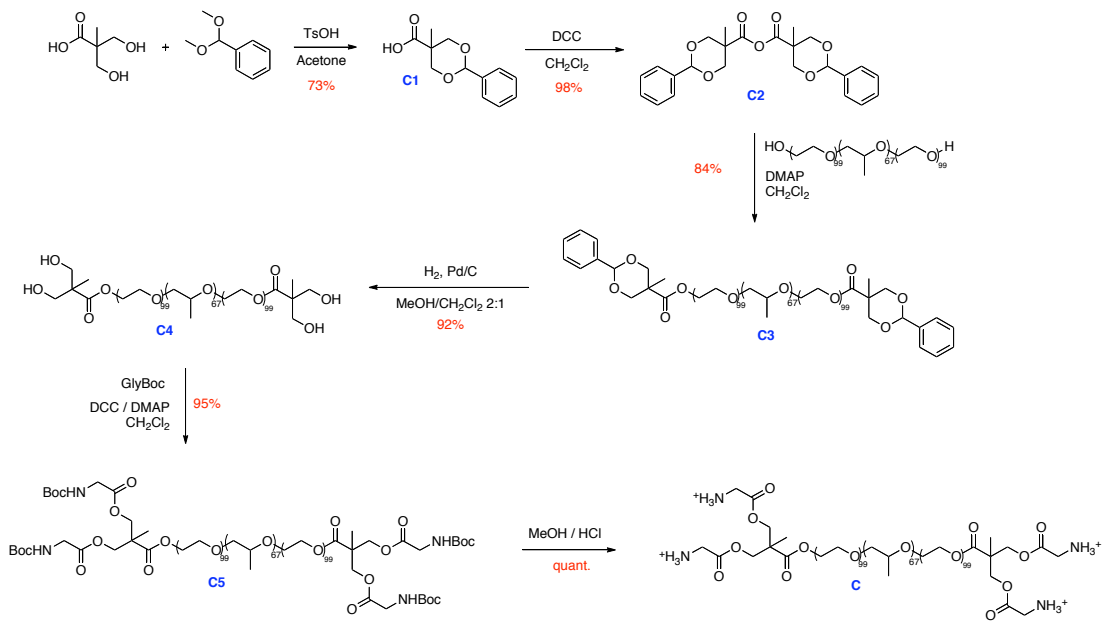

Figure 94: Synthetic scheme for the product C.

[178] H. Ihre, O.L. Padilla De Jesús, J.M.J. Fréchet, *J. Am. Chem. Soc,* **2001**, *123*, 5908-5917.

The final product **C** was obtained as a white powder in a total yield of **52%**.

The structure of the compound **C3** was confirmed in ^{1}H-NMR (Figure 95), ^{13}C-NMR and IR (see experimental part). In ^{1}H-NMR, the union of the protected *bis*-MPA is shown by the shift of **Hg** to upper spectrum (from approx. 3.6 ppm in the commercial pluronic® to 4.32 ppm). The peaks due to the *bis*-MPA monomer structure are situated at 1.01 ppm (s, 6H, **Hh**) and 4.63 ppm (d, 4H, **Hi**). The peak corresponding to the other diastereotopic protons, **Hi'**, appears with the peaks due to the protons of the pluronic® structure: **Hc**, **Hd**, **He**, **Hf**, **Hb**; between 3.35 ppm and 3.79 ppm. The peaks corresponding to the protons of the benzyldene protecting groups can be observed at 5.14 ppm (s, C**H**, 2H, **Hj**), and at 7.28 ppm (m, and 7.39 ppm in the case of the aromatic protons **Hk** **Hl**, **Hm**.

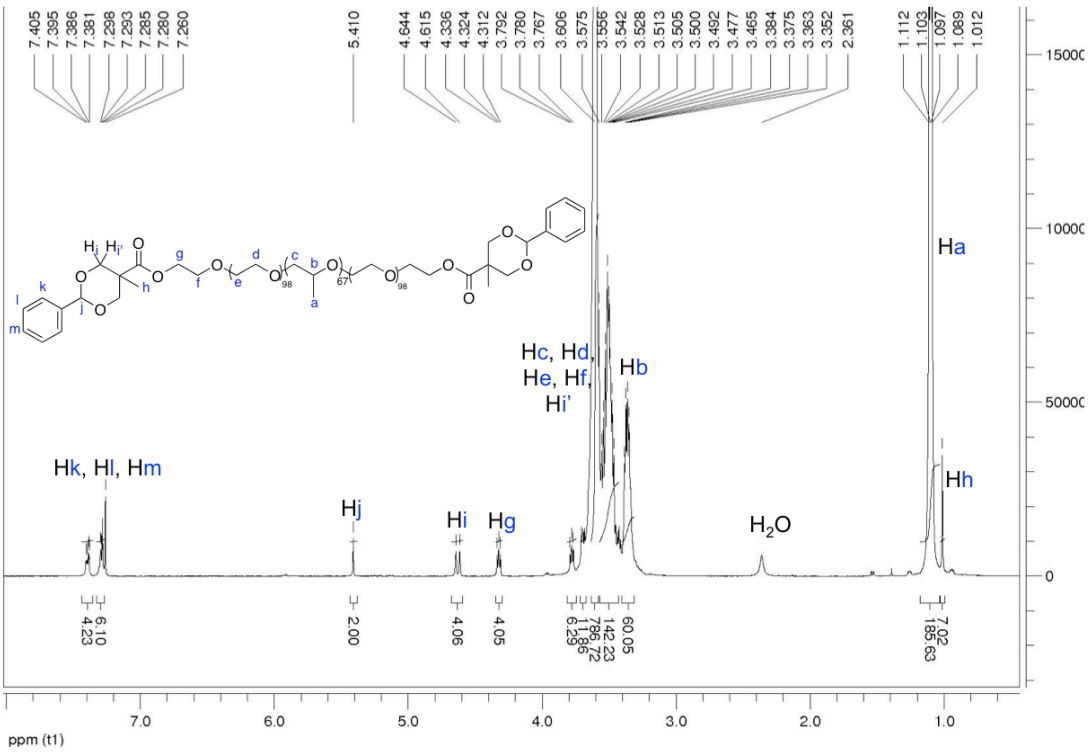

Figure 95: ^{1}H-NMR spectrum of compound C3. 400 MHz, $CDCl_3$ (solvent residual peak at 7.26 ppm), shift in ppm.

The functionalization of the *bis*-MPA modified pluronic **C4** by the protected glycine (**C5**) was shown by the appearance in ^{1}H-NMR of the peak corresponding to the –OCO-C**H$_2$**-NHBoc at 3.81 ppm (d, *J* = 5.6Hz, 8H) and the peak due to the -C**H$_3$**(Boc) at 1.39 ppm (s, 36H). The deprotection of the amines was confirmed by

the absence of the -C**H**$_3$(Boc) peak in ^{1}H-NMR and in IR by the band at 2969 cm^{-1} corresponding to the NH_2 (disappearance of the band at 3328 cm^{-1} corresponding to the **N-H-**Boc).

The compound **D** was obtained by CuAAC between an aminated dendron of third generation, **[G3-*bis*MPA]**, and the pluronic® polymer previously functionalized by an alkyne (see Chapter 1). The structure was confirmed in ^{1}H-NMR, ^{13}C-NMR, and IR analysis.

Encapsulation of antimalarial drugs

Antimalarial drugs

Two commercial hydrophilic antimalarial drugs were encapsulated with the synthetized products **A**, **B**, **C**, **D**: chloroquine and primaquine.

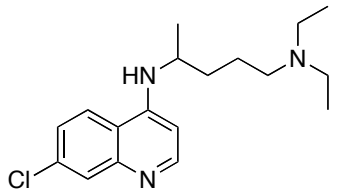

Figure 96: Chloroquine molecule (CQ).

Chloroquine (**CQ**) (Figure 96) is a 4-aminoquinoline drug used in the treatment of malaria. It has several pharmacokinetic and pharmacological advantages over all the other antimalarial drugs despite the CQ-resistance developed by *Plasmodium* strains being substituted by Artemisinin-combinations therapies as a first line of malaria treatment recommended by WHO.[1] The mode of action of CQ is based on its accumulation in the food vacuole of the parasites (lysosomotropic character). The main advantages of CQ therapy are the fast action in blood parasite stages, low toxicity, good bioavailability from oral dosage form, water solubility, high volume of distribution in the body and low cost.

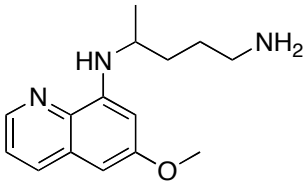

Figure 97: Primaquine molecule (PQ).

Primaquine (**PQ**) (Figure 97) is a member of 8-aminoquinoline drugs used as the essential co-drug with chloroquine in treating all cases of malaria. PQ is the only available drug for preventing relapse of malaria caused by hypnozoites of *P.*

vivax and *P. ovale* (providing radical cure of malaria, in combination with a blood schizontocide). Primaquine is not used in the prevention of malaria, only in the treatment. It has significant activity against *P.vivax* blood stages and some against *P.falciparum*. Primaquine has gametocytocidal activity against all plasmodia. However, its toxicity is a problem; in patients with glucose-6-phosphate dehydrogenase deficiency PQ generally produces hemolysis, which may be severe.

Encapsulation of the drugs inside the nano-carriers

Various methods are used for the encapsulation of hydrophilic and hydrophobic molecules: oil/water emulsion, solvent displacement and interaction deposition, emulsion/solvent diffusion, salting out, etc…[179]

We chose to use the oil/water emulsion method that is based on the emulsification of organic phase (organic volatile solvent + polymers) and aqueous phase (H_2O + drug, in our case) (Figure 98). The first step requires the emulsification of the polymer solution into an aqueous phase and, during the second step, the organic volatile solvent is evaporated inducing the formation of nano and/or microstructures.

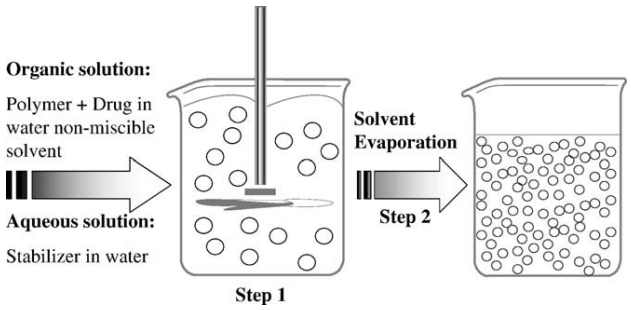

Figure 98: Shematic illustration of the oil/water emulsion method. Adapted from C. Pinto Reis et al.[179.a]

Chloroquine and Primaquine were solubilized in deionized (miliQ) water at the accurate concentrations. The polymer was added in dichloromethane (a solution at 1 mg/mL was previously prepared) and the total volume of water was

[179] a) C. Pinto Reis, R.J. Neufled, A.J. Ribeiro, F. Veiga, *NBM,* **2006***, 2*, 8-21 ; b) S. Vrignaud, J.-P. Benoit, P. Saulnier, *Biomaterials,* **2011***, 32*, 8593-8904.

adjusted. After one hour of stirring and the complete evaporation of dichloromethane, the sample was dialyzed against deionized (miliQ) water to eliminate the free drug and maintain only the nano-objects formed. All the samples were kept at 4°C or -20°C until further analysis to avoid their degradation.

The encapsulation was realized in two different **ratios drug/polymer**:

- a) 5:1 molar ratio (D/P mol/mol)
- b) 1:1 weight ratio (D/P w/w)

The first assay was carried out with the ratio 5:1 D/P mol/mol in order to work with an excess of drug compare to the polymer and to see how many equivalents of drug were able to be encapsulated by the complexes. For example, in Table 2, we can see that 1.10 mg of **CQ** is necessary to reach the 5:1 D/P mol/mol ratio when using 1 mg of the compound **A**. The molecular weight of the dendritic compounds being higher than the molecular weight of the drug molecules (approx. 10 times for A and B and more than 40 times for C and D), we can expect to encapsulate more than one equivalent of drug per polymer, especially in the case of the compounds C and D.

After encapsulation, the excess of drug was eliminated by dialysis against deionized (miliQ) water (cellulose membrane MW 2000) and the amount of drug in the waters of dialysis was quantified by measuring the absorbance at the maximum of absorbance of the drugs in UV-visible spectrometry: A_{max}CQ at 345 nm, A_{max}PQ at 340 nm in water. The amount of drug encapsulated was deduced from the amount of free drug (amount of drug encapsulated = amount of drug loaded – amount of drug in the dialysis waters).

In the Table 13, the results of the encapsulation using the ratio **a**, 5:1 D/P mol/mol, are shown.

Polymer			*CQ added*		CQ encapsulated			
P	**mg[a]**	**µmol[b]**	***mg*[c]**	***µmol*[d]**	**µmol/mgP[e]**	**mg CQ/mgP[f]**	**mol CQ/molP[g]**	**EE[f]**
A	1	0.428	*1.10*	*2.14*	1.73	0.89	4.0	81%
B	1	0.315	*0.81*	*1.57*	1.51	0.78	4.8	96%
C	1	0.072	*0.19*	*0.36*	0.29	0.15	4.0	81%
D	1	0.061	*0.16*	*0.31*	0.32	0.16	5.0	100%

Polymer			*PQ added*		PQ encapsulated			
P	**mg[a]**	**µmol[b]**	***mg*[c]**	***µmol*[d]**	**µmol/mgP[e]**	**mg PQ/mgP[f]**	**mol PQ/molP[g]**	**EE[f]**
A	1	0.428	*0.97*	*2.14*	1.01	0.46	2.4	47%
B	1	0.315	*0.72*	*1.57*	0.95	0.43	3.0	60%
C	1	0.072	*0.16*	*0.36*	0.34	0.16	4.7	98%
D	1	0.061	*0.14*	*0.31*	0.28	0.13	4.6	92%

Table 13: Amount of drug encapsulated using the ratio 5:1 mol of drug/mol of polymer. All the quantites are expressed for 1mg of polymer in 1mL of water.[a]quantity of polymer in mg; [b]quantity of polymer in mol; [c]quantity of drug added in mg; [d]quantitity of drug added in mol; [e]ratio of drug encapsulated in mol per mg of polymer; [f]ratio of drug encapsulated in mg per mg of polymer ; [g]ratio of drug encapsulated in mol per mol of polymer; [h]encapsulation efficiency.

The encapsulation efficiency (EE = 100 x mol of drug added/mol of drug loaded) reached a 100 % in the case of **D(CQ)$_{5:1}$** and a 96 % in the case of **B(CQ)$_{5:1}$**. These high values of EE suggest the possibility of encapsulating a larger quantity of drug inside the nano-structures.

In the case of **CQ**, the lowest values of encapsulation (4 equivalents of drug) were obtained with the compounds **A** and **C.** 4.8 equivalents of CQ were encapsulated by the compound **B,** and the highest value of 5 equivalents of drug per dendritic derivative was obtained with the compound **D**. In the case of **PQ**, the lowest value of encapsulation (2.4 equivalents) was obtained with the compound **A**. With the compound **B** 3 equivalent of drug were encapsulated, and the highest values of encapsulation, 4.6 and 4.7 equivalents of PQ, were obtained with the compounds **C** and **D** respectively.

As it can be seen, after these previous studies, in that in some cases almost the full quantity of drug was loaded inside the nano-objects (see Table 13, compounds B and D in the case of CQ and compounds C and D in the case of PQ), we decided to work with a ratio drug/polymer of 1:1 in weight in order to rich the maximum of drug loading capacity (see Table 14). In the case of the compound A as using a molar ratio of 5:1 (1.10 mg CQ and 0.97 mg PQ) resulted similar than using a ratio of 1:1 in weight, the experiment was not repeated. The results obtained by measuring the absorbance of the dialysis waters are summarized in the Table 14.

Polymer			*CQ added*		CQ encapsulated			
P	**mg[a]**	**µmol[b]**	***mg*[c]**	***µmol*[d]**	**µmol/mgP[e]**	**mg CQ/mgP[f]**	**mol CQ/molP[g]**	**EE[f]**
B	1	0.315	*1*	*1.94*	1.94	1.00	6.2	100%
C	1	0.072	*1*	*1.94*	1.07	0.55	14.9	55%
D	1	0.061	*1*	*1.94*	1.30	0.67	21.2	67%

Polymer			*PQ added*		PQ encapsulated			
P	**mg[a]**	**µmol[b]**	***mg*[c]**	***µmol*[d]**	**µmol/mgP[e]**	**mg PQ/mgP[f]**	**mol PQ/molP[g]**	**EE[f]**
B	1	0.315	1	2.20	1.31	0.60	4.2	60%
C	1	0.072	1	2.20	1.94	0.88	27.0	88%
D	1	0.061	1	2.20	1.29	0.59	21.1	59%

Table 14: Amount of drug encapsulated using the ratio 1:1 w/w. All the quantites are expressed for 1mg of polymer in 1mL of water.[a]quantity of polymer in mg; [b]quantity of polymer in mol; [c]quantity of drug added in mg; [d]quantitity of drug added in mol; [e]ratio of drug encapsulated in mol per mg of polymer; [f]ratio of drug encapsulated in mg per mg of polymer ; [g]ratio of drug encapsulated in mol per mol of polymer; [h]encapsulation efficiency.

For all the compounds, the quantity of drug encapsulated using the ratio 1:1 w/w was superior. In the case of the compound **B**, 1.3 equivalent more of CQ and 1.2 equivalent more of PQ were encapsulated. For the compound **C**, 3.7 times more of CQ and 5.7 times more of PQ were encapsulated. Finally, in the case of the compound **D**, the quantity of drug encapsulated was increased from 4.2 times more equivalents of CQ encapsulated, and 4.6 times for PQ.

The CQ encapsulation efficiency reached 100% with the compound B meaning that probably more drug could be encapsulated while with the other compounds the maximum drug loading seem to have been reached.

These encapsulation studies have shown that all the compounds were able to form macromolecular assemblies that encapsulate a certain amount of drug depending of:

- the amount of drug added,
- the molecule of drug (CQ or PQ),
- the molecule of polymer used (A, B, C or D).

Characterization by SEM

SEM analyses were performed using traditional SEM with gold-coated samples due to the rapidity of the method. As the self-aggregation depends on the concentration, the nature and the condition of formation, techniques like SEM, which work in vacuum conditions, may affect the architecture of the aggregates. As the solvent is completely removed, the variation of the concentration may affect the shape of the nano-objects.

Structures formed by the nano-objects without drug

To study the ability of our amphiphilic compound to self-assemble in water without guest molecules, we use the same oil/water emulsion technique to be able to compare the structures formed.

When the polymers were analyzed without drug, we could observe the formation of objects formed by flexible layers rolled over themselves (Figure 99). The size of the structures is polydisperse. In the case of the compound **A** we can find nano-objects from approx. 500 nm to more than 2 µm. The structures formed by the products **B**, **C** and **D** are less variable, and the sizes are included between approx. 400 nm for the compound **B** and approx. 600 nm for the compounds **C** and **D** (Table 15).

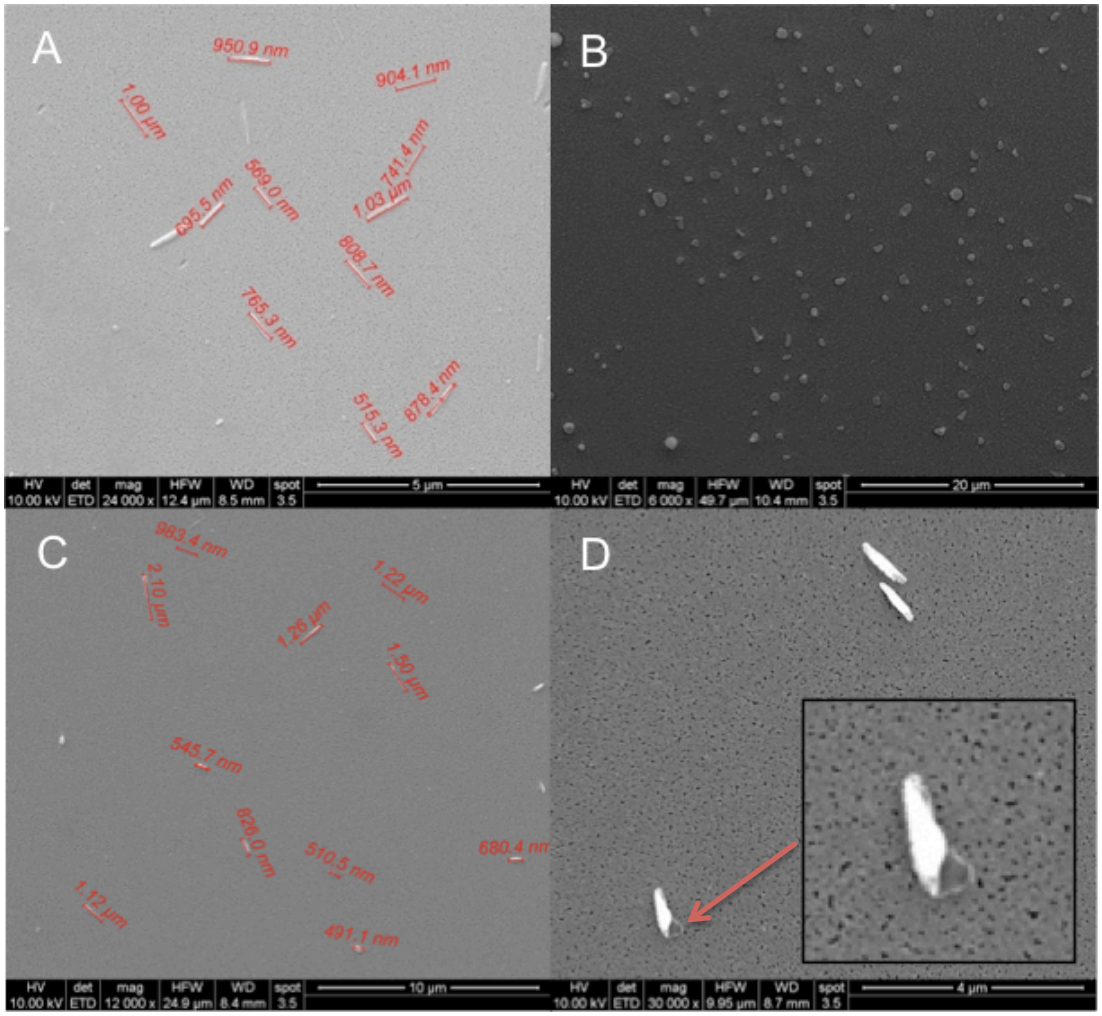

Figure 99: SEM pictures of the structures formed by compound A (A), compound B (B), compound C (C), and compound D (D) in water.

Compound	A	B	C	D
X (nm)	**1221** ± 681	**427** ± 127	**591** ± 219	**601** ± 222
Shape	Layers	Spherical	Layers	Layers

Table 15: Size and shape of structures formed by the compounds A, B, C and D in water. X represents the average size in nm followed by the standard deviation.

The data presented in Table 15 is about the size of the nano-objects formed are extracted from the SEM images. X (nm) is the average size of the structures calculated from more than 10 photos collected (more than 50 structures). SD is the standard deviation from the average number; it gives us an idea of the disparity of the sample. As an example, we can see that for the compound **A**, the size of the

structures is very dispersed (SD=681) and, for the compound **B**, the size of the structures is more homogeneous (SD=127).

Structures formed by the encapsulation of CQ at 5:1 mol D/mol P ratio

The nano-objects formed after encapsulation of **CQ** presented ovoid shapes (Figure 100: SEM pictures of the structures formed by compound A $(CQ)_{5:1}$ (A), compound B $(CQ)_{5:1}$ (B), compound C $(CQ)_{5:1}$ (C), and compound D$(CQ)_{5:1}$ (D), in water after the encapsulation of Chloroquine). The average aspect ratio (AR) was calculated for the different nano-objects following the formula AR=length/width, the closer to one the AR is, the more spherical is the structure. The structures are considered spherical when $1<AR\leq1.2$, ovoid when $1.2<AR\leq3$, elongated when $AR>3$.

In the Figure 20, a clear change in the shape of the structures is observed when the drug is encapsulated. This modification shows that the drug molecules act like a template for the formation of objects approaching a spherical shape. The size of the structures varies from an average of 172 nm for the compounds **C** to 500 nm for the compound **B** (Table 16).

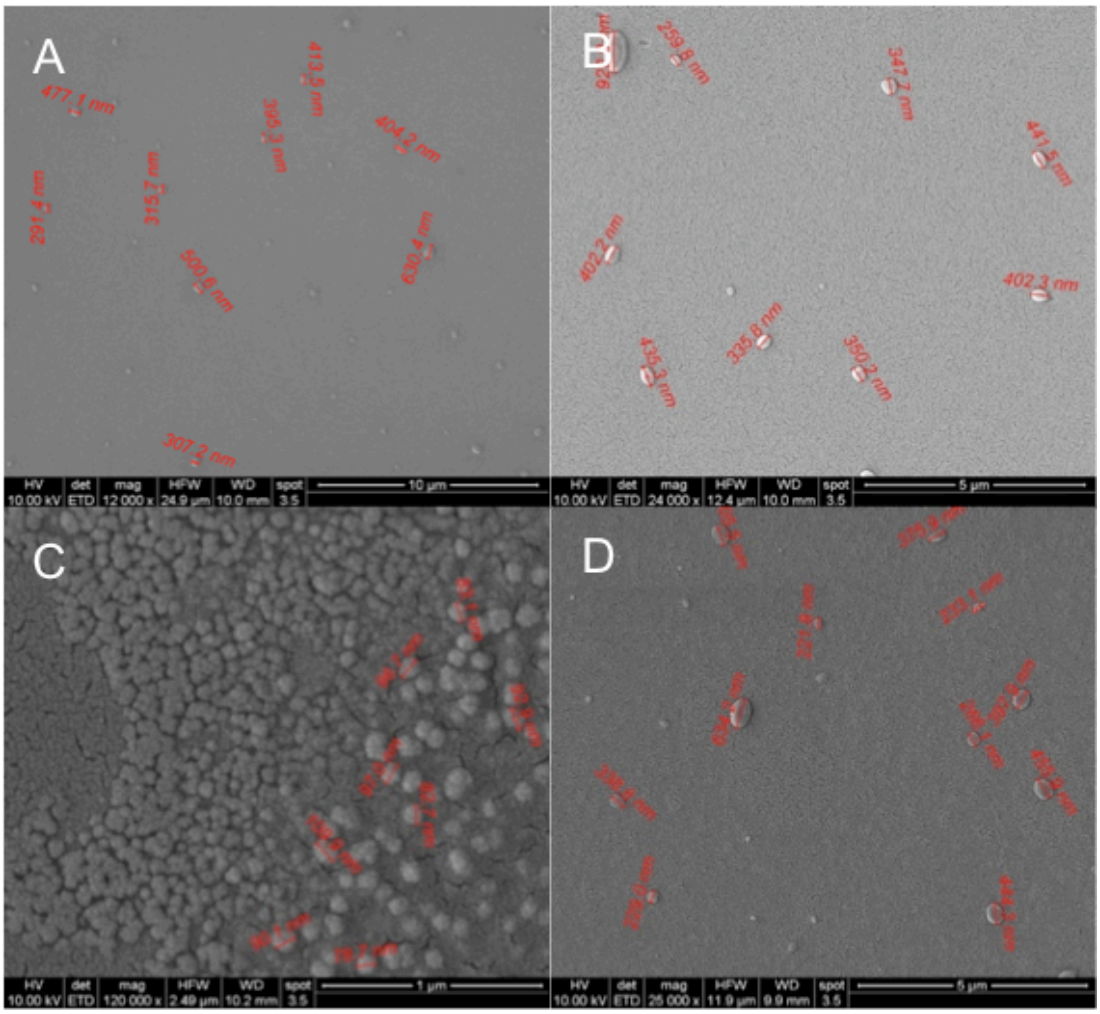

Figure 100: SEM pictures of the structures formed by compound A $(CQ)_{5:1}$ (A), compound B $(CQ)_{5:1}$ (B), compound C $(CQ)_{5:1}$ (C), and compound D$(CQ)_{5:1}$ (D), in water after the encapsulation of Chloroquine.

Compound	A $(CQ)_{5:1}$	B $(CQ)_{5:1}$	C $(CQ)_{5:1}$	D $(CQ)_{5:1}$
X (nm)	**415** ± 109	**500** ± 226	**172** ± 87	**360** ± 131
Shape	spherical	spherical	ovoid	ovoid
AR	**1.13** ± 0.16	**1.17** ± 0.11	**1.46** ± 0.25	**1.30 ±** 0.15

Table 16: Size and shape of structures formed by the compounds A$(CQ)_{5:1}$, B$(CQ)_{5:1}$, C$(CQ)_{5:1}$ and D$(CQ)_{5:1}$ in water. X represents the average size in nm followed by the standard deviation. AR represents the ratio of the major axis size to the minor axis size calculated from more than 20 structures.

Structures formed by the encapsulation of PQ at 5:1 mol D/mol P ratio

When the drug encapsulated is Primaquine, the structures formed are different in terms of shape and size (Figure 101, Table 17). The compound **A(PQ)$_{5:1}$** appears to form ovoid structures of size between 100 nm and 500 nm. The compound **B(PQ)$_{5:1}$** is organized in elongated or rod-like structures of approx. 600 nm in length. The structures formed by **C(PQ)$_{5:1}$** and **D(PQ)$_{5:1}$** are ovoids with lower sizes (between 200 nm and 300 nm).

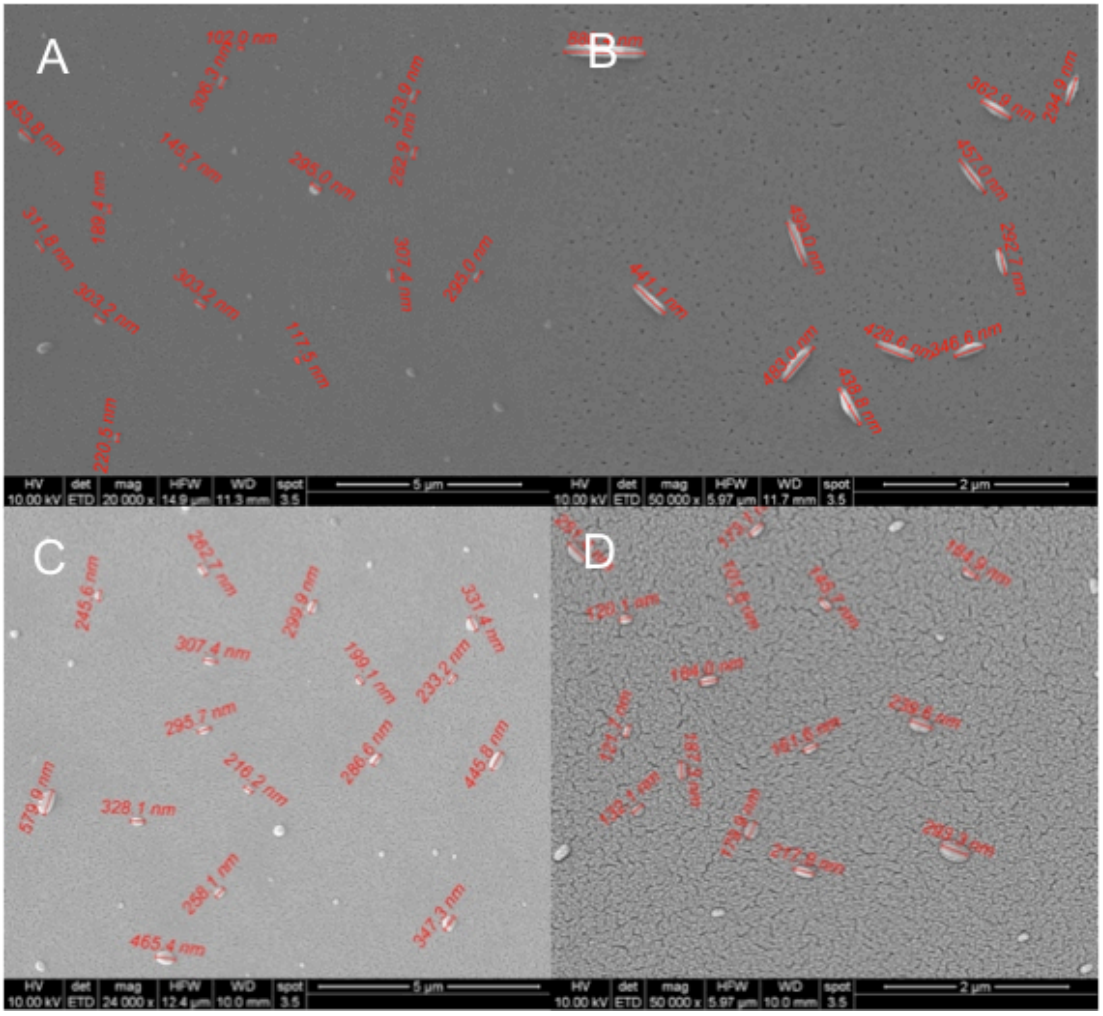

Figure 101: SEM pictures of the structures formed by compound A (PQ)$_{5:1}$ (A), compound B (PQ)$_{5:1}$ (B), compound C(PQ)$_{5:1}$ (C), and compound D(PQ)$_{5:1}$ (D) in water after the encapsulation of Primaquine.

Compound	A $(PQ)_{5:1}$	B $(PQ)_{5:1}$	C $(PQ)_{5:1}$	D $(PQ)_{5:1}$
X (nm)	**386** ± 257	**641** ± 277	**290** ± 78	**178** ± 53
Shape	ovoid	elongated	ovoid	ovoid
AR	**1.71** ± 0.28	**4.66** ± 1.84	**1.23** ± 0.17	**1.73** ± 0.15

Table 17: Size and shape of structures formed by the compounds A$(PQ)_{5:1}$, B$(PQ)_{5:1}$, C$(PQ)_{5:1}$ and D$(PQ)_{5:1}$ in water. X represents the average size in nm followed by the standard deviation. AR represents the ratio of the major axis size to the minor axis size calculated from more than 20 structures.

Structures formed by the encapsulation of CQ at 1:1 w/w ratio

The structures formed after the encapsulation of chloroquine in a ratio 1:1 weight/weight were found to be more spherical than the one formed by the encapsulation at ratio 5:1 mol D/mol P. In the Figure 102, a uniformity of the sizes of the assemblies formed by the different compounds is observed (from approx. 100 nm and 200 nm).

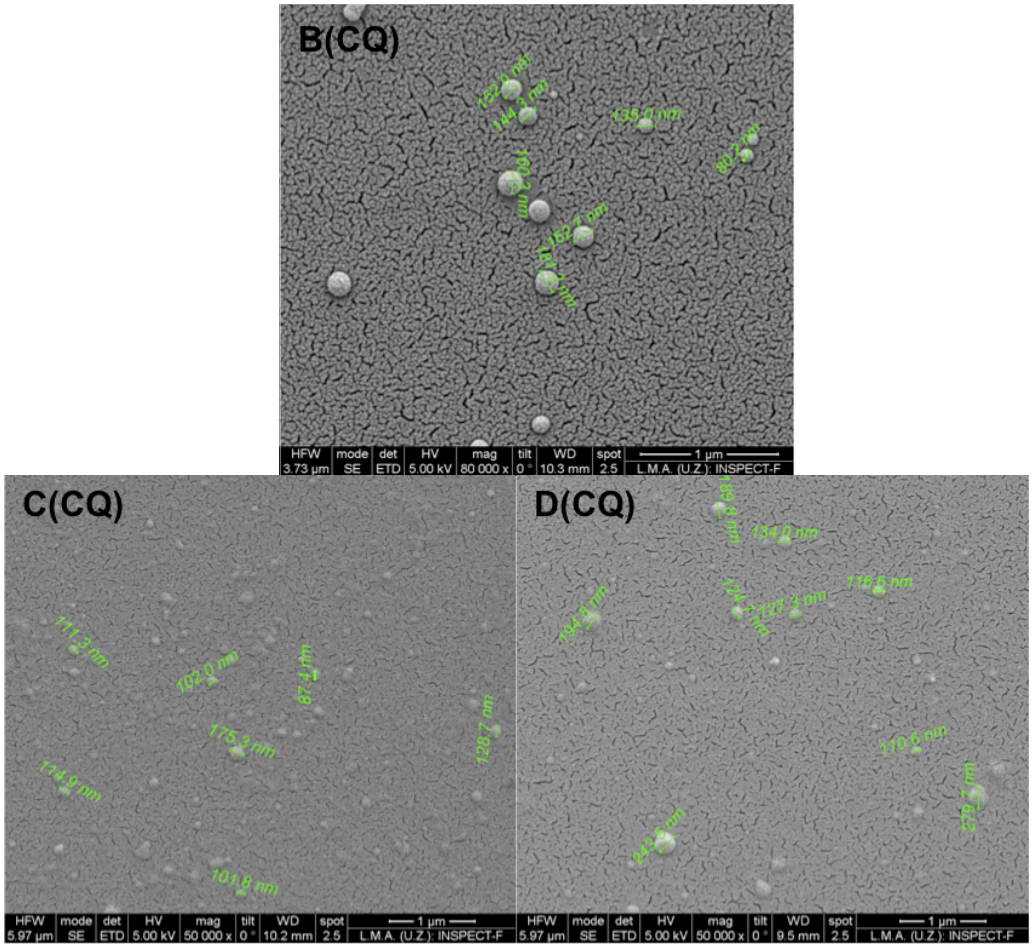

Figure 102: SEM pictures of the structures formed by the compound B $(CQ)_{1:1}$, compound C $(CQ)_{1:1}$, and compound D $(CQ)_{1:1}$ in water after the encapsulation of Chloroquine 1:1 w/w.

Compound	B $(CQ)_{1:1}$	C $(CQ)_{1:1}$	D $(CQ)_{1:1}$
X (nm)	**138** ± 38	**116** ± 23	**156** ± 58
Shape	Spherical	Spherical	Spherical
AR	**1.05** ± 0.04	**1.11** ± 0.09	**1.07** ± 0.06

Table 18: Size and shape of structures formed by the compounds $B(CQ)_{1:1}$, $C(CQ)_{1:1}$ and $D(CQ)_{1:1}$ in water formed at ratio 1:1 w/w. X represents the average size in nm followed by the standard deviation. AR represents the ratio of the major axis size to the minor axis size calculated from more than 20 structures.

The quantity of drug loaded inside the nano-objects was found to have a great influence on the shape of the particle. When the maximum capacity of loading was reached, as here, we could observe a clear tendency to form nano-

objects with a spherical structure. In all the cases, the aspect ratio was found to be very close to 1 (perfect sphere) (Table 18).

Structures formed by the encapsulation of PQ at 1:1 w/w ratio

In the case of primaquine (Figure 103), very small structures were observed for the compounds **B**, **C** and **D**. The resolution of the microscope did not permit to obtain clear images and a good measure of their size. In the case of the **C** and **D**, we could appreciate the tendency of the structures to aggregate forming bigger assemblies. For this reason, the *in vitro* study of the nano-objects will be realized with the structures formed after encapsulation using the ratio 5:1 mol D/mol P. The nano-carriers obtained using the previous encapsulation ratio are more stable and do not form aggregates, their structure and size are also better defined.

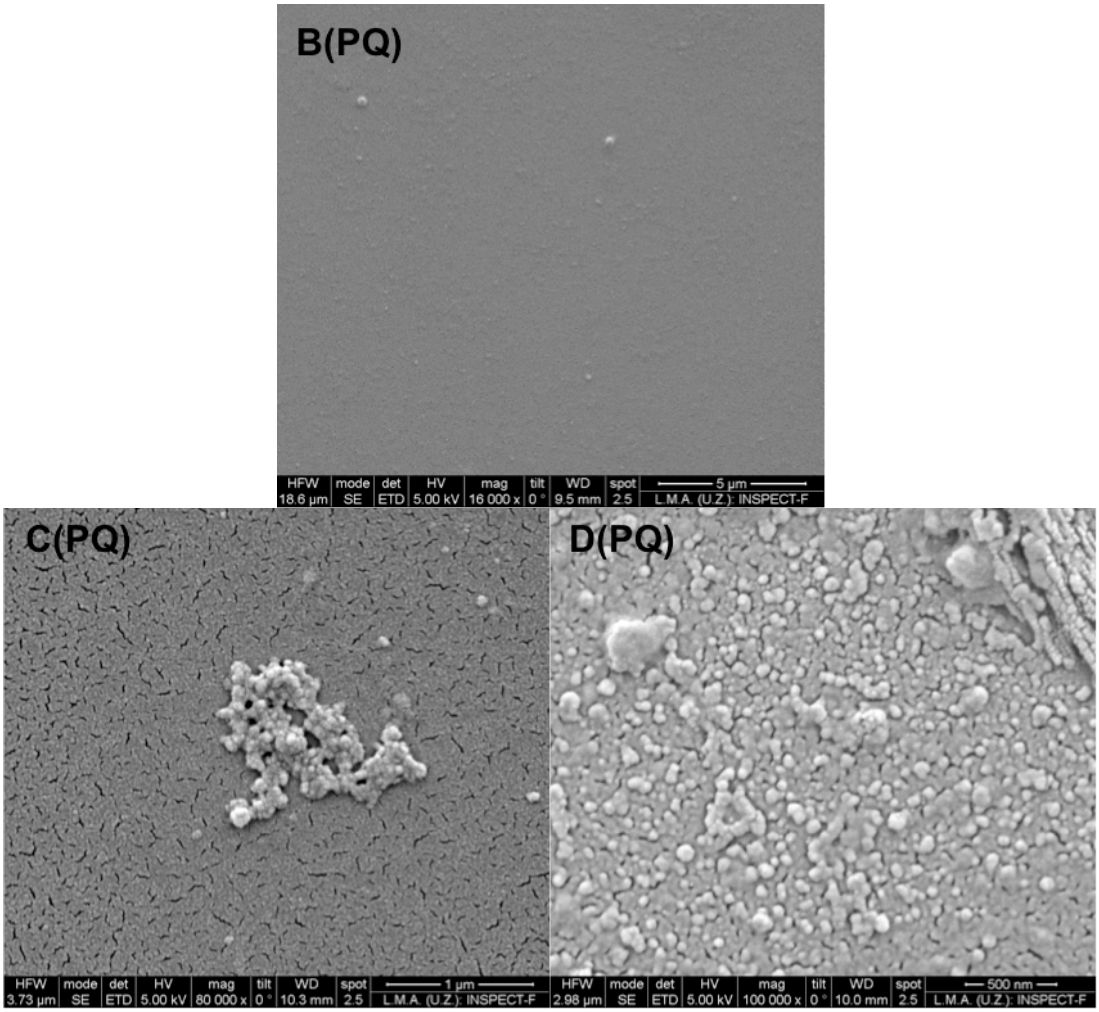

Figure 103: SEM pictures of the structures formed by the compound B $(PQ)_{1:1}$, compound C $(PQ)_{1:1}$, and compound D $(PQ)_{1:1}$ in water after the encapsulation of Primaquine.

Evaluation the nano-objects efficiency as antimalarial drugs vehicles

The growth inhibition assays were carried out on parasites at ring stage. The efficiency of our complexes was compared to the one of free chloroquine and primaquine at the same concentrations of drug. Because of the results of the encapsulation described previously (the nano-objects formed by **C(PQ)** and **D(PQ)** at the ratio 1:1 w/w were not well defined), the growth inhibition assays were realized with the nano-object formed at the encapsulation ratio 5:1 mol of drug/mol of polymer. The study was realized at 5 concentrations (Table 19), C3 correspond to the IC_{50} concentration for late stage parasites.

	Chloroquine		**Primaquine**	
C1	82.4 ng/mL	160 nM	14.1 µg/mL	31 µM
C2	41.2 ng/mL	80 nM	7.04 µg/mL	15.5 µM
C3	**20.6 ng/mL**	**40 nM**	**3.52 µg/mL**	**7.7 µM**
C4	10.3 ng/mL	20 nM	1.76 µg/mL	3.9 µM
C5	5.15 ng/mL	10 nM	0.88 µg/mL	1.9 µM

Table 19: Concentrations of drugs used for the growth inhibition assay.

The concentration of the nano-object was adjusted so that the concentration of drug was the same than the one of the control (Table 20).

		A(drug)	**B(drug)**	**C(drug)**	**D(drug)**
CQ	**C1=82,4 ng/mL**	175 ng/mL	188 ng/mL	635 ng/mL	587 ng/mL
PQ	**C1=14.1 µg/mL**	44.8 µg/mL	46.7 µg/mL	105 µg/mL	123 µg/mL

Table 20: Total concentration of nano-objects formed by A, B, C or D encapsulating CQ or PQ to obtain the desire concentration C1 of pure drugs.

Parasitemia of *P. falciparum* 3D7 cultures was adjusted to 1.5% with more than 90% of parasites at ring stage after sorbitol synchronization. *Plasmodium*

culture was incubated in the presence of each polymer solution for 48 h at 37°C under a gas mixture of 92% N_2, 5% CO_2, and 3% O_2. Parasitemia was determined by microscopic counting of blood smears, or by fluorescence-assisted cell sorting (FACS) and growth inhibition was calculated comparing parasitemias of polymer-treated and control samples. FACS was realized over 50000 cells at 1000 cells per second flow. Each concentration was repeated three times and the standard deviation was calculated by the difference of results between the three measurements. In the Figure 104 is represented the typical dot plot results obtained by flow cytometry. In the graph (b), the two populations of cells that appear correspond to the non-contaminated RBCs (down) and to the parasite contaminated RBCs (up).

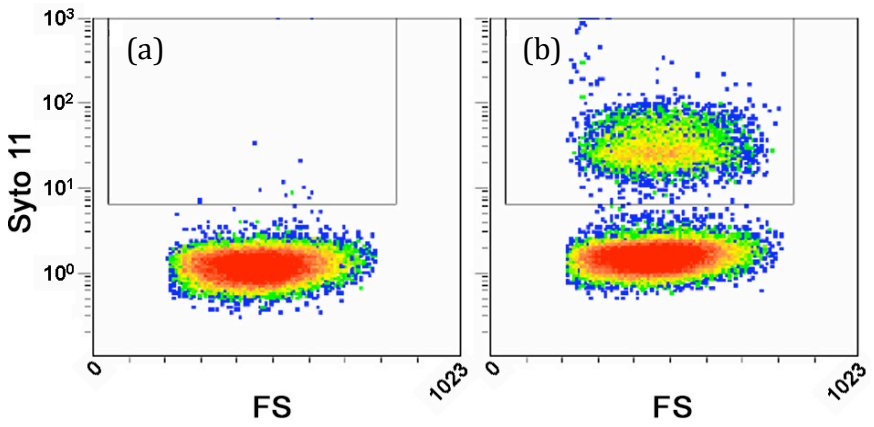

Figure 104: Typical cytometer flow results. In the graph (b), the upper population (inside the rectangle) is the population of RBCs infected by parasites.

Cytotoxicity assays

The cytotoxicity of the nano-objects with encapsulated drugs was evaluated on HUVEC endothelial cells to discard any unspecific effect. The experiment was realized at the same concentrations used for the growth inhibition assays (C1 to C5). No cytotoxicity was observed in the cells after 48h of incubation with the nano-objects, even at the highest concentrations (Figure 105 and Figure 106).

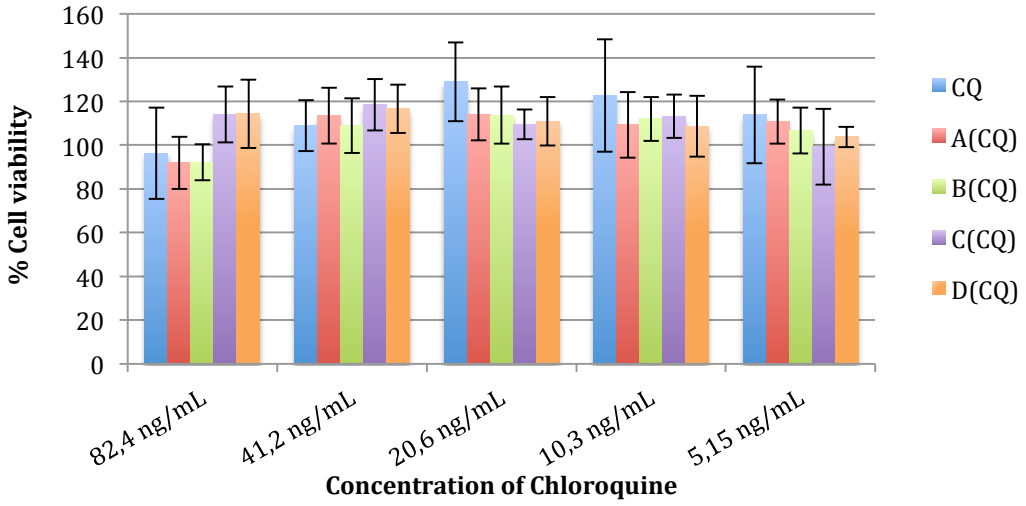

Figure 105: Cell viability of HUVEC cells exposed to CQ and nano-objects containing CQ.

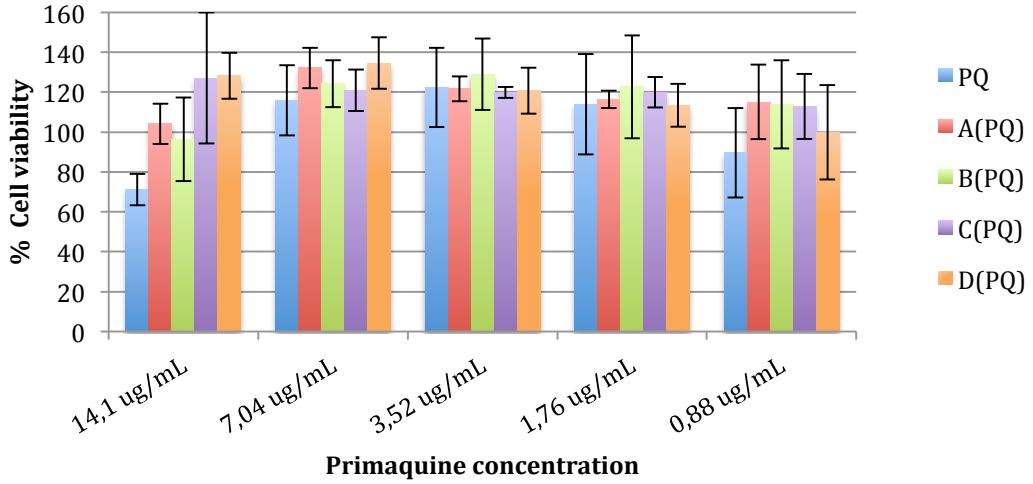

Figure 106: Cell viability of HUVEC cells exposed to PQ and nano-objects containing PQ.

Plasmodium growth inhibition results

In the Figure 107, the data of the first growth inhibition assay with the nano-carriers of chloroquine (Table 21) are graphically represented.

	Free CQ	A(CQ) $_{5:1}$	B(CQ) $_{5:1}$	C(CQ) $_{5:1}$	D(CQ) $_{5:1}$
C1	**90.03 ± 0.84**	91.24 ± 0.62	91.11 ± 0.50	5.34 ± 1.06	**91.38 ± 0.77**
C2	**89.96 ± 0.37**	91.99 ± 1.17	90.06 ± 0.35	5.00 ± 1.73	**90.70 ± 0.73**
C3	**89.96 ± 0.93**	89.79 ± 0.51	70.62 ± 4.37	5.78 ± 1.80	**90.67 ± 0.46**
C4	**86.00 ± 0.41**	87.39 ± 0.21	8.65 ± 1.13	4.97 ± 1.13	**90.87 ± 0.79**
C5	**8.18 ± 1.80**	9.91 ± 2.15	4.26 ± 1.34	4.87 ± 1.32	**90.84 ± 0.86**

Table 21: Results of the growth inhibition assay with chloroquine (CQ) and encapsulated chloroquine on ring stage parasites. The data shown represent the mean growth inhibition result and the standard deviation. C1=82.4 ng/mL, C2=41.2 ng/mL, C3=20.6 ng/mL, C4=10.3 ng/mL, C5=5.15 ng/mL of chloroquine.

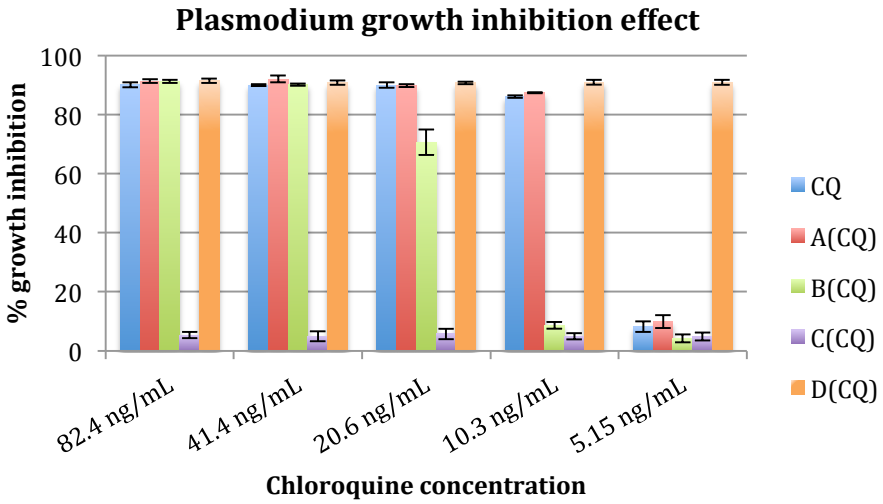

Figure 107: Graphical representation of growth inhibition assay data with CQ and the different nano-objects. 5:1 mol D/mol P ratio obtained during the first assay.

The parasite growth inhibition induced by the compound **A(CQ)$_{5:1}$** was found to be very similar than the one induced by the free drug. From CQ concentrations C1 to C4, an important effect on the parasites was observed, approx. 90% GI, probably due to a quantitative release of the drug by the carrier.

The compound **B(CQ)$_{5:1}$** was as efficient as free **CQ** against the parasites for the highest concentrations C1 and C2, then from C3 its effect started to decrease until being negligible at C4 and C5.

For none of the concentration studied the compound **C(CQ)$_{5:1}$** presented an effect on the parasite, probably due to a poor release of its cargo by the carrier.

Promising results were obtained with the compound **D**. The nano-carriers of **D(CQ)$_{5:1}$** were able to inhibit the growth of the plasmodium more than the free chloroquine. At 10 nmol (C4), the growth inhibition induced by free **CQ** was of 8% whereas with **D(CQ)$_{5:1}$** we obtain a growth inhibition of more than 90%.

For both **D(CQ)$_{5:1}$** and **A(CQ)$_{5:1}$** *in vivo* tests are required in order to study the potentiality of these nano-carriers.

We saw by SEM that the nano-objects formed by the compound **C** and **D** were different in size, the one formed by compound **D** being bigger (between 300-400nm) than the one of compound **C** (approx. 100nm). This could explain the marked difference of activity between the two compounds: the nano-carriers being bigger, more interactions with the RBCs membrane can occur. It is important to consider also that for each case the interaction between the drug and the polymer is unique and explains differences in the release of the cargo by the nanocarriers.

In the Figure 108, the results are illustrated by microscope images of the pRBCs treated with the different polymers and **CQ**. In the part (**f**), we can observe that pRBCs treated with **D(CQ)$_{5:1}$** are almost free of parasites.

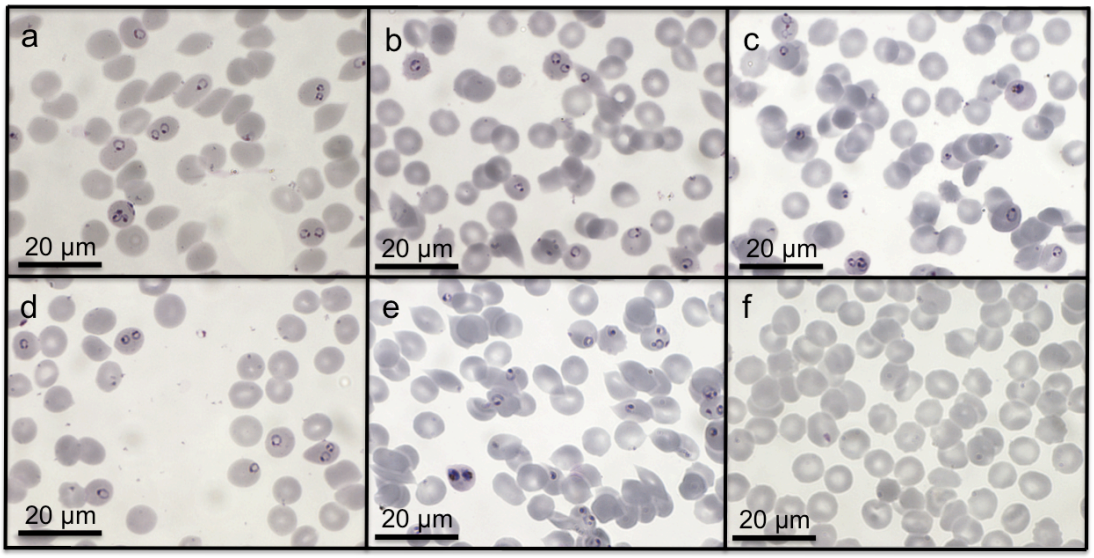

Figure 108: Microscope pictures of stained RBCs infected by plasmodium and treated with chloroquine at 5.15 ng/mL and the four compounds. a: non-treated (control); b: chloroquine; c: $A(CQ)_{5:1}$; d: $B(CQ)_{5:1}$; e: $C(CQ)_{5:1}$; f: $D(CQ)_{5:1}$.

In order to confirm the value of the results obtained, the experiment was repeated at the concentrations C3, C4 and C5 of chloroquine, the average results are presented in the Table 22 show a good correlation between the data obtained in the two experiments.

[CQ] ng/mL	CQ	$A(CQ)_{5:1}$	$B(CQ)_{5:1}$	$C(CQ)_{5:1}$	$D(CQ)_{5:1}$
C3 = 41	**83.4 ± 7.2**	82.4 ± 8.2	70.6 ± 4.4	2.0 ± 3.4	**84.4 ± 8.0**
C4 = 21	**81.5 ± 5.0**	87.4 ± 0.2	3.9 ± 1.6	4.3 ± 4.8	**83.7 ± 8.0**
C5 = 10	**12.6 ± 5.1**	5.9 ± 4.8	2.5 ± 2.2	2.4 ± 2.8	**84.2 ± 7.4**

Table 22: Results of the growth inhibition assay with chloroquine (CQ) and encapsulated chloroquine on ring stage parasites. The data shown represent the mean growth inhibition result (2 experiments) and the standard deviation.

The same experiment was realized with the nano-objects containing **primaquine**. The growth inhibition effect of each compound was calculated from the parasitemia data and is represented in the Figure 29 (data in Table 23).

[PQ]	Free PQ	A(PQ)	B(PQ)	C(PQ)	D(PQ)
C1	**89.54 ± 0.27**	51.02 ± 6.38	87.06 ± 0.47	**87.63 ± 2.14**	76.03 ± 5.78
C2	**86.13 ± 0.84**	14.84 ± 0.98	82.82 ± 6.1	**87.16 ± 1.74**	22.20 ± 6.49
C3	**71.18 ± 1.73**	7.66 ± 1.63	45.70 ± 3.34	**86.06 ± 0.56**	6.99 ± 2.56
C4	**25.58 ± 2.55**	2.11 ± 1.53	25.68 ± 1.4	**85.99 ± 1.79**	2.94 ± 3.44
C5	**8.73 ± 1.46**	2.31 ± 0.92	9.33 ± 7.22	**83.38 ± 2.98**	1.54 ± 5.15

Table 23: Results obtained when the experiment was repeated with the same nano-objects. The data shown represent the mean growth inhibition results (1 experiment) and the standard deviation. C1=14.1 µg/mL, C2=7.04 µg/mL, C3=3.52 µg/mL, C4=1.76 µg/mL, C5=0.88 µg/mL of primaquine.

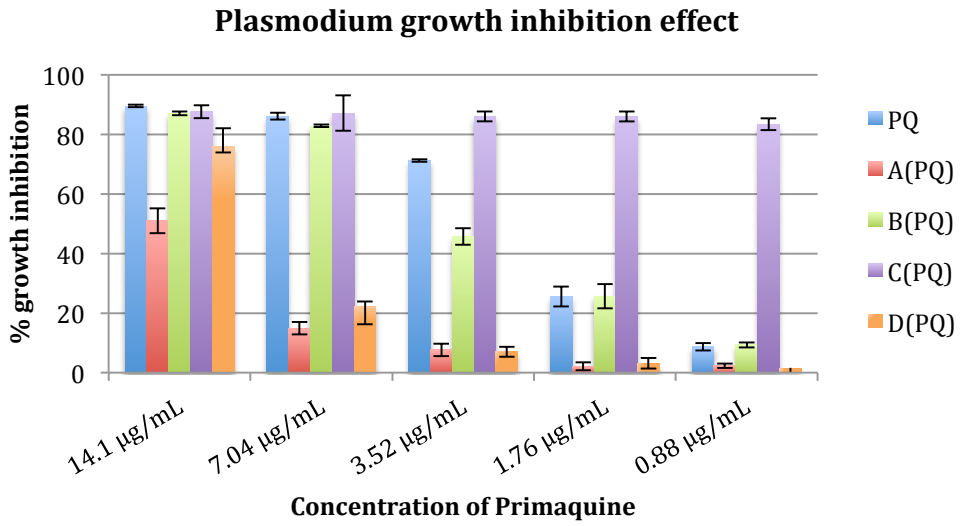

Figure 109: graphical representation of growth inhibition assay results with CQ and the different nano-objects. 5:1 mol D/mol P ratio. 50000 cells, 3 repetitions.

The nano-objects of **A(PQ)$_{5:1}$** induced less growth inhibition of the parasite than free **PQ** from the C1 concentration, and from C2 the effect observed was not significant. The growth inhibition induced by the nano-objects **B(PQ)$_{5:1}$** was found to be similar to the one induced by the free drug. Surprisingly, the nano-objects of **D** were found to be less efficient than free PQ from the first concentration tested (C1), probably because of a difficult release of the drug by the nano-carrier.

In the case of the nano-objects containing primaquine, the most efficient compound was found to be the compound **C(PQ)$_{5:1}$** with a growth inhibition effect higher than the one of the free **PQ** for C3, C4 and C5. The higher difference between the nano-object activity and the drug alone was observed at C5, with a growth inhibition of **83 %** obtained with **C(PQ)**$_{5:1}$ and **9 %** with free **PQ.**

In order to confirm the value of the results obtained, the experiment was repeated and the average data are presented in the Table 24. Also in this case, the results of the Table 24 show a good correlation between the data obtained in the two experiments.

[PQ] µg/mL	PQ	A(PQ)$_{5:1}$	B(PQ)$_{5:1}$	C(PQ)$_{5:1}$	D(PQ)$_{5:1}$
C2 = 15.5	**80.7 ± 5.5**	10.7 ± 4.3	74.3 ± 0.4	**80.3 ± 6.9**	21.0 ± 5.2
C3 = 7.8	**69.1 ± 2.3**	3.9 ± 3.9	45.7 ± 2.8	**79.0 ± 7.1**	8.4 ± 2.3
C4 = 3.9	**26.4 ± 2.6**	1.1 ± 1.3	25.7 ± 4.1	**86.0 ± 0.9**	2.2 ± 1.5
C5 = 1.9	**18.4 ± 9.7**	1.2 ± 1.2	6.6 ± 4.1	**83.4 ± 0.6**	1.5 ± 1.6

Table 24: Results of the growth inhibition assay with primaquine (PQ) and encapsulated primaquine on ring stage parasites. The data shown represent the mean growth inhibition result (2 experiments) and the standard deviation.

The nano-objects formed by pluronic® derivatives C(PQ)$_{5:1}$ and D(CQ)$_{5:1}$ present a higher activity against the parasite in vitro than the free drugs.

The antimalarial effect is directly related with the interactions between the dendritic compound (carrier) and the drug encapsulated (cargo), which affect the size, the shape, and the release of the cargo.

Internalization assays after encapsulation of rhodamine

Nano-objects were formed from the compounds **A**, **B**, **C** and **D** encapsulating **rhodamine** in order to monitor their internalization by fluorescence microscopy.

The structures size and shape of the new nano-object are expected to differ from the ones of **CQ** and **PQ** because of the differences between the molecules encapsulated. The nano-objects were formed following the methodology described previously for the encapsulation of chloroquine and primaquine: the oil/water emulsion method at a ratio 1:1 w/w (1mg of dendritic compound dissolved in dichloromethane was stirred with 1mg of rhodamine, in 1mL of deionized water). The excess of rhodamine was eliminated by dialysis against deionized (miliQ) water (cellulose membrane 1000 MW).

The fluorescence emission of the nano-objects was measured (see in Figure 110) and has shown that the compound **C** ($Emission_{max}$=753) was able to encapsulate the larger quantity of rhodamine, followed by the compound **A** ($Emission_{max}$=597), the compound **D** ($Emission_{max}$=256), and finally the compound **B** ($Emisson_{max}$=30). A light shift of the maximum of fluorescence wavelength is observed when the rhodamine is free ($Emission_{max}$ at 580 nm) than when it is encapsulated inside the nano-objects ($Emission_{max}$ at 577).

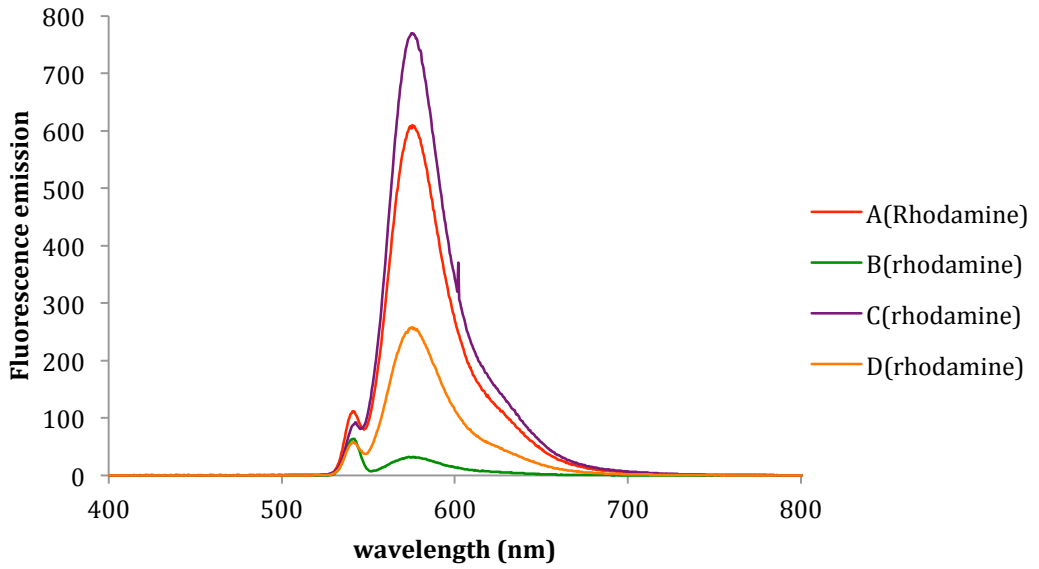

Figure 110: Fluorescence emission of the nano-objects encapsulating rhodamine. Excitation peak at 540 nm.

SEM characterization of the rhodamine-nano-carriers

In all cases, the formation of spherical nano-objects of different sizes has been observed (Figure 111). In the case of the **A(Rho)**, the size of the structures was found to be very polydisperse, with very small objects from approx. 50 nm to bigger ones of approx. 400 nm. The structures formed by **B(Rho)** are more regular, with a diameter between 90 nm and 120 nm. The compounds derived from pluronic® polymer presented smaller assemblies, of approx. 80 nm in the case of **C(Rho)** and of approx. 50 nm in the case of **D(Rho)**.

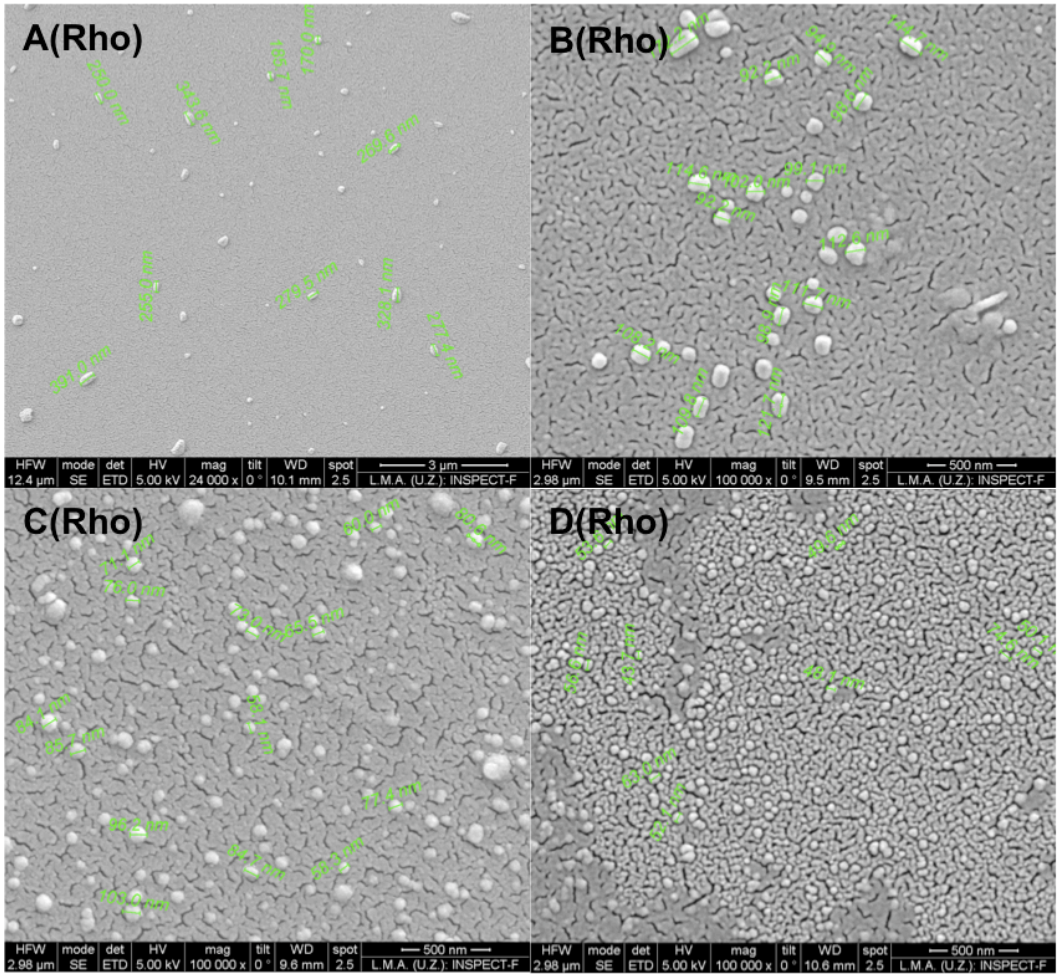

Figure 111: SEM pictures of the nanoobjects formed by rhodamine encapsulated in A, B, C or D (gold coated samples).

As it can be seen in the Table 25, in all cases the aspect ratio was close to one, defining nano-objects with a shape close to spherical. The polydispersity of the samples is reflected by the standard deviation of the average size X(nm), 91 nm in the case of the compound A(Rho) and 7 nm in the case of the compound D(Rho).

Compound	A (Rho)	B (Rho)	C (Rho)	D (Rho)
X (nm)	**188 ± 91**	**94 ± 29**	**70 ± 16**	**50 ± 7**
Shape	Spherical	Spherical	Spherical	Spherical
AR	**1.09 ± 0.11**	**1.17 ± 0.1**	**1.06 ± 0.05**	**1.12 ± 0.09**

Table 25: Size and shape of structures formed by the compounds A(Rho), B(Rho), C(Rho) and D(Rho) in water. X represents the average size in nm followed by the standard deviation. AR represents the ratio of the major axis size to the minor axis size calculated from more than 20 structures.

Internalization of the nano-objects

The internalization of the nano-objects by the RBCs was monitored by fluorescence. In this purpose, the nano-objects encapsulating rhodamine were incubated for 90 minutes with pRBCs. Then the cells were fixed, washed and stained and the results were visualized by confocal microscopy. In blue is represented the parasites nuclei, in red the cell membrane, in purple the hemozoin pigment of the parasite and in white the rhodamine (Figures 112 to Figure 115).

In this assay we expected to find the rhodamine signal in the infected RBCs and not in the healthy RBCs since the presence of the parasite affects the permeability of the membrane. To survive and replicate inside the RBCs, the parasite exports proteins that interact and modify the properties of the host.[180] *Plasmodium falciparum* induces new permeation pathways in *p*RBCs that are involved in the transport of molecules across the erythrocyte membrane.[181] Tarashi and co-workers showed, using a variety of latex beads, that macromolecules up to 50-70 nm in diameter could have a direct access to the intracellular parasites.[182] From these information we can expect that the nano-objects formed by the compound **D** are the most prone to penetrate the cell membrane.

For the internalization experiment, the compounds were incubated 90 minutes with the pRBCs while for the growth inhibition experiment they were incubated 48h with the pRBCs. This might explain why during the GI experiment, the nano-carriers **D(CQ)** and **C(PQ)** could be efficient even having a mean size of respectively 360 nm (AR=1.30) and 290 nm (AR=1.23). Possibly, the nano-carriers interact with the parasites via other pathways, by slow release of the drug. Moreover, the interaction of the nano-carriers with the RBCs might be related to a size/aspect ratio compromise as demonstrated by Mitragotri and colleagues.[183]

---

[180] B.M. Cooke, K. Lingelbach, L.H. Bannister and L. Tilley, *Trends in parasitol.,* **2004***, 20*, 581-589.

[181] K. Kirk, *Physiol. Rev*., **2001**, *81*, 495-537.

[182] I.D. Goodyer, B. Pouvelle, T.G. Schneider, D.P. Trelka, T.F. Taraschi*, Mol. Biochem. Parasitol., **1997**, 87*, 13-28.

[183] a) S.E.A. Gratton, P.A. Ropp, P.D. Pohlhaus, J.C. Luft, V.J. Madden, M.E. Napier, and J.M. DeSimone,

In the Figure 112, we can observe the confocal pictures taken in the case of the compound **A(Rho)**. We can detect the presence of rhodamine in a small amount when the cells infected by the parasite. This could be due to the penetrations of only the small (50 nm) nano-objects inside the *p*RBCs, and not of the bigger ones. Not only the presence of rhodamine is detected inside the *p*RBCs, but also it is detected near the pigment of the parasites.

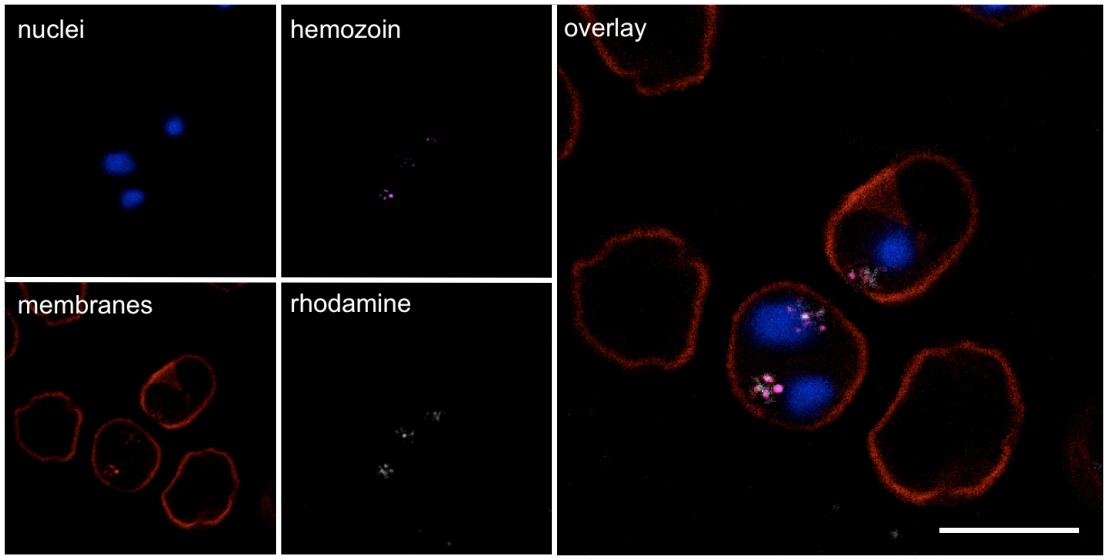

Figure 112: Confocal fluorescence microscopy study of the subcellular localization of the rhodamine encapsulate inside the nano-objects formed by the compound A. DAPI (nuclei) and hemozoin fluorescence (pink) are used to indicate pRBCs. The RBCs plasma membrane is shown in red. The rhodamine fluorescence is shown in white. Scale bar: 5µm.

PNAS, **2008**, *105*, 11613-11618; b) Y. Liu, J. Tan, A. Thomas, D. Ou-Yang, V.R. Muzykantov, *Therapeutic Delivery*, **2012**, *3*, 181-194; c) J.A.Champion, Y.K. Katare, S. Mitragotri, *J. Control. Release*, **2007**, *121*, 3-9; d) G. Sharma, D.T. Valenta, Y. Altman, S. Harvey, H. Xie, S. Mitragotri, J.W. Smith, *J. Control. Release*, **2010**, *147*, 408-412.

In the case of the compound **B(Rho)**, no fluorescence signal was detected (Figure 113), probably because the size of the nano-objects does not allow them to penetrate the cell membrane. The nano-objects formed by this compounds are bigger, varying between 90 nm and 150 nm, and exceed the size limits for internalization. Moreover, the time of incubation (90 min) possibly does not allow sufficiently the release of the nano-object cargo.

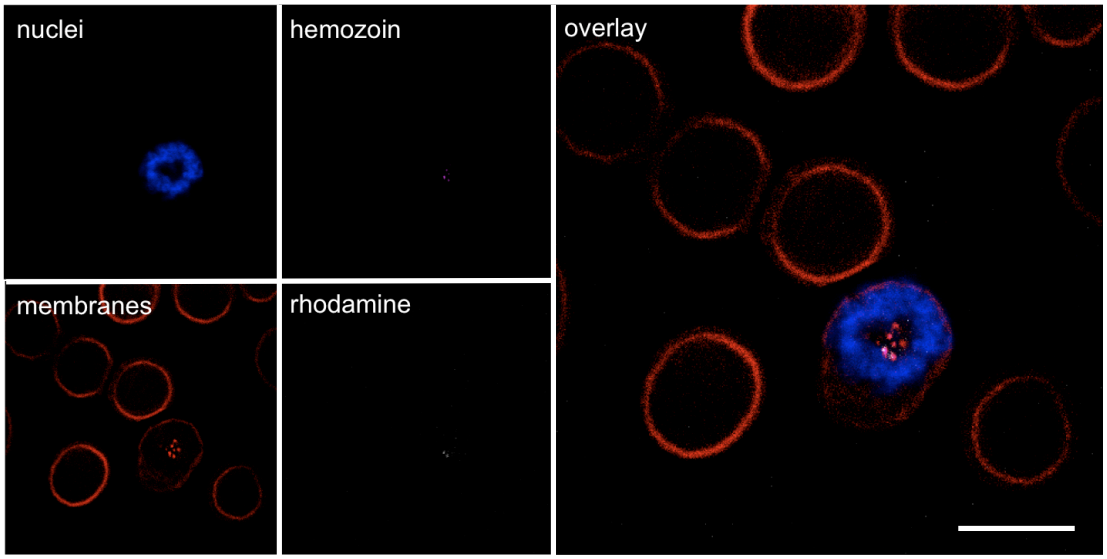

Figure 113: Confocal fluorescence microscopy study of the subcellular localization of the rhodamine encapsulate inside the nano-objects formed by the compound B. DAPI (nuclei) and hemozoin fluorescence (pink) are used to indicate pRBCs. The RBCs plasma membrane is shown in red. The rhodamine fluorescence is shown in white. Scale bar: 5µm.

In the case of the compound **C(Rho)**, the rhodamine presence was detected in a small scale inside the infected red blood cells. These nano-carriers are smaller, with an average size of 80 nm. Again, the fluorescence can be observed next to the parasite hemozoin.

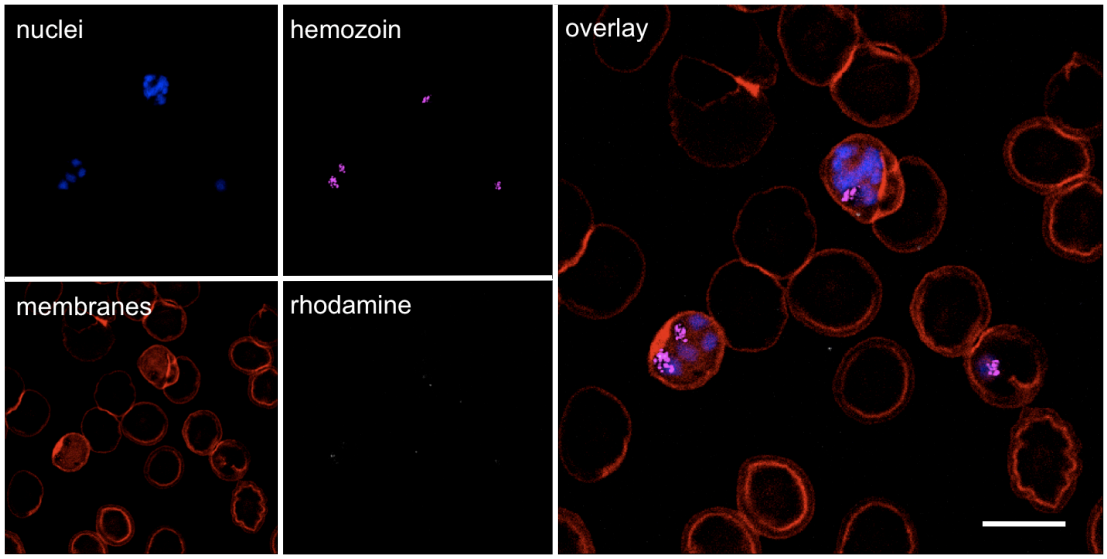

Figure 114: Confocal fluorescence microscopy study of the subcellular localization of the rhodamine encapsulate inside the nano-objects formed by the compound C. DAPI (nuclei) and hemozoin fluorescence (pink) are used to indicate pRBCs. The RBCs plasma membrane is shown in red. The rhodamine fluorescence is shown in white. Scale bar: 5µm.

Finally, in the case of the compound **D(Rho)** (Figure 115), an intense rhodamine signal was observed inside the *p*RBCs. This means that the nano-objects were able to enter inside the contaminated cells thanks to new pathways created by the parasites. Confirming this hypothesis, we can observe that no healthy cell was contaminated. This result was expected because of the size of the nano-objects found by SEM characterization (< 50 nm).

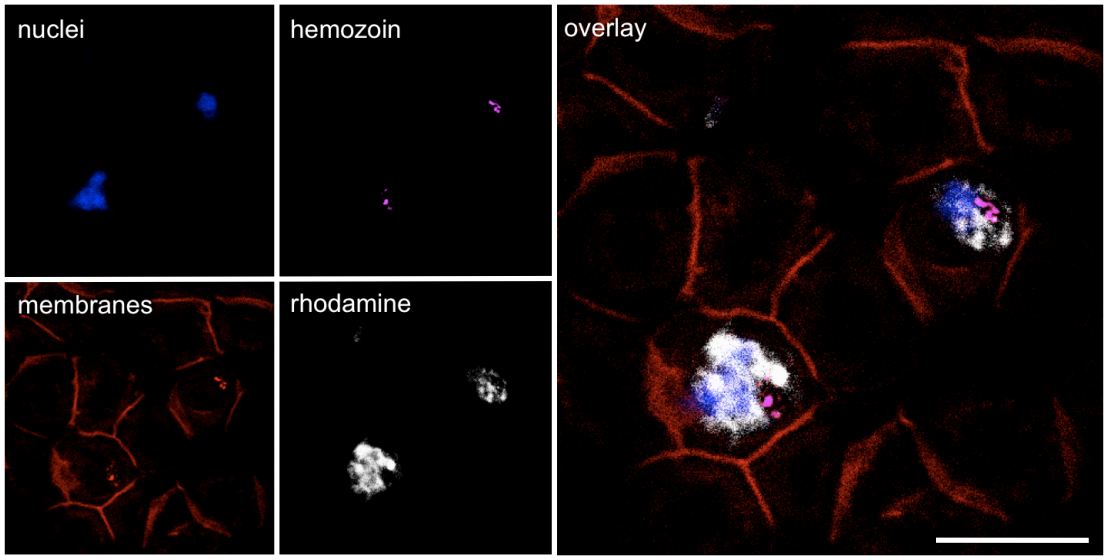

Figure 115: Confocal fluorescence microscopy study of the subcellular localization of the rhodamine encapsulate inside the nano-objects formed by the compound D. DAPI (nuclei) and hemozoin fluorescence are used to indicate pRBCs. The RBCs plasma membrane is shown in red. Scale bar: 5µm.

Taking into account the results of growth inhibition obtained and the results of internalization we can consider that the dendritic derivatives **A**, **C** and **D** are the best candidates for the targeted delivery of antimalarial drugs because they are able to release their cargo selectively into the pRBCs.

Conclusions

None of the compounds studied presented cytotoxicity on HUVEC endothelial cells.

Two nano-objects formed by the compounds derived from pluronic® polymer modified by *bis*-MPA fragments, $\mathbf{D(CQ)_{5:1}}$ and $\mathbf{C(PQ)_{5:1}}$, showed better *Plasmodium* growth inhibition results than their corresponding free drug *in vitro*.

The compounds $\mathbf{A(CQ)_{5:1}}$ and $\mathbf{B(PQ)_{5:1}}$ also worth to be studied *in vivo* as the *in vitro* experiments showed that their cargo can be released quantitatively.

The encapsulation of rhodamine permitted to confirm the specificity of action of small nano-objects thanks to the membrane affectation by the parasite.

Future work:

The promising results obtained with the nano-objects $\mathbf{D(CQ)_{5:1}}$ and $\mathbf{C(PQ)_{5:1}}$ open an interesting via to explore *in vivo* in order to study the applications of antimalarial drugs using nano-carriers based on the dendritic derivatives studied in this PhD thesis.

The results obtained at C5 being promising for this two compounds, future growth inhibition assays could be conduct at lower concentration of drugs.

As continuation, it would be interesting to work with other antimalarial drugs, hydrophilic and hydrophobic ones as Artemether and Lumefantrine. Other molecules synthesized from Pluronic® polymer could be investigated.

Experimental part

Except where otherwise is indicated, all reagents were purchased from Sigma-Aldrich (St-Louis, MO, USA).

The typical procedure for Steglish esterification (A), typical procedure for deprotection of *bis*-MPA alcohol groups (B), and the typical procedure for deprotection of amine groups (C) are described in Chapter 1.

The UV measurements were carried out using a Varian Cary50 Probe UV-visible spectrophotometer. Fluorescence confocal microscopy images were obtained with a Leica TCS SP5 laser scanning confocal microscope.

Synthesis of *bis*-MPA and pluronic® derivatives

($C_{17}H_{35}$)$_4$[G#3]-$CH_2C{\equiv}CH$ (B-3b)

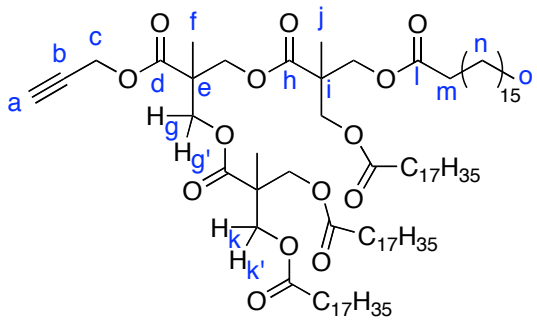

The second generation dendron with free hydroxyl groups B-2b (1.50 g, 3.7 mmol, 1 eq.) was dissolved in dry dichloromethane (75 mL). DMAP (1.36 g, 11.1 mmol, 6 eq.) and stearic acid (6.34 g, 22.3 mmol, 6 eq.) were added. The reaction was allowed to stir under argon atmosphere and was cooled to 0ºC. DCC (4.59 g, 22.27 mmol, 6.0 eq.) was dissolved in dry dichloromethane (25 mmol) and was added dropwise. The reaction was allowed to stir at room temperature during 7 days. Then, the formed DCU was filtered off and the solvent was evaporated under reduce pressure. A mixture of oil and solid was obtained. A few amount of THF was added and the crude was allowed to stir during 20 min at room temperature. Then, the precipitate was filtered off and the solvent was evaporated under vacuum to get a yellow solid which was dissolved in a few amount of dichloromethane and precipitated in cold acetone into a white solid (3.67 g, 67 %).

^{1}H (300 MHz, $CDCl_3$) δ (ppm): 0.88 (t, *J* = 6.6 Hz, 12H, H_o), 1.25 (m, 121 H, H_f, H_j, H_n), 1.57 (m, 8H. H_n), 2.29 (t, *J* = 7.5 Hz, 8H, H_m), 2.50 (t, *J* = 2,4 Hz, 1H, H_a), 4.19 (s, 8H, $H_{g,g'}$, H_k), 4.27 (d, *J* =5.1 Hz, 4H, $H_{k'}$), 4.72 (d, *J* = 2.4 Hz, 2H, H_c).

^{13}C (300 MHz, $CDCl_3$) δ (ppm): 14.0 (C_{m17}), 17.4 (C_f), 17.7 (C_j), 22.6 (C_{m15}), 24.8 (C_{m2}), [29.1, 29.2, 29.4, 29.6] (C_{m3} to C_{m14}), 31.9 (C_{m15}), 34.0 (C_{m1}), 46.4 (C_i), 46.7 (C_e), 52.7 (C_c), 65.0 (C_k), 65.6 (C_g), 75.4 (C_a), 77.1 (C_b), 171.4 (C_d), 172.0 (C_h), 173.1 (C_l).

IR (cm^{-1}, KBr): 3307 (≡C-H), 2919-2851 (C-H), 1736 (C=O).

Calculated $[M]^+$ ($C_{90}H_{164}O_{14}$) *m/z* = 1469.2. Found: ESI+: $[M+Na]^+$ *m/z* = 1492.4.

(NHBoc)$_4$[G#2]-(CH$_2$)$_6$N$_3$

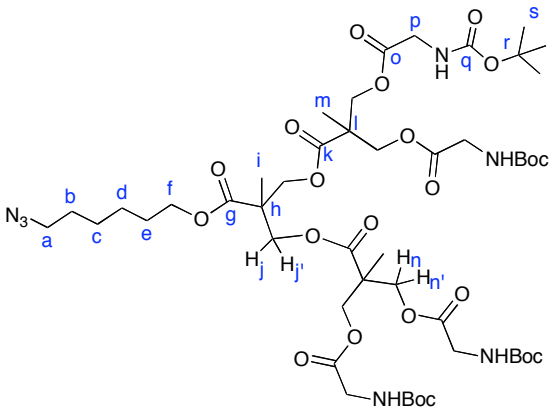

2 g (4.07 mmol) of (OH)$_4$[G#2]-(CH$_2$)$_6$N$_3$ (see synthesis in chapter 1), 3.2 g (18.3 mmol) of GlyBoc and 1.9 g (6.51 mmol) of DPTS were dissolved in 50 mL of dry dichloromethane. The flask was flushed with argon and cooled to 0°C. A solution of 3.8 g (18.3 mmol) of DCC in 5 mL of dry dichloromethane was added dropwise. The reaction was allowed to stir at room temperature, under argon atmosphere for 15 hours. The precipitate was then filtered and the filtrate was concentrated under reduced pressure. The crude product was purified by column chromatography eluting with a mixture 5:5 of Hexane:EtOAc. Yield: 86%. Green oil.

NMR ^{1}H (CDCl$_3$, 300 MHz) δ (ppm): 1.23-1.24 (m, 9H, H$_i$, H$_m$), 1.43 (m, 40H, H$_s$, H$_c$, H$_d$), 1.60-1.65 (m, 4H, H$_b$, H$_e$), 3.27 (t, *J* = 6.6 Hz, 2H, H$_a$), 3.87 (d, *J* = 5.4 Hz, 8H, H$_p$), 4.09-4.13 (m, 2H, H$_f$), 4.23-4.25 (m, 12H, H$_j$, H$_n$), 5.24 (br s, 4H, NH).

NMR ^{13}C (CDCl$_3$, 400 MHz) δ (ppm): 17.6, 17.8, 25.4, 26.3, 28.1, 28.7, 42.3, 46.4, 46.6, 65.5, 65.6, 80.0, 155.8, 169.9, 171.8, 172.2.

IR (cm^{-1}, KBr): 3389 (N-H), 2978-2936 (C-H), 2097 (N$_3$), 1717 (C=O).

Calculated [M]$^+$ (C$_{49}$H$_{81}$N$_7$O$_{22}$) *m/z* = 1120,20. Found: Maldi+: [M+Na]$^+$ *m/z* =1147.2.

3Gpolar(NHBoc)-2Gapolar($C_{17}H_{35}$)$_4$

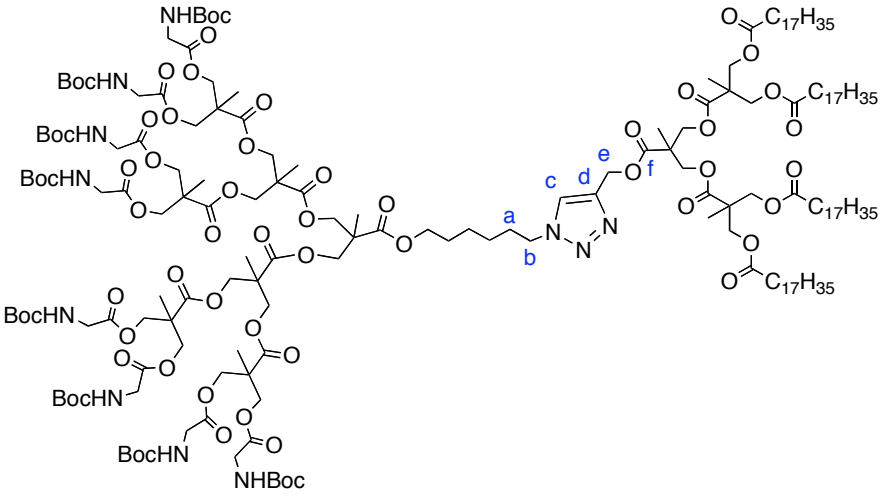

Penta-hydrated copper sulfate (3 mg, 1.13 µmol) and sodium ascorbate (0.45 mg, 2.26 µmol) were agitated in DMF during one hour in order to form Cu(I). At the same time the apolar dendron (37 mg, 25 µmol) and the polar dendron (50 mg, 23 µmol) were solubilized in DMF. After, the solutions were mixed and agitated for 2 days at room temperature, under argon atmosphere. 50 mL of dichloromethane were added and the reaction mixture was washed with brine and water (4 x 10 mL) to remove residues and DMF. The crude was concentrated under reduced pressure and the product was precipitated in cold acetone as a white solid. Yield: 49 %.

NMR ^1H ($CDCl_3$, 300 MHz) δ (ppm): 0.80-0.85 (m, 12H, $CH_{3chains}$), 1.14-1.20 (m, 142H, $CH_{2chains}$, $CH_{3bis\text{-}MPA}$), 1.39 (s, 72H, H_{Boc}), 1.54 (m, 8H), 1.91 (m, 8H, H_{chains}), 2.24 (t, *J* = 7.5 Hz, 8H, H_{chains}), 3.84 (d, *J* =4.8 Hz, 16H, H_{gly}), 4.07-4.35 (m, 42H, H_b, $H_{bis\text{-}MPA}$), 5.19 (s, 2H, H_e), 5.47 (br s, 8H, NH), 7.67 (s, 1H, H_c).

NMR ^{13}C ($CDCl_3$, 400 MHz) δ (ppm): 14.0, 14.1, 17.5, 17.7, 17.8, 20.9, 21.0, 22.6, 24.8, 25.3, 26.1, 28.3, 29.1, 29.2, 29.3, 29.5, 29.7, 30.1, 31.9, 34.0, 42.2, 46.3, 46.4, 46.5, 46.6, 46.7, 50.2, 58.4, 60.3, 64.9, 65.1, 65.4, 65.6, 66.1, 79.9, 124.1 (C_c), 141.9 (C_d), 155.9, 170.1, 171.1, 171.5, 171.8, 171.8, 172.0, 172.1, 173.2.

IR (cm^{-1}, KBr): 3399 (N-H st), 2918-2850 (C-H), 1744 (C=O).

Calculated $[M]^+$ ($C_{187}H_{321}N_{11}O_{60}$) *m/z* = 3683.59. Found: Maldi+: $[M+Na]^+$ *m/z* = 3707.01.

3Gpolar(NH_2)$_8$-2Gapolar($C_{17}H_{35}$)$_4$, compound B

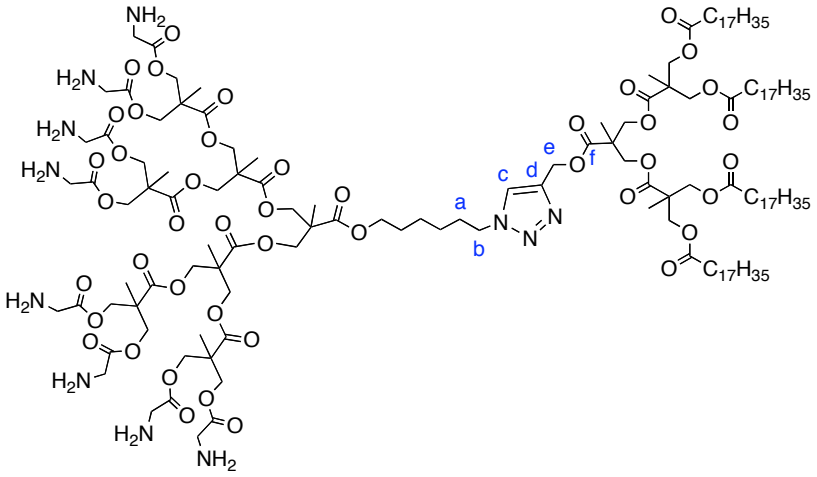

The compound B was obtained following the procedure (C) of deprotection of amine groups. Pale yellow solid, quantitative yield.

NMR ^{1}H (DMSO, 300 MHz) δ (ppm): 0.82-0.86 (m, 12H, $CH_{3chains}$), 0.99-1.10 (m, 30H, $CH_{3bis\text{-}MPA}$), 1.15-1.22 (m, 90H, $CH_{2chains}$,), 1.45-1.52 (m, 8H, $CH_{2chains}$), 1.76-1.81 (m, 8H, H_a), 2.24 (t, *J* = 7.2 Hz, 8H, H_{chains}), 3.44 (d, *J* =4.8 Hz, 16H, H_{gly}), 4.07-4.35 (m, 42H, H_b, $H_{bis\text{-}MPA}$), 5.75 (s, 2H, H_e), 5.47 (br s, 8H, NH), 7.95 (s, 1H, H_c), 8.29 (br s, 16H, NH_2).

NMR ^{13}C ($CDCl_3$, 300 MHz) δ (ppm): 13.8, 16.7-17.0, 22.0, 24.3, 24.4, 28.3-28.9, 31.2, 33.2, 33.6, 34.0, 47.9, 48.1-48.3, 49.3, 50.1, 63.5-63.9, 65.5-65.8, 147.8 (C_d), 168.8, 172.9-173.3, 174.3, 174.4, 175.2, 176.6.

IR (cm^{-1}, KBr): 3433 (N-H), 2917-2850 (C-H), 1741 (C=O).

3Gpolar(NHBoc)$_8$-3Gapolar(C$_{17}$H$_{35}$)$_8$

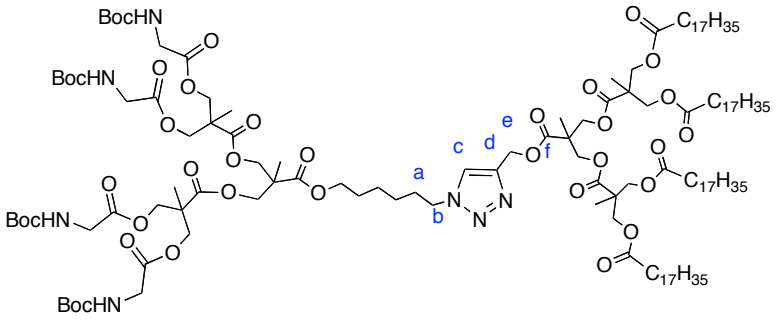

Penta-hydrated copper sulfate (2.7 mg, 9.2 µmol) and sodium ascorbate (3.9 mg, 19.7 µmol) were agitated in DMF during one hour in order to form Cu(I). At the same time the polar dendron (200 mg, 179 µmol) and the apolar dendron (289 mg, 196 µmol) were solubilized in DMF. Then, the two solutions were mixed and agitated for 2 days at room temperature, under argon atmosphere. 50 mL of dichloromethane were added and the reaction mixture was washed with brine and water (4 x 10 mL) to remove DMF. The crude was concentrated under reduced pressure and precipitated in cold MeOH as a white solid and purified by column chromatography eluting with 8:2 hexane/EtOAc . Yield: 49 %.

NMR ^{1}H (CDCl$_3$, 400 MHz) δ (ppm): 0.88 (t, *J* = 6.5 Hz, 12H), 1.18 (s, 6H), 1.25 (m, 122H), 1.39-1.42 (m, 38h), 1.57-1.65 (m, 14H), 1.94 (q, *J* = 3.6 Hz, 2H), 2.28 (t, *J* = 7.5 Hz, 8H), 3.89 (d, J = 5.7 Hz, 8H), 4.04-4.30 (m, 24H), 4.37 (t, *J* = 7.2 Hz, H$_b$), 5.24 (m, 6H, NH, H$_e$) 7.68 (s, 1H, H$_c$).

NMR ^{13}C (CDCl$_3$, 400 MHz) δ (ppm): 14.1, 17.5, 17.2, 17.7, 17.9, 22.6, 24.8, 25.3, 26.1, 28.3, 29.1, 29.2, 29.3, 29.5, 29.6, 29.7, 30.1, 31.9, 34.0, 42.2, 46.3, 46.4, 46.5, 46.6, 50.2 (C$_b$), 58.4 (C$_e$), 64.9, 65.4, 65.5, 65.6, 65.7, 79.9, 124.1 (C$_c$), 142.0 (C$_d$), 155.8, 170.0, 171.8, 172.0, 172.1, 172.2, 173.2.

IR (cm^{-1}, KBr): 3418 (N-H), 2919-2850 (C-H), 1742 (C=O).

Calculated [M]$^+$ (C$_{139}$H$_{245}$N$_7$O$_{36}$) *m/z* = 2590.46. Found: Maldi+: [M+Na]$^+$ *m/z* = 2612.8.

3Gpolar(NH_2)$_8$-3Gapolar($C_{17}H_{35}$)$_8$, compound A

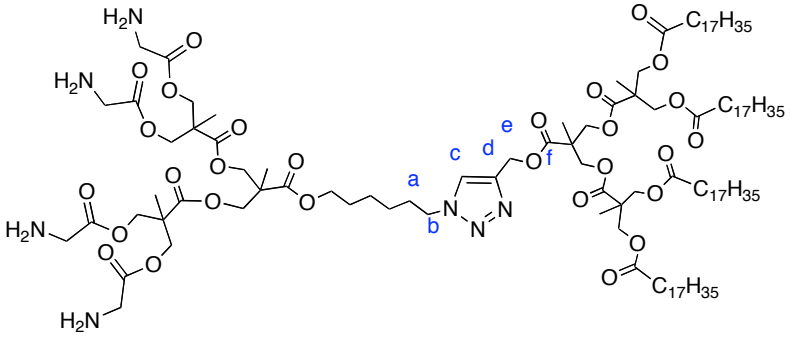

The compound A was obtained following the procedure (C) for deprotection of amine groups. White solid, quantitative yield.

NMR ^{1}H ($CDCl_3$, 400 MHz) δ (ppm): 0.85 (t, *J* = 5.7 Hz, 12H), 1.18-1.40 (m, 140H), 1.58 (m, 12H), 1.80-1.98 (m, 22H), 2.28 (t, *J* = 7.5 Hz, 8H), 4.10-4.37 (m, 34H), 5.24 (s, 2H, H_e), 7.67 (s, 1H, H_c), 8.38 (br s, 8H, NH).

NMR ^{13}C ($CDCl_3$, 400 MHz) δ (ppm): 14.0, 17.5, 17.7, 22.6, 24.8, 25.3, 26.1, 28.3, 29?1, 29.2, 29.3, 29.4, 29.6, 29.7, 30.1, 31.9, 34.0, 46.3, 46.6, 50.2 (C_b), 58.3 (C_e), 64.9, 65.3, 124.1 (C_c), 141.9 (C_d), 167.4, 171.9, 172.1, 173.1.

IR (cm^{-1}, KBr): 3430 (N-H), 2919-2851 (C-H), 1740 (C=O).

Calculated $[M]^+$ ($C_{119}H_{213}N_{16}O_{28}$) *m/z* = 2188.55. Found: Maldi+: $[M+Na]^+$ *m/z* = 2213.2.

[G#1]Pluronic[G#1]

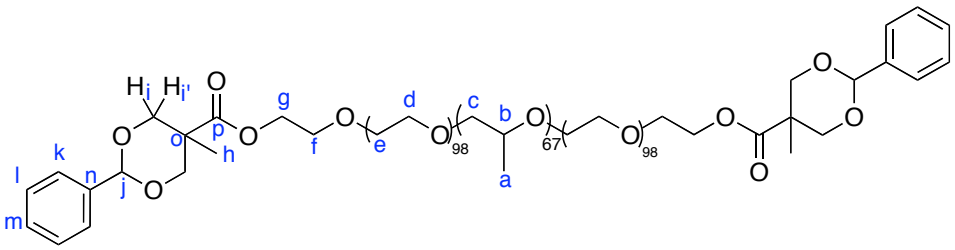

10.04 g (0.80 mmol) of F127 Pluronic were dried at 110°C under vacuum during 1 hour. The product was then dissolved in 50 mL of dry dichloromethane and 116 mg (0.95 mmol) of DMAP was added. After dissolution, 2.03 g (4.76 mmol) of *bis*-MPA benzylidene anhydride (synthesis in Chapter 1, 3-2) were added to the reaction mixture. The reaction was allowed to stir at room temperature, under argon atmosphere during 1 night. Then, 5 mL of methanol were added to the reaction to eliminate the excess of anhydride and the reaction mixture was allowed to stir at room temperature during 6 hours. The crude product was then precipitated dropwise over 1 L of diethylic ether. The precipitate was filtrated after one night at 5°C, and washed with cold diethylic ether. The product was obtained in a 84 % yield (8.73 g, 0.67 mmol) as a white solid after pump drying.

NMR ^{1}H ($CDCl_3$, 400 MHz) δ (ppm): 1.02 (s, 6H, H_h), 1.10 (m, 201H, H_a), 3.36-3.38 (m, 67H, H_b), 3.46-3.79 (m, ≈1030H, H_c, H_d, H_e, H_f, H_i), 4.32 (t, J = 4.8 Hz, 4H, H_g), 4.62 (d, J = 11.6 Hz, 4H, $H_{i'}$), 5.41 (s, 2H, H_j), 7.28 (m, 6H, H_l, H_m), 7.39 (m, 4H, H_k).

NMR ^{13}C ($CDCl_3$, 400 MHz) δ (ppm): 17.1 (C_a), 17.3 (C_a), 17.7 (C_h), 42.2 (C_o), 64.1 (C_g), 68.3 (C_f), 68.4 (C_f), 68.9 (C_f), 70.4 (C_e, C_d), 72.7-73.4 (C_c, C_i), 75.0-75.5 (C_b), 101.6 (C_j), 126.1 (C_k), 128.1 (C_l), 128.8 (C_m), 137.7 (C_n), 173.7 (C_p).

IR (cm^{-1}, thin film over NaCl): 2882 (C-H st), 1734 (C=O), 1114 (C-O-C).

MALDI+: distribution with max at m/z = 13649 and m/z = 5250.

(OH)$_2$[G#1]Pluronic[G#1](OH)$_2$

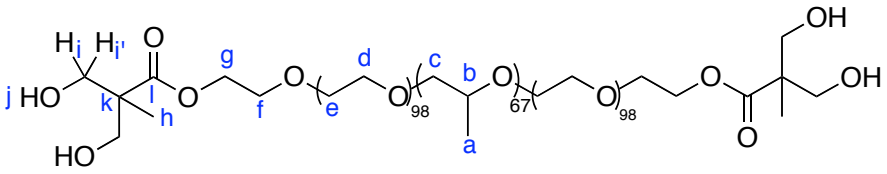

1.88 g (0.14 mmol) of [G#1]Pluronic[G#1] were dissolved in 20 mL of ethyl acetate and 200 mg of palladium on carbon (20 % w) were added. The reaction mixture was allowed to stir at room temperature under hydrogen atmosphere for 1 day. The residue of palladium was filtrated over celite and the solvent evaporated under reduced pressure to give the pure product in a 92 % yield (1.68 g, 0.13 mmol) as a white solid.

NMR ^{1}H ($CDCl_3$, 400 MHz) δ (ppm): 1.10 (m, 207H, H_a, H_h), 3.36 (m, 67H, H_b), 3.48-3.72 (m, ≈1050, H_c, H_d, H_e, H_f, $H_{i,i'}$), 4.32 (t, *J* = 4.8 Hz, 4H, H_g).

NMR ^{13}C ($CDCl_3$, 400 MHz) δ (ppm): 17.1 (C_a), 17.3 (C_a), 17.4 (C_h), 63.3 (C_g), 67.5 (C_i), 68.7 (C_f), 70.5 (C_e, C_d), 72.8-75.5 (C_b, C_c), 175.6 (C_l).

IR (cm^{-1}, thin film over NaCl): 3482 (O-H), 2883 (C-H), 1732 (C=O), 1112 (C-O-C).

MALDI+: distribution with max at *m/z* = 13640.

(NHBoc)$_2$[G#1]Pluronic[G#1](NHBoc)$_2$

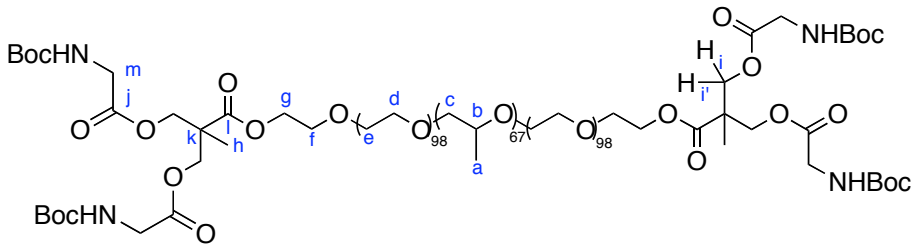

1 g (78 µmol) of $(OH)_2$[G#1]Pluronic[G#1]$(OH)_2$ were dissolved in 50 mL of dry dichloromethane, 164 mg (934 µmol) of GlyBoc and 38 mg (311 µmol) of DMAP were added. After dissolution, 193 mg (934 µmol) of DCC in 10 mL of dry dichloromethane were added to the reaction mixture. The reaction was allowed to stir at room temperature, under argon atmosphere during 2 days. Then, the reaction mixture was cooled to 5°C and the precipitate filtered off. The solvent was evaporated under reduced pressure and the crude product was dissolved in water and dialysed against 300 mL of dichloromethane. After 3 days the dialysed product was collected and the solvent evaporated under reduce pressure. The product was obtained in 95 % yield (997 mg, 74 µmol) as a pale yellow solid after pump drying.

NMR ^{1}H ($CDCl_3$, 400 MHz) δ (ppm): 1.08 (m, 207H, H_a, H_h), 1.39 (s, 36H, H_p), 3.33-3.36 (m, 67H, H_b), 3.45-3.77 (m, ≈ 1030H, H_c, H_d, H_e, H_f, H_i), 3.81 (d, *J* = 5.6 Hz, 8H, H_m), 4.20-4.29 (m, 8H, H_i, H_g).

NMR ^{13}C (MeOD, 400 MHz) δ (ppm): 17.3-17.4 (C_a, C_h), 28.3 (C_p), 42.3 (C_k), 46.3 (C_m), 64.2 (C_g), 65.7 (C_i), 68.8 (C_f), 70.5-70.8 (C_d, C_e), 72.8-73.4 (C_b), 75.1-75.5 (C_c), 79.9 (C_o), 169.9 (C_j, C_n), 172.3 (C_l).

IR (cm^{-1}, thin film over NaCl): 3328 (N-H), 2881 (C-H), 1721 (C=O), 1114 (C-O-C).

MALDI+: distribution with max at *m/z* = 13884 and *m/z* = 5223.

$(NH_2)_2$[G#1]Pluronic[G#1]$(NH_2)_2$, compound C

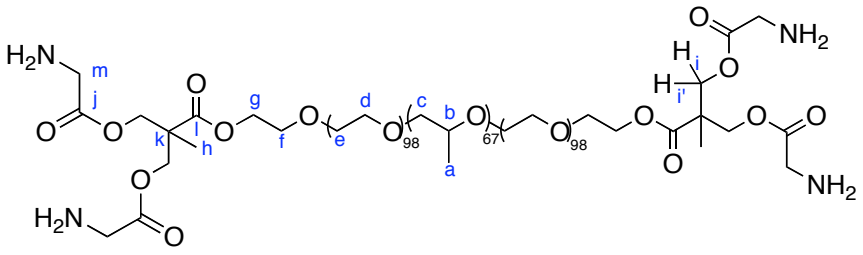

The compound C was obtained following the procedure (C) of deprotection of amines.

NMR ^1H ($CDCl_3$, 400 MHz) δ (ppm): 1.13 (m, 207H, H_a, H_h), 3.29-3.43. (m, 67H, H_b), 3.45-3.77 (m, ≈ 1030H, H_c, H_d, H_e, H_f, H_i, H_m), 4.20-4.29 (m, 8H, $H_{i'}$, H_g), 8.36 (br s, 4H, NH_2).

NMR ^{13}C (MeOD, 400 MHz) δ (ppm): 17.3 (C_a), 17.4 (C_h), 70.2-70.5 (C_d, C_e), 72.8, 72.9, 73.3, 75.1, 75.3, 75.5, 167.4 (C_l), 167.7 (C_i).

IR (cm^{-1}, thin film over NaCl): 2969 (-NH^{3+}, st), 2883 (C-H st), 1750 (C=O), 1114 (C-O-C).

MALDI+: distribution with max at *m/z* = 13987 and *m/z* = 4764.

$(NH_2)_8$[G#3]Pluronic[G#3]$(NH_2)_8$, compound D

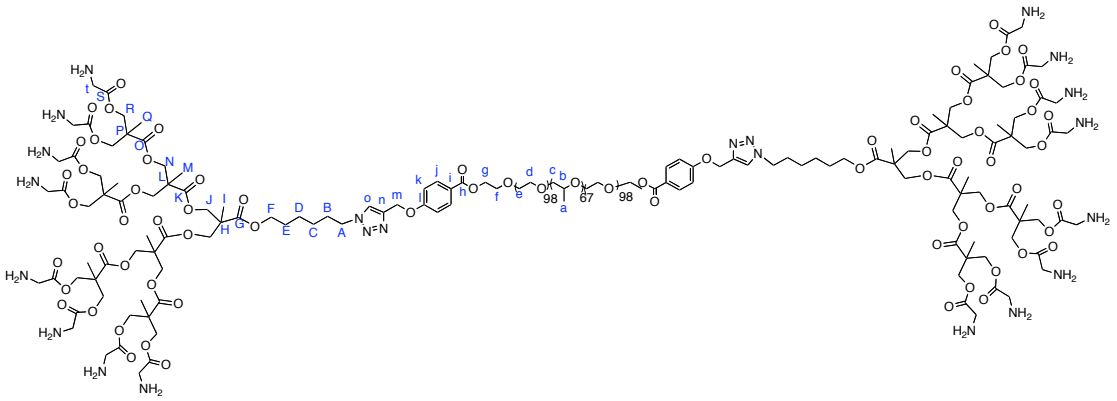

The compound D was obtained following the synthesis method (C). Quantitative yield. Yellow solid.

NMR ^1H (MeOD, 400 MHz) δ (ppm): 1.13-1.15 (m, 201H, H_a), 1.29-1.34 (m, 36H, H_M, H_Q), 1.36-1.67 (m, 8H, H_C, H_D), 3.30-3.33 (m, 69H, H_b, H_A), 3.42-3.69 (m, ≈1080H, H_c, H_d, H_e, H_f), 4.02-4.06 (m, 18H, H_J, H_N), 4.11 (m, 4H, H_g), 4.33-4.35 (m, 32H, H_R), 4.96 (m, 32H, H_T), 5.32 (s, 4H, H_m), 5.49 (s, 2H, H_o), 7.02 (m, 4H, H_i), 8.01 (m, 4H, H_j).

NMR ^{13}C (MeOD, 400 MHz) δ (ppm): 17.7, 71.3-71.5, 74.1, 74.4, 76.6-76.8, 111.4.

IR (cm^{-1}, thin film over NaCl): 2970 (-NH^{3+}, st), 2880 (C-H st), 1742 (C=O), 1112 (C-O-C).

MALDI+: distribution with max at *m/z* = 4991.

Encapsulation of antimalarial drugs

Hydrophilic drugs (chloroquine and primaquine) were dissolved in 1mL of water. The polymers A, B, C and D were dissolved in a small amount of dichloromethane. The two solutions were mixed and stirred until the complete evaporation of the dichloromethane. The excess of drug was removed by dialysis in deionized (miliQ) water. All the samples were kept at 4°C or -20°C until further analysis. The amount of drug encapsulated was determined by and indirect quantification: the amount of free drug was quantified by UV in the residual water of dialysis.

Plasmodium inhibition growth assays

Cultures of *P. falciparum* strains 3D7 and D10 were grown in vitro in group B human RBSCs using previously described conditions.[184] Parasites were cultured at 37°C in Petri dishes containing RBCs in RPMI complete medium under a gas mixture of 92% N_2, 5% CO_2, and 3% 0_2. Synchronized cultures were obtained by 5% sorbitol lysis,[185] and the medium was changed every 2 days maintaining 3 % haematocrit. For culture maintenance, parasitemias were kept below 5% late forms by dilution with washed RBCs.

Parasitemia was adjusted to 1.5% with more than 90% of parasites at ring stage after sorbitol synchronization. 147 µL of this *Plasmodium* culture was plated in 96-well plates and incubated 48h in the presence of antimalarial drug or nanoobjects (3µL at the desired concentration). The same experiment was carried out with late forms of parasites. Parasitemia was determined by microscopic counting of blood smears. Smears were fixed in methanol for a few second and then stained for ten minutes with Giemsa (Merck) diluted 1:10 in Sorenson's Buffer, pH 7.2. After washing with distilled water and drying, the ratio of infected versus non-infected RBCs (Red Blood Cells) was determined by microscopic analysis.

[184] S.L. Cranmer, C. Magowan, J. Liang, R.L. Coppel, B.M. Cooke*, Trans. R. Soc. Trop. Med. Hyg.,* **1997***, 91*, 363-365.
[185] C. Lambros, J.P. Vanderberg, *J. Parasitol.,* **1979***, 65*, 418-420.

Cytotoxicity of nano-objects

Human Umbilical Vein Endothelial Cells (HUVEC) were cultured in DMEM (Invitrogen) supplemented with 10 % heat-inactivated foetal bovine serum (FBS), 1 % penicillin/streptomycin and 10mM glutamine. For cytotoxicity assays, 5000 cells/well were plated in 96-well plates and after 24h at 37°C in 5% CO_2 atm them medium was substituted by 100µL of nanoobjects containing culture medium without FBS, and the plates were incubated for 48h. 10µL of 4-[3-(4-iodophenyl)-2-(4-nitrophenyl)-2H-5-tetrazolio]-1,3-benzene disulfonate labelling reagent (WST-1) was added to each well and the plate was incubated in the same condition for 3h. After thoroughly mixing for 1 min on a shaker, the absorbance of the samples was measured at 440 nm using a Benchmark Plus microplate reader. WST-1 in the absence of cells was used as blank and samples were prepared in triplicate for each experiment.

Immunofluorescence assays

For immunofluorescence assays, pRBCs smears were fixed in an iced-bath of acetone/methanol 90:10 v:v. After PBS washing steps, the parasite nuclei were stained with DAPI (4,6-diamino-2-phenylindole) (Invitrogen Corporation, Carlsbad, CA, USA) and the RBC membrane was labelled with AlexaFluor®350 (Molecular Probes). After the corresponding incubations and PBS washing steps, the samples were mounted with Mowiol (Calbiochem, Merk Chemicals) following standard protocols.

GENERAL CONCLUSIONS

The dendritic compounds based on bis-MPA monomer present low toxicity *in vitro*. Their easy functionalization make these compounds highly polyvalent material.

The ionic dendrimers prepared are good candidates to form electrostatic complexes with plasmid DNA. The ionic dendrimer based on bis-MPA, IbisMPA, combine low citotoxicity and high capacity of forming complexes with pDNA.

Coupling the bis-MPA dendrons functionalized with DOTA ligands to targeting molecules is possible maintaining the activity of the compound as contrast agents. The modification of antibodies by chemical reaction did not affect their selectivity neither their biological activity.

Two amphiphilic compounds synthesized from pluronic® and bis-MPA in which anti-malarial drugs were encapsulated, D(CQ) and C(PQ), permited to improve the growth inhibition of the *Plasmodium* parasite *in vitro* comparing with their respective free drugs.

RESUMEN Y

CONCLUSIONES

Resumen

Esta tesis doctoral está orientada hacia la búsqueda y el estudio de derivados dendríticos biocompatibles con aplicaciones potenciales en biomedicina en los campos de la terapia génica (**capítulo 1**), resonancia magnética de imagen (**capítulo 2**) y transporte de fármacos (**capítulo 3**).

En el **primer capítulo** se describe el estudio de las propiedades de moléculas dendríticas derivadas de dendrímeros *bis*-MPA y de PAMAM para su aplicación en terapia génica. Con este objetivo, se trabajó con dos tipos de moléculas: derivados dendríticos basados en ácido 2,2-*bis*(hidroximetil)propiónico (*bis*-MPA) y dendrimeros iónicos basados en dendrímeros de poliamidas (PAMAM) y de *bis*-MPA.

Se sintetizaron tres derivados de *bis*-MPA (**1**, **2**, **3**) así como cuatro dendrimeros iónicos de PAMAM de diferentes generaciones, con distinto grado de funcionalización para el ácido 2-(2-(2-metoxietoxi)etoxi)acético: **2G-IP-30**, **2G-IP-16**, **5G-IP-254** y **5G-IP-128**. Para completar el estudio se sintetizó un derivado iónico del compuesto **2** de *bis*-MPA, **I*bis*MPA**.

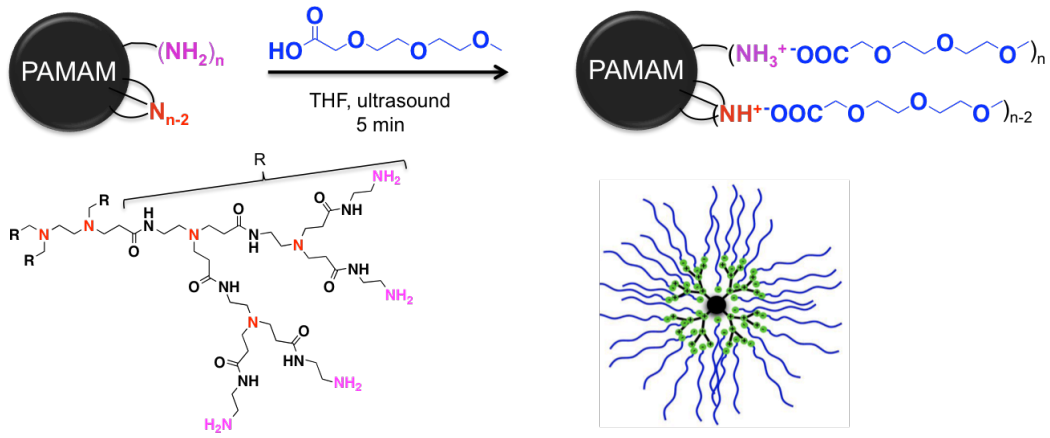

Figura 1: Síntesis de los derivados iónicos del PAMAM.

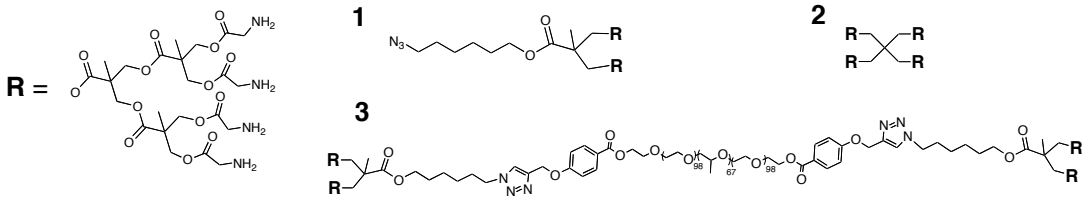

Figura 2: Estructuras de los compuestos derivados de *bis*-MPA: 1, 2 y 3.

Se estudió la viabilidad celular de los compuestos anteriores en dos líneas celulares: células U251MG y células mesenquimales demonstrándose que ningún derivado de *bis*-MPA presenta toxicidad a niveles inferiores a 1 mg/mL, mientras que, por el contrario, los derivados de PAMAM afectan al crecimiento celular desde bajas concentraciones.

Finalmente, se estudió la capacidad de los compuestos para formar complejos con ácidos nucléicos. Con este fin, se realizaron electroforesis en gel de agarosa con los diferentes derivados dendríticos y dos plásmidos de tamaños diferentes: pGFP y pAd a diferentes ratios. Todos los compuestos resultaron capaces de formar complejos con los dos plásmidos, siendo los derivados iónicos de PAMAM los más interesantes. Sin embargo, el compuesto más prometedor fue el **i*bis*MPA** por su baja toxicidad y su alta capacidad para formar complejos electrostáticos con ácidos nucléicos.

Futuros experimentos de transfección *in vitro* permitirán comprobar la eficacia de los compuestos como vectores de ácidos nucleicos.

En el **segundo capítulo** de esta tesis doctoral se estudiaron derivados dendríticos de *bis*-MPA como agentes de contraste.

En primer lugar se llevó a cabo la síntesis de dendrones modificados con ligandos de DOTA que se cargaron con iones de Gd(III) y se midió la relajación de los dendrones preparados. Los dendrones modificados presentaron mayores valores de relajación que el compuesto de referencia, en particular el dendrón de segunda generación que permite aumentar tres veces la relajación.

En segundo lugar se acoplaron con unidades de vectorización: una molécula de ácido fólico y un anticuerpo monoclonal antiHER2. El ácido fólico se unió mediante química “click” catalizada por cobre(I) tras la funcionalización de la molécula por un triple enlace. La unión del anticuerpo se realizó aprovechando los grupos

carbohidratos situados en la parte C_H2 de sus cadenas pesadas. Previamente a este paso se comprobó que el anticuerpo podía ser modificado sin afectar a su actividad biológica y selectividad para los receptores HER2 situados en la membrana de las células. Se midieron de nuevo los valores de relajación de los compuestos preparados. Los resultados confirman que el acoplamiento de los dendrones a moléculas de vectorización mantiene la actividad de los compuestos como agentes de contraste.

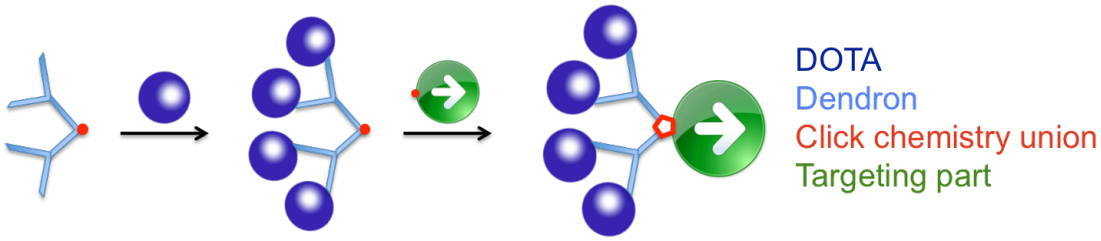

Figura 3: Síntesis de los derivados des *bis*-MPA como agentes de contraste vectorizados.

Posteriores estudios *in vitro* e *in vivo* permitirán completar el estudio de los compuestos preparados.

En el **tercer capítulo** se estudiaron nano-transportadores de fármacos anti-maláricos formados a partir de derivados dendríticos anfífilos.

Con este objetivo, se diseñaron y sintetizaron cuatro compuestos derivados de dendrímeros de *bis*-MPA (A y B) y de polímeros derivados de poloxamer (C y D). Se utilizó el compuesto comercial registrado como pluronic®.

Posteriormente, se estudió la encapsulación de dos fármacos anti-maláricos hidrófilos: la cloroquina (CQ) y la primaquina (PQ). La encapsulación de estos fármacos se realizó mediante un método de emulsión aceite/agua en presencia de los compuestos dendríticos. Los complejos formados fueron estudiados por microscopia electrónica de barrido (SEM).

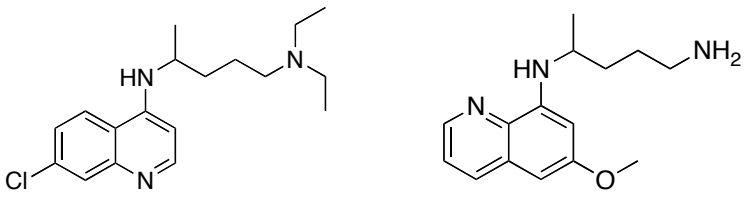

Figure 116: Moleculeculas de cloroquina (CQ, izquierda) y primaquina (PQ, derecha).

Tras haber comprobado la no-toxicidad de los nano-objetos para células endoteliales a las concentraciones necesarias, se estudió la inhibición de crecimiento del parasito *Plasmodium* por los compuestos formados, comparando con la eficacia de los fármacos libres. Con dos de los compuestos derivados del ácido plurónico, D(CQ) y C(PQ), se obtuvieron mejores resultados de inhibición del crecimiento del parásito *in vitro* que con sus correspondientes fármacos libres.

Se llevó a cabo la encapsulación de rodamina con los derivados A, B, C y D, lo cual permitió confirmar la especificidad de acción de nano-objetos pequeños debida a la afectación de la membrana por el parásito.

Conclusiones

- Los derivados dendríticos basados en monómeros de *bis*-MPA tienen una baja toxicidad *in vitro*.
- Su facilidad de funcionalización hace de estos compuestos materiales altamente polivalentes.

- Los dendrímeros iónicos preparados son buenos candidatos para formar complejos electrostáticos con los ácidos nucleicos. El dendrímero **i*bis*MPA** reúne baja toxicidad y alta capacidad para acomplejar pDNA.

- El acoplamiento de dendrones funcionalizados con ligandos de DOTA a moléculas de vectorización mantiene la actividad de los compuestos como agentes de contraste. La modificación de anticuerpos por reacción química no afecta ni a su selectividad ni a su actividad biológica.

- Dos compuestos anfífilos derivados de pluronic® y *bis*-MPA en los cuales se encapsularon antimaláricos, D(CQ) y C(PQ), permitieron mejorar los resultados de inhibición del crecimiento del parásito *in vitro* en relación a los correspondientes fármacos libres.